OPTIMIZED SYNTHESIS OF MECHANOCHEMICALLY GENERATED METAL
COMPLEXES

By

Isaiah Ray Speight

Dissertation

Submitted to the Faculty of the

Graduate School of Vanderbilt University

in partial fulfillment of the requirements

for the degree of

DOCTOR OF PHILOSOPHY

in

Chemistry

MAY 14, 2021

Nashville, Tennessee

Approved by:

Timothy P. Hanusa, Ph. D.

Steven D. Townsend, Ph. D.

Sean B. Seymore, J.D., Ph. D.

Nathan D. Schley, Ph. D.

This work is dedicated to my family, my friends, and my future. Without these three I would not be where I am, and I would not be who I am.

ACKNOWLEDGEMENTS

how far I have come. To my gaming friends, Brandon Dixon, Anthony Fleming, Shaquan Garnett, PMC Corprew Jr., Sean, Warren Powell, Cebastian Allen-Window, Usie Miller, Corey Blackwell, Justin Burke, Adrian Burke, Travis Alexander, Justin Dozier, Jawanza Wilson, Marcus Brent, LT Darius Jones, and LT Cameron Ogletree for the laughs, jokes, games, and joy.

Throughout my chemistry training in specific I have been nothing short of blessed with a multitude of amazing advisors who saw to it that I was pushed, nurtured, encouraged, and supported in all aspects. That starts with Mrs. Shelly Nason, my high school chemistry teacher. Though Mrs. Nason has passed on her spirit of joy, excitement for teaching, and will to motivate and mentor lives on through many of her students, myself included. Mrs. Nason was always there and encouraged me to take the step forward to undergraduate and then graduate school but without her at the start none of this would have been possible. Following Mrs. Nason, I was mentored by two amazing people at Norfolk State University, Dr. Tina Hall and Dr. Anthony Nweke. They both served different purposes in my undergraduate career. Dr. Hall was put on my path to help break and remake me, to teach me how to learn again and to remind me that I did not know it all. Dr. Nweke was put in my life to help me refine my craft, to mold me into a teacher and to encourage me to be a better professional through teaching and learning. These two together gave me an unforgettable experience at NSU that gave me a unique perspective and skillset coming into graduate school.

My mentors through graduate school were numerous, but I would like to call specific attention to Dr. Steven D. Townsend, and Dr. Renã A.S. Robinson. Steve, as he preferred, was always the most honest with me throughout my time at Vanderbilt. When I was falling short, he would immediately tell me and when I was succeeding, he would tell me to not get complacent and keep going. When he saw I was getting too emotionally invested in a reaction that had yet to

be done he would say "Don't outthink the round bottom". Dr. Robinson was a late addition to my mentoring team but a strong addition. She introduced me to NOBCChE and helped put me in positions to develop professionally and to mold my abilities as a leader. Outside of NOBCChE and chemistry, Dr. Robinson always reminded me to keep things in perspective with my personal life and my mental and emotional well-being, encouraging me to take time to evaluate my emotional state and to find life outside of Stevenson 7. Additional thanks to Dr. Tomislav Friščić and his research group. Tomislav welcomed me into his group purely from a hunch when we met at an ACS conference. Since then we have collaborated on two projects, he has introduced me to many amazing scientists, and continues to encourage me to stay up-beat, motivated, and creative. Without Tomislav, one of these chapters would not be present, so I thank you for the contribution to my career and so much more.

Most importantly of all, I would like to thank the Hanusa Research group. Ross, thank you for being a friend and a motivation. Encouraging me, answering my questions, asking me questions, and the work ethic that kept me motivated to work harder. Henry, to being someone to bounce ideas off of, to have those "my chemistry isn't working" conversations, and for appreciating my puns even though you didn't laugh. Lauren, for the fun conversations and the jokes. Dr. Nicholas Boyde, for helping me get settled in the lab, the talks of how to navigate graduate school, and helping put my experiments into action at the earlier stages. All of these things would not have been possible without the guidance of Dr. Timothy Hanusa. Tim, I want to thank you most of all for the support of me making the transition from having an organic chemistry background into the group which is of inorganic focus. The long conversations in your office, the handouts, the tech talks, being a sounding board, and always being supportive of me trying things that our lab normally did not do. Your positive nature, constant joy to learn and to teach, and light-

hearted personality made graduate school fun. I greatly appreciate your wisdom, guidance, and support.

TABLE OF CONTENTS

LIST OF TABLES

LIST OF FIGURES

LIST OF SCHEMES

Common Abbreviations and Symbols

⊶⊶⟶ .... Mechanochemical processing (grinding or milling)

A* .... $[1,3\text{-}(SiMe_3)_2C_3H_3]^-$

KA* .... $K[1,3\text{-}(SiMe_3)_2C_3H_3]$

HA* .... $1,3\text{-}(SiMe_3)_2C_3H_4$

$A*_2$ .... 1,3,4,6-tetrakis(trimethylsilyl)-1,5-hexadiene ($[1,3\text{-}(SiMe_3)_2C_3H_3]_2$)

A^t .... $[1,3\text{-}(tBu)_2C_3H_3]^-$

KA^t .... $K[1,3\text{-}(tBu)_2C_3H_3]$

HA^t .... $1,3\text{-}(tBu)_2C_3H_4$

A^t_2 .... 5,6-di-*tert*-butyl-2,2,9,9-tetramethyldecane ($[1,3\text{-}(tBu)_2C_3H_3]_2$)

TMS .... $SiMe_3$

Ae .... alkaline-earth metal

Cp .... cyclopentadienyl $(C_5H_5)^-$

Im .... imidazole

MeIm 2-methylimidazole

THF .... tetrahydrofuran

Et_2O .... diethyl ether

PhMe .... toluene

NMR .... Nuclear Magnetic Resonance

CHAPTER 1

Mechanochemistry, a contender in synthesis

1.1 Introduction

In the name of simple economics, a traditional goal of synthetic chemistry is to maximize the yield of a desired product from any given reaction. In contrast, the more specific aim of reducing the exposure of humans and the environment to hazardous substances, while simultaneously increasing the efficiency of reactions, was articulated only a few decades ago.[1-2] Under the rubric of *green chemistry*, and codified in the form of "12 principles",[1] this approach strives to employ biologically and environmentally benign solvents, including water, environmentally friendly metals and organic catalysts, and purification methods with minimal use of solvents of any kind.

A general method for reducing solvent use that has been gaining increasing attention in the search for 'greener' synthesis is *mechanochemistry*, which uses mechanical action (e.g., impact and friction) to generate the energy needed for chemical reactions. Although some heat may be involved, mechanochemical reactions are not simply thermal reactions in disguise. The mechanisms involved in mechanochemically promoted reactions are still a matter of considerable dispute, but the grinding and cracking of crystals are accompanied by phenomena not present in solution. For example, the magnitude of the electric field near the tip of a mobile crack has been estimated at $\sim 10^8$ V m^{-1},[3] and the high defect density introduced in crystals by grinding can also serve as a driving force.[4] Such energies can fracture bonds and create radicals in ways that do not occur in solution.

Mechanochemically driven reactions can perform synthetic transformations with little to no solvent on both small (<1 g) and large (kg) scales, decrease the production of waste, and provide access to new compounds not available from solution-mediated reactions. In addition, a wide variety of equipment can be employed for mechanochemical research,[5] ranging from the venerable mortar and pestle, to the mixer and planetary mills, to the recently developed resonant acoustic mixer (RAM) (Figure 1).[6] Such flexibility has helped mechanochemistry become a common tool in a number of chemistry labs.[7] The applications of mechanochemistry continue to expand upon as well. These range from inorganic transformations such as the synthesis of metal hydrides from bulk sources,[8] to organic transformations such as metal-catalyzed cross-coupling reactions,[9] polymerizations,[10] and the formation of metal organic framework (MOF) materials.[11]

Figure 1. Images of a mortar and pestle, Retsch MM400 mixer mill, Retsch PM100 planetary mill, and Resodyn resonance acoustic mixer (left to right).

The Hanusa group has previously observed that mechanochemistry requires different synthetic approaches from those used when solution reactions are used. Parameters such as the compatibility of reagents with the materials of milling vessels, differences in crystal structures and lattice energies, and crystallinity of starting reagents and products can greatly alter the outcome of a mechanochemical reaction. By comparison, lattice structures and crystallite size

are not a concern in solution-based reactions. Even when the outcomes of mechanochemical and solution-mediated reactions are fundamentally the same, such differences in reaction environment can produce more subtle changes, such as shifts in diastereomer ratios.[12]

The four projects that will be discussed in the following chapters are: 1) the optimized synthesis of group 2 amide reagents such as Ca[N(SiMe$_3$)$_2$]$_2$; 2) mechanochemical generation and implementation of fluoro-Grignard reagents; 3) an improved synthesis and application of the 1,3-bis(*tert*-butyl)allyl ligand and derivatives thereof; and 4) the mechanochemical preparation of a low-dimensionality mercury(II) imidazolate framework. These projects incorporate the study of reaction optimization and product formation as a function of reaction conditions, using mechanochemistry to improve or revamp existing solution preparations. There will also be discussion of the importance of diversity and inclusion in the sciences and how to encourage these practices in Appendix 1.

1.2 The driving force

As chemistry has evolved, researchers have learned that using different solvents or multiple solvents in a reaction can expand the range of possible products and transformations that can be performed.[13] Ironically, some chemists found that *avoiding* the use of solvent was also a useful synthetic approach, thus leading them toward the development of solid-state synthesis. Mechanochemistry, defined by the International Union of Pure and Applied Chemistry (IUPAC) as "a chemical reaction that is induced by the direct absorption of mechanical energy", can be approached in a number of forms, such as ball milling, sonochemistry, tribochemistry, and other more specialized varieties.[14]

The focus of this thesis will be in the area of ball milling. Milling reactions were demonstrated as early as the 4th century BCE through the grinding of cinnabar (HgS) in a copper vessel with small amounts of vinegar to produce elemental mercury and copper sulfide (eq 1).[15]

$$HgS + Cu \rightarrow Hg + CuS \qquad\qquad (1)$$

With the intent of distinguishing thermal input from mechanical input, American chemist M. Carey Lee performed an investigation of the reactions of varying metal salts after exposure to heat or milling. Lee observed that silver chloride melted at 455 °C, whereas when ground, decomposition occurred. Hence grinding or milling, even though they involve friction, were not just disguised forms of thermal input.[15]

Aside from the simple removal of solvents, mechanochemical reactions can give access to products that solution phase chemistry may prohibit due to the limited solubility of starting reagents or the instability of products in solution. Product formation in the solid state may be accelerated that would otherwise be slowed due to solvent inhibition, and sometimes the yields or purity of products can be enhanced when solvents are not present (Figure 2). These benefits have been recognized by several research groups, and have led to the growth of mechanochemistry in synthetic organic, inorganic, organometallic, materials, metal-organic framework, and covalent organic framework chemistry. The method has been increasingly adopted in a rapid manner over the past decade, aided by the wide range of equipment (with variable costs) that can be used.[16]
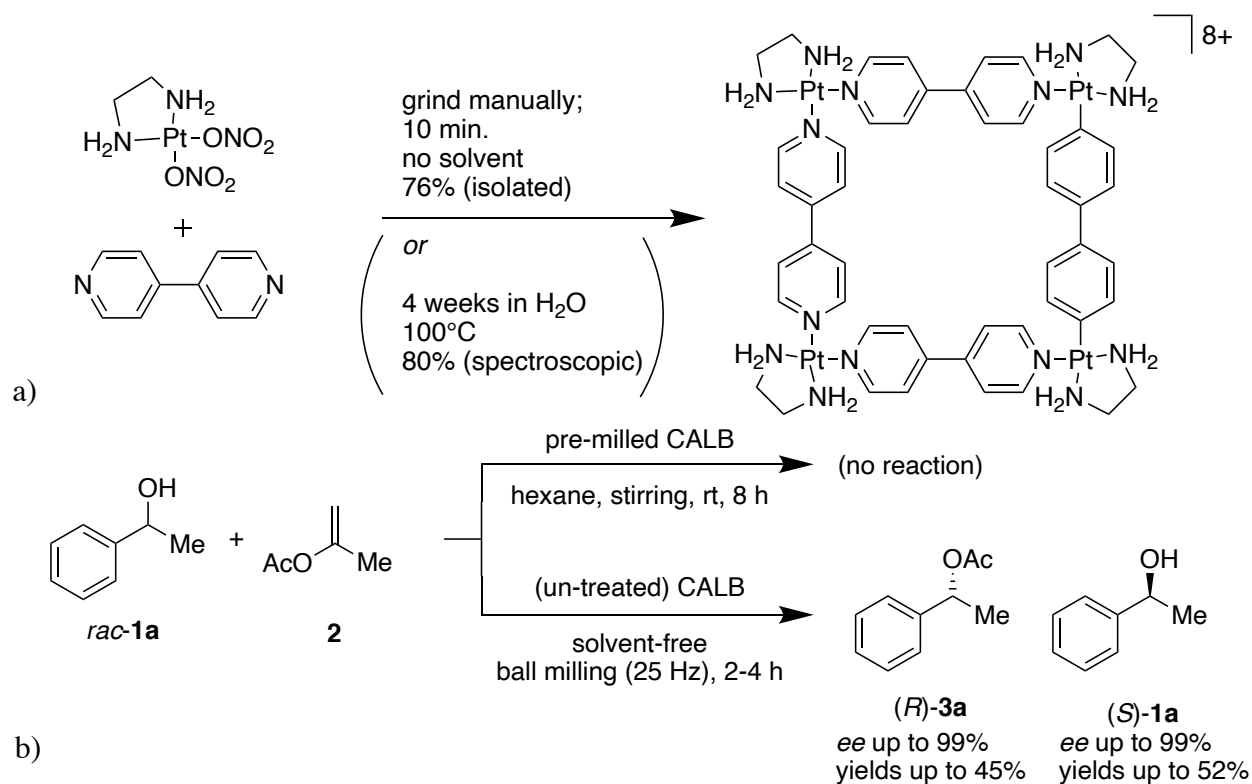
Figure 2. Selected examples of mechanochemical reactions showing improvement over solution methods. a) Mechanochemical formation of platinum bipyridine square complexes are more rapid than under hydrothermal conditions.[17] b) Enzymatic resolution of racemic alcohols by mechanochemical methods gives high *ee* and yields in cases where solution conditions with a premilled enzyme sample gives no yield.[18]

The Hanusa group's first foray into mechanochemistry came with the implementation of stainless steel ball bearings in a glass round bottom flask on a rotary evaporator. From there, the group added a planetary ball mill and mixer/shaker ball mill to the variety of equipment used. The apparatus provided the ability to maintain highly reproducible reaction conditions, higher energy input, and longer reaction times than is possible with the lower cost alternatives. These milling systems allow for flexibility in the motion of the mechanical system, ball bearing size, and material of the ball bearing or milling vessel, which can provide a plethora of experimental conditions to be optimized.

1.3 Mechanochemistry in Organic Synthesis

Mechanochemical reactions have been used at various degrees of sophistication, including at the undergraduate level. Experiments have been developed for use in organic chemistry lab courses with procedures ranging from synthesizing perfumes/detergents to preparing covalent organic frameworks.[19-25] Mechanochemical formation of pharmaceuticals has also been employed in the undergraduate laboratory space.[26] Varying types of mechanochemical equipment have been investigated as well, with reactions such as halogenations being performed manually in a mortar and pestle.[27]

Most organic reactions in the mechanochemical space have been limited by their need for high energy systems and longer reaction times. Nevertheless, these organic systems have been useful in understanding energetic thresholds of the transformations. Mack and coworkers have used mechanochemically mediated Diels-Alder reactions to tease out energetic limitations of mechanochemical reactions, and used heat as a secondary influence to promote reactions that could not be performed by milling alone.[28] By using systems that could be easily quantified with the Arrhenius equation, Mack's group was able to map out energetic thresholds for mechanochemical processes and gather a rough understanding of the systems for which mechanochemistry itself was sufficient, and identify those that would need assistance from thermal activation. Hernandez and coworkers utilized enzymes in mechanochemical reactions to perform asymmetric acylations.[18] With a premilled sample in hexanes, the reaction produced no product, but by milling benzyl alcohols with an acylating agent and *candida antartica* lipase B, they could achieve selective acylation of the *R*- enantiomer over the *S*- enantiomer (Figure 2b). They noted the presence of denatured enzyme in the system, which led them to use higher

loadings to overcome this limitation. The reaction was also scalable to the gram level, providing conversions as high as 49% and *ee* of >99% for the unreacted alcohol and the acylation product,. In addition to scale, Hernandez and coworkers showcased a wide scope of substrates including heterocycles, halides, non-aromatic species, and alkynes, all of which were tolerated by the optimized conditions developed.

As mechanochemistry has expanded, so have its applications, growing into areas such as carbohydrate synthesis,[29] polymer synthesis,[30] and transition metal catalysis.[31] Using the milling jars or containers as reagents themselves has become a popular topic in the mechanochemical space as well. The term "mechanocatalysis" was coined to describe work from the Mack group in which copper milling jars were used in lieu of copper additives in the development of Sonogashira couplings (Figure 3a).[32] Owing to the observance of Glasier coupling products that arose due to the presence of copper iodide in the system in their mechanochemical experiments, investigations of mechanocatalytic conditions were launched. By using a copper ball bearing instead of tungsten carbide, the desired Sonogashira adduct was formed, albeit in lower yields than the reactions that were promoted by copper iodide. By increasing the equivalents of copper in the reaction and milling in a copper vessel, the yield of the reaction can be made comparable to standard solution phase and microwave conditions.

In addition to their work studying Sonogashira chemistry, Mack and coworkers were able to apply their copper milling materials in the synthesis of triazoles via click reactions (Figure 3c).[33] They were able to efficiently synthesize and employ benzyl azides in these reactions. The scope for this system showcased a variety of alkynes (esters, aryl, alkyl) and benzyl halides (*p*-bromo and *p*-nitro), all giving high yields in the upper 90% range. The study

does not, however, discuss *ortho*- or *meta*-substituted arenes, and additionally omits non-aromatic alkynes or halides that are substrates that could further advance this development. Mechanocatalysis has also been utilized in other systems such as Suzuki polymerizations using palladium milling balls, and in the hydrogenations of olefins using diethyl ether and SUS304 stainless steel ball bearings (Figure 3d).[34-35]
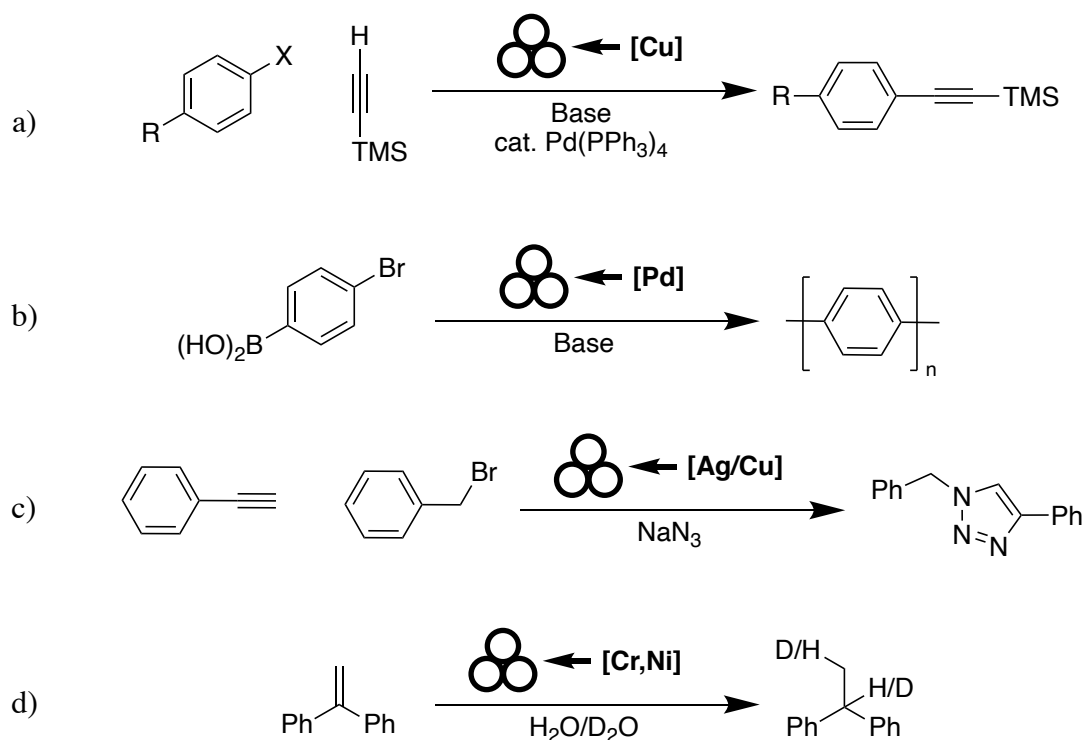
Figure 3. Selected examples of mechanocatalysis. A) The use of copper milling vessels to perform Sonogashira couplings.[32] b) Preparation of aromatic polymers using palladium milling materials to perform Suzuki couplings.[36] c) Ball milling alkynes and benzyl halides with copper or silver materials to perform click reactions to synthesize triazoles.[33] d) Stainless steel reduction of olefins using water or deuterium oxide.[34]

Ito and coworkers have leveraged mechanochemistry in a wide variety of methods. One of their more recent discoveries implements *in-situ* crystallization events of products from a Suzuki-Miyaura coupling to prevent multiarylation of dibrominated aryl species.[37] When performed in toluene, the diarylation occurs readily, forming the diarylated product as the

primary product in comparison to the monoarylated species. In the mechanochemical system, microcrystalline forms of the monoarylated product are believed to be made, which then limits the approach of a second coupling partner and suppresses a second arylation event.

Organic chemists are continuing to explore the areas mechanochemistry can help improve the field of synthesis through catalysis, waste minimization, and facilitating hard-to-achieve organic transformations.[38] With many other boundaries to explore, mechanochemistry will undoubtedly continue to grow to become more commonly used in synthetic organic chemistry.

1.4 Mechanochemistry in inorganic and organometallic synthesis

Mechanochemistry has been an implement in the inorganic chemist's toolbox for some time, dating from one of the very first recorded mechanochemical reactions discussed earlier in this chapter. In very general terms, known inorganic mechanochemical reactions can be divided into seven types of reactions: adduct formation, dehydration, reduction-oxidation (redox), exchange (metathesis), reactions with the vessel (similar to the fundamental thinking behind mechanocatalysis), acid-base, and mixed reactions (such as formations of zeolite frameworks and complex acid-base reactions).[5] Alongside mechanochemical discoveries in inorganic chemistry, the organometallic field has also grown over the course of the 21st century. Our group specifically has explored organometallic mechanochemistry in the past decade, focusing on metathetical synthesis. Consequently, this section will examine inorganic and organometallic metathesis type reactions. Metathesis or exchange reactions can be divided into displacements based on redox processes, acid-base chemistry, or the exchange of counterions between starting species. The discussion herein will center on ion exchange metathesis.

9

In 1880, Spring and coworkers investigated salt metathesis using barium sulfate and sodium carbonate to evaluate the efficacy of mechanochemical methods in synthesis.[39] Reguera and coworkers studied metathesis reactions in the formation of hydrogen difluoride salts.[40] Their study, also performed by manual grinding, systematically evaluated various metal ions in the reaction. Milling ammonium, rubidium, or cesium hydrogen difluorides with potassium bromide produced potassium hydrogen difluoride and the corresponding bromide salt cleanly (i.e., $MHF_2 + KBr \rightarrow KHF_2 + MBr$). Additionally, use of these with sodium halide salts (Cl, Br, I) proved to work well when making the corresponding hydrogen difluoride salt. However, when lithium halide salts were used, a secondary reaction occurred in which the $LiHF_2$ subsequently decomposed to LiF and gaseous HF. Both the heat of the reaction and the grinding itself were the likely causes of the decomposition, unlike in Lea's study of the decomposition of silver salts which showed the two stimuli differ.

Mack and coworkers developed a method to make lithium borohydride, a soft hydride source, via ball milling.[41] The borohydride reagent can be prepared by solution methods by stirring lithium bromide and sodium borohydride in diethyl ether for 48 hours at ambient temperature. In their preparation, ball milling lithium chloride and sodium borohydride for 30 minutes would generate $LiBH_4$. Their study also included generating the reagent in the presence of esters to perform reductions to the corresponding alcohols. Although the reduction times were long, this is a facile way to generate and subsequently use the air-sensitive reagent through metathesis by ball milling.

With respect to organometallic transformations, the Hanusa group has showcased the power of mechanochemistry in metathesis reactions over the past eight years. A cornerstone

10

discovery was the first synthesis of an unsolvated tri(allyl)aluminum complex.[42] Attempts to make a tri(allyl)aluminum species typically results in a solvated aluminum center due to the unsaturated coordination sphere around the metal ion. Our own attempts at formation of an allyl species by solution phase metathesis or by deprotonation using the bis(trimethylsilyl)allyl moiety as the allyl ligand generated the protonated starting material (i.e., a propene) or led to uncharacterizable decomposition products, respectively. Once the system was transitioned from solution-based methods to ball milling, the unsolvated tri(allyl)aluminum complex $Al[1,3\text{-}(SiMe_3)_2C_3H_3]_3$ was observed in yields up to 80% and in reaction times as short as 5 minutes.

Not all metathesis reactions are as facile as the aforementioned aluminum chemistry. Alternative reactions can occur due to reactions with the milling vessel or from the high concentration of reagents. In the synthesis of a tin allyl species, for example, it was found that there are other reaction processes that may occur in the mechanochemical system.[43] When $K[A^*]$ ($A^* = [1,3\text{-}(SiMe_3)_2C_3H_3]^-$) was ball milled with tin(II) chloride, two products were observed depending on milling time,. At shorter times (ca. 5 min), a stannate ($K[SnA^*_3]$) was observed, the product of tin's attempt to fully saturate its coordination sphere with an additional equivalent of KA*. At longer times (15 min), the major product was a tetra(allyl)tin (SnA^*_4), the product of a disproportionation of tin(II)chloride to make tin(IV) and tin(0), the former of which then formed the tetraallyl species. The tetra(allyl)tin can only be synthesized by solid-state synthesis due to the presence of weak interligand London-dispersion interactions that are needed to hold the complex together. When non-polar solvents such as benzene, toluene, or hexanes are introduced to the product, the stability of the complex drastically decreases and leads to complex mixtures of decomposition products.

11

There are many other examples of inorganic and organometallic mechanochemical reactions that have been described, from the formation of metal organic frameworks to nanoparticle synthesis (Figure 4).[44-45] The development of these processes further cements the utility of mechanochemistry as a powerful tool in synthesis. As the field continues to expand, so will the use of more exotic milling techniques such as liquid assisted grinding (LAG), in which a small amount of solvent is added to the milling environment, and the related ionic- and liquid-assisted grinding (ILAG) methods, or the employment of more elaborate milling devices such as twin screw extruders, resonant acoustic mixers (RAM), and perhaps other equipment yet to be developed.
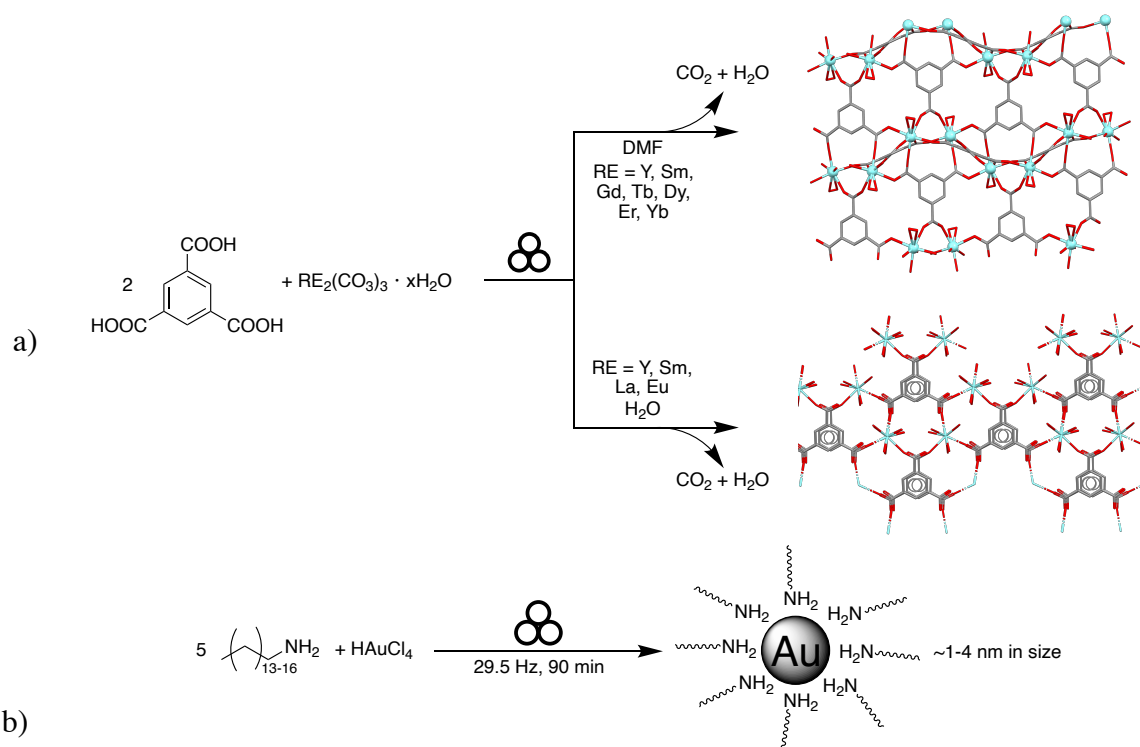
Figure 4. Selected examples of mechanochemical preparation of metal organic frameworks and nanoparticles. A) Formation of rare earth tricarboxylate frameworks with polymorph control through liquid assisted grinding.[46] b) Mechanochemical formation of gold nanoparticles without need of external reducing agents.[47]

1.5 Methods Employed in this Dissertation

Traditional air-sensitive handling techniques were employed for the syntheses described in later chapters. Unless specially mentioned, all reactions were run with rigorous exclusion of air and moisture. Solution-based reactions were conducted either entirely within an inert atmosphere glove box or on a vacuum line with Schlenk techniques. Mechanochemical reactions involved sealing the reaction under nitrogen with an air-tight seal to prevent contamination.

There are a wide range of options for implementing the grinding associated with mechanochemical reactions; these include mortar and pestles, mixer mills, and planetary ball mills. Reactions in this document were performed primarily on a Retsch Planetary Ball Mill (PM 100) or a Retsch Mixer Mill (MM 400 or MM 200). Reactions were conducted for as short as 10 minutes to as long as several hours at a frequency of 10 Hz up to 30 Hz. In most cases, these mechanochemical conditions shed light on new reactivity or new products in comparison to solution-based synthesis.

In addition to these synthetic techniques, nuclear magnetic resonance spectroscopy (NMR), powder X-ray diffraction (PXRD), thermal gravimetric analysis (TGA), infrared spectroscopy (IR), and gas chromatography-mass spectrometry (GC-MS) were also used for characterization of products made at various points in this thesis. Samples were also analyzed by elemental analysis (EA) and X-ray crystallography.

1.6 Conclusions

In this chapter, the broad topics of mechanochemistry and their role in organic and inorganic synthesis were briefly discussed, in addition to a description to the techniques

employed in this thesis. Although this work spans a broad range of synthetic targets, the implementation of mechanochemistry in some facet of the projects unifies the research presented here. Subsequent chapters will discuss the formation of inorganic species, metal organic frameworks, and organometallic reagents, as well as the improved synthesis and application of a bulky allyl ligand and its derivatives.

CHAPTER 2

Mechanochemically directed metathesis in Group 2 chemistry: Calcium amide formation without solvent

2.1 Introduction

Mechanochemically enabled synthesis, specifically that promoted by grinding or milling when no or a minimal amount of solvent is present, can provide access to chemistry different from that observed with solvent-based reactions.[48] The benefits extend across organic,[28, 49-52] organometallic,[53-59] and coordination chemistry,[60-67] and have helped stimulate an upsurge in mechanochemical research in the last decade.[38, 44] Owing to the myriad roles that solvents play in reactions (e.g., facilitating mixing, dispersing heat, altering the polarity of reaction environments, and shifting equilibria, among others), predicting how a given reaction will respond to the removal of solvent(s) is not straightforward. This is particularly true with compounds of the s-block metals, where highly polar bonding is combined with increased ligand lability.[68] Solvent effects play a major role in setting the position of equilibrium in these systems (e.g., Schlenk redistribution in Grignard reagents ($2\ RMgX \rightleftarrows R_2Mg + MgX_2$) is strongly influenced by the polarity of the solvent),[69] and coordinated solvent can affect structure and bonding.[70] We report here that when solvents are removed, ball milling can materially improve the halide metathetical synthesis of the synthetically valuable calcium amido complex $[Ca\{N(SiMe_3)_2\}_2]$ (Figure 5a). These results also suggest that mechanochemistry could offer analogous benefits to other metathetical Group 2 syntheses.
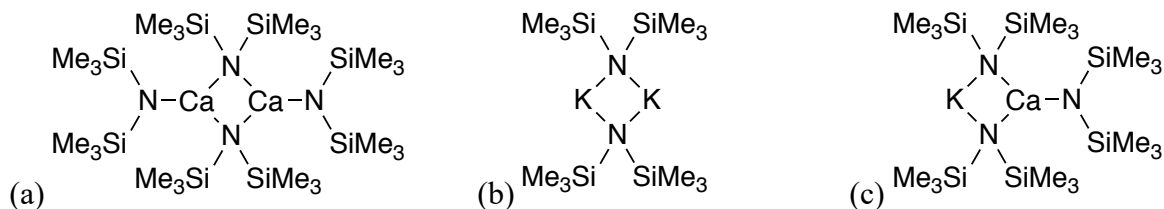
Figure 5. Structures of various amido complexes of interest.

(a) The calcium bis(amido) complex Ca(NR$_2$)$_2$, (b) the potassium amide KNR$_2$, and (c) the potassium calciate K[Ca(NR$_2$)$_3$]. Both Ca(NR$_2$)$_2$[71] and KNR$_2$ [72] crystallize as dimers. R = TMS.

Calcium amides [Ca(NR$_2$)$_2$] are versatile synthetic reagents, as depending on the R group they can serve as hydrocarbon-soluble sources of Ca^{2+} ions for organometallic synthesis,[73-75] and as non-nucleophilic bases for enolization reactions.[76-77] More recently, they have found use as hydrogenation catalysts that can be employed under mild conditions.[78-79] They also catalyze the ring-opening polymerization of lactide, and when paired with coordinating chiral ligands, can influence the stereochemistry of the polymer.[80] These traits are exemplified in the bis(trimethylsilyl)amido derivative, Ca(NR$_2$)$_2$ (R = TMS), one of the most commonly used calcium amido complexes.[81-82] Multiple synthetic routes have been developed for this compound, often involving redox transmetalation/ligand exchange with elemental calcium.[83-84] Several of these syntheses involve toxic mercury[85-86] or tin[71] reagents, and hence metathetical preparations employing calcium sulfonates,[87-88] alkoxides,[89] or iodide (e.g., K[N(TMS)$_2$] (Figure 5b)[90] and CaI$_2$ in diethyl ether[73, 76,91] or toluene[92]) have been employed as well.

These solvent-based syntheses are marked by relatively long reaction times (ranging from 3 hours to 5 days),[86] the frequent formation of solvated species (with THF, DME, or Et$_2$O), and most seriously with the salt metathesis methods, the concomitant generation of calciate species, M{Ca[N(TMS)$_2$]$_3$} (M = Li, K, Figure 5c)), regardless of the stoichiometry of the

starting reagents.[93] The formation of unintended calciates is not unique to the bis(trimethylsilylamido) group, but has been observed during the metathesis formation of calcium complexes containing $[N(Ph)R]^-$ (R = Me, ^{i}Pr) ligands as well.[94]

2.2 Results and Discussion

The generally faster reactions and relative freedom from solvent interactions provided by mechanochemical activation made its use an attractive alternative route for the synthesis of $Ca[N(TMS)_2]_2$. In initial experiments, a typical solution protocol was followed by using stoichiometric amounts of the CaI_2 and potassium amido reagents, i.e., a 1:2 ratio of CaI_2 and $K[N(TMS)_2]$. Grinding the two solids for 10 min at 30 Hz in a mixer mill left a white powder that displayed the peaks characteristic of KI in its powder X-ray diffraction spectrum (Figure 14 in Appendix A2); other products presumably had insufficient crystallinity to be observed. The powder was then extracted with toluene, the extract filtered, and solvent removed from the filtrate. NMR (^{1}H) analysis indicated that a mixture of the amide $Ca[N(TMS)_2]_2$ and the calciate $K\{Ca[N(TMS)_2]_3\}$ was present (Table 1, entry 1). Prolonging the reaction to 30 min (entry 2) and then 60 min (entry 3) decreased the amount of $K\{Ca[N(TMS)_2]_3\}$ relative to $Ca[N(TMS)_2]_2$, but the calciate still comprised nearly half of the mixture, suggesting that its conversion to the neutral amido complex is slow. After adjusting the starting ratio of CaI_2 to $K[N(TMS)_2]$ to 1 : 1, the neutral amido product was isolated in good yield with no evidence for the calciate species (Table 1, entry 4); the use of an even higher ratio of CaI_2 to $K[N(TMS)_2]$ (entry 5) led to a similar yield. Larger scale reactions provided comparable results; i.e., the reactions reported in Table 1, typically conducted with 0.15 g of CaI_2 and 0.1–0.2 g of $K[N(TMS)_2]$, and yielding 60 mg of $Ca[N(TMS)_2]_2$, could be readily scaled up to yield ca. 0.45

g of $Ca[N(TMS)_2]_2$ from a total of 1.3 g of reagents. A sample from one of the larger scale grinds was found by elemental analysis to be essentially free of potassium (< 1%), supporting the NMR results.

Table 1. Effect of molar equivalents on product distributions[a]

Entry	Molar equiv. (CaI$_2$:KNR$_2$)	Time (min)	Yield (%)[b]	Ratio (**1:2**)
1	1 : 2	10	-	1 : 2.5
2	1 : 2	30	-	1 : 1
3	1 : 2	60	-	1.2 : 1
4	1 : 1	10	68	1 : 0
5	1 : 0.5	10	63	1 : 0

[a]Reactions were performed under N_2 on 0.5 mmol scale (CaI$_2$) and milled at 30 Hz with two 8 mm SS ball bearings (3.5 g ball^{-1}) in a Retsch MM400 mill. [b]Typical yield of isolated **1**, with respect to limiting reagent KNR$_2$. **1** – Ca(NR$_2$)$_2$, **2** – K[Ca(NR$_2$)$_3$], R = TMS.

The results from entries 4 and 5 in Table 1 are different from solution synthesis in aromatics. In particular, there is no evidence that the reaction of CaI$_2$ and $K[N(TMS)_2]$ in toluene ever yields pure $Ca[N(TMS)_2]_2$, regardless of the initially used reagent ratio.[93] This is fundamentally a consequence of the different solubilities of CaI$_2$ and $K[N(TMS)_2]$ in aromatic solvents; the very low solubility of CaI$_2$ and the high solubility of $K[N(TMS)_2]$ ensures that the latter will always be in a large excess in solution, thus promoting calciate formation. Under mechanochemical conditions, such solubility differences are less important, and the use of CaI$_2$ in excess of the stoichiometrically required ratio effectively serves to suppress the formation of $K\{Ca[N(TMS)_2]_3\}$.

Table 2. Effect of milling environment on product distribution[a]

Entry	Mill Type	Frequency(Hz)	Ratio (**1:2:3**)
1	Mixer	10	0 : 1 : 4.5
2	Mixer	20	1 : 2 : 0
3	Mixer	25	1 : 0 : 0
4	Mixer	30	1 : 0 : 0
5[b]	Planetary	10 (600 rpm)	0 : 1 : 6.8
6[c]	Planetary	10 (600 rpm)	1 : 0 : 0

[a]Reaction conditions: N_2 atm, 0.5 mmol (CaI_2) scale, 1:1 molar ratio of CaI_2 : **3**, mixer mill (Retsch MM400), two 8 mm stainless steel (SS) ball bearings (3.5 g ball^{-1}), 10 min. [b]Reaction in Retsch PM 100 at 600 rpm with two 8 mm SS ball bearings (3.5 g ball^{-1}). [c]Reaction in Retsch PM 100 at 600 RPM with fifty 4.8 mm ball bearings (0.5 g ball^{-1}). . **1** – $Ca(NR_2)_2$, **2** – $K[Ca(NR_2)_3]$, **3** – KNR_2, R = TMS.

The effect of milling frequency and mill type on product formation was also investigated with a 1:1 ratio of CaI_2 to $K[N(TMS)_2]$ (**Table 2**). In a mixer mill at 10 Hz, a 10 min grind (entry 1) leaves a considerable amount of $K[N(TMS)_2]$ unreacted, but somewhat unexpectantly, yields only the calciate $K\{Ca[N(TMS)_2]_3\}$ rather than any of the neutral amido complex $Ca[N(TMS)_2]_2$, consistent with the former's being the kinetic product of the reaction. Increasing the frequency to 20 Hz (entry 2) consumes all the potassium amide, but still leaves twice the molar amount of calciate compared to the neutral amide. At 25 Hz, the calciate is no longer present, and the result is the same as was previously found at 30 Hz (Table 1, entry 3). When the mill type was changed from a mixer mill to a planetary version, but with the use of only two large ball bearings, milling at 600 rpm (~10 Hz) left proportionally more $K[N(TMS)_2]$ than did the mixer mill (entry 5). Using a larger number of smaller ball bearings to increase the rate of collisions produced results at 600 rpm similar to those from the 30 Hz mixer mill conditions (entry 6).[95-96] The results in **Tables 1** and **2** can be summarized in two steps (Scheme 1): with

a 1:2 ratio of CaI_2 to $K[N(TMS)_2]$, the first represents the rapid formation of the kinetic product calciate $K\{Ca[N(TMS)_2]_3\}$ (eq 1); the second is the slower, incomplete reaction between $K\{Ca[N(TMS)_2]_3\}$, $K[N(TMS)_2]$, and the remaining CaI_2 (eq 2). The effectiveness of the use of larger amounts of CaI_2 (e.g., in the 1:1 reactions) can then be seen as the result of its being a source of additional iodide that scavenges K^+, converting it into KI and preventing the formation of the potassium calciate.

$$2\ CaI_2 + 4\ K[N(TMS)_2] \xrightarrow[rapid]{} \qquad\qquad (1)$$

$$K[Ca\{N(TMS)_2\}_3] + CaI_2 + K[N(TMS)_2] + 2\ KI$$

$$slow \downarrow \qquad\qquad\qquad (2)$$

$$2\ Ca[N(TMS)_2]_2 + 2\ KI$$
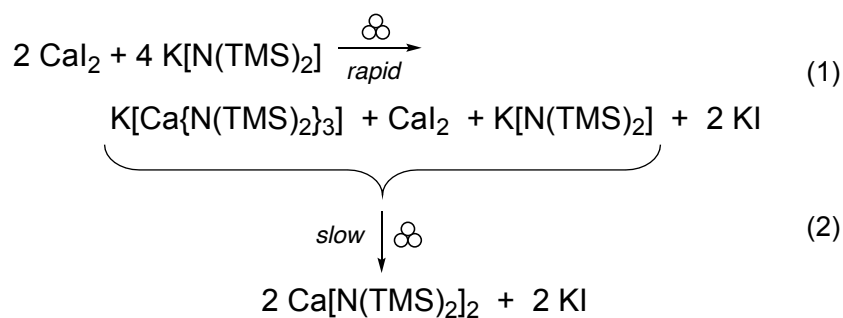
Scheme 1. Proposed formation of $Ca[N(TMS)_2]_2$ from CaI_2 and $K[N(TMS)_2)]$ in a 1:2 molar ratio. The initial reaction produces only the calciate $K\{Ca[N(TMS)_2]_3\}$, which is slowly converted into the neutral amido complex $Ca[N(TMS)_2]_2$ in a second step.

Table 3. Effect of halide identity on product distribution[a]

Halide	Time (min)	Ratio (**1:2:3**)	Yield (%) of **1**[b]
CaI_2	10	1 : 0 : 0	68
	30	1 : 0 : 0	84
	60	1 : 0 : 0	65
$CaBr_2$	10	0 : 5 : 4	-
	30	1 : 10 : 0	9.5
	60	19 : 1 : 0	68
$CaCl_2$	10	0 : 0 : 1	-
	30	0 : 2 : 3	-
	60	0 : 7 : 2	-
CaF_2	10	0 : 0 : 1	-
	30	0 : 0 : 1	-
	60	0 : *trace* : 1	-

[a]Reactions performed on 0.5 mmol scale of CaX_2 salt at 30 Hz in a Retsch MM 400 mill with two 8 mm SS ball bearings (3.5 g ball[-1]). [b]Spectroscopic yield of **1** determined from ^{1}H NMR data. **1** – $Ca(NR_2)_2$, **2** – $K[Ca(NR_2)_3]$, **3** – KNR_2, R = TMS.

A characteristic feature of mechanochemical synthesis is that it can lift restrictions on the solubility requirements for suitable reagents. Calcium iodide is commonly used in halide displacement reactions as it is the most soluble of the dihalides in ethers (a saturated solution in THF is 42 mmol L^{-1}).[97] Of course, the crystal lattice must be disrupted during the reaction whether by solvent or milling, and the greater lattice energy of CaF_2 compared to CaI_2 (U_0 of -626 and -476 kcal mol^{-1}, respectively),[98] for example, would disfavor the fluoride as a source regardless of the reaction environment. To examine this point further, 1:1 mixtures of CaX_2 with $K[N(TMS)_2]$ were ground for various times, and Table 3 displays the relative

amounts of $Ca[N(TMS)_2]_2$ and $K\{Ca[N(TMS)_2]_3\}$ as a function of the calcium salt and milling time. An inverse correlation can be observed between the relative amount of $Ca[N(TMS)_2]_2$ and/or $K\{Ca[N(TMS)_2]_3\}$ and lattice energy (U_0, kcal mol^{-1}); i.e., CaF_2 (trace, -626) < $CaCl_2$ (-535) < $CaBr_2$ (-515) < CaI_2 (-476).[98] Generally the calcium product(s) increase with the milling time, although calcium fluoride does not show any signs of product formation until the one-hour mark, at which point a trace amount ($\lesssim$1%) of $K\{Ca[N(TMS)_2]_3\}$ was detectible (^{1}H NMR). $CaCl_2$ provides only slightly more reactivity, with a 3.5:1 ratio of $K\{Ca[N(TMS)_2]_3\}$: $K[N(TMS)_2]$ after 60 minutes of grinding, but no evidence for the neutral $Ca[N(TMS)_2]_2$. $CaBr_2$ generates the most complete evidence for the shift from $K\{Ca[N(TMS)_2]_3\}$ to $Ca[N(TMS)_2]_2$ with increased grinding time: considerable starting material is left after 10 min, and after 30 min, the ratio of $Ca[N(TMS)_2]_2$: $K\{Ca[N(TMS)_2]_3\}$ is 1:10. After an hour, however, the sample is 95% $Ca[N(TMS)_2]_2$. The recovered weight puts the yield of $Ca[N(TMS)_2]_2$ at 68%, although it was not isolated. Finally, the yield from CaI_2 increased from the 68% observed at 10 min (Table 1, entry 4) to 84% at 30 min. Interestingly, the yield decreases to 65% at one hour of milling. A decrease in yield has been observed after long grinding times in other mechanochemical synthesis as well (e.g., in the formation of ferrocene),[99] and may reflect decomposition assisted by the reaction between the products and by-products that all exist in a single phase, a critical difference from solution-based metathesis, where the alkali metal halide is removed from the reaction environment by precipitation.
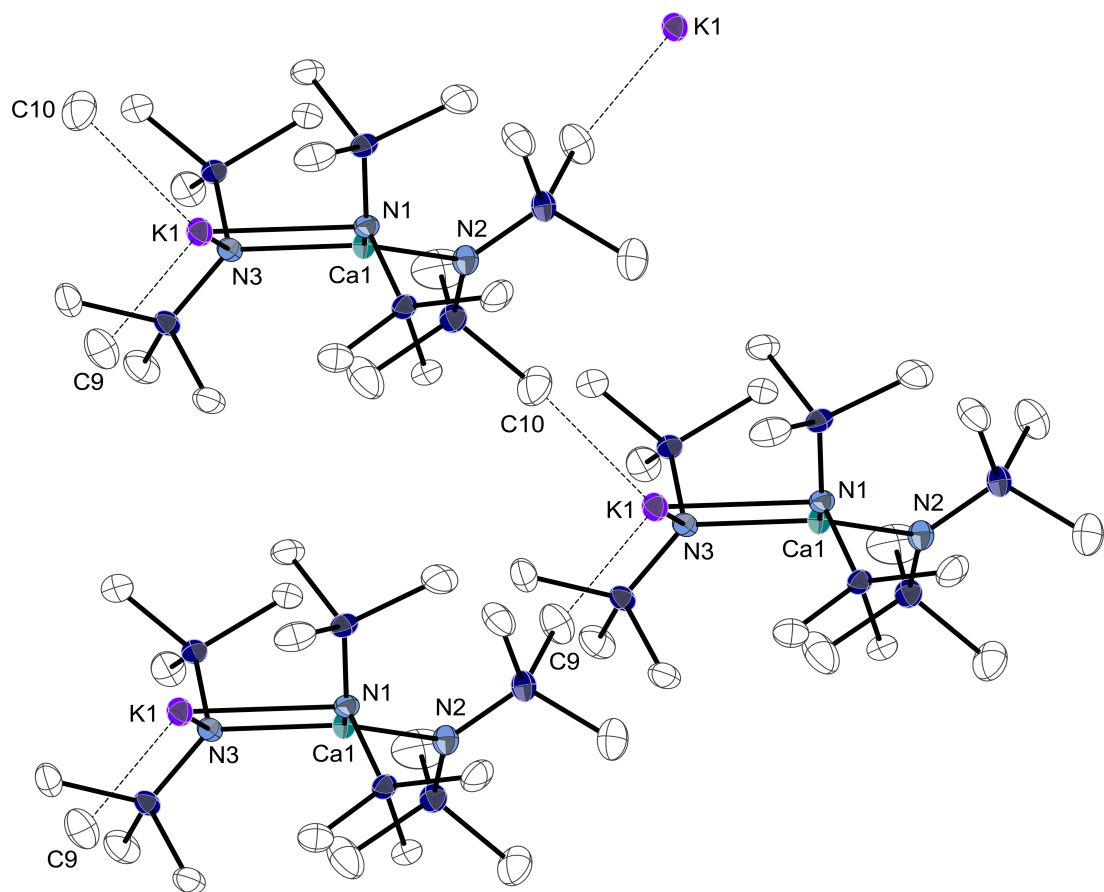
Figure 6. Thermal ellipsoid plot (50% level) of a portion of the crystal lattice of K{Ca[N(TMS)₂]₃}. For clarity, hydrogens have been removed. Select bond distances (Å) and angles (deg): K1–N1 = 2.882(2); K1–N3 = 2.943(2); Ca1–N2 = 2.325(2); Ca1–N1 = 2.386(2); Ca1–N3 = 2.376(2); K1…C9 = 3.235(3); K1…C10 = 3.185(3); N1–K1–N3: 79.96(5); N1–Ca1–N3: 103.60(6); N1–Ca1–N2: 126.17(7); N2–Ca1–N3: 130.19(7).

The rapid formation of the calciate K{Ca[N(TMS)₂]₃} in preference to the neutral bis(amide) Ca[N(TMS)₂]₂ prompted a closer look at the molecule. The X-ray crystal structure of the THF-solvated species [(thf)K{Ca{N(TMS)₂}₃}] has been published,[76] but we were able to grow crystals of the base-free material from hexanes and obtain its structure (Figure 6). As with the THF-solvated version, the molecule comprises a four-membered CaNKN′ ring, with the calcium also bound by a terminal -N(TMS)₂ group. The coordination environment of the potassium consists of two amido groups at distances of 2.882(2) and 2.943(2) Å, and intermolecular K···C(Me) interactions to amido groups at 3.19 and 3.24 Å. There are longer

23

intramolecular contacts (ca. 3.3–3.5 Å) to methyl groups on the bridging amido ligands that help to fill the coordination sphere of the potassium. A chain is formed in the solid state in the THF-solvated analogue by virtue of a K$\cdots$C(Me) interaction.[76] In K{Ca[N(TMS)$_2$]$_3$}, the intermolecular K$\cdots$C interactions take the place of the thf, allowing the molecule to form a sheet-like structure. With the exchange of Mg for Ca, and Li for K, the structure of K{Ca[N(TMS)$_2$]$_3$} is also related to that of [Li{Mg{N(TMS)$_2$}$_3$}];[100] the magnesiate structure is strictly monomeric, with closest intermolecular Me$\cdots$Me′ contacts >3.8 Å. Although detailed information about the formation of K{Ca[N(TMS)$_2$]$_3$} is lacking, it is conceptually possible to replace one [N(TMS)$_2$]$^-$ group in the potassium amide dimer (Figure 1b) with the [CaN(TMS)$_2$]$^-$ fragment to form the calciate. The Ca–(μ-N) bonds found in the structure of K{Ca[N(TMS)$_2$]$_3$} (avg length of 2.36 Å) are 0.12 Å shorter, and hence presumably stronger, than the comparable distance found in the [Ca{N(SiMe$_3$)$_2$}$_2$] dimer (Figure 1a),[82] which may correlate with the former's faster formation and the slowness of its conversion into the neutral bis(amido) complex.

Owing to the success of the implementation of mechanochemistry for the calcium bis(trimethylsilyl) amide salt, we expanded the study with other metals and amido species. In initial studies of other metal amides, use of conditions optimized for the synthesis of calcium amides were employed and a mixture of products was observed. Ball milling magnesium bromide with KN(TMS)$_2$ gave rise to the desired magnesium bis(amide) along with what is believed to be a heteroleptic magnesium amido bromide (MgBr[N(TMS)$_2$]) species. In our brief attempts to optimize the system through varied milling times, magnesium precursors, and reagent ratios, there was always the presence of this intermediate species. In work towards

expansion into the group 3 amide complexes, namely aluminum and indium, complex product distributions were observed as well. In these systems, it was found that a mixture of mono-, bis-, and tris-amido complexes were formed simultaneously when more than 2 equivalents of amide were utilized.

2.3 Conclusions

In summary, we have employed mechanochemical methods to produce $[Ca\{N(TMS)_2\}_2]$ via halide metathesis without employing toxic reagents or coordinating solvents, or requiring the synthesis of intermediate organometallic compounds.[93] Not all the features associated with solvent-based reactions are avoided, i.e., calcium iodide is still the preferred halide, as its lattice is the most easily disrupted (the less expensive $CaBr_2$ also performs well, however, especially at longer grinding times). There is no reason that this method could not be extended to other Group 2 metals or amido ligands and these investigations are ongoing. The critical role that solvents play in directing product formation in s-block chemistry suggests that their removal during reactions by means of mechanochemical assistance may have a substantial impact on the synthesis of a broad range of complexes.

2.4 Experimental Section

General Considerations. All manipulations were performed with the exclusion of air and moisture using standard glovebox techniques. Proton (^{1}H) NMR spectra were obtained on a Bruker AV-400 spectrometer at 400 MHz, and were referenced to the residual proton resonances of C_6D_6. Elemental analysis was performed by ALS, Tucson, AZ.

Materials. Calcium iodide, chloride, bromide, and fluoride, and potassium hexamethyldisilazide were purchased from commercial suppliers and used as received. Toluene was degassed with argon and dried over activated alumina using a solvent purification system, then stored over 4A molecular sieves in a glovebox. Benzene-d_6 was obtained from Cambridge Isotopes and stored over 4A molecular sieves.

Mechanochemical protocol. Ball milling reactions used either 2 stainless steel (440 grade) ball bearings ($^5/_{16}$ in (8 mm), 3.5 g) or 50 stainless steel (440 grade) ball bearings ($^3/_{16}$ in (4.8 mm), 0.44 g) that were thoroughly cleaned with detergent and water, then washed with acetone, and dried in a 125 °C oven prior to use. Planetary milling was performed with a Retsch PM100 mill, 50 mL stainless steel grinding jar type C, and a safety clamp for air-sensitive grinding. Mixer milling was performed with a Retsch MM400 mill with a 15 mL stainless steel Formtech Smartsnap™ grinding jar taped shut for air-sensitive grinding. A typical reaction involved ca. 250 mg total sample weight (1:1 grinding reactions), sealed under an inert atmosphere. The ground mixture was extracted with minimal toluene (<70 mL) and filtered through a fine porosity ground glass frit. The extraction is designed to dissolve the complex, and the filtration removes traces of KI. The filtrate was then dried under vacuum prior to NMR analysis.

Typical preparation of [Ca(N(SiMe₃)₂)₂]. Details for a 1:1 reaction are given here. Inside a glovebox, CaI₂ (146.9 mg, 0.50 mmol) and K[N(SiMe₃)₂] (99.7 mg, 0.50 mmol) were added to a 15 mL stainless steel milling jar with two 8 mm stainless steel ball bearings. The jar was closed tightly, sealed with electrical tape at the seam, brought out of the glovebox, and milled for 10 min at 30 Hz. The jar, still taped, was placed in a C-clamp and returned to the

26

glovebox. When opened, the inside of the jar and balls were coated with a white powder that when extracted with one ca. 30 mL portion of room-temperature toluene and filtered through a fine-porosity ground glass frit, yielded a colorless filtrate. Removal of solvent under vacuum yielded a white solid (61 mg, 68% yield (with respect to the limiting reagent)). The compound was identified by its characteristic NMR shift:[101] ^{1}H NMR (δ/ppm, 400 MHz, C_6D_6): 0.31 ($SiMe_3$).

Larger scale preparation of [Ca[N(SiMe₃)₂)₂]. Details for a scaled-up 1:1 reaction are given here. Inside a glovebox, CaI_2 (817 mg, 2.7 mmol) and $K[N(SiMe_3)_2]$ (554 mg, 2.7 mmol) were added to a 50 mL stainless steel grinding jar with 50 stainless steel ball bearings. The jar was sealed with a safety clamp and milled for 10 minutes at 600 rpm. The reaction was then returned to the glovebox after milling. The jar was opened to reveal a white powder that was extracted with one 60 mL portion of room temperature toluene followed by a second 30 mL portion of the same. The extracts were filtered through a fine-porosity ground glass frit, yielding a colorless filtrate. Removal of solvent under vacuum left a white solid (423 mg, 84% yield (with respect to the limiting reagent)). ^{1}H NMR (C_6D_6, δ/ppm, 400 MHz): 0.31 ($SiMe_3$). Anal. Calcd for $C_{12}H_{36}CaN_2Si_4$ (i.e., $Ca[N(SiMe_3)_2]_2$): Ca, 11.11; K, 0; calcd for $C_{18}H_{54}CaKN_3Si_6$ (i.e., $[KCa(N(SiMe_3)_2)_3]$): Ca, 7.15; K, 6.98. Found: Ca, 11.54; K, 0.64.

X-ray Diffraction (XRD) Measurements. XRD analysis was performed on a Rigaku SmartLab diffractometer equipped with a Cu-Kα radiation source and D/teX Ultra 250 detector operating at 40 kV and 44 mA. XRD samples were prepared by placing raw reaction powder onto a zero-background quartz holder.

(This work was adapted from Speight, I. R., et al. *Chem. Commun.* **2019**, 55, 2202-2205).

CHAPTER 3

Exploration of mechanochemical activation in solid state fluoro-Grignard reactions

3.1 Introduction

For well over a century, the indispensable Grignard reagents have played critical roles in the synthetic chemist's toolbox, and the range of reactions they facilitate is enormous [102-103]. Various methods have been used to promote the so-called 'direct' preparation of Grignard reagents, i.e., the interaction of elemental magnesium with an organic halide, usually in an ethereal solvent [104]. The application of ultrasound [69, 105] or microwave irradiation [106], and the formation of finely divided metal powders have all been used to boost the reactivity of elemental magnesium. Exploration of the latter approach was pioneered by Rieke, who prepared highly reactive metals by reducing metal salts with alkali metals or organoalkalis in ethereal or hydrocarbon media [107-113]. Peripherally related to this technique, in that exceptionally small metal particles are involved, is mechanochemical activation of reactions, typically achieved through grinding or ball milling. The process provides energy input without requiring the use of solvents or the application of elevated temperatures [38, 53, 114-116]. Although the literature on the subject is not large, mechanochemical methods have been employed in Grignard chemistry with various degrees of success.

Mechanochemical approaches have sometimes involved the use of preformed Grignard reagents [117], and Mack determined that as long as the grinding vessel was sealed, the milling of Grignard reagents and substrates need not be performed in rigorously anhydrous or anaerobic

28

environments [118]. The actual generation and subsequent use of Grignard reagents under mechanochemical conditions has been studied in the context of dehalogenation reactions. Complete dechlorination of 1,3,5-trichlorobenzene, for example, is achieved when it is milled with magnesium and *n*-butyl amine. The process involves the stepwise formation of the corresponding Grignard reagents, for which the amine serves as a hydrogen donor, ultimately generating benzene [119]; other organochlorines have been similarly investigated [120-121]. In the search for more general synthetic applications, Harrowfield reported the solvent-free reaction of magnesium with halogenonaphthalenes in a ball mill [122]. The use of at least a four-fold excess of magnesium was required to produce a manipulable solid, instead of an intractable paste. Not surprisingly, the presence of the highly reactive excess magnesium powder complicated further reactions. When quenched with aromatic ketones, for example, McMurry coupling occurred in addition to the alcohol formation expected from reaction with the organomagnesium species (Scheme 2).
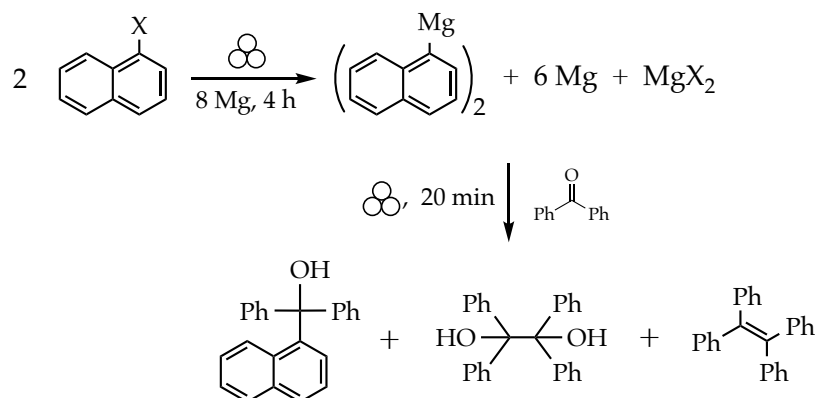
Scheme 2. Products of the milling of Mg with halonaphthalenes (X = Cl, Br)[122]. The tertiary alcohol is the expected product from the Grignard reaction; the diol and alkene are consequences of McMurry coupling from the large amount of finely divided Mg in the reaction. This scheme follows the proposal of Kaupp[123], who suggested that the organomagnesium intermediate in this system is likely dinapthylmagnesium, rather than a napthylmagnesium halide.

Despite the somewhat uncertain prospects for the clean mechanochemical generation of an RMgX species, we were interested in investigating Grignard systems that do not usually work well—if at all—in solution, specifically fluoro-Grignards (RMgF). The C–F bond is roughly 38 kcal mol^{-1} stronger than the next strongest carbon-halogen bond (C–Cl) [124], and the attempted reaction of elemental magnesium with an organofluorine in solution is usually unsuccessful [125]. Exploration of this issue dates back a century, beginning with the work of Swarts in 1921 [126], and an array of methods has been used in efforts to provide a more reactive magnesium source [127]; some of the early strategies have been reviewed [128].

It should be noted that the preparation of fluoro-Grignard reagents has been described via indirect routes from organomagnesium compounds, including other Grignard reagents [129]. For example, the reaction of EtMgBr with perfluoraryl compounds in the presence of certain transition metal halide catalysts (e.g., $CoCl_2$, $NiCl_2$, CuI) was used to generate the corresponding ArMgF species that then underwent the expected Grignard reactions [127]. Similarly, the reaction of MgR_2 (R = Me, Et, Bu, Ph) with fluorinating agents such as $BF_3 \cdot OEt_2$, Bu_3SnF, and SiF_4 produced the associated RMgF species, although not always in high purity [128]. Crabtree reported the use of the thermally sensitive magnesium anthracene ($MgC_{14}H_{10}$) to activate perfluorinated alkyl or aryl compounds, followed by reaction with CO_2 to produce carboxylic acids, albeit in low to moderate yields (6–34%). Reaction of the same organofluorines with elemental magnesium yielded no product, but neither did the reaction of perfluoronaphthalene with ($MgC_{14}H_{10}$) [130].

Despite these reports, the lure of a direct route to fluoro-Grignards remains, as it would avoid the need for prior synthesis of an organomagnesium reagent that might not be readily

accessible, and hence the potential range of R groups could be larger. Rieke's first work with finely divided magnesium (Mg*) focused on organochlorines and -bromines, but fluorobenzene was examined as well [107]. The refluxing of fluorobenzene with Mg* in diglyme for 1 hr, followed with treatment with CO_2, produced benzoic acid in very low yield (ca. 5%) [131,132]. Evidence for the formation of fluoro-Grignards by these bulk synthetic methods is indirect; e.g., the formation of the expected reaction products (e.g., after hydrolysis or treatment with CO_2), which is consistent the formation of RMgF species as intermediates. For the sake of completeness, it should be mentioned that magnesium vapor has been used to prepare fluoro-Grignards at low temperatures. For example, when excited state (^3P) magnesium atoms produced from laser ablation experiments were allowed to react with methyl halides diluted in an argon matrix, Grignard molecules CH_3MgX, including the fluoride species, CH_3MgF, were identified [133]. Similarly, cluster Grignard reagents, $C_6H_5Mg_nX$, including the combination ($n = 4$, X = F) have been produced by metal vapor synthesis [134-135]. Finally, although it does not involve the reaction of organometallic compounds, it might be mentioned that the reaction of (BDI)Mg–Mg(BDI) (BDI = κ^2-{2,6-$^iPr_2C_6H_3NCMe$}$_2CH$) [136-137] with a series of perfluorinated and polyfluorinated arenes generates (BDI)MgF by a process deemed 'equivalent' to Grignard formation in solution [138].

We report here the use of mechanochemical activation of Mg with fluorinated naphthalenes, in which it is clear that C–F bond activation has occurred, although there are still practical issues that must be overcome prior to more general development of the method. There have been cautions raised about the potentially explosive nature of fluorinated Grignards [125], but no such difficulties were encountered with the monofluoro organics used here.

3.2 Results/discussion

3.2.1 Exploration of mechanochemically generated Grignard reagents

Owing to the paucity of literature on mechanochemically driven Grignard chemistry, and to the potential sensitivity of reaction outcomes to the specific equipment and conditions employed, we selected several homocoupling reactions as calibration points for reactivity. In these cases, there are no other potential organic products other than ones generated from the Grignard reagents themselves. For this initial study, aromatic substrates were chosen as more likely to provide greater reactivity than the saturated equivalents [130]. As noted above, Harrowfield found that a considerable excess (at least 4X stoichiometric levels) of magnesium metal was required when milling it in Grignard reactions [122]. The use of smaller amounts led to pasty mixtures that could not be easily manipulated. We found a similar situation to be true, but perhaps because of our use of finer Mg powder (325 mesh) than in Harrowfield's experiments (50 mesh), 8 equiv. of Mg were required to produce a friable reaction product. In attempts to prevent the formation of pastes while using fewer equivalents of Mg (i.e., in line with Harrowfield's conditions), sodium chloride was used as a grinding agent. However, the reaction mixture post milling was a hardened mass rather than a free-flowing powder.

$$Mg, Ph_2CO$$
$$600\ rpm$$
$$Air,\ 2\ h$$

(Trace)
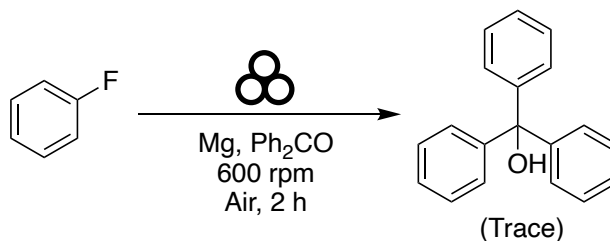
Scheme 3. Formation of triphenylmethanol by mechanochemical milling.

Initial investigation into carbonyl addition showed that milling fluorobenzene with benzophenone and 8 equiv. of magnesium powder in a planetary milling jar in air for 2 hours produced trace amounts of triphenylmethanol which was identified by GC (Scheme 3). After this positive, but limited result, multiple modifications were made in hopes of increasing the reactivity of the generated Grignard species, all while maintaining ease of reaction set up. The reactions were milled for longer times, magnesium turnings were utilized rather than magnesium powder, and other additives were introduced into the system; none of these changes produced a product of interest. 1,2-dihaloethanes were examined for the possibility of boosting reactivity in the system and aiding in Grignard formation, however the introduction of this additive seemed to favor formation of pinacol-coupled products rather than the expected Grignard addition product (Scheme 4). This is apparently due to the rapid formation of the keto-radical in the reaction system in comparison to the formation of the Grignard reagent, leading to rapid and efficient coupling of the radical species.
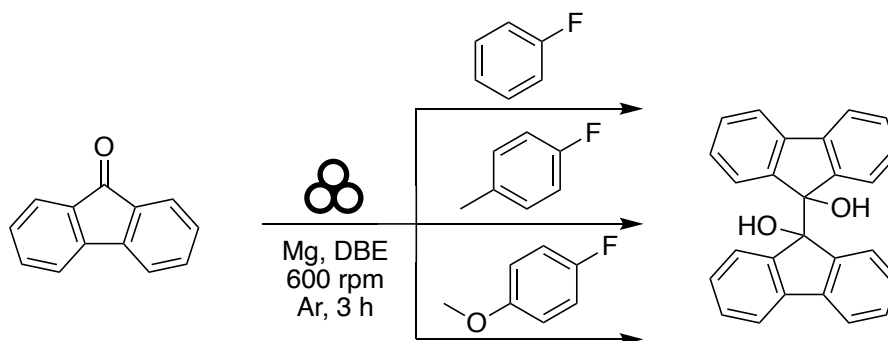
Scheme 4. Formation of pinacol coupled products via mechanochemical milling.

Fewer equiv. of magnesium were used with the intent of reducing the amount of pinacol product, but none of the desired product was observed if less than 8 equiv. were used. The formation and addition reactions were subsequently split into a two-step system to remove the

competing reactions for Grignard formation and radical formation. This unfortunately did not improve the reaction yield. Performing the milling reactions under an argon-flushed glove bag and then ultimately in a nitrogen-filled glovebox in efforts to prevent moisture and oxygen interference also gave no positive results. After attempts to perform carbonyl additions proved complicated and irreproducible, a system that isolated the Grignard reagent and focused on its reactivity was employed. Homocoupling of the generated Grignard reagents was studied to help avoid inconsistency in the reactivity of the electrophiles.

A series of coupling reagents whose efficacy has been established in solution chemistry ($FeCl_3$, $MnCl_2$, $Fe(acac)_3$, $NiBr_2 \cdot DME$, and 3,3′,5,5′-tetra-*tert*-butylbisquinone) were chosen[139-142], and bromobenzene was used as the substrate. Milling experiments were carried out using 100 mg of PhBr, 8 equiv. of Mg, and one equiv. of coupling reagent, performed under the conditions stated in Section 4.1. The only reagent that coupled to form the product, biphenyl, was iron(III) chloride (Scheme 5). It should be noted that biphenyl is a common contaminant in solution reactions involving PhMgBr [143], but it was not observed under these conditions in the absence of $FeCl_3$.
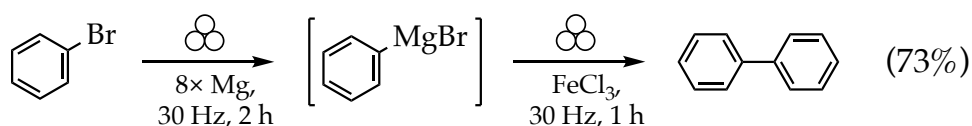
Scheme 5. Homocoupling of bromobenzene using iron(III) chloride under mechanochemical conditions.
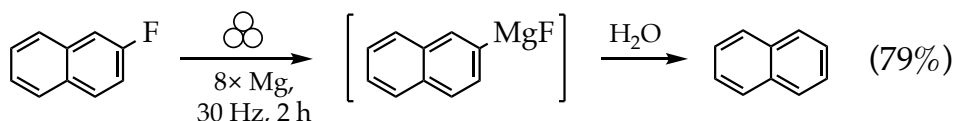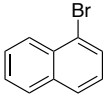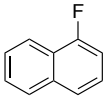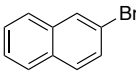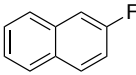
Scheme 6. Quenching of a mechanochemically generated fluoro-Grignard reagent.

For the initial screening of an organofluorine, 2-fluoronapthalene was selected. Milling it with 8 equiv. of Mg for 2 hours left a black powder that when extracted with THF, the extract filtered, and the filtrate treated with water, left naphthalene in 79% yield (Scheme 6). Attempts were made to isolate the fluoro-Grignard intermediate by treatment of the ground mixture with 1,4-dioxane followed by filtration, or quenching with iodine, TMSCl, and MeI; however, none of these efforts yielded any of the expected products.

In order to examine more completely the reactivity differences between two sets of halogenated compounds, 1- and 2- bromo- and fluoronaphthalenes were treated with magnesium under the same conditions as used for bromobenzene (Table 4). Regardless of the halide used, the yield of the isolated product binapthalene was almost identical, roughly 20%.

Table 4. Comparison of halide and isomer reactivity in homocoupling reactions with mechanochemically generated Grignard reagents.[a]

$$(naph)X \xrightarrow[\substack{Mg, 30 Hz \\ 2 h, RT}]{} [(naph)MgX] \xrightarrow[\substack{FeCl_3 \\ 30 Hz, 1 h, RT}]{} (naph)_2$$

Aryl Halide	Isolated Yield
1-bromonaphthalene	22%
1-fluoronaphthalene	20%
2-bromonaphthalene	21%
2-fluoronaphthalene	22%

[a]Conditions: halonapthalene (1 equiv.), Mg powder (8 equiv.), FeCl₃ (1 equiv.), two 8mm stainless steel ball bearings (3.3g/ball), N₂ atmosphere, isolated yields after column chromatography.

Curiously, although in line with other reports of the low reactivity of RMgF species towards CO_2 [130-131], the presumptive fluoro-Grignards described here were relatively unreactive toward carbonyl addition. Generation of the Grignard reagent was followed by either mechanochemical quenching or treatment of a solution of an electrophile (i.e., benzaldehyde, benzophenone) with the ground powder in order to minimize pinacol and McMurray-type coupling from the excess magnesium powder, yet no product was isolated. Addition of Et_2O as a liquid assisted grinding (LAG) agent also gave no product formation. The addition of lithium chloride to make a Turbo-Grignard reagent (RMgX-LiCl) and the addition of Lewis acids, such as $BF_3 \cdot OEt_2$ that doubles as LAG agent, were not successful. There may be poorly understood matrix effects that are interfering with subsequent reactivity.

3.2.2 Charge Analysis of Grignard Reagents

Geometry optimization of the (napht)MgX and (napht)$_2$Mg compounds was conducted with the dispersion-corrected B3PW91-D3BJ functional and the def2TZVP basis set on all atoms (see Section 3.4 for details). Charge estimation was conducted under the Natural Population Analysis (NPA) protocol (Figure 7). Interestingly, the Mg atom (or MgX unit) seems to serve as a buffer to the charge on the α-carbon in each species. In both halonaphthalenes, the difference in the carbon charge between the fluoro- and bromo- variants is no more than 0.03 units. Although there is a slightly more negative charge on the α-carbons in the 2-halonaphthalene as compared to the 1-halo isomer, it does not exceed 0.05 units. The pattern in the (napht)$_2$Mg species is similar, in that the charge on the α-carbon in the two complexes differs by no more than 0.04 units.
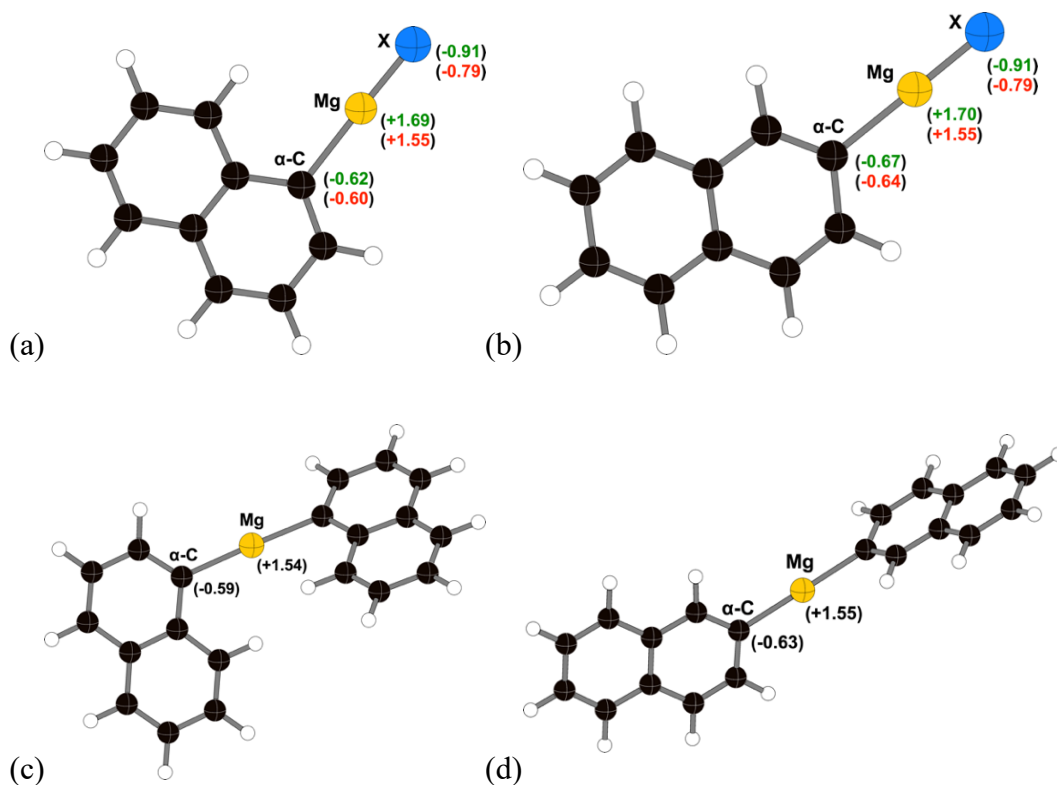
Figure 7. **NPA charges on halogen, Mg, and α-C in modeled Grignard species.** Charges are modeled in (a) naphthalen-1-ylmagnesium bromide (fluoride); (b) naphthalen-2-ylmagnesium bromide (fluoride); (c) bis(1-naphthyl)magnesium; and (d) bis(2-naphthyl)magnesium. In (a) and (b), the top values (in green) correspond to the fluoro species, and the bottom values (in red) correspond to the bromo species. The (naphth)$_2$Mg complexes were optimized under C$_2$ symmetry, so the charges on both $\underline{\alpha}$-carbons in each molecule are the same.

The α-carbon charges for all the molecules fall in the range of -0.63±0.04. It then should not be surprising that little difference is observed between the reactivity of the fluoro- and bromo- species if, once the halogen bond is broken, the nucleophilic carbon is effectively unbiased toward the identity of the halogen that was present prior to activation. It also suggests that it may be difficult to distinguish between a (naphthyl)MgX or a (naphthyl)$_2$Mg species in the coupling reactions.

3.3 Conclusion

Mechanochemically induced Grignard reagent formation by the direct ball milling of magnesium metal and an organohalogen (X = Cl, Br) has previously been demonstrated to provide products and yields comparable to those obtained in solution reactions.[122] Extension of this technique to fluoronaphthalenes induces activation of the C–F bond as well, although yields of e.g., homocoupled naphthalenes under the conditions used here, are low (ca. 20%). Density functional theory calculations indicate that charges on the α-carbon in the naphthalenes are similar in all cases. Thus, although it is clear that activation of the C–F bond of the fluoronaphthalenes has occurred, whether a (naphthyl)MgF or a (naphthyl)$_2$Mg species is involved in the coupling reactions is uncertain. Mechanochemical promotion of Grignard reagents offers many other variables in the search for improved conditions (e.g., magnesium source, composition of the grinding balls, geometry of the milling apparatus, temperature of the milling, etc.) and thus it is likely that further optimization of reaction conditions is possible.

3.4 Experimental

General Considerations. All manipulations were performed with the exclusion of air and moisture using standard glovebox techniques. Proton (^{1}H) NMR and carbon (^{13}C) spectra were obtained on a Bruker AV-400 spectrometer at 400 MHz, and were referenced to the residual proton resonances of CDCl$_3$.

Materials. Bromobenzene (purity ≥98%), 1-bromonaphthalene (purity ≥98%), 1-fluoronaphthalene (purity ≥98%), 2-bromonaphthalene (purity ≥98%) and 4-fluorotoluene (purity 97%) were purchased from Oakwood Products Inc.; and 2-fluoronaphthalene (purity ≥98%) was purchased from Fisher Scientific. Bromobenzene, 1-bromonaphthalene, 1-

fluoronaphthalene, and 4-fluorotoluene were all degassed and stored under a nitrogen atmosphere without further manipulation. Magnesium powder (purity 99%, ~325 mesh) was purchased from Strem Chemicals and stored under a nitrogen atmosphere without further manipulation. Iron(III) chloride was purchased from Sigma-Aldrich, dried under vacuum over an oil bath, and stored under nitrogen. Toluene was degassed with argon and dried over activated alumina, then stored over 4A molecular sieves in a nitrogen atmosphere glovebox. Anhydrous tetrahydrofuran (THF) was stored over 4A molecular sieves in a nitrogen atmosphere glovebox. CDCl$_3$ was obtained from Cambridge Isotopes.

Mechanochemical protocol. Ball milling reactions used either two stainless steel (440 grade) ball bearings ($^5/_{16}$ in (8 mm), 3.5 g) or fifty stainless steel (440 grade) ball bearings ($^3/_{16}$ in (4.8 mm), 0.44 g) that were thoroughly cleaned with detergent and water, then washed with acetone, and dried in a 125 °C oven prior to use. Planetary milling was performed with a Retsch PM100 mill, 50 mL stainless steel grinding jar type C, and a safety clamp for air-sensitive grinding. Mixer milling was performed with a Retsch MM400 mill with a 15 mL stainless steel Formtech Smartsnap™ grinding jar taped shut for air-sensitive grinding. A typical reaction involved ca. 250 mg total sample weight (1:1 grinding reactions), sealed under an inert atmosphere. The ground mixture was extracted with minimal toluene (<70 mL) and filtered through a fine porosity ground glass frit. The extraction is designed to dissolve the complex, and the filtration removes traces of KI. The filtrate was then dried under vacuum prior to NMR analysis.

General Procedure for Homocoupling Reactions. In a typical procedure, a 15 mL stainless steel Formtech milling jar was loaded with two 8 mm stainless steel (440 grade) ball

bearings (3.3 g each). In a nitrogen atmosphere glovebox, the aryl halide (100 mg, 1 equiv.) and the magnesium powder (8 equiv.) were added to the milling jar. The jar was sealed tightly and electrical tape was used to protect the atmosphere inside the milling jar. The jar was removed from the glovebox, placed in a Retsch MM 400 mixer mill and milled for the specified time and frequency (2 h, 30 Hz). The jar was returned to the glovebox in a c-clamp, and $FeCl_3$ (1 equiv.) was added to the ground reaction mixture. The jar was resealed, removed from the glovebox, and remilled (1 h, 30 Hz). Upon its return to the glovebox, the ground mixture was extracted with toluene (ca. 60 mL) and filtered through a medium porosity ground glass frit. The filtrate was treated with 15 mL of deionized water. Standard workup was completed by purifying the crude materials with column chromatography using hexanes as the eluent. The dried isolated products were identified by their characteristic ^{1}H NMR spectra on a Bruker AV-400 spectrometer at 400 MHz [144-146].

General Procedure for Quenching Reactions. The procedure above was followed, but following the initial milling reaction, the material was extracted with THF (ca. 40 mL), and the filtrate treated with 15 mL of deionized water. Workup was as above, but no column purification was used. Products were identified by their characteristic ^{1}H NMR spectra on a Bruker AV-400 spectrometer at 400 MHz.

General Procedure for Carbonyl Addition Reactions. In a typical procedure, a 15 mL stainless steel Formtech milling jar was loaded with two 8 mm stainless steel (440 grade) ball bearings (3.3 g each). To the jar, magnesium powder (8 equiv.) and the aryl halide (100 mg, 1 equiv.) were added to the milling jar. The jar was sealed tightly, and after grinding in a Retsch MM 400 mixer mill (2 h, 30 Hz), it was returned to the glovebox, and benzophenone (1

equiv.) was added to the ground reaction mixture. The jar was resealed and remilled (1 h, 30 Hz). The ground mixture was extracted with ~40 mL of dry THF and filtered through a medium porosity ground glass fritted funnel. The filtrate was treated with 15 mL of saturated ammonium chloride along with 15 mL of toluene. The mixture was transferred into a separatory funnel and the layers were separated. The organic layer was then washed with a 15 mL portion of deionized water. The aqueous layers were extracted once with 15 mL of toluene, the organics combined and washed with a 15 mL portion of brine. The organics were then collected, dried over magnesium sulfate, and filtered into a 100 mL round bottom flask. The solvent was removed by rotary evaporation and the crude material was purified with column chromatography (hexanes:ethyl acetate) to reveal unreacted electrophile and other unidentified species.

General Procedures for Computational Analysis. All calculations were performed with the Gaussian 16W suite of programs [147]. The B3PW91 functional, which incorporates Becke's three-parameter exchange functional with the 1991 gradient-corrected correlation functional of Perdew and Wang, was used [148]. To add dispersion correction, Grimme's D3 correction[149] with additional Becke-Johnson damping was used [150] (Gaussian keyword: empiricaldispersion=GD3BJ). The def2TZVP basis set was used on all atoms [151]. The (napth)MgX molecules were optimized under C_s symmetry; the (napth)$_2$Mg complexes were run under C_2 symmetry. Atomic charges were estimated with the Natural Population Analysis protocol (v 3.1) [152-153].

(This work was adapted from Speight, I. R., et al. *Molecules*, **2020**, 25(3), 570).

CHAPTER 4

An improved synthesis and use of *tert*-butyl substituted allyl and alkoxide ligands

4.1 Introduction

Many transition metal-catalyzed processes are known that utilize, generate, or are proposed to go through a metal allyl intermediate or other species.[154] Many research groups, such as the Dong group, have relied on metal allyl species as intermediates for coupling reactions, and rhodium catalysts in particular have been used in a variety of cross coupling contexts.[155-157] The transition metal allyl has become a staple in many olefin and alkyne couplings to form ring species, as precatalysts for cross couplings, and as reagents for polymerization.[158] The Hazari group, as well as others, have developed many substituted allyl species to diversify their catalysts and their utility, yet when utilizing 1,3- substituted systems (Figure 8) have opted to employ the related indenyl species due to its stability and high control in substituent orientation.[159-161]
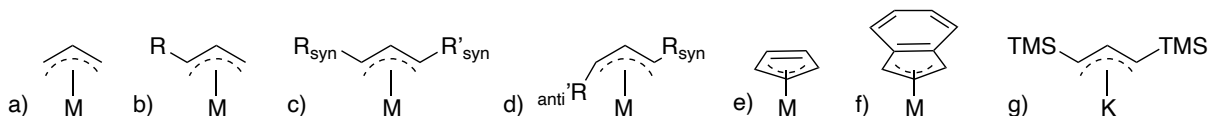
Figure 8. Illustration of different η^3-π-allyl complexes using a) unsubstituted allyl ($C_3H_5^-$), b) mono-substituted allyl, c) 1,3-substituted allyl with both substituents *syn* to the center hydrogen, d) 1,3-substituted allyl with one substituent *syn* and one substituent *anti* to the center hydrogen, e) a slipped cyclopentadienyl ring, f) indenyl ligand, and g) 1,3-bis(trimethylsilyl)allyl potassium salt.[162]

The Hanusa group, however, has chosen a different approach to metal ligand design by employing trimethylsilyl (TMS) groups as the substituents on the allyl moiety.[163-165] The TMS substituent adds significant steric bulk while retaining the fundamental electronics of the allyl system. In addition to bulk, the TMS group helps to moderate some of the extremely high

reactivity characteristic of unsubstituted metal allyl complexes. By increasing the number of TMS groups, not only have the resulting metal complexes become much more thermally stable, but they have also exhibited unique reactivity such as the ability to initiate difficult polymerization reactions.

In studies designed to expand the variety of metal allyl complexes, the Hanusa group has focused on the 1,3-bis(trimethylsilyl)allyl (A*) ligand, and more recently has added mechanochemical methods to the synthetic repertoire. This has greatly aided efforts in the last eight years to prepare unsolvated metal allyl species. This use of solvent-free synthesis allowed the isolation of the unsolvated aluminum tris(1,3-bis(trimethylsilyl)allyl) species, for example, which can only be obtained through mechanochemical methods.[42] Though use of the TMS-substituted allyl has been extremely useful, silyl groups are typically labile under conditions that employ the use of fluoride-containing precursors or acidic media, thus limiting their exploitation under such conditions.[166-168] This has driven efforts to develop an all-carbon analogue of the substituted allyl ligand to minimize the potential for substituent loss while maintaining the relative steric bulk profile that has proven to be valuable in making unsolvated metal allyl species.

In our efforts to find a suitable counterpart to the A* ligand, we examined the potential advantages of replacing the TMS groups with *tert*-butyl (tBu) substituents. Metal complexes containing such ligands would allow for direct comparisons with their TMS-substituted counterparts, and hence clarify the role that the silyl groups play in metal allyl chemistry. Additionally, the attempted synthesis of 2nd- and 3rd-row transition metal complexes that contain the A* ligand has met with little success, and the availability of a purely hydrocarbon-

based ligand might provide access to palladium, platinum, and other late transition metal complexes of catalytic interest.

The synthesis of 1,3-bis(*tert*-butyl)allyl ligand (A^t) has been reported previously by Fraenkel and co-workers through the formation of a lithiated species which was then utilized for NMR studies (Scheme 7).[169] Key transformations in Fraenkel's route include the use of LAH for the reduction of the allylic ketone, formation of the thioether via substitution, and stannylation through iterative metallations (Li, Sn). The use of potentially dangerous reagents (LiDMAN, SnMe$_3$Cl, MeLi, and LAH), in addition to the absence of other studies of the A^t ligand in other contexts sparked our interest, as there were optimizations that could be made to the synthesis and provide other variants of this potentially useful ligand. This chapter will discuss current efforts toward an improved synthesis of the 1,3-bis(*tert*-butyl)allyl ligand as well as the discovery of other bulky ligands that could potentially be of value to the organometallic community.
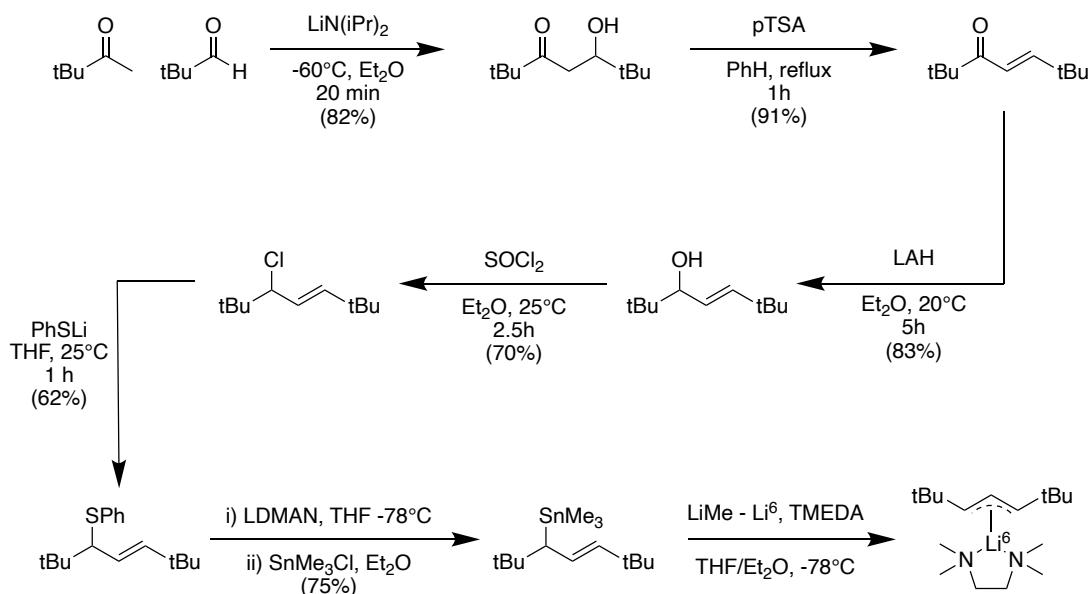
Scheme 7. Preparation of 1,3-bis(*tert*-butyl)allyl lithium by Fraenkel and coworkers.

44

4.2 Results and discussion

4.2.1 Progress towards potassium 1,3-bis-tert-butylallyl

Two fundamental approaches were considered for obtaining the potassium salt of the 1,3-bis-*tert*-butylallyl anion, i.e., deprotonation of the all-hydrocarbon olefin (HA^t), or lithium-halogen exchange of an allylic halide. We envisioned reaching the product by starting from the use of common organic reactions such as an aldol condensation or a Wittig olefination (Figure 5). The route to the olefin was focused on the use of a Wittig reaction between the phosphonium salt of a neopentyl halide and the corresponding aldehyde.
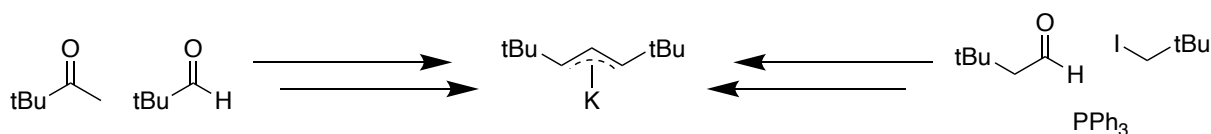
Figure 9. Proposed starting points to 1,3-bis-*tert*-butylallyl potassium.

Preparation of the neopentyl triphenylphosphonium salts proved to be sensitive to reaction conditions such as heat, reaction time, and purification/storage of the final product. Refluxing triphenylphosphine in a solution of neopentyl bromide in xylenes did not yield the appropriate phosphonium salt, and only triphenylphosphine was recovered. When triphenylphosphine was refluxed for 24 hours in neat neopentyl iodide, the corresponding salt was obtained after precipitation of the hot solution in ethyl acetate. When THF or acetone were used as the precipitation and washing solvents, or when the isolated product was stored in air, the product color would change from white/off-white to yellow, and in some cases, orange. This coloration change is attributed to slow oxidation of the product; the oxidized material could

be removed by washing the product in ethyl acetate, followed by storage under vacuum or under a nitrogen atmosphere.

The phosphonium salt was then utilized in formation of the propene precursor after optimization of reaction conditions. The olefination product was purified by column chromatography and identified by its characteristic proton NMR spectrum. It is key to note that the product was isolated as a solution in toluene which arises from the use of a mixed solvent system (Scheme 8), as removal of toluene under vacuum would remove the product as well. With the propene in hand, multiple attempts to deprotonate it were made but none were successful. The conditions used for the synthesis of KA* (i.e., deprotonation of the silyl-substituted propene with nBuLi, followed by transmetallation with potassium *tert*-butoxide) did not produce the potassium salt of the hydrocarbon, but rather an insoluble orange powder. The reaction was then repeated with other bases (KBz) and combinations of bases (tBuLi and KOtBu), but no product was observed. Either black or insoluble powders were isolated which could not be examined with NMR due to their low solubility in benzene-d6. After multiple attempts to improve this route, the decision to explore a route that employed a halide intermediate was made.
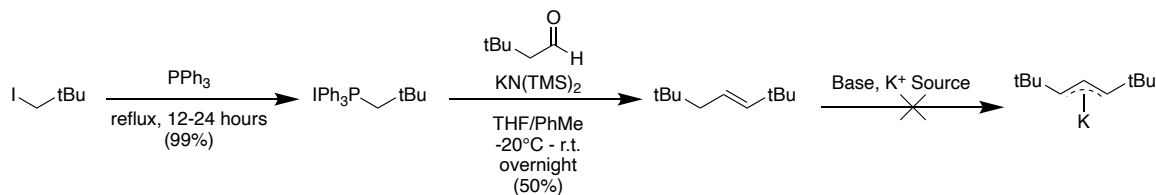
Scheme 8. Attempted synthesis of the potassium allyl species via Wittig reaction.

The route presented by Fraenkel and co-workers employed a seven-step synthesis to the lithium allyl species which utilized reagents such as lithium aluminum hydride (LAH),

trimethyltin chloride, lithium dimethyl aminonaphthalide (LDMAN), and toxic solvents such as benzene. Fraenkel's route provided a route to the ligand of interest, but there were features of it that could be modified to make the synthesis more simple, accessible, and scalable. Aldol condensation of pinacolone and pivaldehyde to form the propene backbone proved to be straightforward and scalable (up to 20 g scale), while also removing the need for specific conditions for storage and purification. Subsequent sodium borohydride reduction, in lieu of using LAH, produced the alcohol in good yield; this procedure can also be performed on a multigram scale (up to 8 g). In addition to large-scale solution preparations, the allylic ketone and allylic alcohol can be prepared by mechanochemical methods, which suggests other methods such as resonant acoustic mixing (RAM) could be used to scale the system to quantities similar to solution preparation.

The alcohol was then converted to the allylic bromide by two methods, either treatment with aqueous hydrobromic acid and sulfuric acid or treatment with thionyl bromide. The aqueous HBr conditions were adopted due to simplified workup involved and improved yield in comparison to the thionyl bromide conditions.

Treatment of the allyl halide with n-butyl lithium led to the formation of a white precipitate that was identified as lithium bromide; it was accompanied by a side product from reaction of the lithium allyl with butylbromide (Scheme 9). Changing the base used from n-butyl to *tert*-butyl, lowering the overall reaction temperature to -78 °C, and increasing the base equivalents from one to two to promote the formation of lithium bromide via elimination proved effective in improving the process. The reaction was then treated with potassium *tert*-butoxide and the product of interest was isolated in conjunction with another unidentified species.
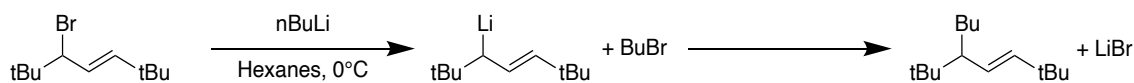
Scheme 9. Substitution reaction of butylbromide with Li[A^t].

A direct synthesis approach was performed by treating the allyl halide with potassium metal overnight in THF, which led to formation of the product without a large mixture of other undesired species. Although other side products such as the hydrodehalogenation product were observed, the potassium salt could be identified by characteristic allyl signals in the proton NMR spectrum. The product was observed to have a *syn, anti*-conformation of the *tert*-butyl groups as opposed to the *syn, syn* relationship that is seen in the trimethylsilyl allyl salt. Investigation into ways to improve the synthesis of the potassium salt as well as understanding the preferred orientation of the *tert*-butyl groups in the potassium species is ongoing.
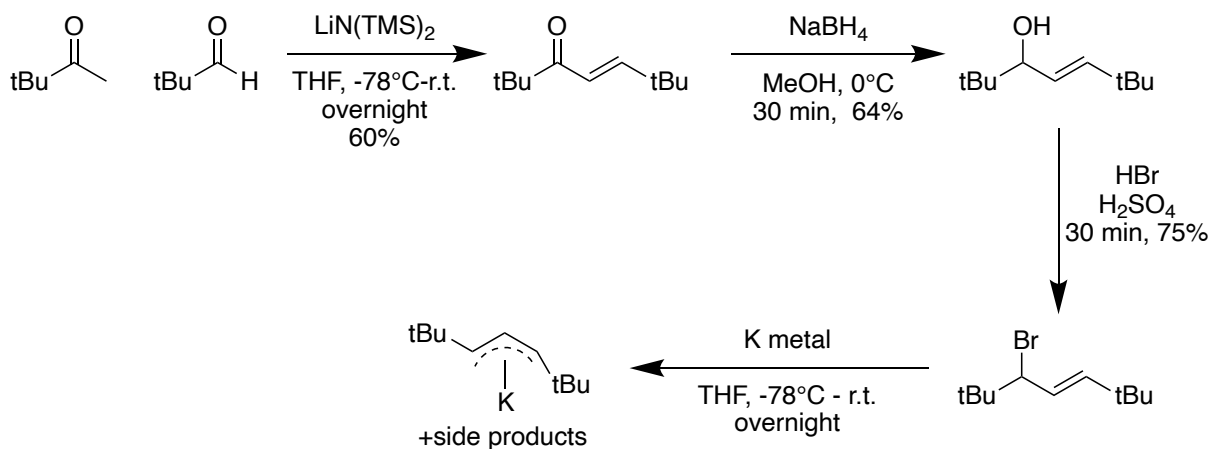
Scheme 10. Synthesis of potassium allyl species via the new route.

4.2.2 Synthesis of metal complexes containing the 1,3-bis-tert-butylallyl ligand

While synthesizing the potassium allyl salt had its own difficulties, its synthetic route allows for the preparation of other metal complexes along the way. For example, the allylic

48

alcohol can be utilized for the synthesis of bulky metal alkoxides, which could benefit from the multiple functional groups that are present (alkoxide and olefin). Alternatively, the allyl halide could be utilized for metal insertion reactions to produce transition metal complexes. With these ideas in mind, the allyl halide was used in attempts to make several metal complexes.

Treatment of bipotassium tetrachloropalladate, $K_2[PdCl_4]$, with the *tert*-butyl allyl bromide in water at elevated temperature for multiple days gave no color change and no product of interest. In an attempt to make a nickel complex, the allyl bromide was treated with bis(triphenylphosphine)nickel dicarbonyl in benzene at elevated temperature, which immediately resulted in a color change from a pale-yellow solution to a maple-colored solution. The solvent was removed under vacuum and treated with a small volume of hexanes to give a deep red solution along with a light green precipitate. Separation of the red solution from this precipitate followed by removal of the solvent gave rise to a deep red oil which was identified as a nickel allyl bromide species. The isolated species shows no evidence for coordinated phosphine by ^{1}H and ^{31}P NMR, but the substituents on the allyl ligand were found to be in a *syn*,*anti*-relationship, which is not uncommon for first-row transition metal complexes.[165] Over a few hours, the complex changed color and form from a deep red oil to a forest green solid. The NMR spectra of the species does not change despite the color change. It is unclear what causes the color shift other than perhaps weak solvent interactions from residual solvent not detected in the NMR spectra or a highly colored impurity that may have evaporated or decomposed over time to leave solely the product of interest. Further studies of the material must be performed.

In addition to synthesis of the nickel species, formation of a cobalt carbonyl complex was sought. Treatment of dicobalt octacarbonyl under phase transfer conditions with the allyl bromide gives rise to a yellow oil tentatively identified as a cobalt allyl tricarbonyl complex in low yield (Scheme 11). The compound behaves similarly to its trimethylsilyl allyl counterpart in terms of color and stability.[170] The complex slowly decomposes to a blue solid over a 12-hour period which has led to difficulty in characterization by any method other than ^{1}H NMR.
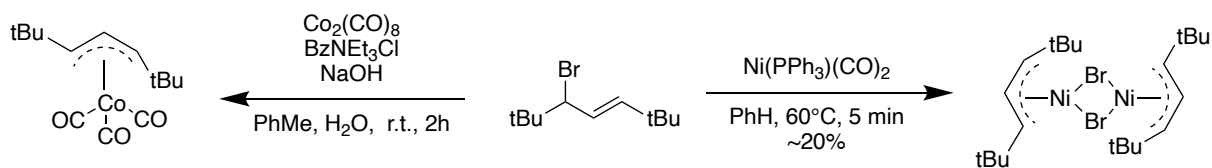
Scheme 11. Synthesis of cobalt and nickel A^t products via oxidative insertion.

4.2.3 Synthesis of a bulky diketone and diol

Initial attempts to optimize the aldol condensation for the *tert*-butyl allylic ketone on route to the potassium allyl salt gave rise to a unique isolated species. Modification of the reaction conditions to have pinacolone in excess gave rise to a double addition product, a highly crystalline diketone species that was isolated in moderate yield (Scheme 12). The crystal structure of the compound shows that the carbonyls face the same face of the molecule (Figure 10a).
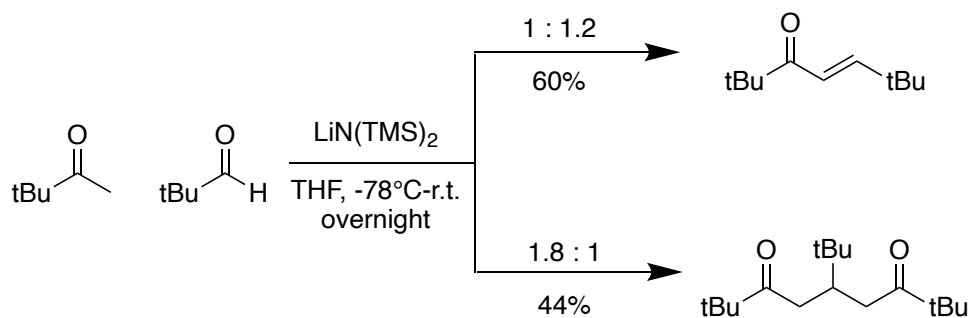
Scheme 12. Molar equivalence influence on the aldol condensation used to form A^t.
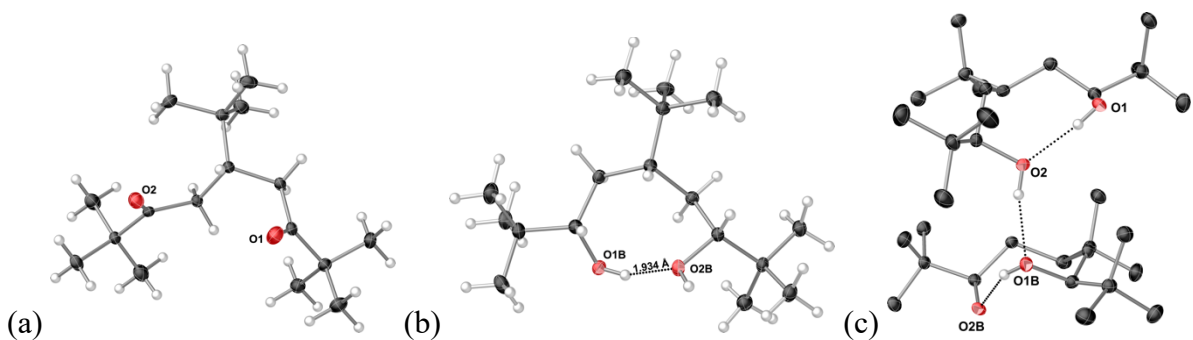
Figure 10. Crystal structures of (a) 5-(*tert*-butyl)-2,2,8,8-tetramethylnonane-3,7-dione and 5-(*tert*-butyl)-2,2,8,8-tetramethylnonane-3,7-diol ((b) single and (c) dimer unit).

Once the compound was reduced to a diol, a *meso* compound was identified (Figure 6b). The reduction of the diketone has not been fully optimized; however, crystals of the product have been obtained and confirm the *meso* configuration as well as a pseudo-8-membered ring structure that arises from a hydrogen bond interaction between the alcohols. Additionally, the hydrogen bond network extends through the structure and is not limited to intramolecular interactions.

4.3 Conclusions and future directions

A *tert*-butyl substituted allylic halide can be accessed in three total steps from commercially available starting materials. Additionally, we can perform all steps on a multigram scale (20 g scale for aldol condensation, 8 g scale for reduction, 5 g scale for halogenation) while only using purification techniques such as recrystallization and distillation. This synthetic route also removes the need for more specialized or difficult to handle reagents such as LAH and LDMAN, and removes the use of toxic chemicals such as trimethyltin chloride and benzene. The potassium allyl has been observed in a complex mixture of the desired product and other species but is observed to have a *syn,anti*-orientation of the *tert*-butyl substituents. In

addition to this, we have synthesized allyl species containing nickel and observed an allyl species containing cobalt, starting from the allylic bromide precursor.

Further exploration of this series will expand on uses for the A^t ligand and the bulky tri-(*tert*-butyl)-diol and diketone. The route to the allyl moiety also opens a plethora of pathways to other species such as an allylic alkoxide which could provide dual functionality as a loosely bound π-donor via the olefin. Additionally, the alcohol can be transformed into a variety of different species through very simple chemical manipulations. Amines, other halides, phosphines, and sulfides are all feasible products that could prove useful in the continued development of the A^t system. The sterically hindered diol could be a useful reagent for the development of bulky metal alkoxides and through the implementation of substoichiometric conditions, dimeric alkoxides could be formed. Through these species we can potentially access a broad series of transition metal complexes, bifunctional alkoxide main group species, and develop new and exciting species for catalysis, polymerization initiation, and other applications.

4.4 Experimental

General methods and materials. All syntheses were conducted under rigorous exclusion of air and moisture using Schlenk line and glovebox techniques unless noted otherwise. Proton (^{1}H) and carbon (^{13}C) NMR spectra were obtained at ambient temperature on a Bruker AV-400 MHz spectrometer. Proton and carbon spectra were referenced to the residual resonances of C_6D_6 and $CDCl_3$.

Pivaldehyde, pinacolone, neopentyl iodide, triphenylphosphine, lithium hexamethyldisilazane in THF, and sodium borohydride were purchased from Oakwood

Products. Thionyl bromide, thionyl chloride, and potassium metal were purchased from Sigma Aldrich. Anhydrous inhibitor-free tetrahydrofuran (THF) was stored over molecular sieves prior to use. Hexanes and diethyl ether were distilled under nitrogen in the presence of potassium metal prior to use. Deuterated benzene and deuterated chloroform were purchased from Cambridge Isotopes. Dicobalt octacarbonyl, and bis(triphenylphosphine)dicarbonyl nickel(0) were purchased from Strem Chemicals.

Preparation of 2,2,6,6-tetramethylhept-4-en-3-one.

Method A. An oven-dried 500 mL Schlenk flask was equipped with a Teflon stirring bar and placed in a nitrogen-filled glovebox. 100 mL of THF was added to the flask and the opening sealed with a ribbed septum. The flask was removed from the glovebox and placed on a Schlenk line. Pinacolone (7.43 mL, 59.4 mmol, 1 equiv.) was added to the flask via syringe. The THF solution was chilled to -78 °C for 10 minutes prior to manipulation. An oven-dried 125 mL flask was filled with 60 mL of 1.0 M LiHMDS in THF and sealed with a ribbed septum. The LiHMDS was transferred using a cannula into the reaction flask and the solution was stirred for 15 minutes at -78 °C. After stirring, pivaldehyde (7.10 mL, 65.4 mmol, 1.1 equiv.) was added to the reaction via syringe. The ice bath was removed from the reaction flask and stirred at room temperature overnight. After the reaction was complete, 50 mL of saturated ammonium chloride was added to the reaction along with 50 mL of diethyl ether. The mixture was transferred to a 500 mL separatory funnel and the layers were separated. The organic layer was washed twice with 50 mL portions of deionized water. The aqueous washes were collected and extracted with 50 mL of diethyl ether. The organics were then combined, washed with 100 mL

of brine, separated, and dried over magnesium sulfate before being filtered into a 500 mL round bottom flask.

The volatiles were removed via rotary evaporator to leave a yellow/amber liquid. The liquid was transferred to an Erlenmeyer flask. Cold methanol (-78 °C) was added to the flask slowly to promote recrystallization. The methanol/crude product mixture was placed in the ice bath and methanol was added until a roughly 1:1 mixture was obtained. The product was observed as a white powder and recovered by filtration. The product was then placed in vials and placed on high vacuum to remove any residual methanol and other volatile impurities. The product was identified by its characteristic NMR spectrum.[169] Yield: 6.9 g (69%).

Method B. Pinacolone (1.49 mL, 11.9 mmol, 1.0 equiv.), pivaldehyde (1.29 mL, 11.9 mmol, 1.0 equiv.), and sodium hydroxide (476 mg, 11.9 mmol, 1.0 equiv.) were evenly distributed into two 15 mL Formtech Smartsnap™ stainless steel milling jars with two 8 mm stainless steel ball bearings per jar. The jars were closed, and the reaction was milled for 30 minutes at 30 Hz. The jars were then opened, revealing a slurry. The reaction mixture was treated with 8 mL of 10% HCl (2 mL per jar section) and combined in a 125 mL Erlenmeyer flask. The jars were rinsed with 20 mL of diethyl ether (5 mL per jar section). Organic and aqueous portions were combined in a 125 mL separatory funnel. The aqueous layer was removed and extracted with an additional 10 mL of diethyl ether. The organics were combined, washed with 5 mL of brine, separated, and dried over magnesium sulfate before filtration into a 100 mL round bottom flask. The volatiles were removed by rotary evaporation and the crude product placed on high vacuum to remove any remaining volatile impurities. The product was

isolated with no further purification. The product was identified by its characteristic NMR spectrum.[169] Yield: 1.88 g (94%).

2,2,6,6-tetramethylhept-4-en-3-ol. A 250 mL round bottom flask was equipped with a stirring bar. The flask was charged with 2,2,6,6-tetramethylhept-4-en-3-one (8.00 g, 47.5 mmol, 1 equiv.) and methanol (50 mL). The solution was cooled to 0 °C in an ice bath, and sodium borohydride (1.80 g, 47.5 mmol, 1 equiv.) was added slowly to the flask. The reaction was stirred at 0 °C for 60 minutes after the last addition of sodium borohydride. The reaction was kept cool and 10 mL of saturated Rochelle's salt solution was slowly added to quench the reaction mixture. The quenched solution was diluted with 40 mL of diethyl ether and filtered into a 250 mL round bottom flask. The volatiles were removed to give a pale-yellow emulsion. The material was dried over sodium sulfate to remove all water from the product. The product was transferred with a pipet into a vial and stored with no further purification. The product was identified by its characteristic NMR spectrum.[171] Yield: 5.05 g (63%).

5-bromo-2,2,6,6-tetramethyl-hept-4-ene.

Method A. A 100 mL vial was equipped with a Teflon stirring bar and allylic alcohol (5.00 g, 29.4 mmol, 1 equiv.). The flask was placed in an ice bath and 40% hydrobromic acid in water (16.6 mL, 147 mmol, 5 equiv.) was added to the flask and stirred. Concentrated sulfuric acid (1.56 mL, 29.4 mmol, 1 equiv.) was added to the chilled reaction, and the mixture was stirred vigorously for 30 minutes. Hexanes (40 mL) was added to the flask and stirring was continued briefly. The flask was removed from the ice bath and the reaction mixture was transferred to a 125 mL separatory funnel and the acidic layers were removed. The organics were washed once with 5 mL of deionized water, 5 mL of brine, and dried over magnesium

sulfate. The solution was filtered into a 100 mL round bottom flask and volatiles were removed using a rotary evaporator. The product was isolated without further purification. The compound was identified by its characteristic NMR spectrum.[171] Yield: 4.80 g (70%).

Method B. A 50 mL round bottom flask was wrapped in aluminum foil and equipped with a Teflon stirring bar. The flask was charged with allylic alcohol (1.89 g, 11.1 mmol, 1 equiv.) and 11 mL of diethyl ether. Thionyl bromide (3.01 mL, 38.8 mmol, 3.5 equiv.) was added to the flask slowly. The reaction was stirred for 2.5 hours at room temperature. When the reaction was observed to be complete by TLC (10% EtOAc in hexanes), the flask was placed in a 0 °C ice bath and slowly quenched with 2 mL of deionized water. The reaction was transferred to a 50 mL separatory funnel. Layers were separated and the organics were washed with 5 mL of saturated sodium thiosulfate. The aqueous washes were combined and extracted with 5 mL of diethyl ether. The organics were combined, washed with brine, dried over magnesium sulfate, and filtered into a 50 mL round bottom flask. The volatiles were removed via rotary evaporator to leave a yellow liquid. The product was isolated without further purification. The compound was identified by its characteristic NMR spectrum.[171] Yield: 1.09 g, 40%.

Potassium 1,3-(di-*tert*)-butylallyl. An oven-dried 50 mL Schlenk flask was transferred to a nitrogen-filled glovebox, equipped with a magnetic stirrer bar, and charged with 4 mL THF and potassium metal (33.5 mg, 0.86 mmol, 2 equiv.). Allylic bromide (100 mg, 0.43 mmol) was degassed in a 20 mL vial. The Schlenk flask containing potassium in THF was placed on a Schlenk line and cooled to -78 °C. The degassed allylic bromide was injected via syringe into the flask and the reaction was stirred at low temperature for 4 hours. The flask was then returned to the glovebox and stirred overnight. The reaction was then concentrated to a solid consisting

of a mixture of the proto-dehalogenated product, potassium metallated product, and other impurities. The K[A^t] appears to have an η^3-π system that displays a *syn,anti*-orientation of the *tert*-butyl groups on the allyl. Due to the presence of undesired products in the isolated material increasing the complexity of the ^{13}C NMR spectrum, only the resonances of the ^{1}H NMR spectrum are listed. ^{1}H NMR (400 MHz, C$_6$D$_6$, 298 K): δ 0.87 (s, 9H, C(CH$_3$)$_3$), 0.96 (s, 9H, C(CH$_3$)$_3$), 4.23 (d, 1H, *J* = 10.35 Hz, C-H), 5.36 (dd, 1H, *J* = 15.55 Hz, *J* = 11.50, C-H), 5.67 (dd, 1H, *J* = 15.40 Hz, *J* = 10.36, C-H).

5-(*tert*-butyl)-2,2,8,8-tetramethylnonane-3,7-dione. A 1 L flask with a 24/40 addition arm attachment was flame dried, joints greased and assembled, and a Teflon stirring bar added before being flushed with nitrogen gas on a Schlenk line. A separate oven-dried 500 mL Schlenk flask was placed in a nitrogen-filled glovebox and filled with 200 mL of dry diethyl ether. The flask was removed from the glovebox and placed on a Schlenk line. The diethyl ether was transferred via cannulation. Pinacolone (22.3 mL, 178 mmol, 1.8 equiv.) was added to the THF and stirred. The resulting solution was cooled to -78 °C and LiHMDS (1.0M, 178 mL, 1.8 equiv.) was added to the flask. The solution was stirred at low temperature for 15 minutes. Pivaldehyde (10.6 mL, 97.6 mmol, 1 equiv.) was added to the flask, the reaction removed from the ice bath and stirred at room temperature overnight. The reaction was quenched with 200 mL of saturated ammonium chloride and the contents of the flask were transferred to a 1 L separatory funnel. The organics were washed twice with two 100 mL portions of deionized water and the washes were combined. The aqueous washes were then extracted twice with 60 mL portions of diethyl ether. The organics were combined, washed with brine, and dried over magnesium sulfate. The dried organics were filtered into a 1 L flask and concentrated with a rotary evaporator to give a viscous amber oil. When agitated with a pipette, the oil slowly

crystallized to give light tan needles. The product was obtained without further purification (11.7 g, 45%). ^{1}H NMR (400 MHz, CDCl$_3$, 298 K): δ 0.86 (s, 9H, C(CH$_3$)$_3$), 1.14 (s, 18H, C(CH$_3$)$_3$), 2.26 (dd, 2H, J = 17.01 Hz, 7.91 Hz, C-H$_{methylene}$), 2.49 (m, 1H, C-H$_{methyne}$), 2.67 (dd, 2H, J = 16.95 Hz, 3.93 Hz, J = 1.62, C-H$_{methylene}$). ^{13}C NMR (100 MHz, C$_6$D$_6$, 298 K): δ 27.08 (CH$_3$), 27.70 (CH$_2$), 33.56 (CMe$_3$), 37.67 (CMe$_3$), 38.33 (CMe$_3$), 44.61 (CH(tBu)), 215.54 (C$_{sp2}$-O).

5-(*tert*-butyl)-2,2,8,8-tetramethylnonane-3,7-diol. 5-(*tert*-butyl)-2,2,8,8-tetramethyl-nonane-3,8-dione (1.00 g, 3.73 mmol, 1 equiv.) was dissolved in 13 mL of ethanol (90%) in a 100 mL round bottom flask. The solution was cooled in an ice bath and stirred. Sodium borohydride (705 mg, 18.6 mmol, 4 equiv.) was added to the flask slowly. Upon completion of the addition, the ice bath was removed, and the reaction was allowed to stir for 14 hours. The reaction was then quenched with 15 mL of a 10% (v/v) HCl solution and stirred for 10 minutes. The mixture was diluted with 30 mL of diethyl ether and transferred to a separatory funnel. The aqueous portion was removed, and the organic layer was returned to the flask along with 15 mL of a saturated solution of Rochelle's salt and an additional 30 mL portion of diethyl ether. The mixture was returned to the separatory funnel and the aqueous portion was removed. The organic portion was washed with 10 mL of Rochelle's salt solution and separated. The isolated layer was dried over magnesium sulfate, filtered, and concentrated to afford a white powder and a colorless oil. The mixture was separated with column chromatography (10:90 ethyl acetate:hexanes). The isolated product was a white crystalline solid (209.0 mg, 21%). ^{1}H NMR (400 MHz, CDCl$_3$, 298 K): δ 0.87 (s, 9H, C(CH$_3$)$_3$), 0.90 (s, 18H, C(CH$_3$)$_3$), 1.18 (m, 2H, C-H$_{methylene}$), 1.41 (quin, 1H, J = 3.96 Hz, C-H$_{methyne}$), 1.79 (dd, 2H, J = 3.70 Hz, J = 1.62, C-H), 1.83 (dd, 2H, J = 3.70 Hz, J = 1.62, C-H), 3.19 (s, 2H, OH), 3.32 (dd, 2H, J = 10.88 Hz, J =

1.56, C-H). ^{13}C NMR (100 MHz, C$_6$D$_6$, 298 K): δ 25.66 (CH$_3$), 27.23 (CH$_2$), 34.46 (CMe$_3$), 35.20 (CMe$_3$), 35.37 (CMe$_3$), 45.95 (CH(tBu)), 82.98 (C-OH).

1,3-bis-_tert-_butylallyl nickel bromide. In a nitrogen atmosphere glovebox, Ni(CO)$_2$(PPh$_3$)$_2$ (500 mg, 0.78 mmol) and dry benzene (11.5 mL, 68 mM) were placed in a 50 mL Schlenk flask equipped with a Teflon stirring bar. The flask was sealed with a rubber septum and removed from the glovebox. The solution was placed in a 60 °C oil bath and stirred. To the stirring heated solution, 5-bromo-2,2,6,6-tetramethyl-hept-4-ene (182 mg, 0.78 mmol, 1 equiv.) was added by syringe to the reaction system. The reaction was allowed to continue for 10 minutes at elevated temperature before removal from the oil bath. The mixture was returned to the glovebox and the volatiles removed from the flask via vacuum. The resulting material was treated with 2 mL of hexanes to afford a red oil. The oil was transferred to a glass vial and the hexanes was removed in vacuo to afford a deep red purple oil (59.6 mg, 21.6%).^{1}H NMR (400 MHz, C$_6$D$_6$, 298 K): δ 0.87 (s, 9H, C(CH$_3$)$_3$), 0.96 (s, 9H, C(CH$_3$)$_3$), 4.24 (d, 1H, J = 10.35, anti C-H), 5.37 (d, 1H, J = 15.42 Hz, syn C-H), 5.67 (dd, 2H, J = 15.40 Hz, J = 10.35, C$_{(2)}$-H). ^{13}C NMR (100 MHz, C$_6$D$_6$, 298 K): δ 27.34 (CH$_3$), 29.24 (CH$_3$), 35.84 (anti C-H), 70.2 (syn C-H), 124.76 (C$_{(2)}$-H).

1,3-bis-_tert-_butylallyl cobalt tricarbonyl. A 250 mL Schlenk flask was charged with a stirring bar, NaOH (8 g, 200 mmol), and triethylbenzyl ammonium chloride (300 mg, 1.32 mmol). The reagents were dissolved in 40 mL of deionized water. The mixture was then degassed 3 times to remove any air, then flushed with nitrogen to create an inert atmosphere. In a nitrogen atmosphere glovebox, dicobalt octacarbonyl (300 mg, 0.88 mmol) was added to a Schlenk flask with 30 mL of dry toluene. The Schlenk flask was removed from the glove box and BrA^t (205 mg, 0.88 mmol, 1 equiv.) was added by syringe. The mixture was stirred and

then transferred by cannula to the flask with the aqueous portions. The reaction was allowed to stir vigorously at room temperature for two hours, after which time a deep orange organic layer and a vivid blue aqueous layer were observed. The materials were transferred to a glove bag and placed under an argon atmosphere. The layers were separated, and the organics dried over magnesium sulfate, followed by gravity filtration into a 100 mL round bottom flask. The organic solution was bright yellow. The flask was sealed with a septum and transferred to a nitrogen glovebox. The organic solvent was removed in vacuo. A yellow oil (60 mg) was observed along with a brown residue lining the walls of the flask. The yellow oil was found to have retained some toluene. Due to the steady decomposition of the product, only the ^{1}H NMR resonances are listed. ^{1}H NMR (400 MHz, C_6D_6, 298 K): δ 0.88 (s, 9H, $C(CH_3)_3$), 0.96 (s, 9H, $C(CH_3)_3$), 4.23 (d, 1H, J = 10.34, anti C-H), 5.38 (d, 1H, J = 15.39 Hz, syn C-H), 5.67 (dd, 2H, J = 15.36 Hz, J = 10.37, $C_{(2)}$-H).

General Procedures for X-ray Crystallography

A suitable crystal of each sample was selected for analysis and mounted in a polyimide loop. All measurements were made on a Rigaku Oxford Diffraction Supernova Eos CCD with filtered Cu-Kα radiation at a temperature of 100 K. Using Olex2,[172] the structure was solved with the ShelXT[173] structure solution program using Direct Methods and refined with the ShelXL refinement package[174] using least squares minimization. Prof. Nathan Schley performed the data collection and structure solution.

CHAPTER 5

Disappearing polymorphs in metal-organic framework chemistry

5.1 Background

Metal-organic frameworks (or MOFs) have become of interest to many chemists and companies alike due to the immense utility of these species. Owing to their often-porous structures, wide variety of metal ion and linker compatibility, and tunable synthesis to form different framework structures, MOFs have taken a fast lane to the forefront of many materials chemists' minds. The ability to use these pores for catalysis, gas adsorption, purification systems, and many more applications has also played a heavy role in the interest in MOF chemistry.[175] Farha and coworkers have demonstrated the use of MOFs to protect from mustard gas simulants via oxidation using ambient air. [176] NU-400, a zirconium-based MOF linked by pyrene-2,7-dicarboxylic acid, can completely and selectively oxidize 2-chloroethyl ethyl sulfide, a sulfur mustard simulant, to the corresponding sulfoxide completely and selectively in 50 minutes under UV irradiation in oxygen saturated conditions. When under air without oxygen presaturation, NU-400 exhibits high photocatalytic activity, even in comparison to previously explored MOFs such as NU-1000 (a mesoporous framework linked by the larger 4,4′,4′′,4′′′-(pyrene-1,3,6,8-tetrayl)tetrabenzoic acid linked framework).

MOFs are composed of metal-containing units, often referred to as secondary building units (SBUs), and organic linkers that form strong bonds to support the framework.[177] Typically, these frameworks are open crystalline materials that are permanently porous due to the extremely strong bonds made and the rigidity of the linkers. The pore sizes can be altered through either varying ratios of SBUs and linkers, reaction conditions, host solvent presence or

removal, or through post synthetic modification of the framework. There are, however, examples of MOFs that are collapsible after the removal of a guest molecule from the pore or are not porous at all. There is a large amount of debate regarding whether porosity or the presence of a porous network is the true marker of whether a species is a MOF or simply a coordination solid.[178] For the purposes of this thesis and this study, porosity will be used as a descriptor rather than a limiter.

Traditionally, metal-organic frameworks are made through solution-based methods, but with the rise of mechanochemistry many have been synthesized with the ball mill. Ball milling of metal precursors with different organic linkers has been a common method of MOF preparation. Stuart James and coworkers were able to generate a copper isonicotinic acid MOF through ball milling which contained residual water from the reaction in the pores of the system.[179] The product was of square grid (*sql-*) topology and was generated rapidly (10 min) in high purity and crystallinity. This particular synthesis was solvent-free in its entirety; however, some solvent can prove useful in MOF chemistry. 1,3,5-Benzenetricarboxylic acid (BTC) MOFs containing rare earth metals were originally prepared using solution methods requiring long reaction times (over 24 hours) and were limited to yttrium, terbium, and dysprosium. James and coworkers once again were able to synthesize these species through liquid assisted grinding (LAG) in a much shorter period in comparison to the solution preparations. In addition to these products, frameworks containing samarium, erbium, gadolinium, and ytterbium, and heterometallic species were developed. Performing the grinding experiments with different LAG additives also gave rise to different polymorphs of these MOFs. When DMF was used as the additive in the milling reaction, a porous, 3D framework was obtained; however, when water was the additive, a 2D linear framework was recovered.[46]

The focus of this chapter is zeolitic imidazolate frameworks (ZIFs) and the synthesis and properties of them. The interest in these ZIFs is due to their highly modular utility. ZIFs have been shown to be active for a surplus of catalytic transformations alone or when paired with nanoparticles as a cocatalyst. For example, Kong and coworkers were able to demonstrate that monodispersed ZIF-8 (a Zn^{2+}/MeIm framework) nanoparticles are active in catalyzing Knoevenagel condensations between benzaldehyde and malononitrile.[180] The nanoparticles were strategically prepared by dispersion in methanol, DMF, and DMSO in order to achieve unusually large nanoporosity. The study also notes that the materials made have improved hydrothermal stability and CO_2 adsorption capacity in comparison to ZIF-8 materials made by other methods.

The Friščić group has also explored ZIF application and synthesis via mechanochemistry, recently focusing on showcasing the utility of ZIFs as potential fuels sources.[181] Their work has also delved into the mechanochemical generation of many different substituted imidazolate framework species, including the synthesis of cornerstone frameworks such as ZIF-L and ZIF-8 (frameworks composed of Zn^{2+}/MeIm at varying ratios and topologies). The Friščić group has showcased that the use of resonant acoustic mixers (RAM) can increase the production of ZIF-L and ZIF-8 up to gram scale, and ZIF-L can be synthesized in 25 g quantities. With systems such as these in place, the formation of ZIFs will become more facile than ever, and will reduce the need for copious amounts of solvents. These developments will make batch scale preparations safer and environmentally sustainable.

Although there have been many advancements in the MOF and ZIF field in recent years, these investigations have not taken a look at the heavier transition and main-group metals and

their influence on structure and function of ZIFs. This chapter will take a brief look into the incorporation of heavier atoms in ZIF synthesis, and how such heavy atom ZIFs can display unique bonding motifs and shed light on the factors influencing polymorphism.

5.2 Introduction

Metal-organic frameworks are one of the most active and prolific areas of contemporary materials chemistry, due to their modular design that permits rational incorporation of a diverse range of metal ions and suitably functionalized organic linkers into functional solid-state structures.[178, 182-183] While a significant amount of effort has been invested into developing materials with new and/or improved properties,[184-187] fundamental and systematic studies of how the stability and topology of MOFs are affected by component choice and structure have remained less developed.[188-192] Popular MOF designs have mostly focused on lighter main group (*e.g.* Li,[193] Mg,[194] Al[195]) and first-row transition metals[196-200] with the exception of NbOFFIVE, UiO- and NU-type MOFs based on Nb, Zr, or Hf.[201-204] While lanthanide-based systems are known, including examples of naturally-occurring MOFs (*e.g.* the cerium-based deveroite),[205-208] and recent work has started exploring elements of the 6th period (*e.g.* Th, U, Np) as nodes, the properties and formation of MOFs with heavier members of the periodic table remain poorly explored.[209-214] Consequently, it is unknown to what extent such heavy elements are compatible with, and can bring novelty to, MOF designs. This is particularly relevant for topologically-flexible MOFs, a case in point being zeolitic imidazolate frameworks (ZIFs)[215] and other azolates,[216] that are prone to polymorphism and will adopt a wide range of topologies depending on metal and linker choice.[217-218] While it is well known that such networks can adopt different topologies depending on inclusion of solvent guests, the behavior of true

framework polymorphs, i.e., structurally different materials of identical chemical composition in which there are no included guests, remains a poorly explored area of MOF chemistry that has only recently sparked the interest of the research community.[219-226] Although the most popular ZIFs (e.g., sodalite-topology ZIF-8, ZIF-67) are based on open, microporous structures, it has been shown that their behavior reflects that of inorganic tetrahedral solids,[191-192, 227-228] with thermodynamically stable true polymorphs of such materials being dense, sometimes interpenetrated, three-dimensional (3D) frameworks of *zni-*, *dia-* or *qtz-*topology.[217-226]

We report here the unusual destabilization of such an interpenetrated, dense *dia-*topology ZIF (Figure 11a) relative to a layered structure based on two-dimensional (2D) *sql-*sheets, in a mercury(II) imidazolate framework. Stabilization of the 2D structure is due to weak interactions that include short C-H···Hg contacts, providing a unique example of intermolecular agostic interactions contributing to thermodynamic selection of a MOF structure. While the herein reported new *sql-*polymorph of mercury(II) imidazolate is readily obtained using different solution and solid-state techniques, the originally reported *dia-*topology was almost impossible to reproduce, except as a fleeting intermediate phase. The difficulty of obtaining a previously reported crystalline phase has been well documented in crystal engineering of organic molecular solids, as the "disappearing polymorph" phenomenon which is explained by the metastable nature of the first reported polymorph with respect to a subsequently observed, thermodynamically more stable, phase. As this phenomenon has to date been observed only in discrete molecular organic solids,[229-230] the herein presented work represents, to the best of our knowledge, the first documented example of the disappearing polymorph phenomenon not only in MOFs, but also in the broader context of coordination compounds and network solids.[229-230]
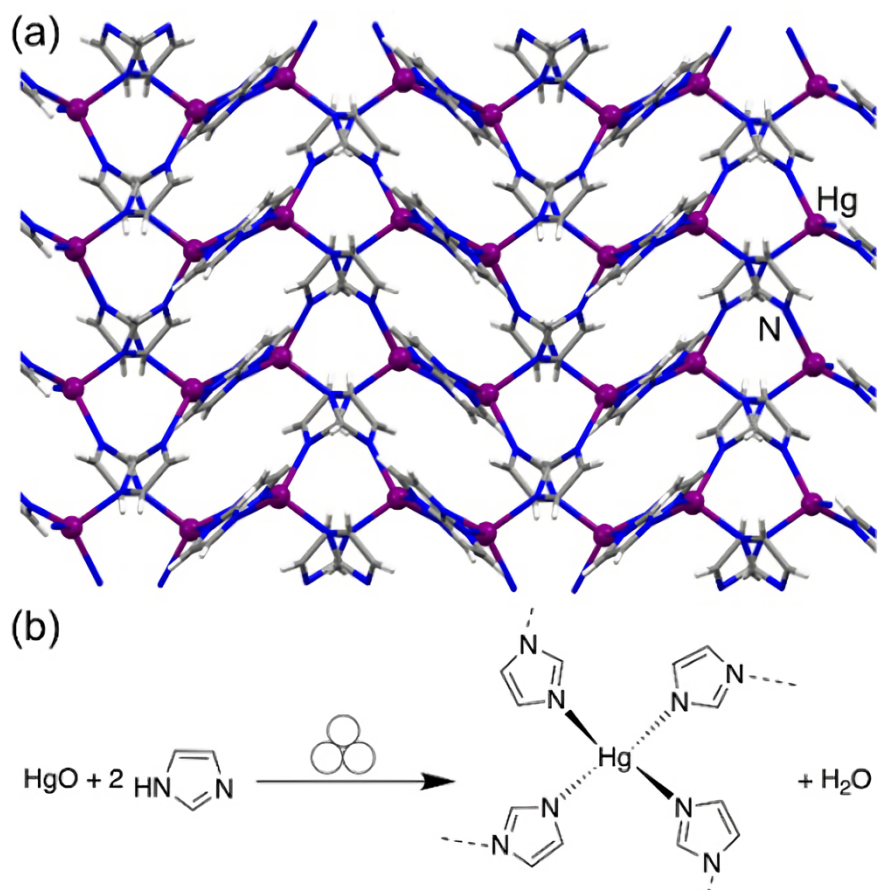
Figure 11. (a) View of the previously reported crystal structure of interpenetrated *dia*-Hg(Im)$_2$ and **(b)** the herein explored mechanochemical reaction.

Mercury (as Hg^{2+}) is attractive for investigating the effect of heavy elements on ZIF chemistry, as it is the heaviest accessible homologue of Zn^{2+}, the most extensively used node in ZIF design.[211, 214-226] As ZIFs with Cd^{2+} have also been studied,[231-233] using Hg^{2+} as a node offers a unique opportunity to explore MOF formation across an entire series of homologous transition metals.[234] To date, there has been only one report of a mercury-based imidazolate framework, the *dia*-topology mercury(II) imidazolate Hg(**Im**)$_2$.[235-237] The framework (CSD code BAYPUN) was reported to be isostructural to its cadmium analogue *dia*-Cd(**Im**)$_2$ that represents the dense, stable polymorph among several known Cd(**Im**)$_2$ structures.[231-233] Both

dia-Cd(**Im**)$_2$ and -Hg(**Im**)$_2$ were first reported in 2003 to be formed by precipitation from aqueous solution, and were structurally characterized from powder X-ray diffraction (PXRD) data by Masciocchi *et al*. (Figure 11a).[237] In 2006, Fernández-Bertrán *et al.* attempted the synthesis of Hg(**Im**)$_2$ mechanochemically,[238-239] and established that manual grinding of HgO and imidazole (H**Im**) led to partial formation of a material with hexagonal symmetry, distinct from *dia*-Hg(**Im**)$_2$.

5.3 Results and Discussion

Intrigued by the apparent difference in mechanochemical and solution-based routes to Hg(**Im**)$_2$, we re-investigated the mechanochemical reaction by ball milling HgO and H**Im** in the respective 1:2 stoichiometric ratio (Figure 11b), a methodology previously shown to be highly successful in making zinc ZIFs.[217-218] Milling was performed in a 25 mL Teflon jar, using one ZrO$_2$ ball (3.25 g). Chemical reaction upon milling was evident by a change in color of the reaction mixture from orange (due to HgO) to colorless. After 30 min milling, PXRD analysis revealed the total absence of Bragg reflections of reactants, indicating complete conversion (Figure 12a). Unexpectedly, the product exhibited X-ray reflections that did not match either the *dia*-Hg(**Im**)$_2$ structure or the product of Fernández-Bertrán *et al*.[238]
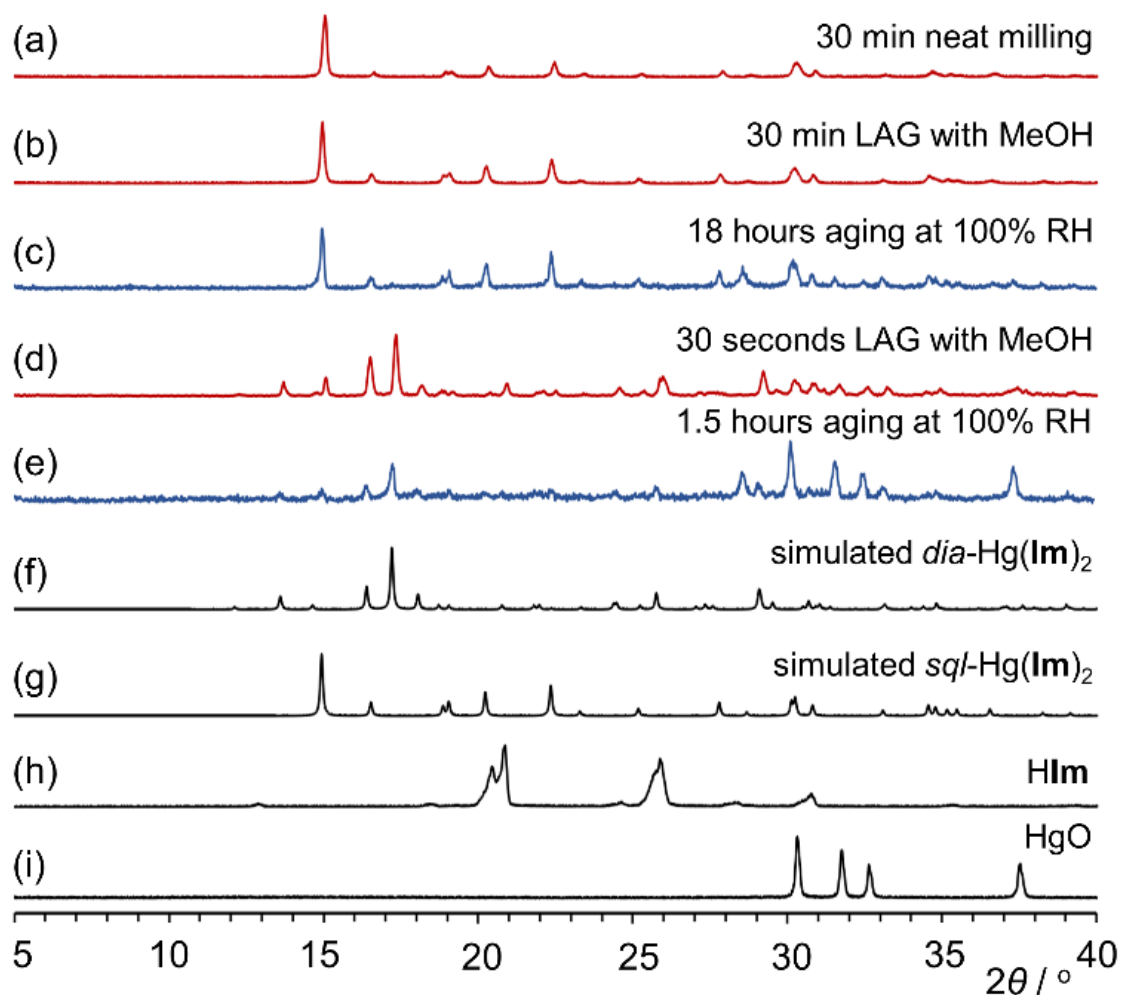
Figure 12. Comparison of selected PXRD patterns for the reactions of HgO and HIm: (a) after 30 min neat milling; (b) after 30 min LAG with MeOH; (c) after 18 h aging at 100% RH; (d) after 30 sec LAG with MeOH; (e) after 1.5 h aging at 100% RH; (f) simulated for dia-Hg(**Im**)$_2$ (CSD BAYPUN); (g) simulated for sql-Hg(**Im**)$_2$ and measured for: (h) **HIm**; (i) HgO.

The reaction was repeated with liquid-assisted grinding (LAG),[240] a method in which the reaction progress is accelerated and directed by small amounts of a liquid. The outcome of the mechanochemical reaction did not change upon LAG with different liquids, including methanol (MeOH, Figure 12b), *N,N*-dimethylformamide (DMF), acetonitrile (MeCN), or water. Moreover, attempts to prepare the known dia-Hg(**Im**)$_2$ by following the reported[237]

solution synthesis were unsuccessful, yielding a microcrystalline powder with a PXRD pattern identical to that of the material made by milling. Thermogravimetric analysis (TGA) of the product revealed no weight loss until the decomposition temperature of ca. 200 °C, indicating that the material does not contain guest solvent. Comparison of the samples with scanning electron microscopy (SEM) prepared mechanochemically and from solution revealed particles of similar block-shaped morphology. However, different methods of preparation led to differences in particle sizes: mechanochemically made material exhibited particles with sizes of ca. 200-1000 nm, whereas solution-made material consisted of elongated blocks mostly in the 10-20 μm range (see Appendix 5).

The PXRD pattern of mechanochemically prepared material was readily indexed to an orthorhombic unit cell in the space group $P2_12_12$, with $a = 9.4089(4)$ Å, $b = 7.6414(3)$ Å, $c = 5.3625(2)$ Å, and $V = 385.55(3)$ Å^3. Structure solution and Rietveld refinement revealed a polymorph of Hg(**Im**)$_2$ based on two-dimensional (2D) sheets with a square-grid (*sql*) topology (Figures 13a,b).

In contrast to the previously reported *dia*-Hg(**Im**)$_2$, in which Hg^{2+} adopts a roughly tetrahedral coordination with N-Hg-N angles in the range of 98.3-117.7° and Hg-N bonds in the range of 2.18-2.32 Å, the geometry of Hg^{2+} in *sql*-Hg(**Im**)$_2$ is highly distorted, best described as "see-saw" (Figure 13c). Specifically, the environment of each Hg^{2+} is defined by two shorter (2.18(2) Å) Hg-N bonds at an angle of 156.1(6)°, and a pair of longer ones (2.31(2) Å), at an angle of 104.6(7)° (Figure 9d).
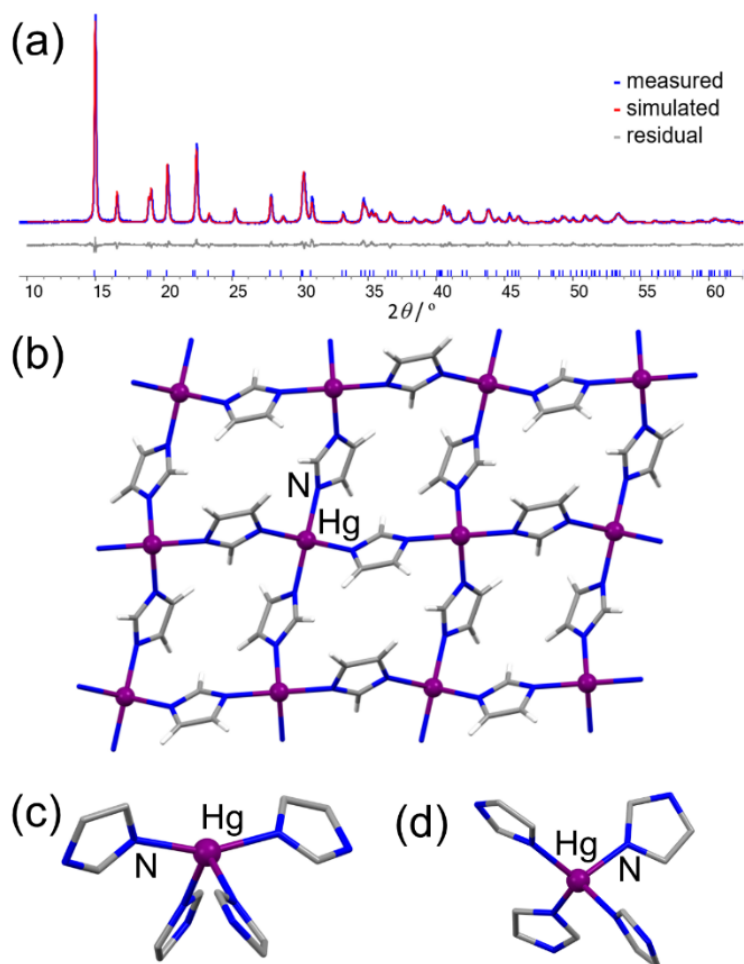
Figure 13. (a) Final Rietveld refinement fit for the structure of *sql*-Hg(**Im**)$_2$: the experimental PXRD pattern is shown in blue, the calculated pattern in red, and the difference curve in grey. (b) view of a single layer of *sql*-Hg(**Im**)$_2$ along the crystallographic *c*-axis. Comparison of the coordination geometries of the metal node in: (c) *sql*-Hg(**Im**)$_2$ and (d) *dia*-Hg(**Im**)$_2$, with hydrogen atoms omitted for clarity.
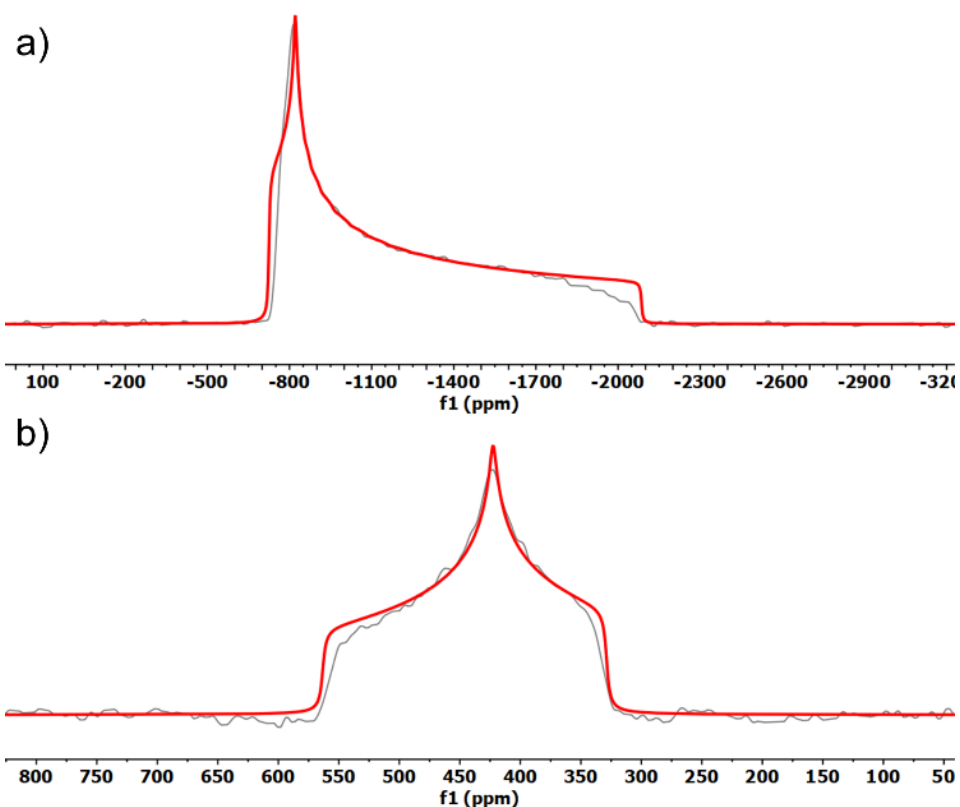
Figure 14. a) Overlay of the fit (red) to the static solid-state ^{199}Hg NMR powder pattern of *sql*-Hg(**Im**)$_2$ (grey). The pattern shows that the chemical shift tensor at the mercury nucleus has nearly axial symmetry (isotropic chemical shift δ_{iso} = -1212.5 ppm, span Ω = 1366 ppm, skew κ = 0.9); b) overlay of the fit (red) to the static solid-state ^{113}Cd NMR powder pattern of *dia*-Cd(**Im**)$_2$ (grey). The pattern shows non-axial chemical shift anisotropy (isotropic chemical shift δ_{iso} = 438.2 ppm, span Ω = 235.0 ppm, skew κ = -0.2).

The geometry can be described more quantifiably by means of the τ_4[241] and τ_4' [242] structural parameters, which are derived from metal-centered bond angles. Values of τ_4 close to 1 imply a tetrahedral geometry, those close to 0 a square planar arrangement, and intermediate values are associated with various sawhorse structures. For the *sql*-Hg(**Im**)$_2$ structure, τ_4 = 0.60 and τ_4' = 0.28. This value of τ_4 corresponds to a sawhorse geometry, slightly distorted toward a tetrahedral configuration. In this case, the low value of τ_4' indicates that the effective coordination number of the metal may actually be higher than 4, a situation first noticed in a complex with Hg$\cdots\pi$ interactions.[243] In the present case, additional short H$\cdots$Hg

contacts, described in more detail below, appear to fulfill this role. In contrast to other reported *sql*-topology ZIFs, Ni(**Im**)$_2$ (CSD ALIDUU)[244] and zinc benzimidazolate (CSD KOLYAM),[245] where neighboring layers arrange in an offset way, the sheets in *sql*-Hg(**Im**)$_2$ stack directly on top of each other (see Appendix 5). The coordination of Hg^{2+} in *sql*-Hg(**Im**)$_2$ is consistent with its axially-symmetric ^{199}Hg solid-state nuclear magnetic resonance (ssNMR) powder pattern (Figure 14a),[246] very different from the anisotropic ^{113}Cd pattern observed in *dia*-Cd(**Im**)$_2$ (Figure 14b) and which would have been expected also for the ^{199}Hg spectrum of isostructural *dia*-Hg(**Im**)$_2$.

We were surprised that all explored mechanochemical and solution-based experiments yielded only *sql*-Hg(**Im**)$_2$, without any evidence of the previously reported polymorph *dia*-Hg(**Im**)$_2$, or the hexagonal phase reported by Fernández-Bertrán.[238] Moreover, thermal analysis of *sql*-Hg(**Im**)$_2$, including differential scanning calorimetry, thermogravimetric analysis and variable-temperature PXRD all confirmed that the material retained its structure until chemical decomposition at ca. 150 °C. In contrast to unsuccessful attempts to synthesize *dia*-Hg(**Im**)$_2$, we readily reproduced the dense phase of zinc imidazolate (*zni*-Zn(**Im**)$_2$) and the dense *dia*-Cd(**Im**)$_2$ phase reported by Masciocchi *et al.*[237] and others,[229] using either mechanochemical or solution synthesis (see Appendix 5). In an attempt to reproduce any of the reported Hg(**Im**)$_2$ phases, we explored a milder synthetic route, by aging[247-248] a 1:2 stoichiometric mixture of HgO and H**Im** at 100% relative humidity. Real-time PXRD monitoring[249] (Figure 15a) revealed X-ray reflections of *dia*-Hg(**Im**)$_2$ (Figures 8e,c), and Rietveld analysis of the *in situ* data revealed that the content of *dia*-Hg(**Im**)$_2$ increases for ca. 90 min, after which it diminishes and *sql*-Hg(**Im**)$_2$ appears (Figure 15b). After 140 min, the PXRD pattern exhibits only *sql*-Hg(**Im**)$_2$. The initial, short-lived appearance of *dia*-Hg(**Im**)$_2$ in aging led us to explore the milling reaction

of HgO and H**Im** at short reaction times. Indeed, PXRD analysis after 30 seconds LAG with MeOH revealed the appearance of *dia*-Hg(**Im**)$_2$ along with unreacted HgO and H**Im** (Figure 8d). After 1 min, the reaction mixture exhibits only reflections of *sql*-Hg(**Im**)$_2$.

The difficulty in reproducing the previously reported *dia*-Hg(**Im**)$_2$ phase resembles the disappearing polymorphs[229-230] phenomenon reported in molecular organic crystalline solids, in which a first-reported polymorph is subsequently found to be metastable and difficult to reproduce compared to a later obtained, and usually more stable, polymorph. However, such behavior has not yet been reported for metal-containing systems with either molecular or network structures. So far, investigations of phase landscapes for ZIFs based on four-coordinate metal atoms have shown resemblance to zeolites and other tetrahedral structures, with the phases of greater density being the more stable ones. For *dia*- and *sql*-Hg(**Im**)$_2$, the relative stabilities are not readily deduced from their calculated densities, which are very similar: 2.87 and 2.88 g cm^{-3}, respectively. However, the difficulty in synthesizing the *dia*-phase, and the *dia*→*sql* transformation seen in aging and milling, indicates that the *sql*-form should be the thermodynamically more stable phase in the Hg(**Im**)$_2$ system.[217-218]
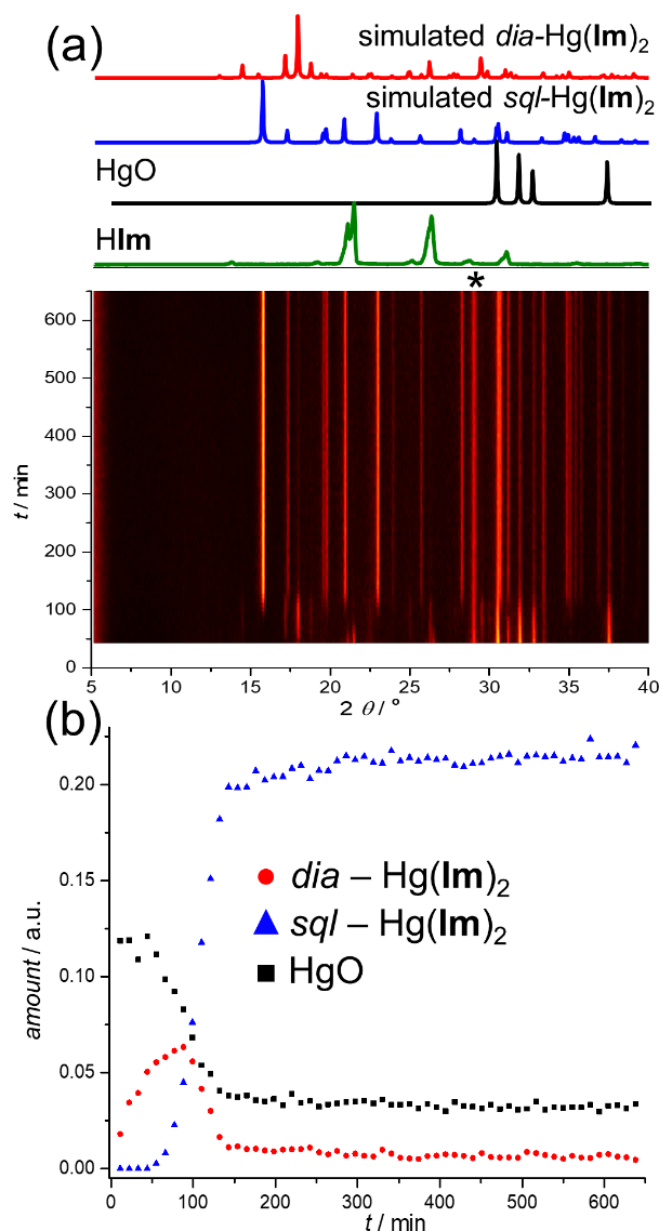
Figure 15. Real-time monitoring of the aging reaction of HgO and HIm by PXRD: (a) time-resolved diffractogram, with diffraction patterns of selected phases shown on top, and Bragg reflection of CeO_2 standard labeled with '*'; (b) reaction profile based on Rietveld fitting, demonstrating changes in amount of HgO, *dia*- and *sql*-Hg(**Im**)$_2$. Quantitative kinetics analysis was hindered by preferred orientation in the static reaction mixture.

The stability of the *sql*-form was supported by slurry shaking experiments, as there were no changes in sample PXRD patterns upon shaking of *sql*-Hg(**Im**)$_2$ in either water or common organic solvents (MeOH, ethanol, CH_3CN, $CHCl_3$, acetone) over two days (see Appendix 5).

74

The stability of *sql*-Hg(**Im**)$_2$ was also validated by periodic density functional theory (DFT) calculations, performed with the periodic DFT code CRYSTAL17[250] using the hybrid B3LYP[251-252] functional combined with the Grimme D3 semiempirical dispersion correction,[253] which showed that the *sql*-form is 10.21 kJ mol^{-1} lower in energy than the *dia*-one. This contrasts with Zn(**Im**)$_2$[254] and Cd(**Im**)$_2$, whose most stable forms exhibit three-dimensional (3D) *zni*- and *dia*-topologies, respectively. The unexpected difference between our study and previous reports on Hg(**Im**)$_2$ prompted us to perform similar calculations on the known *dia*-Cd(**Im**)$_2$, as well as on the hypothetical *sql*-Cd(**Im**)$_2$ structure that was obtained by DFT optimization of a structural model obtained by replacing all mercury atoms in *sql*-Hg(**Im**)$_2$ with cadmium. In this case, the two structures were found to have essentially indistinguishable energies, with *sql*-Cd(**Im**)$_2$ being just 0.39 kJ mol^{-1} more stable. The improved stability of the *dia*-structure in Cd(**Im**)$_2$ is consistent with the herein confirmed experimental reproducibility and multiple previous observations of *dia*-Cd(**Im**)$_2$.[231-233]

Stabilization of the 2D *sql*-structure in Hg(**Im**)$_2$, compared to a more extensively connected, interpenetrated 3D *dia*-framework, is unexpected and, we believe, associated with weak interactions between layers. This view is supported by calculations of the relative stabilities of *dia*- and *sql*-Hg(**Im**)$_2$ using the B3LYP functional uncorrected for dispersion. Under such conditions, which artificially ignore the contributions of van der Waals interactions, the stabilities of the two structures become inverted, with the *dia*-form becoming 7.81 kJ mol^{-1} more stable.

Whereas the *sql*-Hg(**Im**)$_2$ structure reveals short contacts between neighboring layers, readily interpreted as C-H$\cdots\pi$ and $\pi\cdots\pi$ interactions, it also exhibits short H$\cdots$Hg contacts at

3.26(3) Å, not present in the *dia*-form. Each Hg atom participates in two such contacts with symmetry-related imidazolate groups (Figure 16). Most proposed van der Waals radii for Hg range from 2.00 to 2.53 Å,[255-256] indicating that these contacts might be roughly 10% shorter than the sum of van der Waals radii of H (1.20 Å) and Hg. The shortness of these contacts lends itself to two possible explanations. The contacts can be interpreted either as hydrogen-bonding interactions of the C-H···Hg type, where the σ*-orbital C-H moiety is interacting with available electron density on the metal atom, or a C-H···Hg agostic interaction,[257-258] where the empty orbitals on the metal ion are associated with the σ-electron density of the C-H bond.[259-261] Of these two interpretations, the formation of weak agostic bonds is the more likely one, as the Hg atom is expected to be electron-deficient in its +2 oxidation state and when associated with four electronegative azolate ligands.
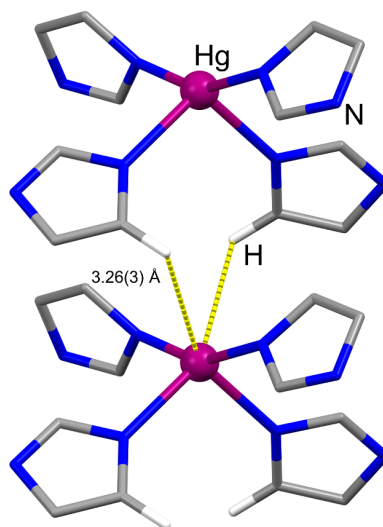
Figure 16. Fragment of the crystal structure of *sql*-Hg(Im)$_2$ illustrating the short H···Hg contacts between neighboring metal-organic layers. Hydrogen atoms, except the ones relevant for illustrating the H···Hg contacts, have been omitted for clarity.

To better understand the nature of C-H···Hg interactions as well as the unique appearance and energetic stability of *sql*-Hg(**Im**)$_2$, as opposed to its hypothetical *sql*-Cd(**Im**)$_2$ analogue, we performed Bader's quantum theory of atoms in molecules (QTAIM)[262-263] analysis on the DFT-optimized structures. Specifically, we searched for bond critical points (BCPs) as evidence for structure-stabilizing interactions. The experimental *sql*-Hg(**Im**)$_2$ structure and the computationally generated isostructural *sql*-Cd(**Im**)$_2$ structure display a very similar distribution of non-covalent BCPs (Figure 17), with the exception of one BCP in the vicinity of the Hg atom (Figure 17a). This critical point, which is the highest in the *sql*-Hg(**Im**)$_2$ structure, reveals a moderate bonding interaction (0.074 electrons Å^{-3}) between the C-H group and the Hg atom in neighboring layers (Figures 17a,b, see also Appendix 5). This BCP coincides with the experimentally noted short H···Hg contact between layers and, importantly, it is retained regardless of whether the dispersion correction is applied in structure optimization or not. The second highest BCP in the *sql*-Hg(**Im**)$_2$ structure is also located near the metal atom, but clearly represents a stabilizing C-H···N hydrogen bonding interaction.

The electron density analysis is different for the putative *sql*-Cd(**Im**)$_2$ structure, which does not exhibit any BCPs involving the metal center. Instead, the highest BCP in the *sql*-Cd(**Im**)$_2$ structure overlaps with the second-highest BCP of *sql*-Hg(**Im**)$_2$ and corresponds to a stabilizing C-H···N hydrogen-bonding interaction between the metal-organic sheets (Figures 17c,d, see also Appendix 5).
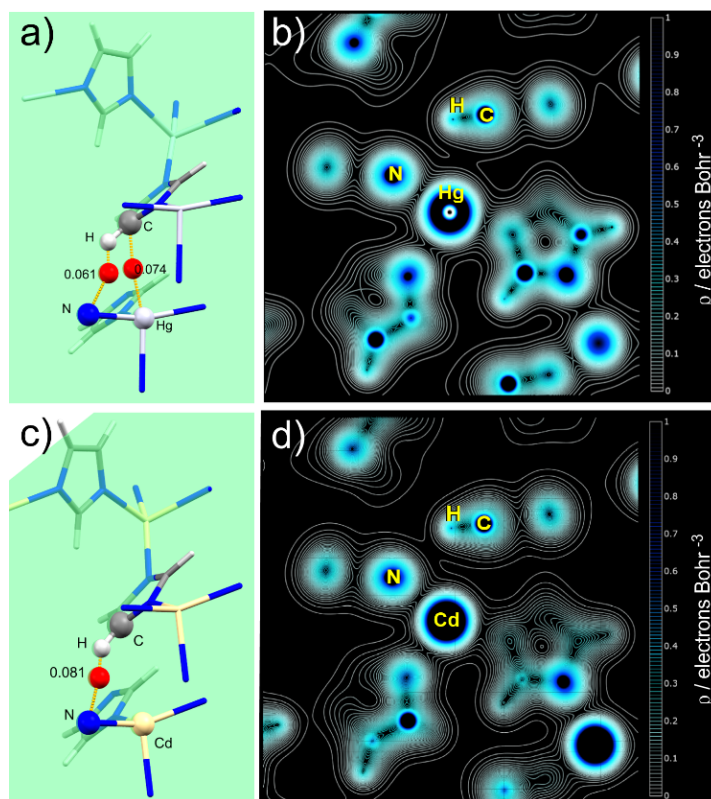
Figure 17. The highest bond critical points (BCPs) for the experimental *sql*-Hg(Im)$_2$ and theoretically generated *sql*-Cd(Im)$_2$ structures: a) structure plot showing a C-H$\cdots$Hg bonding interaction with a BCP with electron density (ρ) of 0.074 electrons Å^{-3} as well as a C-H$\cdots$N bonding interaction with a BCP with ρ of 0.061 electrons Å^{-3} in *sql*-Hg(**Im**)$_2$; b) 2D contour plot showing the electron density distribution in *sql*-Hg(**Im**)$_2$. c) Structure plot showing a C-H$\cdots$N bonding interaction with a BCP with ρ of 0.081 electrons Å^{-3} in *sql*-Cd(**Im**)$_2$; d) 2D contour plot showing the electron density distribution in *sql*-Cd(**Im**)$_2$. In all cases the green plane shows the orientation of the contour plot slices. The plots indicate that the dominant interaction between the 2D layers of *sql*-Hg(**Im**)$_2$ framework occurs *via* the metal atom, in contrast to the hypothetical analogous structure based on cadmium (see Appendix 5).

The Bader analysis shows that the short H$\cdots$Hg contacts in *sql*-Hg(**Im**)$_2$ are clearly of a stabilizing nature, and the positioning of their corresponding BCPs indicates a "side-on" interaction of the hydrocarbon moiety and the Hg atom, which implies the participation of the C-H bond σ-electron density. Finally, the pair of short C-H$\cdots$Hg contacts in *sql*-Hg(**Im**)$_2$ can be interpreted as completing the unusual see-saw geometry, established by nitrogen azolate ligands, into a distorted octahedron. All of these observations are consistent[261] with the appearance of weak C-H$\cdots$Hg agostic bonds[257-258, 261, 263-265] between metal-organic layers, that

contribute to the overall stabilization of the *sql*-Hg(**Im**)$_2$ structure. As BCPs corresponding to such stabilizing contacts do not appear in the hypothetical *sql*-Cd(**Im**)$_2$ structure, they also provide a possible explanation for the difference in structural preferences of dense phases of mercury(II) and cadmium(II) imidazolates.

5.4 Conclusion

In summary, a re-investigation of an early report of mechanochemical MOF formation has revealed a novel, layered polymorph of a unique mercury(II) imidazolate framework. Experiment and theory indicate that the layered polymorph is thermodynamically more stable than the previously reported interpenetrated *dia*-framework, evidently due to weak intermolecular forces that include interlayer agostic C-H···Hg contacts. At the same time, we were unable to obtain the originally reported *dia*-structure in pure form and have observed it only as a fleeting intermediate during solid-state synthesis, sometimes not lasting more than a minute. The difficulty in reproducing the *dia*-polymorph makes mercury(II) imidazolate, to the best of our knowledge, the first documented example of the disappearing polymorph phenomenon in coordination chemistry. This new parallel with crystal engineering of organic solids[266] is of high relevance for the ongoing commercialization of MOFs.[175] By analogy with organic pharmaceutical solids,[230] where polymorphism and problems of phase nucleation[267] are recognized as major challenges in their development and industrial manufacture, the discovery of the disappearing phenomenon in coordination networks is of relevance in the commercial development of MOFs, as some of the previously reported materials might prove difficult to reproduce.

The demonstrated stabilization of a layered structure makes a striking contrast between Hg^{2+} and its congeners Cd^{2+} and Zn^{2+}, whose imidazolates in their most stable form favor 3D frameworks, highlighting the potential for differences in MOF formation when using a heavy element compared to its lighter congeners, and suggesting a possible role for even weak agostic interactions[257-263] in directing polymorphism in MOF structures. We believe that the results of this work are of significance for understanding the formation of layered MOFs, which have recently become of considerable interest as functional materials,[268-270] and are pursuing further studies of systems based on heavy elements.

5.5 Experimental

General Considerations. The herein provided information is a general overview of selected procedures only. More extensive descriptions and data on experimental and computational procedures, structure analysis, as well as selected X-ray diffraction, infrared and solid-state NMR spectroscopy data are provided in Appendix 5.

Crystallographic data. CCDC 1948341 *sql*-Hg(**Im**)$_2$ contains the supplementary crystallographic data for this chapter. These data can be obtained free of charge from the Cambridge Crystallographic Data Centre.

Materials. HgO (≥99%) and imidazole (**HIm**) (≥99%) were purchased from Aldrich. Methanol (MeOH), *N*,*N*-dimethylformamide (DMF), and acetonitrile (MeCN) were purchased from ACP Chemicals. All chemicals were used without further purification. *Mercury compounds should be treated with rigorous safety precautions due to their toxicity.* Care was taken at all times to avoid contact with solid, solution, and air-borne particulate mercury compounds. All reactions, equipment, and waste were treated and disposed of properly.

Mechanochemical protocol. Reactions were conducted in a Teflon milling jar of 25 mL volume, using one 7 mm diameter (weight ~3.2 g) zirconia ball, and either a Retsch MM400 or Retsch MM200 mill operating at 25 Hz. In a typical experiment, a solid mixture of HgO (108.3 mg, 0.50 mmol) and H**Im** (68.1 mg, 1.00 mmol, 1:2 stoichiometric ratio with respect to total mercury content) was placed in a 25 mL Teflon jar along with either 50 μL of MeOH, MeCN, DMF, water, or no additive, and the reaction mixture was milled for a period of 30 min. The material was analyzed without further treatment.

Synthesis of *sql*-Hg(Im)₂ from solution. A 250 mL round bottom flask was charged with a Teflon stirring bar, mercury(II) acetate (5.00 g, 15.7 mmol, 1 equiv.), and H**Im** (4.25 g, 62.4 mmol, 4 equiv.). Next, 100 mL of de-ionized water was added to the flask and the solution was stirred. Aqueous ammonia (28% v/v) (7.01 mL, 68.1 mmol) was added slowly down the side of the flask. The reaction was allowed to stir at ambient temperature for 3 h. The reaction was then filtered and the isolated material was washed twice with 25 mL portions of de-ionized water, washed once with 25 mL of methanol and then dried.

Reactions by aging. Samples of HgO (108.3 mg, 0.50 mmol, 1 equiv.) and H**Im** (68.1 mg, 1 mmol, 2 equiv.) were ground separately in a mortar and pestle. The two solids were placed in a vial along with CeO₂ (17.6 mg, 10% w/w) as an internal X-ray diffraction standard. The mixture was agitated in a vial to create a homogenous mixture. A small portion of the mixture was then transferred to a custom designed PXRD sample holder[271] with two grooves ground into the surface. In each groove was placed 200 μL of water to act as a source of humidity. The holder was covered with a small sheet of Saran wrap to seal the chamber and generate a

saturated humidity atmosphere. Samples were aged under this atmosphere for 17.5 h, with PXRD patterns recorded periodically every 11.4 min.

(This work was adapted from Speight, I. R., et al. *Chem.– Eur. J.* **2020**, 26, 1811-1818).

Section A1

A Diverse View of Science to Catalyse Change

A1.1 Introduction

From the structure of DNA[272], to computer science[273], and space-station batteries[274], several key scientific discoveries that enhance our lives today, were made by marginalized scientists. These three scientists, Rosalind E. Franklin, Alan M. Turing, and Olga D. González-Sanabria, did not conform to the cultural expectations of how scientists should look and behave. Unfortunately, marginalized scientists are often viewed as just a resource rather than the lifeblood that constitutes science itself. Thinking of the future and all the life-threatening societal challenges that lie ahead, it is clear that we need to embrace scientists from all walks of life and corners of the globe. An awareness of science policy is essential to safeguarding our future.

Science policy deals with creating the framework and codes of conduct that determine how science can best serve society[275,276-277]. Discussions around science policy are often accompanied by anecdotes of 'good' and 'bad' practices regarding the merits of diversity and inclusion. Excellence and truth, which flow inexorably from diversity and inclusion, are the bedrocks upon which science should influence political and economic outcomes. A vital area of science policy is to support the professional development of marginalized scientists, an objective that must be acted upon by scientific leaders and communicators.

A1.2 Diversity 101

To paraphrase Zimmerman and Anastas[278] on the topic of green chemistry, if people are confused about what diversity, equity, and inclusion (DEI) are, it is difficult to imagine that from confusion will arise a clear path on how to implement them. If we want to achieve DEI in science, we need to be clear about the definitions of the following key terms.

Diversity. The ways in which people differ, encompassing all the characteristics that make one individual or group distinctive[279]. The dimensions of diversity include, but are not limited to (i)

83

ethnic or national origins, skin color or nationality, (ii) gender, gender identity, and gender expression, (iii) sexual orientation, (iv) background (socio-economic status, immigration status, or class), (v) religion or belief (including absence of belief), (vi) civil or marital status, (vii) pregnancy and maternity, paternity, parental leave, and (viii) age and (ix) disability[280].

Equity. The fair treatment, access and opportunity that leads to the advancement of all peoples. Equity is about striving to identify and remove barriers that have prevented the full participation of some groups. Improving equity means increasing justice and fairness within the processes of institutions or systems, as well as communication and sharing of resources. Addressing issues of equity requires a deep understanding of the sources of disparity in our society[281].

Inclusion. The act of creating an environment in which any individual or group feels (i) welcomed, (ii) safe, (iii) supported, (iv) respected and (v) valued to participate. An inclusive and welcoming culture embraces differences and offers respect in words and actions to all people. It is important to note that while an inclusive group is by definition diverse, a diverse group is not always inclusive. Increasingly, recognition of implicit bias helps organizations to be constructive about addressing issues of inclusion[282].

Implicit bias. People are not neutral in judgement and behavior, but instead have experience-based associations and preferences or aversions without being consciously aware of them[283].

Microaggressions. These are often manifestations of implicit bias, typically in the form of comments or actions[284].

Marginalized scientists. Scientists who are at the periphery of social, economic and scientific discussions.

The reason marginalized scientists leave science, technology, engineering and mathematics (STEM) is not an accident. It results from the historic expectations of how a scientist should be perceived[285] and, in turn, the different treatment of scientists who don't conform to those expectations. The pursuit of equity will dismantle these beliefs, driving policy development and creating equal access to positions of leadership and opportunities for all.

This article is a message for (i) current and future scientists, (ii) students, mentors and educators, (iii) science communicators, (iv) publishers and (v) science policy makers. It has two purposes: (1) Provide marginalized scientists and their allies with a space to talk about their approach towards scientific advancement, mentorship and how to challenge systemic injustice, and (2) Provide actionable advice to implement equity in academia and related businesses and organizations.

A1.3 Identifying and quantifying inequity

Science can only expand the research questions and problems defined as important with a broad pool of life experiences and knowledge. Non-diverse academic environments are closed communities that reinforce traditional stereotypes of who gets to be a scientist. This situation is analogous to the political science phenomena known as 'echo chambers'[286]. Each country has its own demographics, and consequently the make-up of marginalized populations may differ. Most well-represented scientists — that means scientists that conform to the cultural expectations of how scientists should look and behave — do not know or understand the challenges that exist for marginalized scientists. The first step towards beginning to understand these challenges is to listen to marginalized scientists. This must then be followed by collecting reliable data, informed by the individual experiences of marginalized scientists[287-288].

For example, in the UK, a 2018 report by the Royal Society of Chemistry (RSC) noted that the percentage of students from minority groups falls from 26% at the undergraduate level to 14% at the postgraduate level[289]. Unfortunately, this study was not able to show the ethnicity data for staff in higher-education settings. This incomplete dataset highlights the need for transparent and consistent reporting of DEI data from universities. The RSC also shared that the percentage of minority ethnic chemical scientists in academia appears to drop significantly with increasing career stage[268]. Meanwhile, in the US, a study by *C&EN* found that 12.3% of the US population is Black, yet only 1.6% of chemistry professors at the top 50 US universities are Black[290].

Mapping the diversity landscape of academia across hierarchies is vital to understanding the severity of the underrepresentation of marginalized scientists. This data should be collected and reported on a regular basis so that progress can be monitored transparently. This

information gathering will give organizations a quantitative perspective of diversity in their communities, and provide context to create equitable policies and practices.

A1.4 Supporting marginalized scientists

Discrimination and lack of social connections in the scientific community have a negative impact on the experiences and performance of marginalized scientists[291-293], ranging from poor physical and mental health, to low self-esteem[294-296]. The psychological cost of not feeling socially or professionally connected is impactful, persistent, and has a similar effect as physical pain[294, 297]. Regardless of minority status, marginalized populations experience a higher amount of stress[298].

Every member of the scientific community has a duty to act and create support structures that promote the career development of marginalized scientists. Below are some examples of specific support systems, and how they play a key role in a marginalized scientist's career.

Mentorship. Supporting the personal and professional growth, development and success of scientists through the provision of career and mental-health advice[299]. Mentorship has an overall positive effect on retention and career success of mentees across STEM disciplines[272]. Despite current efforts in DEI, however, marginalized individuals enrolled in STEM degree programs typically receive less mentorship than their well-represented peers[300-301]. Research has shown that marginalized scientists already dedicate more hours of service engaging in invisible work, including mentorship, than their peers[302-303]. This imbalance reduces their available time to perform tasks that are deemed more valuable for career progression. Mentoring marginalized scientists should also be the responsibility of well-represented scientists.

Online peer communities. Communities such as #ScienceTwitter are free resources to build connections, learn about career opportunities, and share expert advice[304]. These platforms can increase the visibility and reach of scientific work[305]. Scientists can increase their visibility and use their audience to promote marginalized colleagues.

Financial support. The barriers for marginalized scientists pursuing and engaging in scientific careers can be reduced through financial support[306]. Scientists and scientific organizations need

to create and promote equitable financial aid opportunities that support marginalized scientists in career development and be mindful of the costs of participating in networking events.

Effective inclusion and diversity support. These systems can identify, and address, the negative experiences of marginalized researchers; they must be approachable, trustworthy and accountable. Research suggests that such support is best provided through independent and impartial structures[279].

Recognizing the work of marginalized scientists. It is crucial that the achievements of marginalized scientists be valued, respected and credited appropriately[307-308]. This recognition involves (i) reading their work, (ii) engaging in their discoveries, (iii) cooperating in joint research projects, (iv) citing their work and (v) nominating them for leadership positions and awards.

A1.5 Expanding and redefining excellence

Excellence in science is often equated to fundamental discoveries with broad societal impact. The conventional view of excellence was historically shaped within non-diverse communities that celebrate heroes of science like Isaac Newton, Thomas Edison, and Albert Einstein as pop-culture icons — geniuses isolated from societal context[309]. This narrow perception of excellence results in funneling of resources into the hands of already recognized, established and well-represented scientists — the perceived heroes of tomorrow. Further, it limits the progress of science and the development of fundamentally new ideas, and interdisciplinary fields of investigation[310].

Diversity in science has helped to bring forward advances in areas that the well-represented cannot fathom, because they do not share the problems and perspectives of marginalized scientists. Furthermore, the technical and societal problems that marginalized scientists value are not weighted equally. It is not only that well-represented scientists have a narrower conception of what constitutes excellence, but also many of them will fail to attain the level of excellence that the achievements of marginalized scientists already have in contemporary society.

If we want to renew our understanding of excellence, we must also renew the composition of the bodies that define it. This renewal could be achieved through the tenure and promotion process. In order for the promotion process to be equitable, all the achievements of scientists in research, teaching, and service must be included in the redefinition of excellence[311].

Academics should care about DEI because marginalized scientists matter. Academia has been slower to embrace diversity than the private sector where diversity has been linked to the financial bottom line, in that the more diverse the corporation, the more valuable and profitable is the company[312]. A broad understanding of excellence embraces the diversity of the creators and beneficiaries of science. As institutions redefine excellence to include all, the benefits for all will be tremendous[267-313].

A1.6 Inclusion in the publishing space

Scientific communication throughout the mass media and academic outlets remains the fundamental pillar of the relationship between scientists and society[314]. Participants in the publishing process, however, do not yet universally reflect the diversity of the scientific community, which itself does not reflect the diversity of society as a whole[315]. This lack of diversity reduces the participation of marginalized groups when it comes to publishing. Their inclusion will not occur until stakeholders from all parts of the scientific community are represented at all levels of the publishing process. This change means: (i) shaping journal policies, (ii) influencing daily operations, (iii) choosing reviewers, (iv) giving guidance to editorial staff and (v) hiring more diverse teams. Marginalized scientists need to play leadership roles in the establishment of advisory and editorial boards within publishing houses.

Journals can create a more equitable and trustworthy publishing process by stating their mission initiatives clearly and making direct statements addressing any kind of bias against marginalized groups. These statements should be updated annually and be supported by data analysis on the diversity of (i) frontline editorial teams, (ii) reviewers, and (iii) authors both of submitted manuscripts and accepted articles. Given this transparent information, publishers can identify biases and take steps to eliminate them. A larger and equitable talent pool would also unburden the marginalized scientists who are currently stretched thin across editorial positions.

A1.7 Conclusion

The uptake of DEI support structures has started to address shortcomings, and we see an upward — but often anecdotal — trend in the inclusion of some marginalized groups in STEM. These efforts, however, focus on dealing with the consequences, rather than eliminating systemic discrimination and implicit bias in academia[316]. All scientists can contribute to reducing the impact of implicit bias by accepting, learning, and identifying their own biases through active and continuous self-assessment. For example, Project Implicit, a non-profit organization, has developed a set of online tools for understanding attitudes, stereotypes and other hidden biases that influence perception, judgment and action[317].

Reducing the inequalities in STEM requires a data-based, holistic approach to DEI. We all need to become advocates of marginalized scientists and give them equitable opportunities to advance their careers because it is ultimately the right thing to do. Additionally, the result will not only be a broader pool of future talents, but also an unprecedented level of excellence that a more colorful and inclusive scientific community can attain.

We have collected statements from scientists that come from all walks of life to share how they value DEI initiatives. These statements contain individual calls to action, as well as broader advice to the younger scientists. We hope that you find them interesting and, in the words of Michael Polanyi[318], use them for "coordination by mutual adjustment of independent initiatives." Let us use these statements to learn from each other as we do in science.

(This work was adapted from: Urbina-Blanco, C. A.; Jilani, S. Z.; Speight, I. R.; et al., *Nature Chem.*, **2020**, 12, 773-776; *J. Am. Chem. Soc.,* **2020**, 142, 34, 14393-14396; *Chem. Sci.,* **2020**, 11, 9043-9047; *Angew. Chem. Int. Ed.* **2020**, 59, 18306-18310; *Can. J. Chem.,* **2020**, 98, 10, 597-600; *Croat. Chem. Acta,* **2020**, 93, 1, 77-81.)

Appendix A2

Supplementary information for Chapter 2
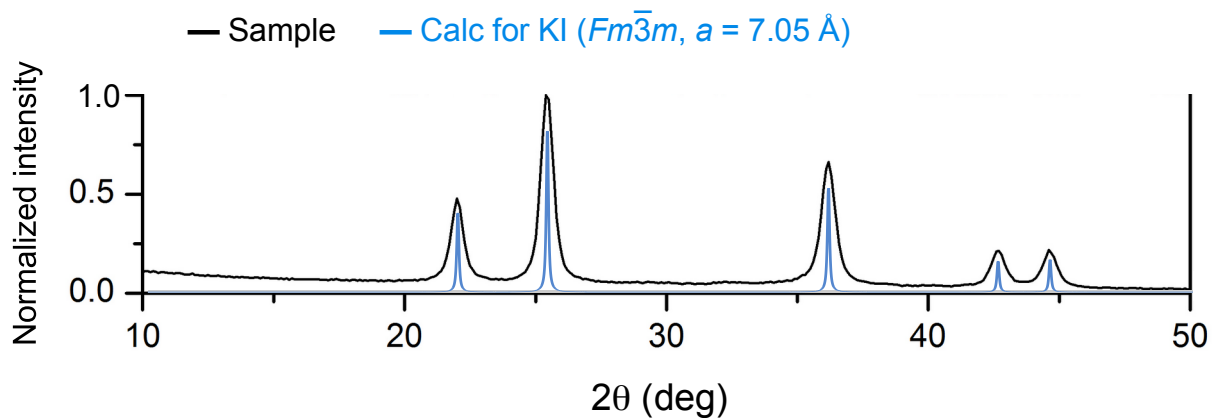
Figure 18. Powder XRD of unextracted milled sample (1 CaI$_2$: 2 K[N(TMS)$_2$])

Table 5. Crystal data and summary of X-Ray collection for K{Ca[N(TMS)$_2$]$_3$}

Identification code	vand70	
Empirical formula	C$_{18}$H$_{54}$CaKN$_3$Si$_6$	
Formula weight	560.36	
Temperature	123(2) K	
Wavelength	0.71073 Å	
Crystal system	Triclinic	
Space group	$P\overline{1}$	
Unit cell dimensions	a = 8.6477(8) Å	α = 93.148(5) °
	b = 11.2357(9) Å	β = 91.419(2) °
	c = 19.398(2) Å	γ = 111.817(2) °
Volume	1745.0(3) Å^3	
Z	2	
Density (calculated)	1.066 g/cm^3	
Absorption coefficient	0.516 mm^{-1}	
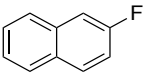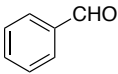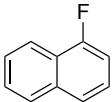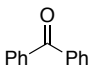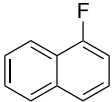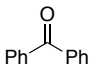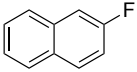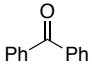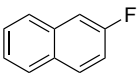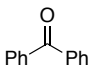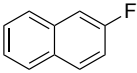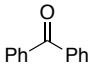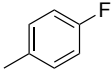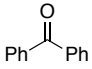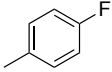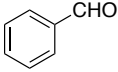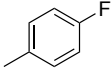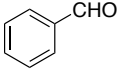
F(000)	612
Crystal size	0.32 x 0.28 x 0.24 mm^3
Crystal color, habit	Colorless block
Theta range for data collection	1.96 to 27.01 °
Index ranges	$-11 \leq h \leq 10, -14 \leq k \leq 14, 0 \leq l \leq 24$
Reflections collected	25 442
Independent reflections	7444 [R(int) = 0.0000]
Completeness to theta = 25.00 °	99.8 %
Absorption correction	Multi-scan
Refinement method	Full-matrix least-squares on F^2
Data / restraints / parameters	7444 / 0 / 263
Goodness-of-fit on *F*^{2}	1.062
Final R indices [*I*>2sigma(I)]	R$_1$ = 0.0327, *w*R$_2$ = 0.0794
R indices (all data)	R$_1$ = 0.0422, *w*R$_2$ = 0.0840
Largest diff. peak and hole	0.358 and -0.289 e Å^{-3}
Twinning	Full rotational twin (50/50)

Appendix 3

Supplementary information for Chapter 3

Table 6. Carbonyl addition attempts with mechanochemically generated Grignard reagents.

Aryl Fluoride	Electrophile	Deviations	Reaction Time (1st step / 2nd step)
		None	2 h / 15 min
		Three, 8 mm stainless steel ball bearings (3.3 g ball^{-1}) were used. Second step milled at 15 Hz.	2 h / 15 min
		Three, 8 mm stainless steel ball bearings (3.3 g ball^{-1}) were used. First and second step milled at 15 Hz.	2 h / 15 min
		Second step stirred in THF with electrophile.	2 h / 1 h
		Second step stirred in diethyl ether w/ 0.7 equiv. electrophile.	2 h / 4 h
		First step milled w/ 2.25 equiv. LiCl. Second step stirred in diethyl ether with electrophile.	2 h / 1 h
		First step milled w/ 0.5 equiv. BF$_3$•OEt$_2$. Second step stirred in THF w/ 0.5 equiv. electrophile.	1 h / 1 h
		First step milled w/ 0.5 equiv. BF$_3$•OEt$_2$. Second step stirred in THF w/ 0.5 equiv. electrophile.	1 h / 1 h
		First step milled w/ 0.5 equiv. BF$_3$•OEt$_2$. Second step stirred in THF w/ 0.5 equiv. electrophile.	2 h / 1 h

| | | First step milled w/ 0.5 equiv. AlCl₃. Second step stirred in THF w/ 0.5 equiv. electrophile. | 1 h / 48 h |
| | | First step milled w/ 0.5 equiv. AlCl₃. Second step stirred in THF w/ 0.5 equiv. electrophile. | 1 h / 48 h |

Optimized conditions can be found in 3.4 Experimental.

Table 7. Coordinates of geometry-optimized structures

(1-Napth)MgF   E = -685.2725495 au

C	-1.694462	2.132906	0.000000
C	-1.349022	0.808442	0.000000
C	0.000000	0.383273	0.000000
C	1.007829	1.394115	0.000000
C	0.627998	2.754996	0.000000
C	-0.690998	3.120149	0.000000
H	-2.737978	2.424219	0.000000
H	-2.140610	0.059085	0.000000
C	0.355035	-0.999560	0.000000
C	2.364658	1.002361	0.000000
H	1.405979	3.511030	0.000000
H	-0.967609	4.167702	0.000000
C	2.704353	-0.321758	0.000000
C	1.699938	-1.312292	0.000000
H	3.130637	1.770362	0.000000
H	3.748127	-0.615519	0.000000
H	2.025210	-2.349610	0.000000
Mg	-1.121802	-2.447352	0.000000
F	-2.350455	-3.708316	0.000000

(1-Napth)MgBr   E = -3159.6043071 au

C	3.044587	1.143825	0.000000
C	1.735420	0.744593	0.000000
C	1.366701	-0.620956	0.000000
C	2.417361	-1.586830	0.000000
C	3.761529	-1.151502	0.000000
C	4.072002	0.181413	0.000000
H	3.293132	2.198319	0.000000
H	0.954148	1.505060	0.000000
C	0.000000	-1.033111	0.000000
C	2.080613	-2.958515	0.000000
H	4.548895	-1.897743	0.000000
H	5.107255	0.500960	0.000000
C	0.771405	-3.352012	0.000000
C	-0.259426	-2.388927	0.000000
H	2.879102	-3.692626	0.000000
H	0.520268	-4.406836	0.000000
H	-1.282944	-2.755056	0.000000
Mg	-1.494384	0.393345	0.000000
Br	-3.200811	1.998855	0.000000

(2-Napth)MgF   E = -685.270615

C	-3.353126	-1.674406	0.000000
C	-2.090985	-2.204436	0.000000
C	-0.955493	-1.364634	0.000000
C	-1.140343	0.045475	0.000000

94

C	-2.455887	0.561051	0.000000
C	-3.537757	-0.277341	0.000000
H	0.509303	-2.944942	0.000000
H	-4.217099	-2.328488	0.000000
H	-1.945636	-3.279256	0.000000
C	0.363090	-1.869457	0.000000
C	0.000000	0.883432	0.000000
H	-2.594408	1.637029	0.000000
H	-4.541909	0.130065	0.000000
C	1.292255	0.393492	0.000000
C	1.439210	-1.022976	0.000000
H	-0.192373	1.954990	0.000000
H	2.432266	-1.464277	0.000000
Mg	2.900952	1.687924	0.000000
F	4.263626	2.802066	0.000000

(2-Napth)MgBr   E = -3159.6022192

C	-5.076790	0.144234	0.000000
C	-4.191758	1.188671	0.000000
C	-2.799020	0.954556	0.000000
C	-2.325112	-0.386539	0.000000
C	-3.264228	-1.442194	0.000000
C	-4.608562	-1.184807	0.000000
H	-2.209115	3.027239	0.000000
H	-6.143276	0.336051	0.000000
H	-4.549367	2.212559	0.000000
C	-1.852388	2.002239	0.000000

C	-0.928990	-0.617043	0.000000
H	-2.900498	-2.464192	0.000000
H	-5.319044	-2.002988	0.000000
C	0.000000	0.406033	0.000000
C	-0.509440	1.735509	0.000000
H	-0.614077	-1.659124	0.000000
H	0.176287	2.578452	0.000000
Mg	2.018717	-0.020021	0.000000
Br	4.304920	-0.531192	0.000000

(1-Napth)₂Mg   E = -970.6598966

C	0.661013	4.256252	-2.364660
C	0.102360	4.902032	-1.294841
C	-0.239851	4.200607	-0.116925
C	0.000000	2.795409	-0.040294
C	0.581296	2.171988	-1.170082
C	0.904787	2.871167	-2.301716
H	-0.998792	5.920723	0.939262
H	0.918150	4.807242	-3.261542
H	-0.086644	5.969575	-1.337049
C	-0.816533	4.852809	0.995170
C	-0.337804	2.054776	1.134116
H	0.782181	1.101325	-1.140495
H	1.349130	2.362057	-3.148699
C	-0.899341	2.758002	2.181851
C	-1.138834	4.147153	2.121054
H	-1.178135	2.246319	3.100186

96

H	-1.581656	4.654056	2.971509
Mg	0.000000	0.000000	1.169132
C	0.337804	-2.054776	1.134116
C	0.000000	-2.795409	-0.040294
C	0.899341	-2.758002	2.181851
C	-0.581296	-2.171988	-1.170082
C	0.239851	-4.200607	-0.116925
C	1.138834	-4.147153	2.121054
H	1.178135	-2.246319	3.100186
C	-0.904787	-2.871167	-2.301716
H	-0.782181	-1.101325	-1.140495
C	-0.102360	-4.902032	-1.294841
C	0.816533	-4.852809	0.995170
H	1.581656	-4.654056	2.971509
C	-0.661013	-4.256252	-2.364660
H	-1.349130	-2.362057	-3.148699
H	0.086644	-5.969575	-1.337049
H	0.998792	-5.920723	0.939262
H	-0.918150	-4.807242	-3.261542

(2-Napth)₂Mg   E = -970.6556937

C	0.000000	7.038719	-0.548307
C	0.767552	6.299791	0.311463
C	0.624573	4.896562	0.383460
C	-0.331727	4.256784	-0.452660
C	-1.108282	5.047731	-1.328965
C	-0.947946	6.406291	-1.377315

97

H	2.126697	4.580162	1.895682
H	0.118710	8.114894	-0.594785
H	1.498082	6.783652	0.950826
C	1.395376	4.096789	1.255375
C	-0.471159	2.850296	-0.377251
H	-1.837075	4.557432	-1.965833
H	-1.549741	7.001732	-2.053892
C	0.279894	2.060720	0.473622
C	1.226427	2.738444	1.294875
H	-1.216063	2.407514	-1.037398
H	1.846151	2.170595	1.984385
Mg	0.000000	0.000000	0.502538
C	-0.279894	-2.060720	0.473622
C	0.471159	-2.850296	-0.377251
C	0.331727	-4.256784	-0.452660
C	-0.624573	-4.896562	0.383460
C	-1.395376	-4.096789	1.255375
C	-1.226427	-2.738444	1.294875
H	1.837075	-4.557432	-1.965833
H	1.216063	-2.407514	-1.037398
C	1.108282	-5.047731	-1.328965
C	-0.767552	-6.299791	0.311463
H	-2.126697	-4.580162	1.895682
H	-1.846151	-2.170595	1.984385
C	0.000000	-7.038719	-0.548307
C	0.947946	-6.406291	-1.377315
H	-1.498082	-6.783652	0.950826
H	-0.118710	-8.114894	-0.594785
H	1.549741	-7.001732	-2.053892

Supplementary information for Chapter 4

Figure 19. ^{1}H NMR of NiBrA^t in C$_6$D$_6$
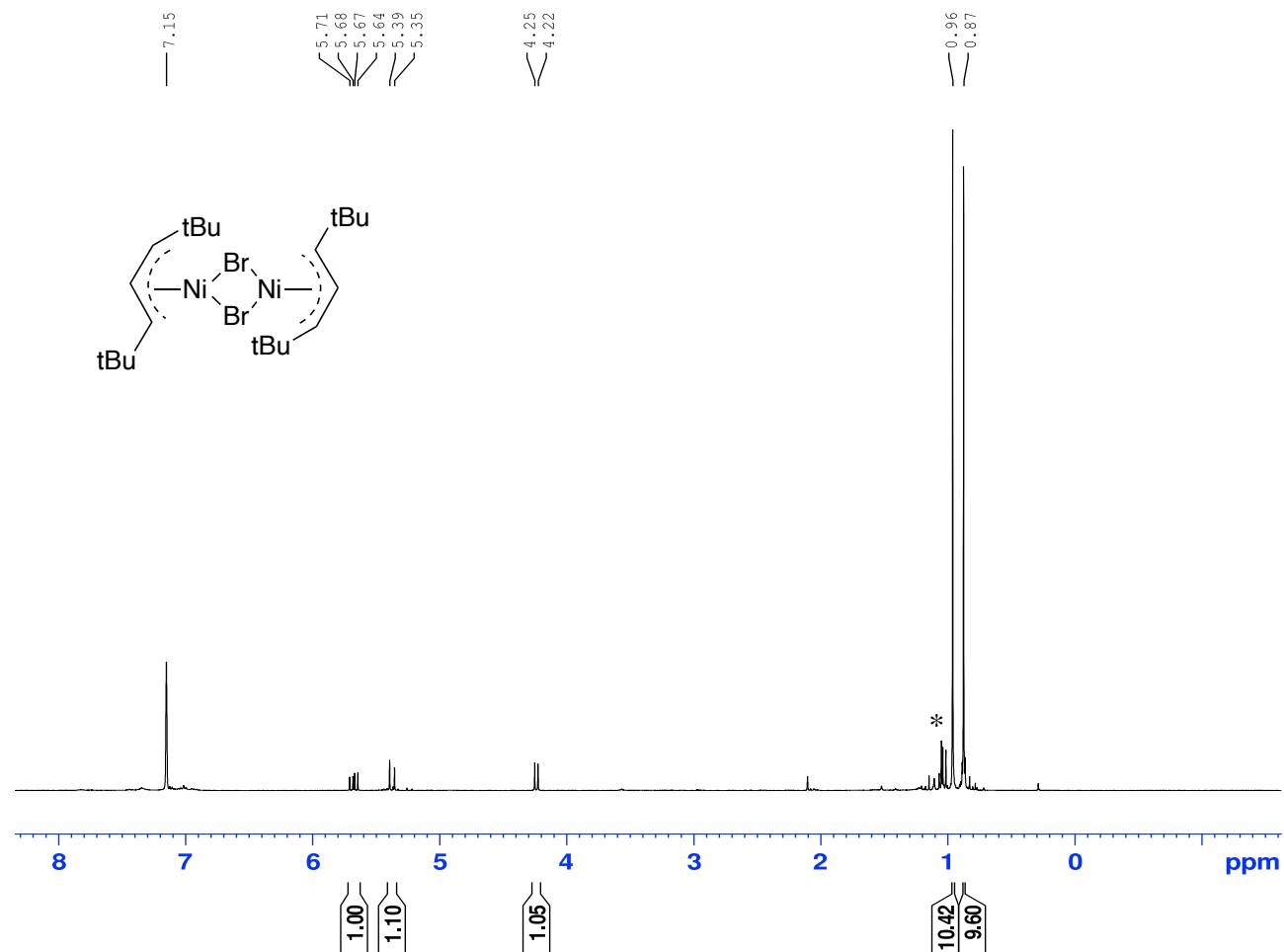
Figure 20. ^{13}C NMR of NiBrA^t in C$_6$D$_6$

144.32
128.22
127.98
127.74
124.76
70.29
35.84
29.25
27.34
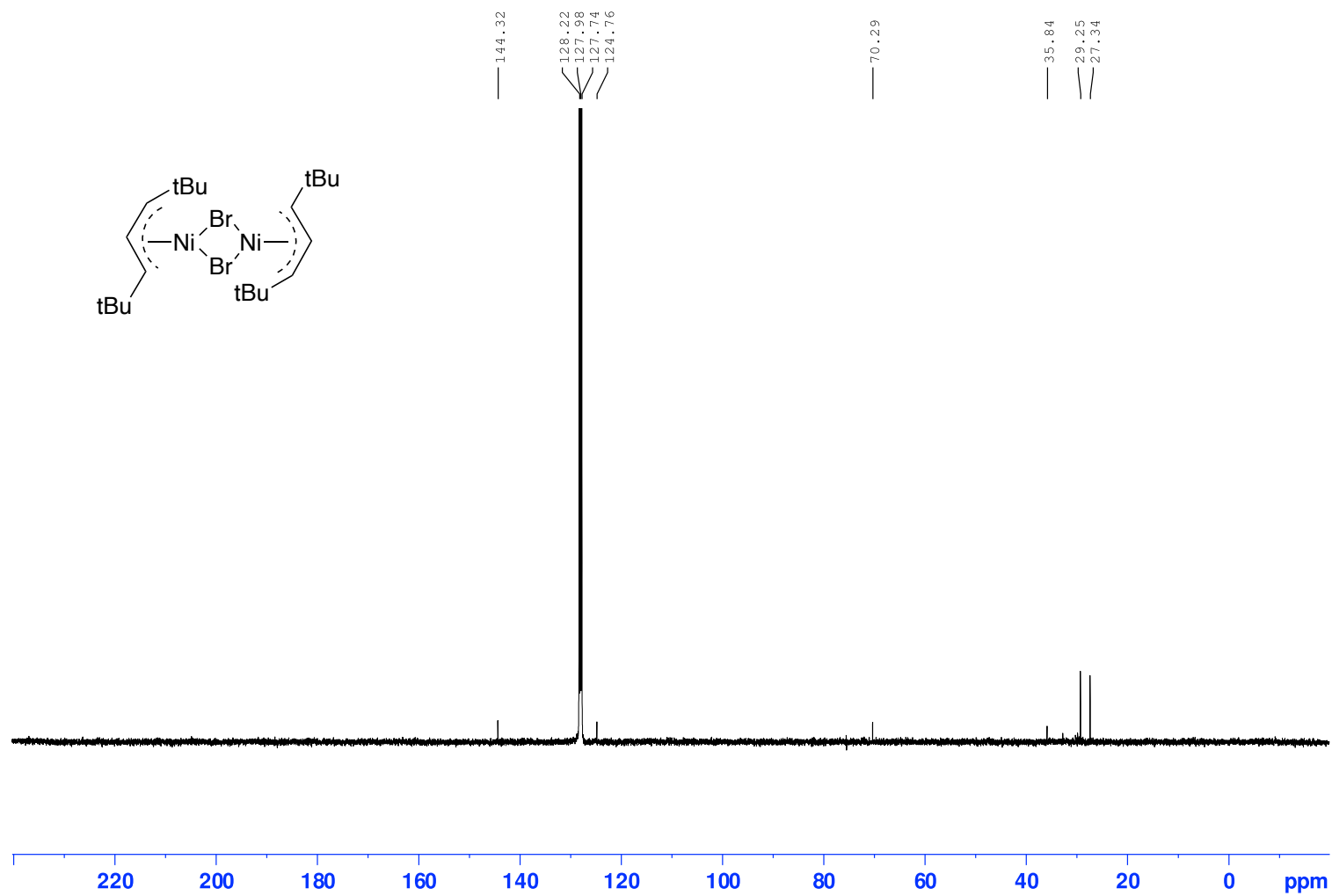
Figure 21. ^{1}H NMR of CoA^t(CO)$_3$ in C$_6$D$_6$
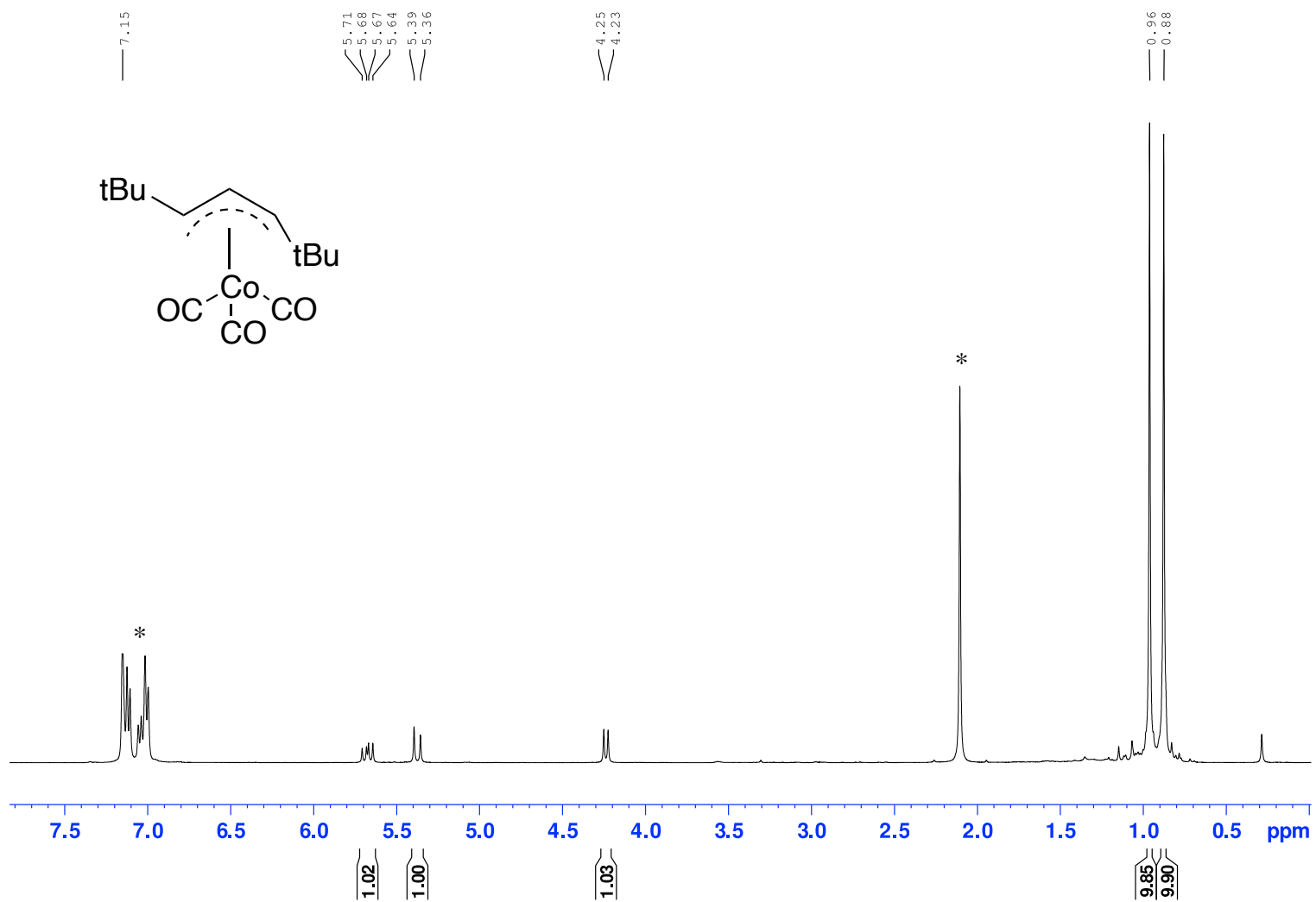
Figure 22. ^{13}C NMR of CoA^t(CO)$_3$ in C$_6$D$_6$
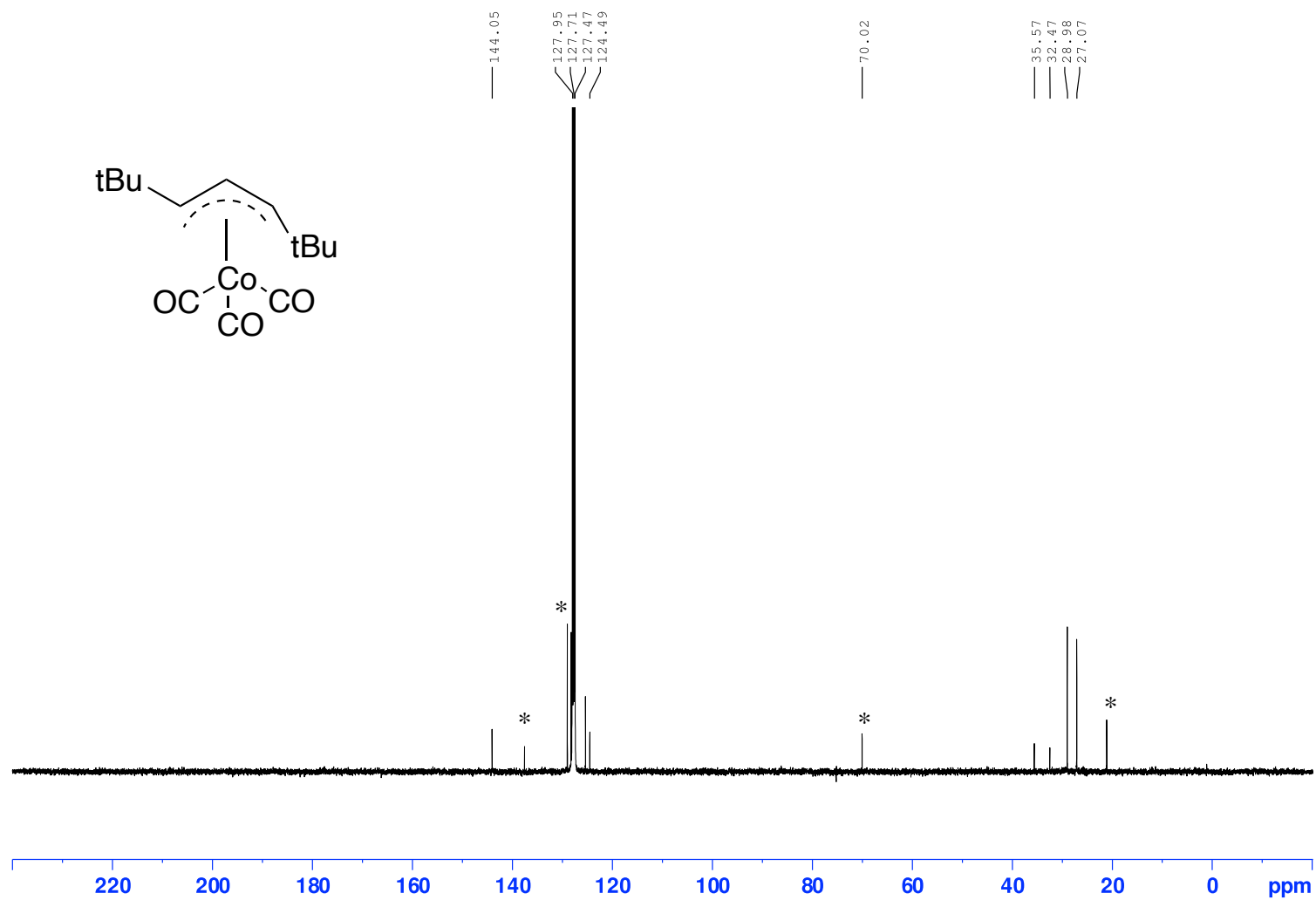
Figure 23. ^{1}H NMR of 5-(tert-butyl)-2,2,8,8-tetramethylnonane-3,7-dione in CDCl$_3$
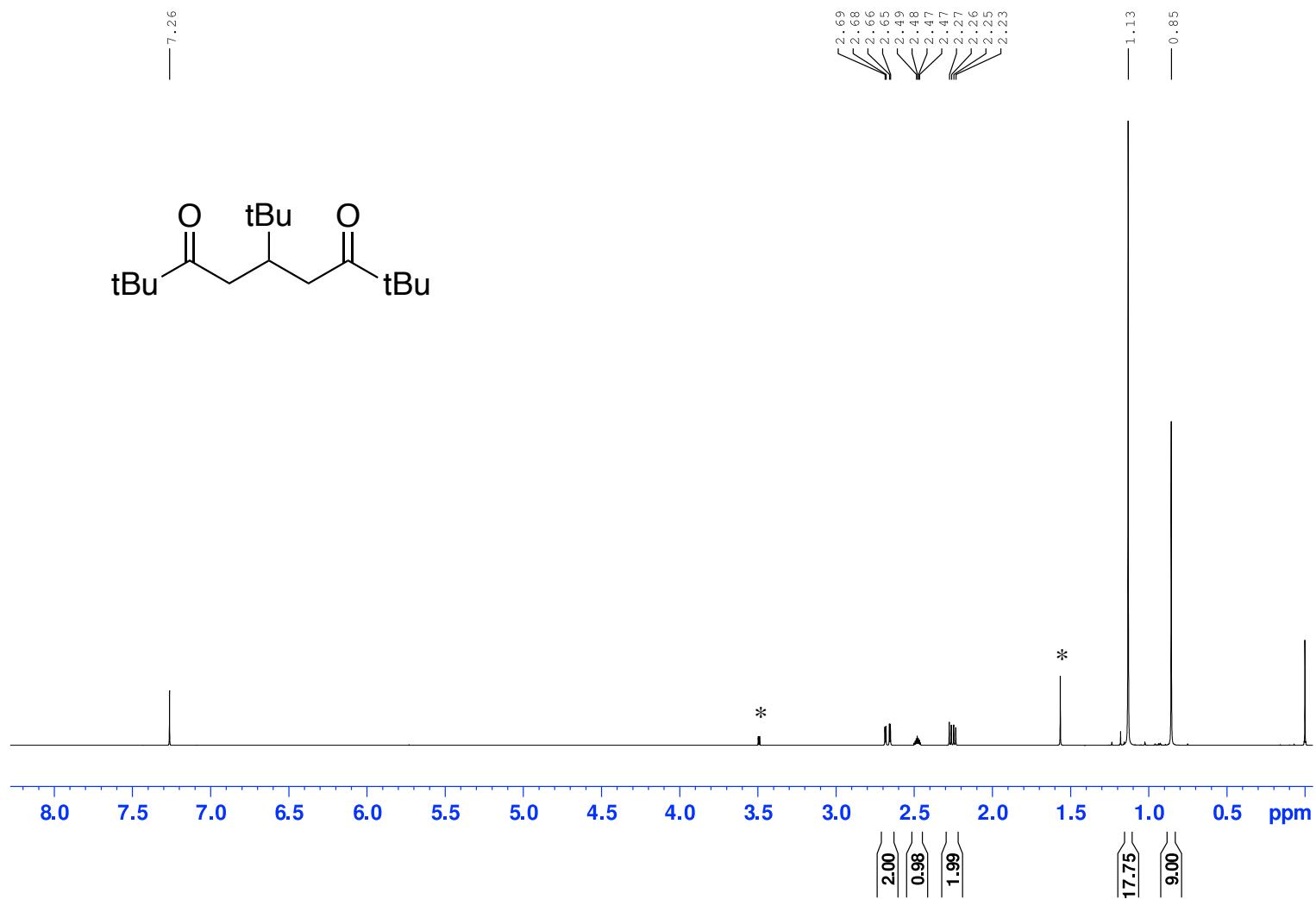
Figure 24. ^{13}C NMR of 5-(tert-butyl)-2,2,8,8-tetramethylnonane-3,7-dione in CDCl$_3$
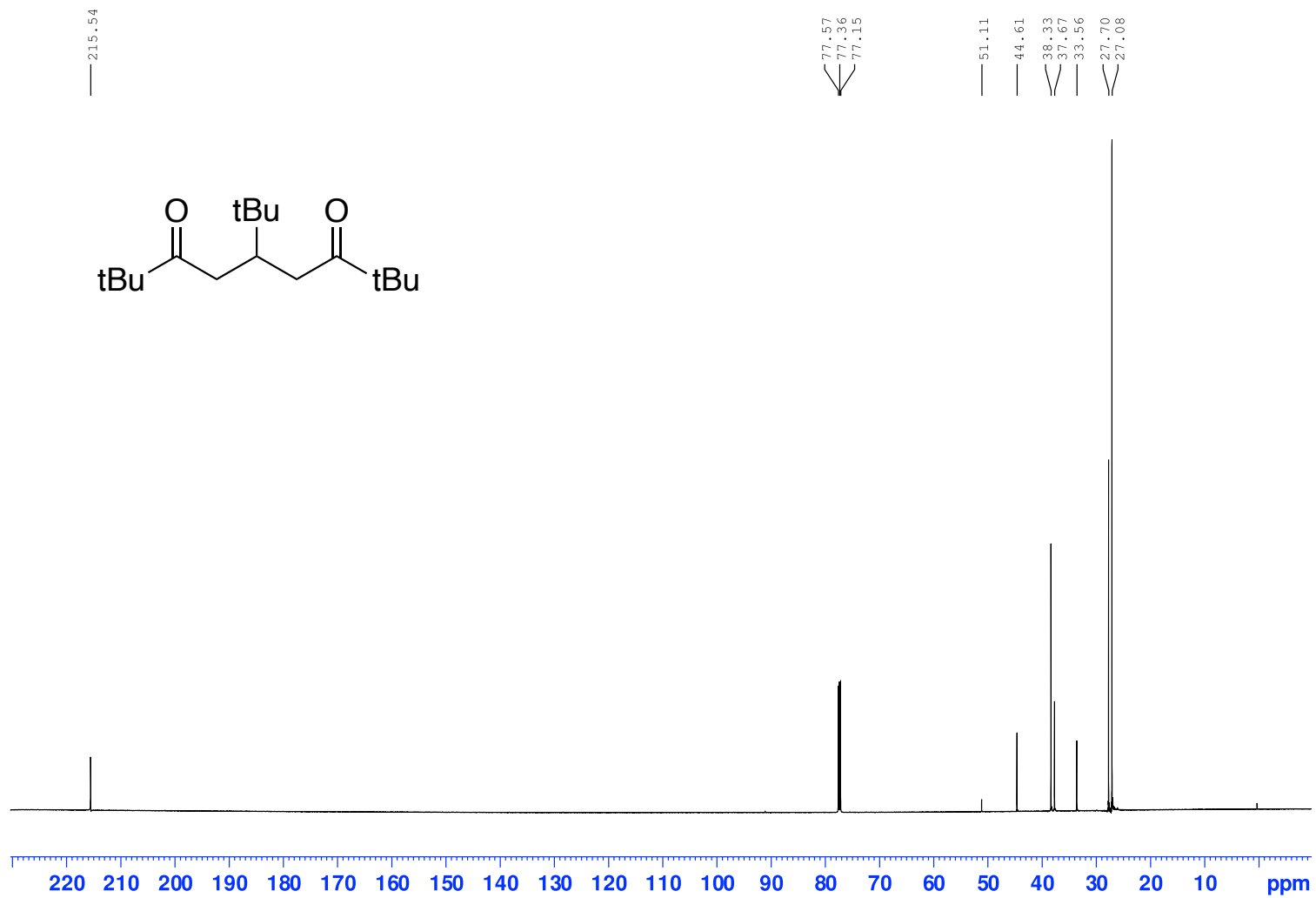
Figure 25. ^{1}H NMR of 5-(tert-butyl)-2,2,8,8-tetramethylnonane-3,7-diol in CDCl$_3$
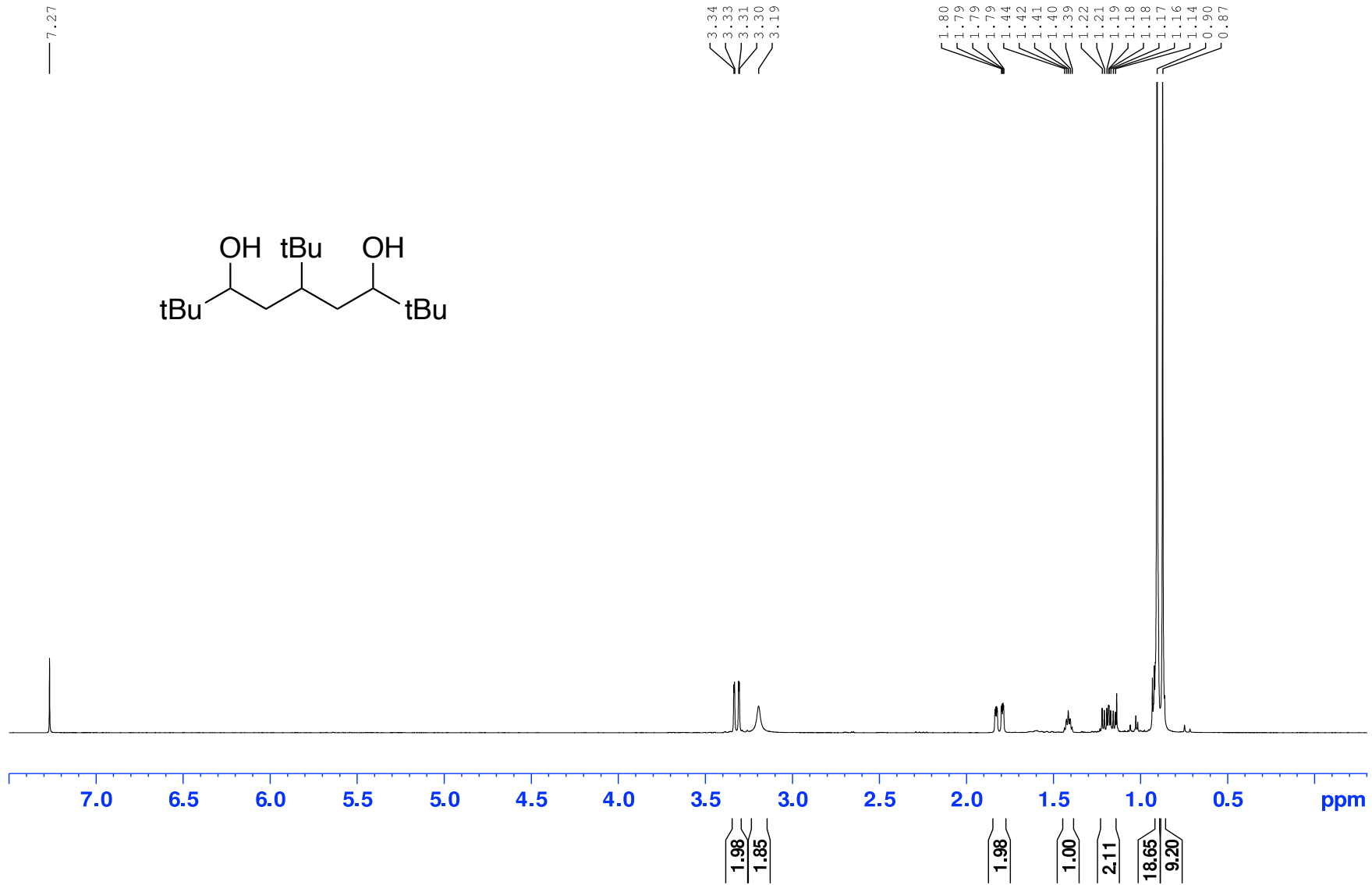
Figure 26. ^{13}C NMR of 5-(tert-butyl)-2,2,8,8-tetramethylnonane-3,7-diol in CDCl$_3$
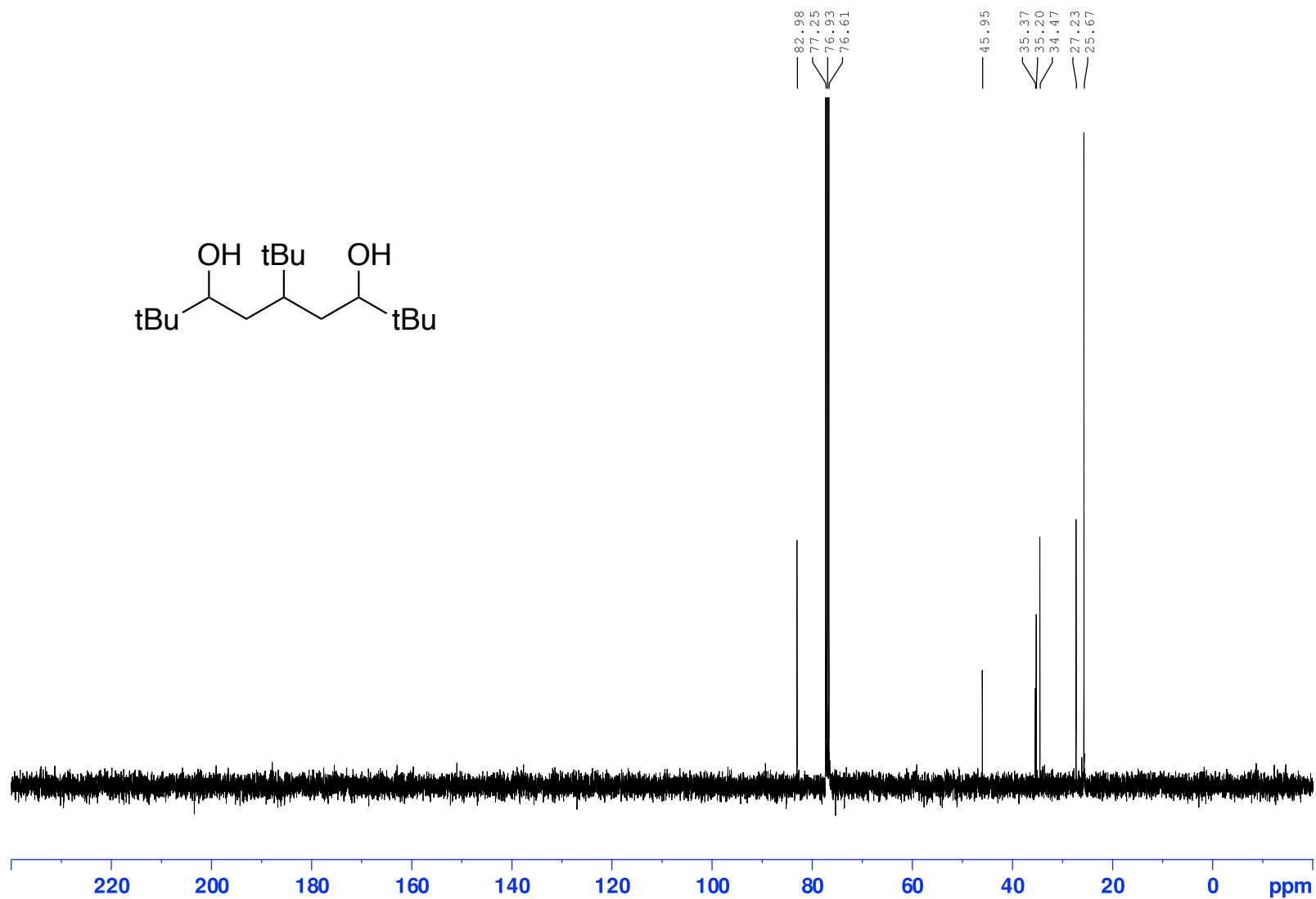
Figure 27. ^{1}H NMR of 1,3-bis-tert-butylallyl potassium in C_6D_6
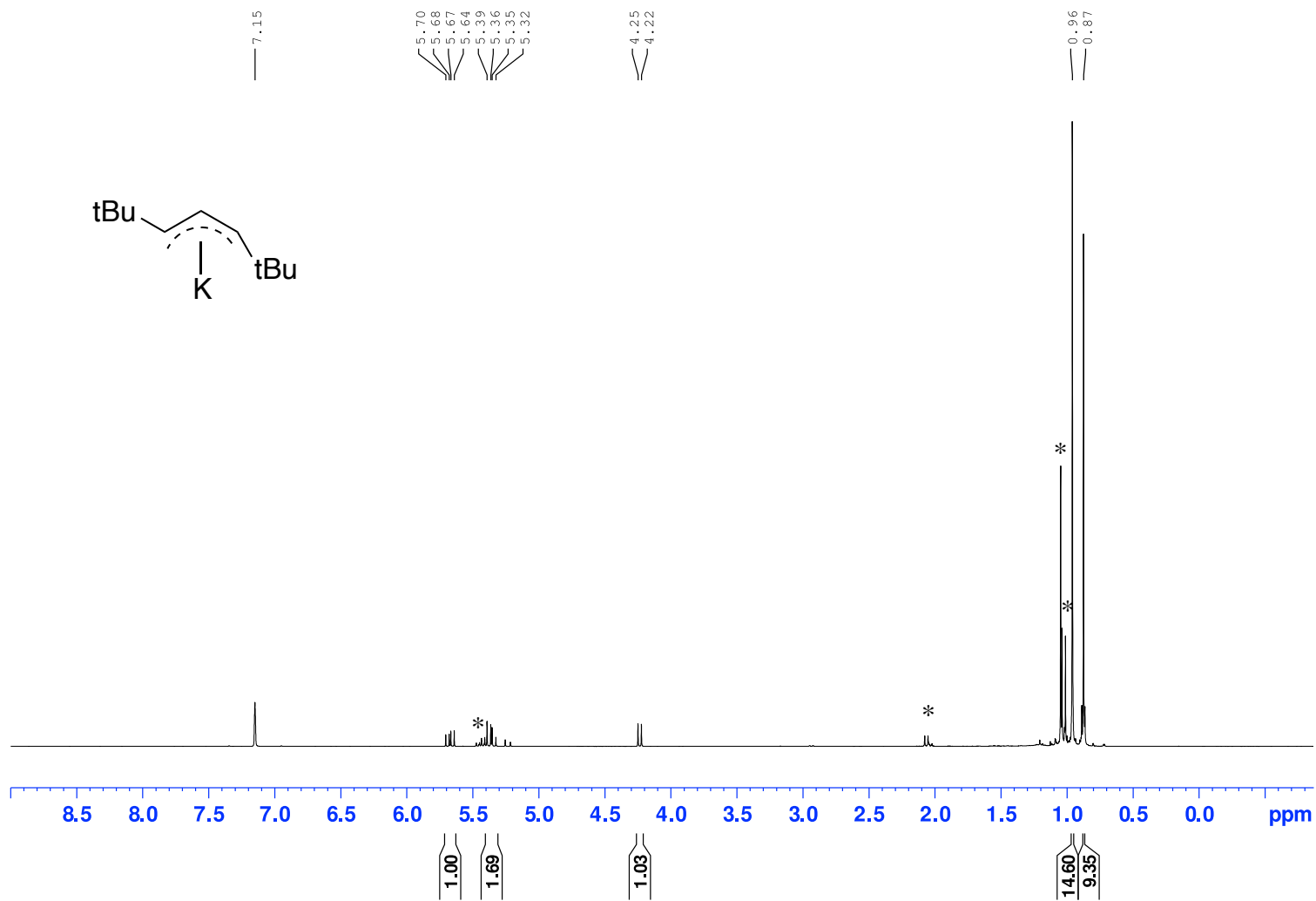
Figure 28. ^{13}C NMR of 1,3-bis-*tert*-butylallyl potassium in C_6D_6
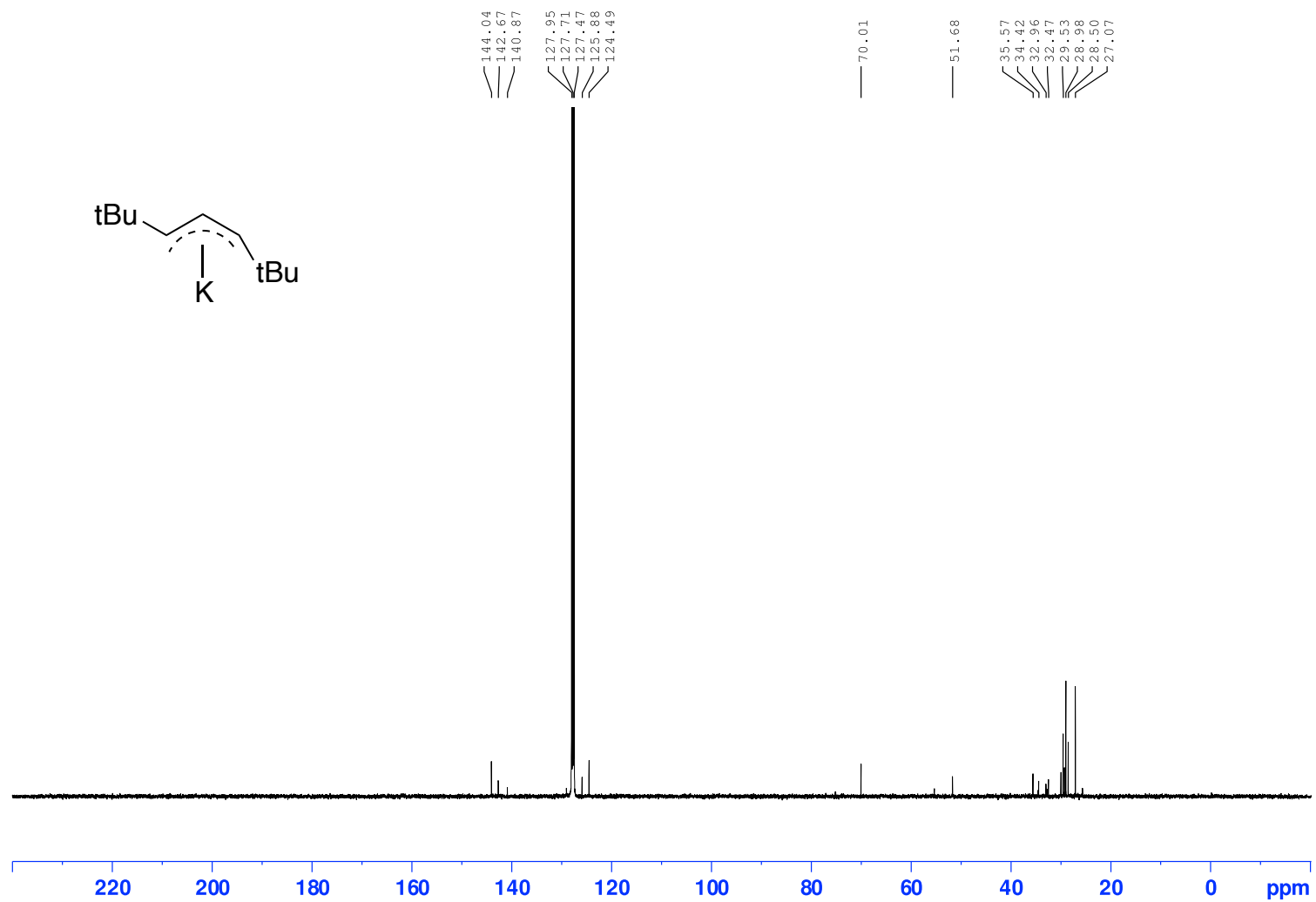
Table 8. Crystallographic data and summary of X-ray collection for 5-(*tert*-butyl)-2,2,8,8-tetramethylnonane-3,7-dione.

Identification code	IRS-e-0040
Empirical formula	$C_{17}H_{32}O_2$
Formula weight	268.42
Temperature	100.00 (10) K
Wavelength	1.54184 Å
Crystal system	Monoclinic
Space group	$P2_1/c$
Unit cell dimensions	a = 10.0722(1) Å $\alpha = 90°$
	b = 15.3500(1) Å $\beta = 92.721(10)°$
	c = 11.0263(1) Å $\gamma = 90°$
Volume	1702.84(3) Å^3
Z	4
Density (calculated)	1.047 g/cm^3
Absorption coefficient	0.507 mm^{-1}
F(000)	600
Crystal size	0.408 x 0.131 x 0.126 mm^3
Crystal color, habit	Colorless needle
Theta range for data collection	4.395 to 73.326 °
Index ranges	$-12 \leq h \leq 12, -19 \leq k \leq 18, -13 \leq l \leq 9$
Reflections collected	16 703
Independent reflections	3380 [R(int) = 0.0225]
Completeness to theta = 25.00 °	100.0 %
Absorption correction	Gaussian
Max. and min. transmission	1.000 and 0.676

Refinement method	Full-matrix least-squares on F^2
Data / restraints / parameters	3380 / 0 / 181
Goodness-of-fit on F^2	1.073
Final R indices [I>2sigma(I)]	$R_1 = 0.0362$, $wR_2 = 0.0922$
R indices (all data)	$R_1 = 0.0381$, $wR_2 = 0.0937$
Extinction coefficient	n/a
Largest diff. peak and hole	0.255 and -0.222 e/ $Å^{-3}$

Table 9. Atomic coordinates (x 10^5) and equivalent isotropic displacement parameters ($Å^2$ x 10^4) for 5-(*tert*-butyl)-2,2,8,8-tetramethylnonane-3,7-dione. U(eq) is defined as one third of the trace of the orthogonalized U_{ij} tensor.

	x	y	z	U(eq)
O(1)	54377(7)	27724(5)	59311(6)	227(2)
O(2)	17168(7)	21803(5)	46566(7)	208(2)
C(1)	73277(9)	24042(6)	47853(9)	151(2)
C(2)	59806(9)	28375(6)	49737(9)	138(2)
C(3)	53419(9)	33648(6)	39321(9)	143(2)
C(4)	38188(9)	32750(6)	38246(9)	134(2)
C(5)	34896(9)	23643(6)	33093(9)	146(2)
C(6)	22836(9)	19107(6)	37843(9)	135(2)
C(7)	18084(9)	10749(6)	31257(9)	158(2)
C(8)	78928(11)	20172(7)	59758(10)	224(2)
C(9)	70946(10)	16663(7)	38525(9)	193(2)
C(10)	83104(10)	30822(7)	43272(9)	186(2)
C(11)	29793(11)	5357(7)	26981(12)	279(3)
C(12)	9996(11)	5272(7)	39811(10)	223(2)
C(13)	9184(12)	13562(7)	20206(10)	253(2)
C(14)	31477(10)	40296(6)	30798(9)	170(2)
C(15)	16483(10)	38620(7)	28952(11)	253(2)
C(16)	33265(11)	48869(7)	37875(10)	240(2)
C(17)	37403(11)	41320(7)	18293(9)	218(2)

Table 10. Bond lengths [Å] and angles [°] for 5-(*tert*-butyl)-2,2,8,8-tetramethylnonane-3,7-dione.

O(1)-C(2)	1.2159(12)
O(2)-C(6)	1.2142(12)
C(1)-C(2)	1.5340(13)
C(1)-C(8)	1.5261(14)
C(1)-C(9)	1.5405(13)
C(1)-C(10)	1.5380(14)
C(2)-C(3)	1.5225(13)
C(3)-H(3A)	0.9700
C(3)-H(3B)	0.9700
C(3)-C(4)	1.5392(13)
C(4)-H(4)	0.9800
C(4)-C(5)	1.5392(13)
C(4)-C(14)	1.5557(13)
C(5)-H(5A)	0.9700
C(5)-H(5B)	0.9700
C(5)-C(6)	1.5150(12)
C(6)-C(7)	1.5393(13)
C(7)-C(11)	1.5334(14)
C(7)-C(12)	1.5273(13)
C(7)-C(13)	1.5398(14)
C(8)-H(8A)	0.9600
C(8)-H(8B)	0.9600
C(8)-H(8C)	0.9600
C(9)-H(9A)	0.9600
C(9)-H(9B)	0.9600
C(9)-H(9C)	0.9600
C(10)-H(10A)	0.9600
C(10)-H(10B)	0.9600
C(10)-H(10C)	0.9600
C(11)-H(11A)	0.9600
C(11)-H(11B)	0.9600

C(11)-H(11C)	0.9600
C(12)-H(12A)	0.9600
C(12)-H(12B)	0.9600
C(12)-H(12C)	0.9600
C(13)-H(13A)	0.9600
C(13)-H(13B)	0.9600
C(13)-H(13C)	0.9600
C(14)-C(15)	1.5359(14)
C(14)-C(16)	1.5361(14)
C(14)-C(17)	1.5363(14)
C(15)-H(15A)	0.9600
C(15)-H(15B)	0.9600
C(15)-H(15C)	0.9600
C(16)-H(16A)	0.9600
C(16)-H(16B)	0.9600
C(16)-H(16C)	0.9600
C(17)-H(17A)	0.9600
C(17)-H(17B)	0.9600
C(17)-H(17C)	0.9600
C(2)-C(1)-C(9)	107.55(8)
C(2)-C(1)-C(10)	109.77(8)
C(8)-C(1)-C(2)	110.39(8)
C(8)-C(1)-C(9)	109.08(8)
C(8)-C(1)-C(10)	109.05(8)
C(10)-C(1)-C(9)	111.00(8)
O(1)-C(2)-C(1)	121.27(9)
O(1)-C(2)-C(3)	120.48(9)
C(3)-C(2)-C(1)	118.24(8)
C(2)-C(3)-H(3A)	108.9
C(2)-C(3)-H(3B)	108.9
C(2)-C(3)-C(4)	113.23(8)
H(3A)-C(3)-H(3B)	107.7
C(4)-C(3)-H(3A)	108.9
C(4)-C(3)-H(3B)	108.9

C(3)-C(4)-H(4)	107.6
C(3)-C(4)-C(14)	112.36(8)
C(5)-C(4)-C(3)	107.83(7)
C(5)-C(4)-H(4)	107.6
C(5)-C(4)-C(14)	113.63(8)
C(14)-C(4)-H(4)	107.6
C(4)-C(5)-H(5A)	108.1
C(4)-C(5)-H(5B)	108.1
H(5A)-C(5)-H(5B)	107.3
C(6)-C(5)-C(4)	116.87(8)
C(6)-C(5)-H(5A)	108.1
C(6)-C(5)-H(5B)	108.1
O(2)-C(6)-C(5)	122.14(9)
O(2)-C(6)-C(7)	120.69(8)
C(5)-C(6)-C(7)	117.16(8)
C(6)-C(7)-C(13)	107.21(8)
C(11)-C(7)-C(6)	111.62(8)
C(11)-C(7)-C(13)	109.60(9)
C(12)-C(7)-C(6)	109.30(8)
C(12)-C(7)-C(11)	109.47(9)
C(12)-C(7)-C(13)	109.60(8)
C(1)-C(8)-H(8A)	109.5
C(1)-C(8)-H(8B)	109.5
C(1)-C(8)-H(8C)	109.5
H(8A)-C(8)-H(8B)	109.5
H(8A)-C(8)-H(8C)	109.5
H(8B)-C(8)-H(8C)	109.5
C(1)-C(9)-H(9A)	109.5
C(1)-C(9)-H(9B)	109.5
C(1)-C(9)-H(9C)	109.5
H(9A)-C(9)-H(9B)	109.5
H(9A)-C(9)-H(9C)	109.5
H(9B)-C(9)-H(9C)	109.5
C(1)-C(10)-H(10A)	109.5
C(1)-C(10)-H(10B)	109.5

C(1)-C(10)-H(10C)	109.5
H(10A)-C(10)-H(10B)	109.5
H(10A)-C(10)-H(10C)	109.5
H(10B)-C(10)-H(10C)	109.5
C(7)-C(11)-H(11A)	109.5
C(7)-C(11)-H(11B)	109.5
C(7)-C(11)-H(11C)	109.5
H(11A)-C(11)-H(11B)	109.5
H(11A)-C(11)-H(11C)	109.5
H(11B)-C(11)-H(11C)	109.5
C(7)-C(12)-H(12A)	109.5
C(7)-C(12)-H(12B)	109.5
C(7)-C(12)-H(12C)	109.5
H(12A)-C(12)-H(12B)	109.5
H(12A)-C(12)-H(12C)	109.5
H(12B)-C(12)-H(12C)	109.5
C(7)-C(13)-H(13A)	109.5
C(7)-C(13)-H(13B)	109.5
C(7)-C(13)-H(13C)	109.5
H(13A)-C(13)-H(13B)	109.5
H(13A)-C(13)-H(13C)	109.5
H(13B)-C(13)-H(13C)	109.5
C(15)-C(14)-C(4)	110.19(8)
C(15)-C(14)-C(16)	107.56(9)
C(15)-C(14)-C(17)	108.64(9)
C(16)-C(14)-C(4)	109.40(8)
C(16)-C(14)-C(17)	109.09(8)
C(17)-C(14)-C(4)	111.86(8)
C(14)-C(15)-H(15A)	109.5
C(14)-C(15)-H(15B)	109.5
C(14)-C(15)-H(15C)	109.5
H(15A)-C(15)-H(15B)	109.5
H(15A)-C(15)-H(15C)	109.5
H(15B)-C(15)-H(15C)	109.5
C(14)-C(16)-H(16A)	109.5

C(14)-C(16)-H(16B)	109.5					
C(14)-C(16)-H(16C)	109.5					
H(16A)-C(16)-H(16B)	109.5					
H(16A)-C(16)-H(16C)	109.5					
H(16B)-C(16)-H(16C)	109.5					
C(14)-C(17)-H(17A)	109.5					
C(14)-C(17)-H(17B)	109.5					
C(14)-C(17)-H(17C)	109.5					
H(17A)-C(17)-H(17B)	109.5					
H(17A)-C(17)-H(17C)	109.5					
H(17B)-C(17)-H(17C)	109.5					

Symmetry transformations used to generate equivalent atoms:

Table 11. Anisotropic displacement parameters (Å^2 x 10^4) for 5-(*tert*-butyl)-2,2,8,8-tetramethylnonane-3,7-dione. The anisotropic displacement factor exponent takes the form: $-2\pi^2 \left[h^2 a^{*2} U_{11} + \ldots + 2\, h\, k\, a^* b^* U_{12} \right]$

	U_{11}	U_{22}	U_{33}	U_{23}	U_{11}	U_{12}
O(1)	186(4)	345(4)	152(4)	35(3)	40(3)	31(3)
O(2)	207(4)	202(4)	222(4)	-17(3)	80(3)	-9(3)
C(1)	144(4)	169(5)	139(5)	-8(4)	2(4)	12(4)
C(2)	135(4)	140(4)	139(5)	-14(3)	-1(4)	-29(3)
C(3)	138(4)	139(4)	153(5)	8(4)	2(3)	-18(3)
C(4)	128(4)	126(4)	147(4)	0(3)	4(3)	-6(3)
C(5)	124(4)	128(4)	186(5)	-8(4)	23(4)	-3(3)
C(6)	116(4)	130(4)	158(5)	27(3)	-7(3)	16(3)
C(7)	143(4)	140(4)	189(5)	7(4)	-5(4)	-22(4)
C(8)	216(5)	272(6)	182(5)	23(4)	-9(4)	62(4)
C(9)	204(5)	173(5)	203(5)	-36(4)	16(4)	13(4)
C(10)	141(5)	230(5)	188(5)	-25(4)	11(4)	-21(4)
C(11)	242(5)	164(5)	436(7)	-96(5)	67(5)	-13(4)
C(12)	218(5)	203(5)	246(5)	50(4)	-22(4)	-80(4)
C(13)	295(6)	249(6)	207(5)	36(4)	-73(4)	-70(4)

C(14)	168(5)	133(5)	206(5)	12(4)	-30(4)	3(4)
C(15)	171(5)	209(5)	372(6)	53(5)	-58(4)	30(4)
C(16)	293(6)	139(5)	284(6)	-13(4)	-33(4)	36(4)
C(17)	265(5)	190(5)	194(5)	47(4)	-44(4)	-26(4)

Table 12. Hydrogen coordinates (x 10^4) and isotropic displacement parameters (Å^2 x 10^3) for 5-(*tert*-butyl)-2,2,8,8-tetramethylnonane-3,7-dione.

	x	y	z	U(eq)
H(3A)	5707	3176	3177	17
H(3B)	5569	3974	4048	17
H(4)	3492	3301	4647	16
H(5A)	3362	2415	2435	17
H(5B)	4256	1993	3472	17
H(8A)	8020	2472	6567	34
H(8B)	8730	1743	5842	34
H(8C)	7284	1593	6267	34
H(9A)	6512	1238	4174	29
H(9B)	7929	1399	3688	29
H(9C)	6698	1902	3114	29
H(10A)	7977	3312	3563	28
H(10B)	9157	2811	4226	28
H(10C)	8411	3547	4907	28
H(11A)	3457	868	2124	42
H(11B)	2651	10	2320	42
H(11C)	3563	392	3383	42
H(12A)	1552	361	4676	34
H(12B)	678	15	3564	34
H(12C)	260	862	4241	34
H(13A)	186	1694	2290	38
H(13B)	587	849	1597	38
H(13C)	1428	1702	1485	38
H(15A)	1504	3352	2403	38

H(15B)	1233	4355	2498	38
H(15C)	1271	3775	3669	38
H(16A)	2981	4821	4579	36
H(16B)	2856	5345	3358	36
H(16C)	4254	5030	3868	36
H(17A)	4664	4282	1933	33
H(17B)	3276	4584	1383	33
H(17C)	3652	3593	1391	33

Table 13. Crystallographic data and summary of X-ray collection for 5-(*tert*-butyl)-2,2,8,8-tetramethylnonane-3,7-diol.

Identification code	IRS-e-0038
Empirical formula	$C_{17}H_{36}O_2$
Formula weight	272.46
Temperature	100.00(10) K
Wavelength	1.54184 Å
Crystal system	Monoclinic
Space group	$P2_1$
Unit cell dimensions	a = 10.19113(9) Å $\alpha = 90°$
	b = 18.06166(12) Å $\beta = 108.7450(10)°$
	c = 10.28106(9) Å $\gamma = 90°$
Volume	1729.05(3) $Å^3$
Z	4
Density (calculated)	1.010 g/cm^3
Absorption coefficient	0.482 mm^{-1}
F(000)	616.0
Crystal size	0.412 x 0.11 x 0.091 mm^3

Crystal color, habit	Colorless needle
Theta range for data collection	4.542 to 73.387°
Index ranges	$-12 \leq h \leq 7$, $-22 \leq k \leq 22$, $-12 \leq l \leq 12$
Reflections collected	16331
Independent reflections	6892 [R(int) = 0.0250]
Completeness to theta = 25.00 °	100 %
Absorption correction	Gaussian
Max. and min. transmission	1.000 and 0.610
Refinement method	Full-matrix least-squares on F^2
Data / restraints / parameters	6892 / 1 / 365
Goodness-of-fit on F^2	1.037
Final R indices [I>2sigma(I)]	$R_1 = 0.0303$, $wR_2 = 0.0762$
R indices (all data)	$R_1 = 0.0313$, $wR_2 = 0.0771$
Absolute structure parameter	0.05(6)
Extinction coefficient	n/a
Largest diff. peak and hole	0.159 and -0.144 e Å^{-3}

Table 14. Atomic coordinates (x 10^5) and equivalent isotropic displacement parameters (Å^2 x 10^4) for 5-(*tert*-butyl)-2,2,8,8-tetramethylnonane-3,7-diol. U(eq) is defined as one third of the trace of the orthogonalized U_{ij} tensor.

	x	y	z	U(eq)
O(1)	42113(12)	39924(6)	37498(12)	162(2)
O(2)	52746(13)	29039(7)	55852(12)	188(3)
C(1)	20442(19)	43898(10)	20949(18)	185(4)
C(2)	27332(17)	39171(9)	33923(17)	149(3)
C(3)	22407(18)	40949(9)	46153(17)	167(3)
C(4)	27090(18)	35250(9)	57971(17)	154(3)

C(5)	41924(18)	36966(9)	67649(17)	156(3)
C(6)	51831(18)	30412(9)	69286(17)	151(3)
C(7)	66463(19)	31460(10)	79816(18)	186(4)
C(8)	21990(20)	52204(10)	24027(19)	222(4)
C(9)	27200(20)	41975(12)	10050(20)	283(4)
C(10)	4917(19)	41917(11)	15180(20)	245(4)
C(11)	16197(18)	34381(10)	65613(18)	184(4)
C(12)	2900(20)	30907(12)	55910(20)	267(4)
C(13)	12800(20)	41886(10)	70740(20)	233(4)
C(14)	21530(20)	29090(11)	77928(19)	233(4)
C(15)	74720(20)	24297(11)	80420(20)	270(4)
C(16)	65300(20)	32957(13)	94089(19)	310(5)
C(17)	74080(20)	37865(11)	75640(20)	290(4)
O(1B)	41611(13)	65054(6)	51065(12)	165(3)
O(2B)	55577(12)	52886(6)	47753(13)	171(3)
C(1B)	33852(18)	67179(10)	70701(18)	175(4)
C(2B)	45278(17)	63778(9)	65655(17)	154(3)
C(3B)	60023(18)	66503(9)	73052(17)	155(3)
C(4B)	71490(17)	61275(9)	71703(17)	140(3)
C(5B)	73197(17)	61648(9)	57220(17)	146(3)
C(6B)	69877(17)	54330(9)	49325(17)	145(3)
C(7B)	72509(17)	54129(9)	35279(17)	152(3)
C(8B)	33920(20)	75656(10)	70200(20)	218(4)
C(9B)	19788(19)	64323(11)	61520(20)	250(4)
C(10B)	36000(20)	64599(11)	85490(20)	259(4)
C(11B)	85502(18)	62342(10)	83544(17)	166(3)
C(12B)	83650(20)	60917(11)	97603(19)	237(4)
C(13B)	91251(19)	70160(10)	83464(19)	212(4)
C(14B)	96073(19)	56627(10)	81992(19)	201(4)
C(15B)	71000(20)	46089(10)	30140(20)	215(4)
C(16B)	87370(18)	56713(11)	37067(19)	204(4)
C(17B)	62110(20)	59010(11)	24659(19)	213(4)

Table 15. Bond lengths [Å] and angles [°] for 5-(*tert*-butyl)-2,2,8,8-tetramethylnonane-3,7-diol.

O(1)-H(1)	0.8200
O(1)-C(2)	1.438(2)
O(2)-H(2)	0.8200
O(2)-C(6)	1.435(2)
C(1)-C(2)	1.549(2)
C(1)-C(8)	1.531(2)
C(1)-C(9)	1.532(3)
C(1)-C(10)	1.543(2)
C(2)-H(2A)	0.9800
C(2)-C(3)	1.530(2)
C(3)-H(3A)	0.9700
C(3)-H(3B)	0.9700
C(3)-C(4)	1.546(2)
C(4)-H(4)	0.9800
C(4)-C(5)	1.551(2)
C(4)-C(11)	1.560(2)
C(5)-H(5A)	0.9700
C(5)-H(5B)	0.9700
C(5)-C(6)	1.530(2)
C(6)-H(6)	0.9800
C(6)-C(7)	1.547(2)
C(7)-C(15)	1.534(3)
C(7)-C(16)	1.534(3)
C(7)-C(17)	1.530(3)
C(8)-H(8A)	0.9600
C(8)-H(8B)	0.9600
C(8)-H(8C)	0.9600
C(9)-H(9A)	0.9600
C(9)-H(9B)	0.9600
C(9)-H(9C)	0.9600

C(10)-H(10A)	0.9600
C(10)-H(10B)	0.9600
C(10)-H(10C)	0.9600
C(11)-C(12)	1.535(3)
C(11)-C(13)	1.534(2)
C(11)-C(14)	1.539(2)
C(12)-H(12A)	0.9600
C(12)-H(12B)	0.9600
C(12)-H(12C)	0.9600
C(13)-H(13A)	0.9600
C(13)-H(13B)	0.9600
C(13)-H(13C)	0.9600
C(14)-H(14A)	0.9600
C(14)-H(14B)	0.9600
C(14)-H(14C)	0.9600
C(15)-H(15A)	0.9600
C(15)-H(15B)	0.9600
C(15)-H(15C)	0.9600
C(16)-H(16A)	0.9600
C(16)-H(16B)	0.9600
C(16)-H(16C)	0.9600
C(17)-H(17A)	0.9600
C(17)-H(17B)	0.9600
C(17)-H(17C)	0.9600
O(1B)-H(1B)	0.8200
O(1B)-C(2B)	1.443(2)
O(2B)-H(2B)	0.8200
O(2B)-C(6B)	1.4376(19)
C(1B)-C(2B)	1.546(2)
C(1B)-C(8B)	1.532(2)
C(1B)-C(9B)	1.530(2)
C(1B)-C(10B)	1.538(2)
C(2B)-H(2BA)	0.9800
C(2B)-C(3B)	1.531(2)
C(3B)-H(3BA)	0.9700

C(3B)-H(3BB)	0.9700
C(3B)-C(4B)	1.543(2)
C(4B)-H(4B)	0.9800
C(4B)-C(5B)	1.555(2)
C(4B)-C(11B)	1.562(2)
C(5B)-H(5BA)	0.9700
C(5B)-H(5BB)	0.9700
C(5B)-C(6B)	1.531(2)
C(6B)-H(6B)	0.9800
C(6B)-C(7B)	1.552(2)
C(7B)-C(15B)	1.536(2)
C(7B)-C(16B)	1.538(2)
C(7B)-C(17B)	1.533(2)
C(8B)-H(8BA)	0.9600
C(8B)-H(8BB)	0.9600
C(8B)-H(8BC)	0.9600
C(9B)-H(9BA)	0.9600
C(9B)-H(9BB)	0.9600
C(9B)-H(9BC)	0.9600
C(10B)-H(10D)	0.9600
C(10B)-H(10E)	0.9600
C(10B)-H(10F)	0.9600
C(11B)-C(12B)	1.538(2)
C(11B)-C(13B)	1.530(2)
C(11B)-C(14B)	1.537(2)
C(12B)-H(12D)	0.9600
C(12B)-H(12E)	0.9600
C(12B)-H(12F)	0.9600
C(13B)-H(13D)	0.9600
C(13B)-H(13E)	0.9600
C(13B)-H(13F)	0.9600
C(14B)-H(14D)	0.9600
C(14B)-H(14E)	0.9600
C(14B)-H(14F)	0.9600
C(15B)-H(15D)	0.9600

C(15B)-H(15E)	0.9600
C(15B)-H(15F)	0.9600
C(16B)-H(16D)	0.9600
C(16B)-H(16E)	0.9600
C(16B)-H(16F)	0.9600
C(17B)-H(17D)	0.9600
C(17B)-H(17E)	0.9600
C(17B)-H(17F)	0.9600
C(2)-O(1)-H(1)	109.5
C(6)-O(2)-H(2)	109.5
C(8)-C(1)-C(2)	111.97(14)
C(8)-C(1)-C(9)	109.44(16)
C(8)-C(1)-C(10)	109.35(15)
C(9)-C(1)-C(2)	108.59(15)
C(9)-C(1)-C(10)	108.25(15)
C(10)-C(1)-C(2)	109.16(15)
O(1)-C(2)-C(1)	108.41(13)
O(1)-C(2)-H(2A)	107.4
O(1)-C(2)-C(3)	111.32(13)
C(1)-C(2)-H(2A)	107.4
C(3)-C(2)-C(1)	114.48(14)
C(3)-C(2)-H(2A)	107.4
C(2)-C(3)-H(3A)	108.8
C(2)-C(3)-H(3B)	108.8
C(2)-C(3)-C(4)	113.96(14)
H(3A)-C(3)-H(3B)	107.7
C(4)-C(3)-H(3A)	108.8
C(4)-C(3)-H(3B)	108.8
C(3)-C(4)-H(4)	106.5
C(3)-C(4)-C(5)	111.23(14)
C(3)-C(4)-C(11)	111.88(14)
C(5)-C(4)-H(4)	106.5
C(5)-C(4)-C(11)	113.68(13)
C(11)-C(4)-H(4)	106.5

C(4)-C(5)-H(5A)	109.0
C(4)-C(5)-H(5B)	109.0
H(5A)-C(5)-H(5B)	107.8
C(6)-C(5)-C(4)	112.87(13)
C(6)-C(5)-H(5A)	109.0
C(6)-C(5)-H(5B)	109.0
O(2)-C(6)-C(5)	105.81(13)
O(2)-C(6)-H(6)	108.2
O(2)-C(6)-C(7)	110.39(14)
C(5)-C(6)-H(6)	108.2
C(5)-C(6)-C(7)	115.84(14)
C(7)-C(6)-H(6)	108.2
C(15)-C(7)-C(6)	108.55(14)
C(16)-C(7)-C(6)	109.71(15)
C(16)-C(7)-C(15)	108.69(16)
C(17)-C(7)-C(6)	111.00(15)
C(17)-C(7)-C(15)	109.12(16)
C(17)-C(7)-C(16)	109.72(17)
C(1)-C(8)-H(8A)	109.5
C(1)-C(8)-H(8B)	109.5
C(1)-C(8)-H(8C)	109.5
H(8A)-C(8)-H(8B)	109.5
H(8A)-C(8)-H(8C)	109.5
H(8B)-C(8)-H(8C)	109.5
C(1)-C(9)-H(9A)	109.5
C(1)-C(9)-H(9B)	109.5
C(1)-C(9)-H(9C)	109.5
H(9A)-C(9)-H(9B)	109.5
H(9A)-C(9)-H(9C)	109.5
H(9B)-C(9)-H(9C)	109.5
C(1)-C(10)-H(10A)	109.5
C(1)-C(10)-H(10B)	109.5
C(1)-C(10)-H(10C)	109.5
H(10A)-C(10)-H(10B)	109.5
H(10A)-C(10)-H(10C)	109.5

H(10B)-C(10)-H(10C)	109.5
C(12)-C(11)-C(4)	109.65(14)
C(12)-C(11)-C(14)	106.59(15)
C(13)-C(11)-C(4)	111.07(14)
C(13)-C(11)-C(12)	109.58(15)
C(13)-C(11)-C(14)	108.97(15)
C(14)-C(11)-C(4)	110.87(14)
C(11)-C(12)-H(12A)	109.5
C(11)-C(12)-H(12B)	109.5
C(11)-C(12)-H(12C)	109.5
H(12A)-C(12)-H(12B)	109.5
H(12A)-C(12)-H(12C)	109.5
H(12B)-C(12)-H(12C)	109.5
C(11)-C(13)-H(13A)	109.5
C(11)-C(13)-H(13B)	109.5
C(11)-C(13)-H(13C)	109.5
H(13A)-C(13)-H(13B)	109.5
H(13A)-C(13)-H(13C)	109.5
H(13B)-C(13)-H(13C)	109.5
C(11)-C(14)-H(14A)	109.5
C(11)-C(14)-H(14B)	109.5
C(11)-C(14)-H(14C)	109.5
H(14A)-C(14)-H(14B)	109.5
H(14A)-C(14)-H(14C)	109.5
H(14B)-C(14)-H(14C)	109.5
C(7)-C(15)-H(15A)	109.5
C(7)-C(15)-H(15B)	109.5
C(7)-C(15)-H(15C)	109.5
H(15A)-C(15)-H(15B)	109.5
H(15A)-C(15)-H(15C)	109.5
H(15B)-C(15)-H(15C)	109.5
C(7)-C(16)-H(16A)	109.5
C(7)-C(16)-H(16B)	109.5
C(7)-C(16)-H(16C)	109.5
H(16A)-C(16)-H(16B)	109.5

125

H(16A)-C(16)-H(16C)	109.5
H(16B)-C(16)-H(16C)	109.5
C(7)-C(17)-H(17A)	109.5
C(7)-C(17)-H(17B)	109.5
C(7)-C(17)-H(17C)	109.5
H(17A)-C(17)-H(17B)	109.5
H(17A)-C(17)-H(17C)	109.5
H(17B)-C(17)-H(17C)	109.5
C(2B)-O(1B)-H(1B)	109.5
C(6B)-O(2B)-H(2B)	109.5
C(8B)-C(1B)-C(2B)	111.95(14)
C(8B)-C(1B)-C(10B)	109.58(15)
C(9B)-C(1B)-C(2B)	108.44(14)
C(9B)-C(1B)-C(8B)	109.25(16)
C(9B)-C(1B)-C(10B)	108.36(15)
C(10B)-C(1B)-C(2B)	109.18(14)
O(1B)-C(2B)-C(1B)	108.30(13)
O(1B)-C(2B)-H(2BA)	107.4
O(1B)-C(2B)-C(3B)	110.48(13)
C(1B)-C(2B)-H(2BA)	107.4
C(3B)-C(2B)-C(1B)	115.49(14)
C(3B)-C(2B)-H(2BA)	107.4
C(2B)-C(3B)-H(3BA)	108.7
C(2B)-C(3B)-H(3BB)	108.7
C(2B)-C(3B)-C(4B)	114.17(14)
H(3BA)-C(3B)-H(3BB)	107.6
C(4B)-C(3B)-H(3BA)	108.7
C(4B)-C(3B)-H(3BB)	108.7
C(3B)-C(4B)-H(4B)	106.2
C(3B)-C(4B)-C(5B)	112.36(14)
C(3B)-C(4B)-C(11B)	112.55(13)
C(5B)-C(4B)-H(4B)	106.2
C(5B)-C(4B)-C(11B)	112.66(13)
C(11B)-C(4B)-H(4B)	106.2
C(4B)-C(5B)-H(5BA)	108.9

C(4B)-C(5B)-H(5BB)	108.9
H(5BA)-C(5B)-H(5BB)	107.7
C(6B)-C(5B)-C(4B)	113.36(13)
C(6B)-C(5B)-H(5BA)	108.9
C(6B)-C(5B)-H(5BB)	108.9
O(2B)-C(6B)-C(5B)	105.05(13)
O(2B)-C(6B)-H(6B)	108.1
O(2B)-C(6B)-C(7B)	111.30(13)
C(5B)-C(6B)-H(6B)	108.1
C(5B)-C(6B)-C(7B)	116.02(13)
C(7B)-C(6B)-H(6B)	108.1
C(15B)-C(7B)-C(6B)	108.32(14)
C(15B)-C(7B)-C(16B)	108.28(14)
C(16B)-C(7B)-C(6B)	109.86(13)
C(17B)-C(7B)-C(6B)	111.27(13)
C(17B)-C(7B)-C(15B)	109.19(15)
C(17B)-C(7B)-C(16B)	109.85(14)
C(1B)-C(8B)-H(8BA)	109.5
C(1B)-C(8B)-H(8BB)	109.5
C(1B)-C(8B)-H(8BC)	109.5
H(8BA)-C(8B)-H(8BB)	109.5
H(8BA)-C(8B)-H(8BC)	109.5
H(8BB)-C(8B)-H(8BC)	109.5
C(1B)-C(9B)-H(9BA)	109.5
C(1B)-C(9B)-H(9BB)	109.5
C(1B)-C(9B)-H(9BC)	109.5
H(9BA)-C(9B)-H(9BB)	109.5
H(9BA)-C(9B)-H(9BC)	109.5
H(9BB)-C(9B)-H(9BC)	109.5
C(1B)-C(10B)-H(10D)	109.5
C(1B)-C(10B)-H(10E)	109.5
C(1B)-C(10B)-H(10F)	109.5
H(10D)-C(10B)-H(10E)	109.5
H(10D)-C(10B)-H(10F)	109.5
H(10E)-C(10B)-H(10F)	109.5

C(12B)-C(11B)-C(4B)	110.74(14)
C(13B)-C(11B)-C(4B)	111.43(14)
C(13B)-C(11B)-C(12B)	108.80(15)
C(13B)-C(11B)-C(14B)	109.69(14)
C(14B)-C(11B)-C(4B)	109.39(14)
C(14B)-C(11B)-C(12B)	106.67(14)
C(11B)-C(12B)-H(12D)	109.5
C(11B)-C(12B)-H(12E)	109.5
C(11B)-C(12B)-H(12F)	109.5
H(12D)-C(12B)-H(12E)	109.5
H(12D)-C(12B)-H(12F)	109.5
H(12E)-C(12B)-H(12F)	109.5
C(11B)-C(13B)-H(13D)	109.5
C(11B)-C(13B)-H(13E)	109.5
C(11B)-C(13B)-H(13F)	109.5
H(13D)-C(13B)-H(13E)	109.5
H(13D)-C(13B)-H(13F)	109.5
H(13E)-C(13B)-H(13F)	109.5
C(11B)-C(14B)-H(14D)	109.5
C(11B)-C(14B)-H(14E)	109.5
C(11B)-C(14B)-H(14F)	109.5
H(14D)-C(14B)-H(14E)	109.5
H(14D)-C(14B)-H(14F)	109.5
H(14E)-C(14B)-H(14F)	109.5
C(7B)-C(15B)-H(15D)	109.5
C(7B)-C(15B)-H(15E)	109.5
C(7B)-C(15B)-H(15F)	109.5
H(15D)-C(15B)-H(15E)	109.5
H(15D)-C(15B)-H(15F)	109.5
H(15E)-C(15B)-H(15F)	109.5
C(7B)-C(16B)-H(16D)	109.5
C(7B)-C(16B)-H(16E)	109.5
C(7B)-C(16B)-H(16F)	109.5
H(16D)-C(16B)-H(16E)	109.5
H(16D)-C(16B)-H(16F)	109.5

H(16E)-C(16B)-H(16F)   109.5

C(7B)-C(17B)-H(17D)   109.5

C(7B)-C(17B)-H(17E)   109.5

C(7B)-C(17B)-H(17F)   109.5

H(17D)-C(17B)-H(17E)   109.5

H(17D)-C(17B)-H(17F)   109.5

H(17E)-C(17B)-H(17F)   109.5

_____

Symmetry transformations used to generate equivalent atoms:

Table 16. Anisotropic displacement parameters ($Å^2$ x 10^4) for 5-(*tert*-butyl)-2,2,8,8-tetramethylnonane-3,7-diol. The anisotropic displacement factor exponent takes the form: $-2\pi^2$ [h^2 $a^{*2}U_{11}$ + ... + 2 h k a* b* U_{12}]

	U_{11}	U_{22}	U_{33}	U_{23}	U_{13}	U_{12}
O(1)	150(6)	142(6)	178(6)	24(4)	33(5)	7(5)
O(2)	248(7)	171(6)	140(6)	2(5)	57(5)	77(5)
C(1)	191(9)	192(9)	143(8)	-3(7)	14(7)	7(7)
C(2)	146(8)	141(7)	150(8)	-12(6)	34(6)	-13(6)
C(3)	166(8)	166(8)	166(8)	-4(6)	51(7)	22(6)
C(4)	171(8)	142(8)	149(8)	-22(6)	50(7)	10(6)
C(5)	176(9)	148(7)	146(8)	-14(6)	53(7)	2(7)
C(6)	176(8)	145(8)	133(8)	0(6)	50(6)	-13(7)
C(7)	180(9)	191(8)	165(8)	21(6)	22(7)	-4(7)
C(8)	234(9)	188(9)	200(9)	34(7)	7(7)	-6(7)
C(9)	323(11)	353(11)	165(9)	28(8)	66(8)	52(9)
C(10)	207(9)	224(9)	232(9)	0(7)	-31(7)	-9(8)
C(11)	187(9)	176(8)	212(8)	-6(7)	94(7)	12(7)
C(12)	199(9)	306(10)	315(10)	-15(8)	110(8)	-26(8)
C(13)	280(10)	218(9)	246(9)	5(7)	148(8)	63(8)
C(14)	266(10)	224(9)	254(9)	26(8)	148(8)	17(8)
C(15)	220(10)	259(10)	267(10)	45(8)	-11(8)	50(8)
C(16)	305(11)	410(12)	163(9)	-20(8)	2(8)	21(9)
C(17)	198(10)	243(10)	386(12)	54(8)	34(8)	-61(8)

O(1B)	180(6)	167(6)	152(6)	-8(4)	59(5)	14(5)
O(2B)	163(6)	149(6)	228(6)	-51(5)	101(5)	-33(5)
C(1B)	170(8)	168(8)	209(9)	4(6)	91(7)	10(7)
C(2B)	162(8)	147(7)	157(8)	21(6)	57(7)	12(7)
C(3B)	169(8)	155(8)	147(8)	-12(6)	59(7)	15(6)
C(4B)	150(8)	123(7)	148(8)	-5(6)	52(6)	-5(6)
C(5B)	143(8)	145(8)	156(8)	2(6)	57(6)	-14(6)
C(6B)	141(8)	142(8)	163(8)	-3(6)	62(6)	5(6)
C(7B)	159(8)	158(8)	154(8)	-15(6)	71(6)	8(7)
C(8B)	234(9)	183(8)	275(9)	-10(7)	135(8)	34(7)
C(9B)	162(9)	261(10)	346(11)	-14(8)	110(8)	-15(8)
C(10B)	298(10)	290(10)	247(10)	55(8)	167(8)	46(8)
C(11B)	161(8)	184(8)	139(8)	10(6)	31(7)	23(7)
C(12B)	241(10)	311(10)	155(9)	35(7)	59(7)	60(8)
C(13B)	193(9)	193(9)	212(9)	-26(7)	10(7)	-10(7)
C(14B)	180(9)	200(8)	223(9)	20(7)	64(7)	25(7)
C(15B)	242(9)	198(9)	235(9)	-56(7)	120(8)	-10(7)
C(16B)	180(9)	245(9)	211(9)	-12(7)	98(7)	-15(7)
C(17B)	226(9)	244(9)	174(9)	32(7)	70(7)	25(7)

Table 17. Hydrogen coordinates (x 10⁴) and isotropic displacement parameters (Å² x 10³) for 5-(*tert*-butyl)-2,2,8,8-tetramethylnonane-3,7-diol.

	x	y	z	U(eq)
H(1)	4591	3656	4269	24
H(2)	5507	2473	5535	28
H(2A)	2504	3398	3145	18
H(3A)	1237	4120	4297	20
H(3B)	2588	4579	4970	20
H(4)	2759	3045	5370	18
H(5A)	4558	4116	6403	19
H(5B)	4146	3834	7661	19
H(6)	4757	2608	7204	18
H(8A)	1713	5348	3032	33
H(8B)	1817	5494	1565	33
H(8C)	3162	5340	2805	33
H(9A)	3682	4332	1334	42
H(9B)	2265	4465	176	42
H(9C)	2637	3675	823	42
H(10A)	392	3667	1377	37
H(10B)	82	4442	660	37
H(10C)	36	4343	2159	37
H(12A)	-113	3419	4832	40
H(12B)	-357	3010	6080	40
H(12C)	507	2627	5253	40
H(13A)	2118	4413	7656	35
H(13B)	650	4117	7584	35
H(13C)	862	4506	6303	35
H(14A)	2386	2441	7483	35
H(14B)	1445	2838	8211	35
H(14C)	2961	3118	8453	35
H(15A)	7014	2029	8332	41
H(15B)	8388	2489	8683	41

H(15C)	7532	2323	7148	41
H(16A)	6145	3780	9424	47
H(16B)	7433	3270	10085	47
H(16C)	5938	2931	9611	47
H(17A)	7446	3700	6656	43
H(17B)	8333	3820	8198	43
H(17C)	6924	4241	7577	43
H(1B)	4489	6176	4757	25
H(2B)	5353	4871	4465	26
H(2BA)	4518	5841	6706	18
H(3BA)	6115	6714	8272	19
H(3BB)	6122	7132	6940	19
H(4B)	6838	5624	7269	17
H(5BA)	6714	6547	5190	18
H(5BB)	8266	6305	5821	18
H(6B)	7549	5043	5515	17
H(8BA)	4264	7747	7615	33
H(8BB)	2656	7755	7318	33
H(8BC)	3261	7726	6097	33
H(9BA)	1825	6592	5224	37
H(9BB)	1260	6625	6473	37
H(9BC)	1970	5901	6183	37
H(10D)	3645	5929	8588	39
H(10E)	2839	6627	8833	39
H(10F)	4449	6663	9151	39
H(12D)	7772	6465	9935	36
H(12E)	9252	6109	10465	36
H(12F)	7956	5613	9759	36
H(13D)	9217	7116	7463	32
H(13E)	10016	7053	9040	32
H(13F)	8503	7369	8531	32
H(14D)	9244	5173	8205	30
H(14E)	10456	5714	8948	30
H(14F)	9783	5745	7347	30
H(15D)	7774	4304	3659	32

H(15E)	7246	4587	2137	32
H(15F)	6186	4433	2923	32
H(16D)	8812	6193	3896	31
H(16E)	8950	5574	2879	31
H(16F)	9376	5408	4457	31
H(17D)	5291	5711	2300	32
H(17E)	6428	5899	1624	32
H(17F)	6262	6398	2808	32

Appendix 5

Supplementary information for Chapter 5

A5.1 Thermal analysis

Thermogravimetric analyses (TGA) were performed utilizing 2 mg of sample on a TGA/DSC 1 system with a sulfur trap attached to avoid release of mercury vapors to the open atmosphere. The system was operated on a PC with STAR^e software. Samples were heated from 25-600 °C at a rate of 10 °C/min under flowing air. The balance and purge flow were 40 mL min^{-1} and 25 mL min^{-1}, respectively.

A5.2 Powder X-ray diffraction (PXRD) collection

Powder X-ray diffraction (PXRD) patterns were collected using a Bruker D2 Phaser powder diffractometer equipped with a Cu-Ka ($\lambda = 1.5418$ Å) source and Lynxeye detector. The patters were collected in the angle region of 4° and 40° (2θ) with a step size of 0.05°. PXRD patterns used for structure solution-refinement were collected in the angle region between 4° and 70° (2θ) with a step size of 0.02° and 6.0 s counting per step.

A5.3 Structure determination from powder X-ray data

The PXRD pattern of *sql*-Hg(**Im**)$_2$ was indexed using the DASH 3.4.2 program suite[319] and the 2 DICVOL06 algorithm[320], giving the following unit cell with orthorhombic metric symmetry: $a = 9.41$ Å, $b = 7.64$ Å, $c = 5.36$ Å ($V = 385.3$ Å^3). The space group was assigned as $P2_12_12$. From consideration of the density and volume of the unit cell, there are two formula units of Hg(**Im**)$_2$ ($Z = 2$) in the unit cell. Profile fitting using the Pawley method[321] in the TOPAS6[322]

program gave a reasonable quality of fit (Rp = 5.74%, Rwp = 8.69%), and refined unit cell parameters of a = 9.4089(4) Å, b = 7.6414(3) Å and c = 5.3625(2) Å. The refined unit cell parameters were used in the subsequent structure-solution calculation. Structure solution was carried out using the simulated annealing technique in the program DASH 3.4.2. The crystal structure was defined by 9 variables: six variables for the imidazolate fragment (three positional variables and three orientational variables), and three positional variables for the Hg^{2+} cation. The structure solution was then used as the starting model for Rietveld refinement, carried out in TOPAS6 program.[323] In the Rietveld refinement, standard restraints were applied to bond lengths and bond angles, and planar restraints were applied to the imidazolate group. The final Rietveld refinement gave a reasonable fit to the powder XRD data (Rp = 7.09%, Rwp = 9.22%).

A5.4 Solid-state nuclear magnetic resonance (NMR) spectroscopy

All MAS spectra and the static ^{113}Cd powder pattern were acquired on a Varian VNMRS (now Agilent, Santa Clara, CA, USA) spectrometer operating at 399.8 MHz for ^{1}H, 100.5 MHz for ^{13}C, 89.5 MHz for ^{199}Hg, 88.7 MHz for ^{113}Cd, and 40.5 MHz for ^{15}N using a 4 mm double-resonance Varian Chemagnetics T3 probe (now Agilent, Santa Clara, CA, USA). Approximately 70 mg of sample were center-packed into rotors using either Teflon or boron nitride inserts, and spun at between 8 and 15 kHz for MAS. The static ^{199}Hg spectrum of *sql*-Hg(**Im**)$_2$ was acquired on a Varian VNMRS spectrometer operating at 499.9 MHz for ^{1}H and 89.5 MHz for ^{199}Hg using a 6 mm double-resonance Varian Chemagnetics T3 probe. The ^{13}C CPMAS spectrum was acquired in 512 scans under spinning at 8 kHz, using a recycle delay of 10 s with a contact time of 4 ms at a ^{13}C rf field of approximately 60 kHz. SPINAL-64 decoupling at an rf field of 90 kHz was applied during acquisition. Spectra were referenced

using the carbonyl carbon signal in glycine at 176.4 ppm with respect to TMS.[324] The ^{15}N

CPMAS spectrum of *sql*-Hg(**Im**)$_2$ was acquired under spinning at 8 kHz in 7260 scans, with a

contact time of 3 ms at a ^{15}N rf field of approximately 45 kHz. The recycle delay was 10 s.

SPINAL-64 decoupling at an rf field of 70 kHz was applied during acquisition. Spectra were

referenced using the nitrogen signal in glycine at 33.4 ppm with respect to liquid ammonia.[325]

The ^{199}Hg BRAIN-CP/WURST-CPMG[246] spectrum of *sql*-Hg(**Im**)$_2$ was acquired in 896 scans

using a recycle delay of 8 s. A 4 μs (62.5 kHz) π/2 excitation pulse was used on the ^{1}H channel

and 40 kHz of spin-locking power was applied on both channels for the optimized contact time.

The WURST spin-locking pulse of ^{199}Hg was swept over 400 kHz in 6000 points. The CPMG

refocusing portion of the sequence used 50 μs WURST-80 pulses, with $\nu_1 = 35$ kHz and 800

kHz sweep ranges. The spectral width was 500 kHz (2 μs dwell time). The acquisition period

of a single echo was 0.56 ms and 29 echoes were acquired in each scan. All ^{199}Hg spectra were

referenced using the isotropic ^{199}Hg chemical shift of mercuric acetate at -2495 ppm with

respect to Hg(CH$_3$)$_2$.[326] Two ^{199}Hg CPMAS spectra (not shown) were acquired of *sql*-Hg(**Im**)$_2$,

one under spinning at 8 kHz (768 scans) and the other spinning at 10 kHz (2048 scans). In both,

a contact time of 8 ms was used at a ^{199}Hg rf field of approximately 50 kHz. SPINAL-64

decoupling at an rf field of 90 kHz was applied during acquisition and the recycle delay was 5

s. The ^{113}Cd static spectrum of *dia*-Cd(**Im**)$_2$was acquired using cross-polarization at an rf field

of approximately 50 kHz in 6144 scans using a 5 s recycle delay. Spectra were referenced to

Cd(NO$_3$)$_2$ at -102.2 ppm with respect to Cd(ClO$_4$)$_2$·6H$_2$O.[327] ^{1}H single-pulse spectra were

acquired with spinning at 15 kHz and were referenced to adamantane at 1.87 ppm[328] with

respect to TMS. High resolution ^{1}H spectra were acquired using the windowed PMLG-5[329]

sequence with 100 kHz rf (16.3 μs pulses and 1 μs acquisition) for a total of 10 ms acquisition

in 4 scans (recycle delay of 4 s). The PMLG spectra were referenced and scaled using a spectrum of α-glycine whose signals were referenced to 8.4 ppm and 3.4 ppm (the center of the CH_2 signals) with respect to TMS.[330]

A5.5 Fourier-transform infrared attenuated total reflectance (FTIR-ATR) spectroscopy

Infrared spectra were obtained using a Bruker Alpha FT-IR spectrometer (Bruker Optics Ltd., Milton, ON, Canada) decorated by diamond crystal in the range of 4000-450 cm^{-1} and with resolution of 4 cm^{-1}, and are reported in wavenumber (cm^{-1}) units for the most significant absorption bands.

A5.6 Scanning Electron Microscopy (SEM)

Scanning electron microscopy images were obtained using a FEI Quanta FEG 450 scanning electron microscope. Samples were suspended in hexanes and deposited onto carbon tape, then vacuum sputtered with platinum.

A5.7 Synthesis of *dia*-Cd(Im)$_2$ framework from solution

A solution of $Cd(NO_3)_2$ (500.0 mg, 2.12 mmol) in 17 mL of MeOH was added to a 100 mL round bottom flask equipped with a Teflon stirring bar. To the stirring solution, H**Im** (288.7 mg, 4.24 mmol, 2 equiv.) dissolved in 7 mL of MeOH was added all at once. NaOH (169.5 mg, 4.24 mmol, 2 equiv.) was dissolved in 1 mL of deionized water and added dropwise to the stirring solution. After 5 min of stirring, a white precipitate formed. The reaction was vacuum filtered and the filtrate was washed twice with 10 mL portions of methanol and twice with 10

mL portions of deionized water. To ensure its dryness, the product was placed in a 45 °C oven for 30 minutes. The product was identified by its characteristic PXRD pattern.

A5.8 Synthesis of *zni*-Zn(Im)$_2$ framework by milling

A solid mixture of ZnO (75.0 mg, 0.94 mmol) and H**Im** (123.0 mg, 1.80 mmol, 2 equiv.) was placed in a 25 mL Teflon milling jar with 2 zirconia balls (3.25 g each) and 100 µL of MeOH. The reaction was milled at 30 Hz for 1 h to give a white free-flowing powder. The material was analyzed without further treatment and identified by its characteristic PXRD pattern.

A5.9 Slurry experiments on *sql*-Hg(Im)$_2$

To a small glass vial equipped with a Teflon stirring bar was added 50 mg of the mechanochemically generated *sql*-Hg(**Im**)$_2$ and 1 mL of solvent (water, acetone, MeCN, CHCl$_3$, MeOH, or EtOH). The slurry was stirred at room temperature for 2 days, after which the products were filtered and immediately analyzed with powder X-ray diffraction (See Figure 27).

A5.10 Geometry optimization of MOFs

The *dia*- and *sql*- structures of Hg(**Im**)$_2$ and Cd(**Im**)$_2$ were geometry-optimized using the periodic DFT code CRYSTAL17[250] using the hybrid B3LYP[251-252] functional supplemented with the Grimme D3[253] semiempirical dispersion correction. The wavefunctions were constructed using the POB-TZVP basis set (H, C, N, Cd)[331-332] and a double-zeta basis set for Hg.[333] Effective core potentials (ECPs) were used for Cd and Hg atoms.[334] The electronic 1st Brillouin zone was sampled with a 0.05 Å^{-1} Monkhorst-Pack k-point spacing. Crystal structures

were optimized with respect to atom coordinates and unit cell parameters, subject to the symmetry constraints of their respective space groups. The following convergence criteria were used for geometry optimization: maximum force on atom $4.5 \cdot 10^{-4}$ Ha Bohr^{-1}, RMS force $3.0 \cdot 10^{-4}$ Ha Bohr^{-1}, maximum atom displacement $1.8 \cdot 10^{-3}$ Bohr, RMS atom displacement $1.2 \cdot 10^{-3}$ Bohr. The energies of all crystal structures were corrected for basis set superposition error (BSSE) using the counterpoise method with ghost atoms located up to 5 Å away from the reference molecule.

A5.11 Bader analysis of MOFs

Topological analysis of the calculated electron density for the optimized *sql* structures of Hg(**Im**)$_2$ and Cd(**Im**)$_2$ was performed using the TOPOND program accessed through the CRYSTAL Properties module. In the case of Hg(**Im**)$_2$, the electron density obtained from the final geometry optimization step was used in the analysis. For Cd(**Im**)$_2$ a single point calculation using a double zeta basis set for Cd atom was performed.[335] This was necessary, as the *f*-functions in the original POB_TZVP basis set for Cd could not be processed by the TOPOND code. Critical points were searched using an automated eigenvector following algorithm. The contour electron density and Laplacian contour plots (Figures 34) were drawn with the aid of the CRYSPLOT visualization tool.
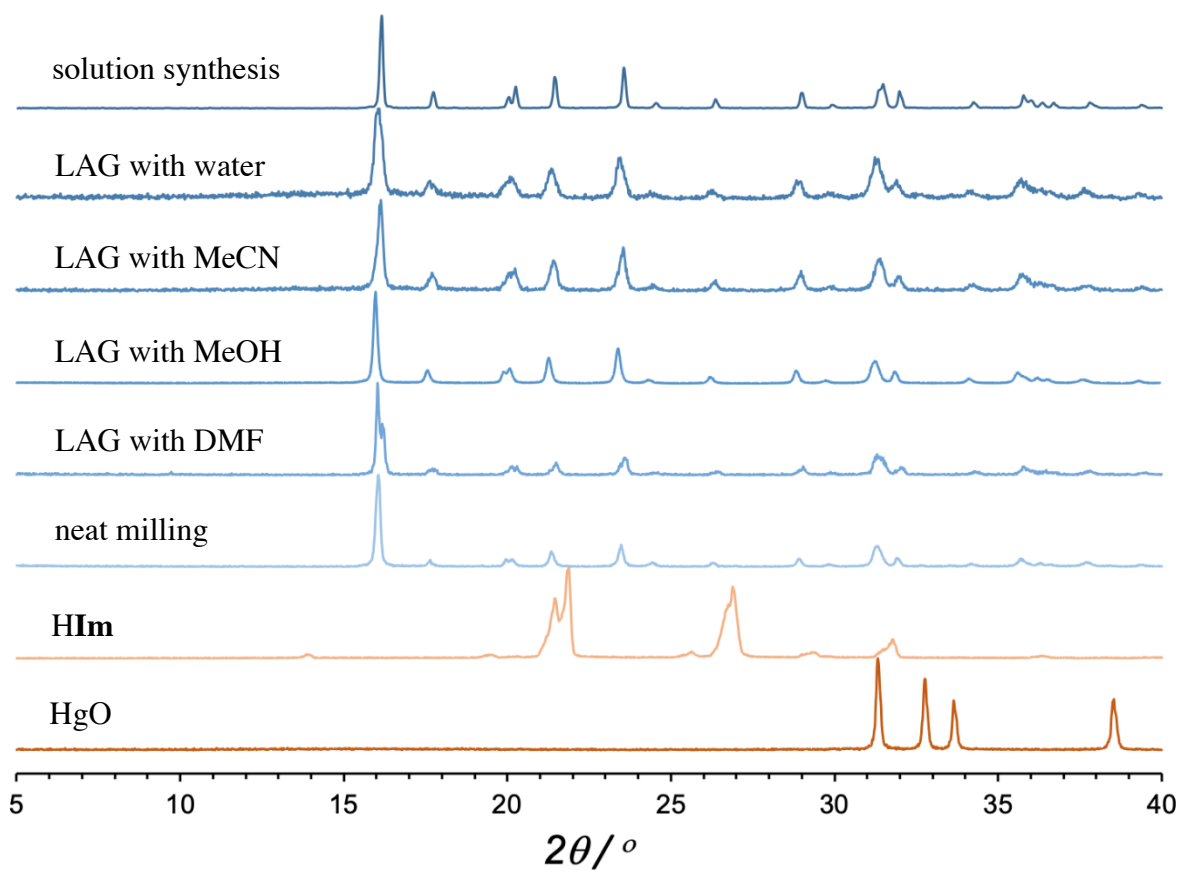
Figure 29. Selected PXRD patterns for Hg(Im)$_2$ product obtained from solution synthesis or by mechanochemical reaction of 1 HgO + 2 HIm by neat milling or LAG with different solvent additives. All milling reactions were performed in a 25 mL Teflon jar using one 7 mm diameter (3.2 g weight) zirconia ball, and either a Retsch MM400 or MM200 mill operating at 25 Hz for 30 minutes. For LAG reactions, 50 μL of a liquid phase were added to the reaction mixture.
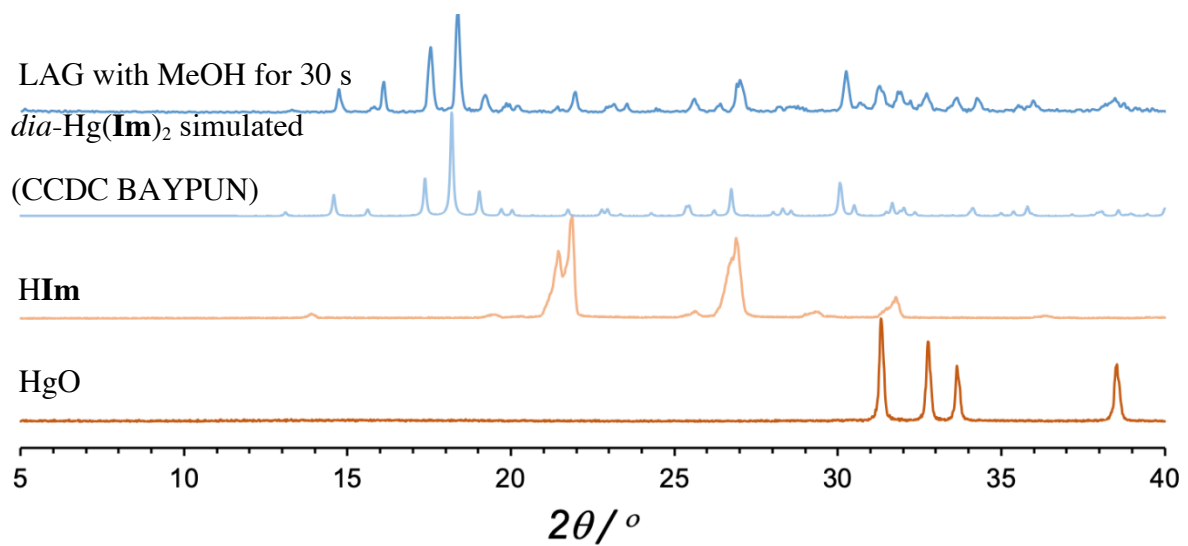
Figure 30. Selected PXRD patterns for attempts of mechanochemical synthesis of *dia*-Hg(Im)$_2$ by LAG. All reactions were performed in a 25 mL Teflon jar using one 7 mm diameter (3.2 g weight) zirconia ball, and a Retsch MM400 or MM200 mill operating at 25 Hz. In all reactions, 50 μL of MeOH was added.
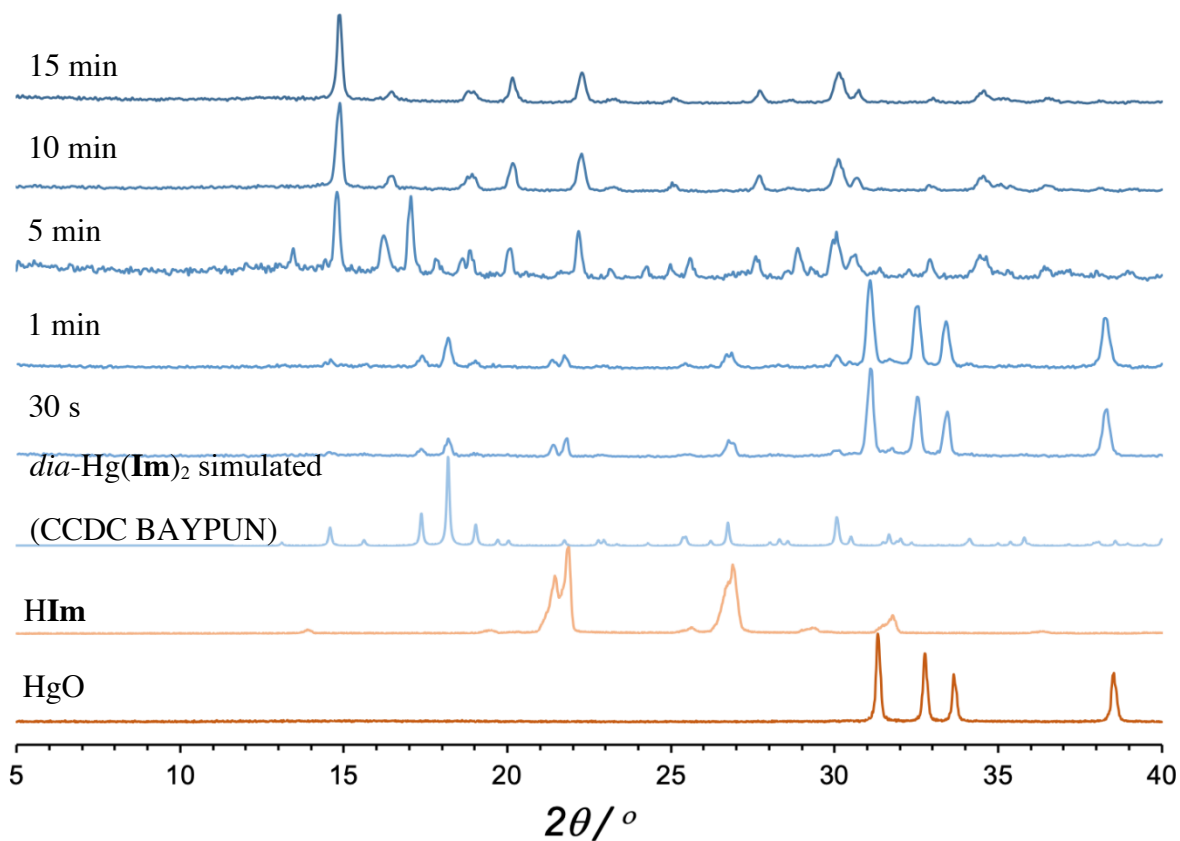
Figure 31. Selected PXRD patterns for attempts of mechanochemical synthesis of *dia*-Hg(Im)$_2$ by neat milling. All reactions were performed in a 25 mL Teflon jar using one 7 mm diameter (3.2 g weight) zirconia ball, and a Retsch MM400 or MM200 mill operating at 25 Hz.
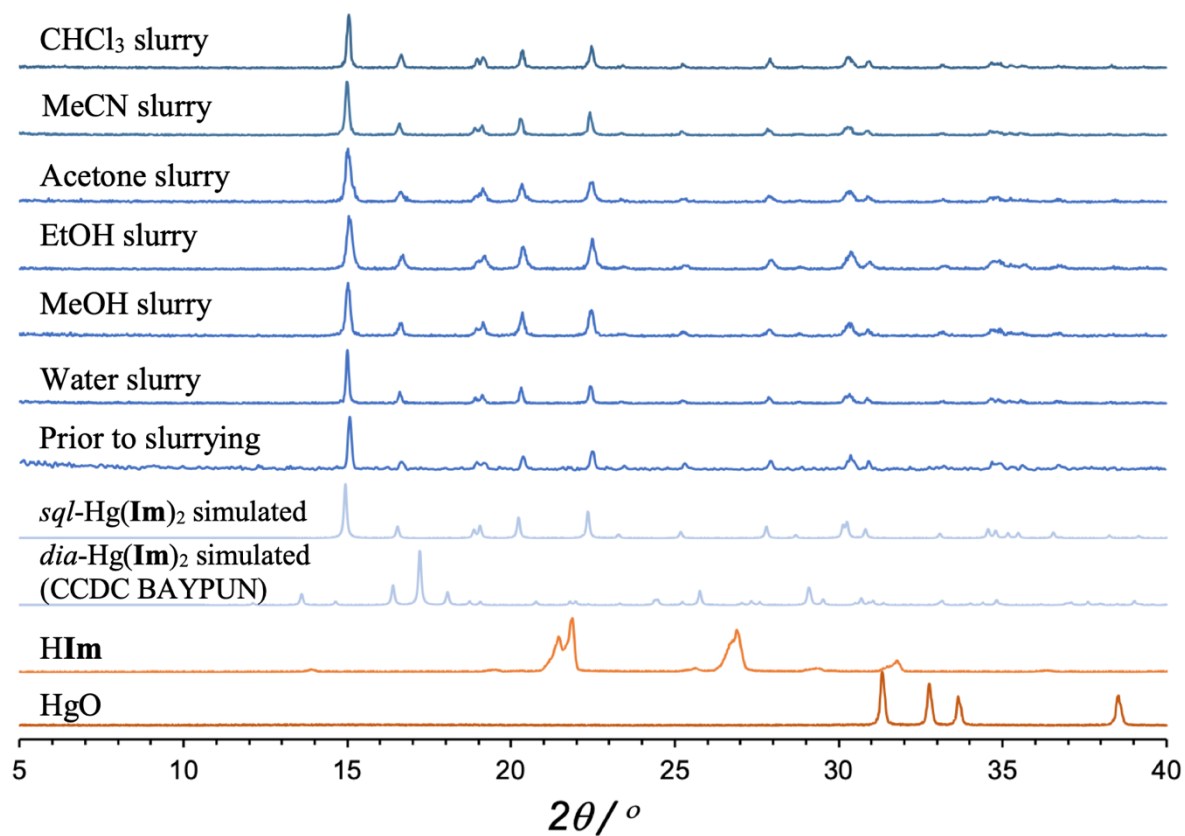
Figure 32. Comparison of PXRD patterns from slurrying experiments involving *sql*-Hg(Im)$_2$. All experiments were performed in glass vials with 1 mL of solvent and 50 mg of pure framework material at room temperature for 2 days.
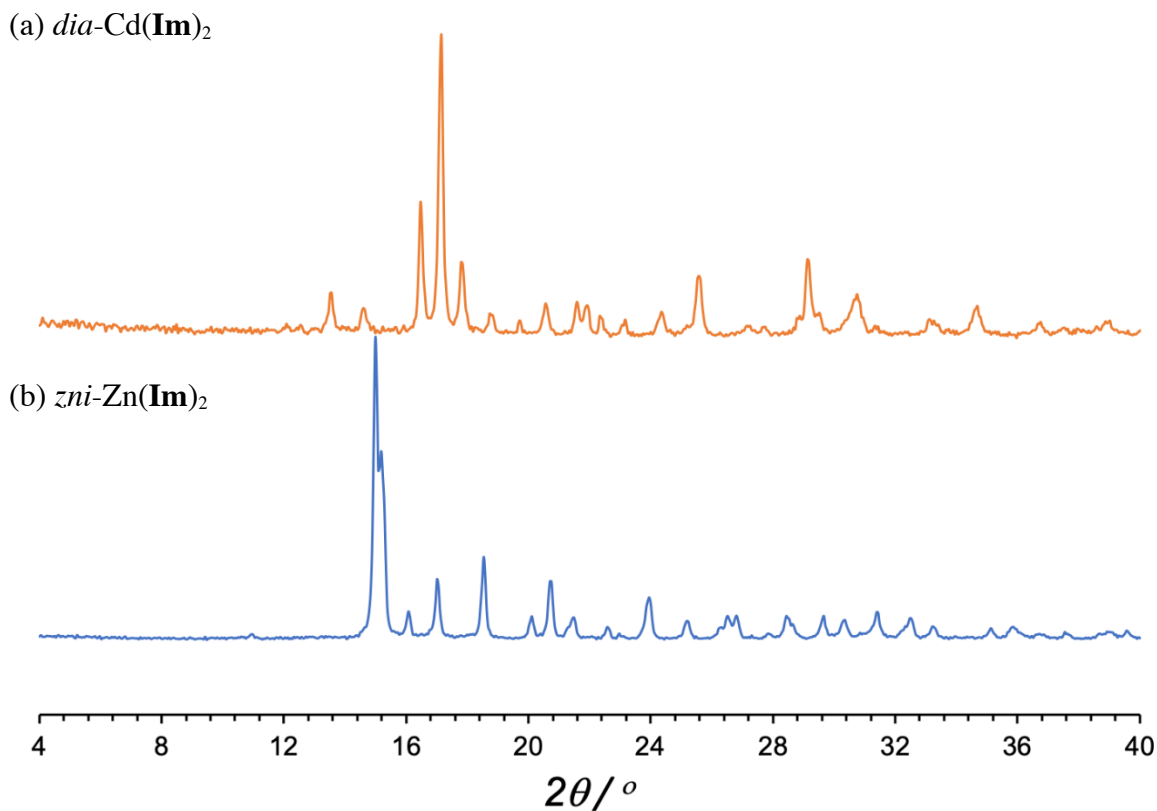
Figure 33. Experimental powder patterns for (a) *dia*-Cd(Im)$_2$ and (b) *zni*-Zn(Im)$_2$ prepared from solution. The measured patterns match the ones calculated for the previously reported structures, confirming the reproducible formation of three-dimensional dense frameworks in case of cadmium and zinc nodes.
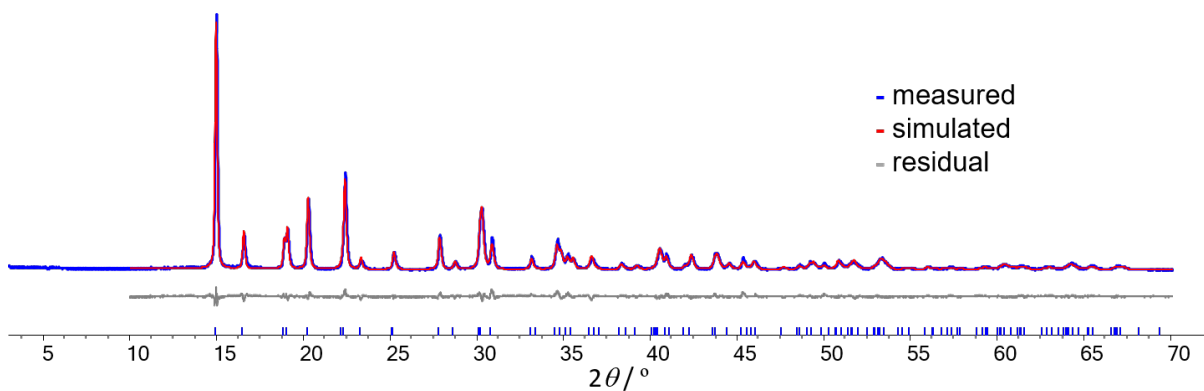
Figure 34. The final Rietveld fit for the *sql*–Hg(Im)$_2$ structure. Experimental pattern is shown in blue, calculated pattern in red, and difference curve in grey.

Table 18. Crystallographic data for structure of *sql*-Hg(Im)$_2$ polymorph determined from powder X-ray diffraction data.

|	*sql*–Hg(**Im**)$_2$
Formula	Hg(C$_3$H$_3$N$_2$)$_2$
M_r	334.73
Crystal system	orthorhombic
CSD deposition code	1948341
a / Å	9.4089(4)
b / Å	7.6414(3)
c / Å	5.3625(2)
α (°)	90
β (°)	90
γ (°)	90
V / Å^3	385.549(3)
Space group	$P2_12_12$
ϱ_c (g cm^{-3})	2.8835
Radiation type	Cu-$K\alpha$ ($\lambda = 1.5418$ Å)
$F(000)$	300
R_{wp} (%)	9.2
R_p (%)	7.1
R_{Bragg} (%)	2.7
χ^2	1.63
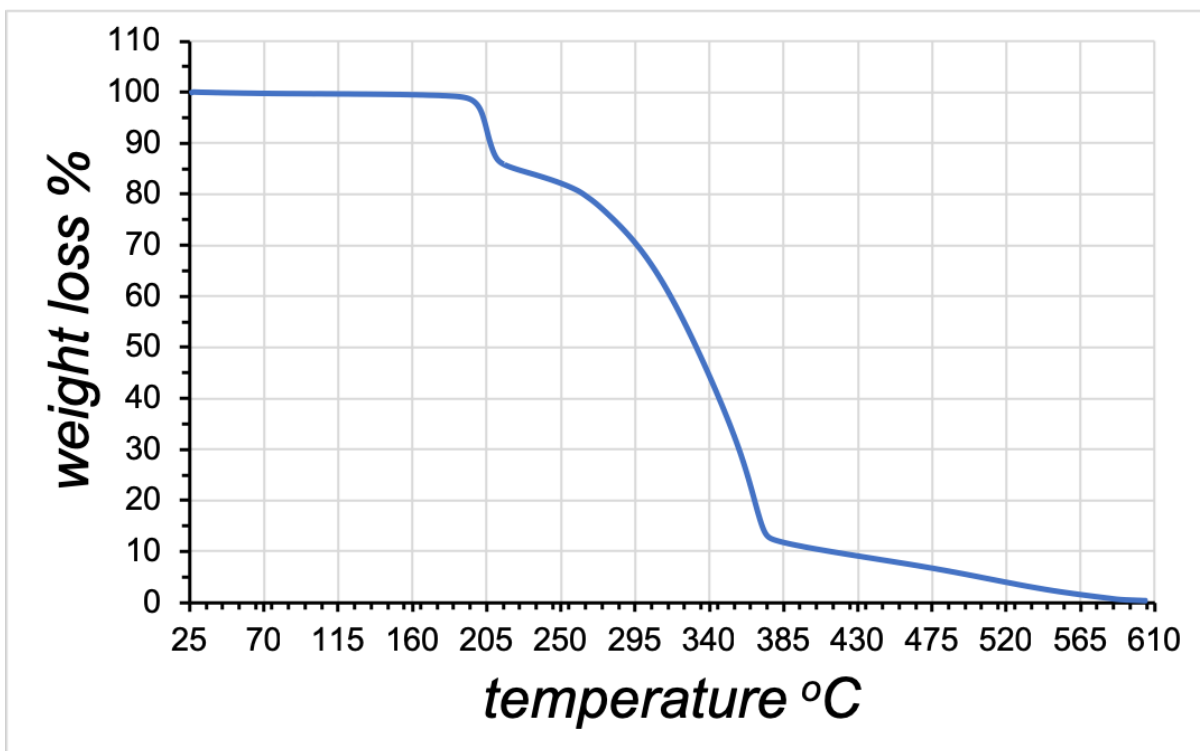
Figure 35. TGA thermogram of *sql*-Hg(Im)$_2$ framework prepared by LAG with MeOH.
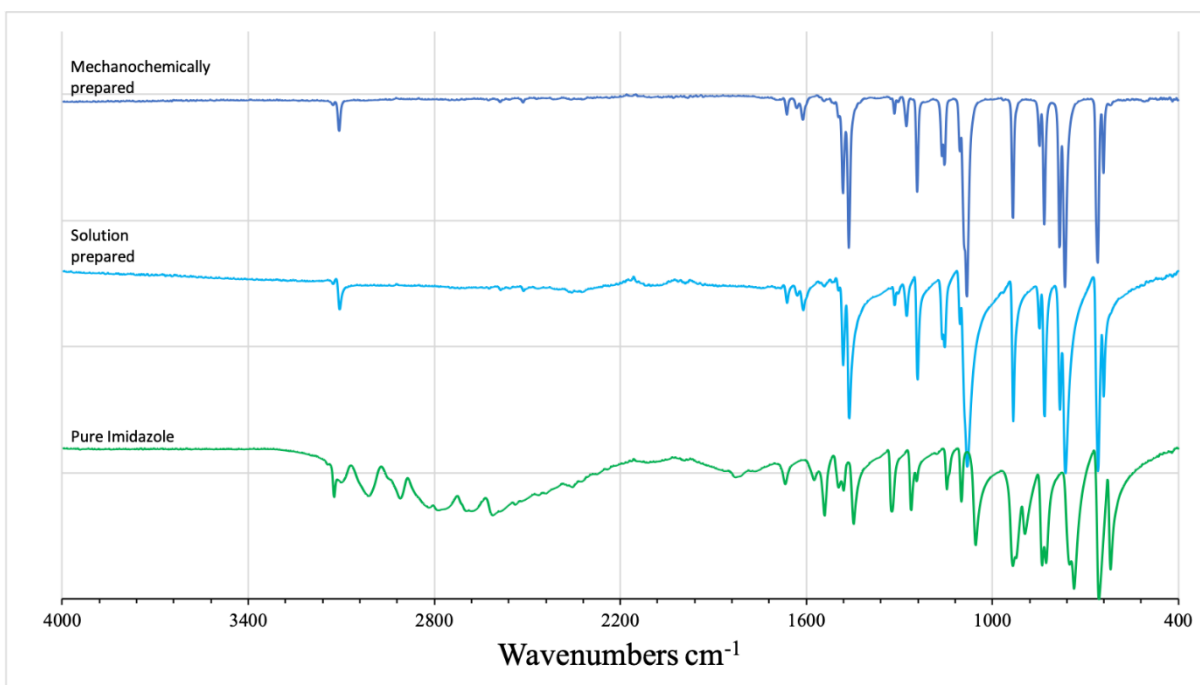
Figure 36. FTIR–ATR spectra of *sql*-Hg(Im)$_2$ products and relevant starting materials (from top to bottom): Mechanochemically prepared sample, with MeOH used as the LAG additive; solution-prepared *sql*-Hg(Im)$_2$; solid HIm ligand.

146
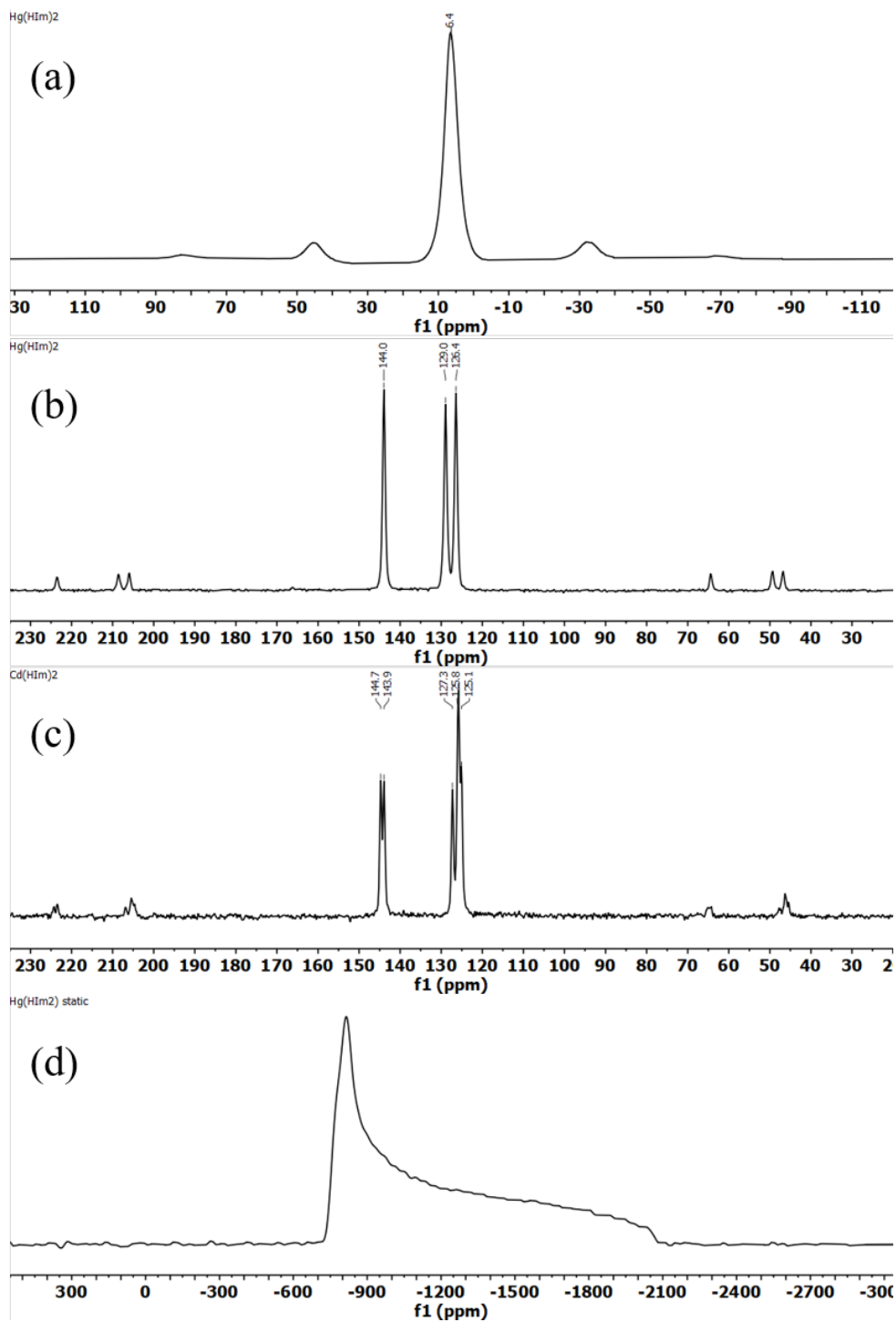
Figure 37. Solid-state NMR spectra of *sql*-Hg(Im)$_2$: a) ^{1}H; b) ^{13}C; c) ^{15}N; and d) ^{199}Hg (static). In (a), (b), and (c), only the center bands are labeled with chemical shift values; the other signals are spinning sidebands.
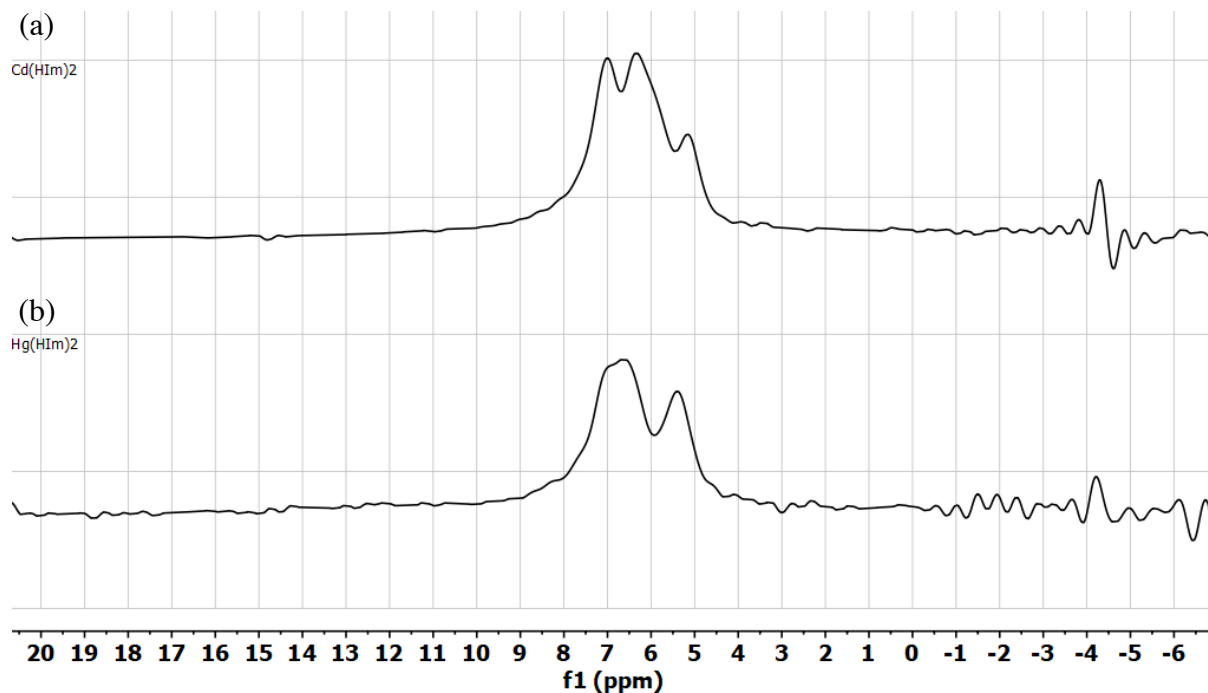
Figure 38. ^{1}H PMLG-5 ssNMR spectra for: (a) *dia*-Cd(Im)$_2$, and (b) *sql*-Hg(Im)$_2$. The signals between 5 and 8 ppm are real signals; those at lower ppm values are artifacts of the windowed PMLG sequence.
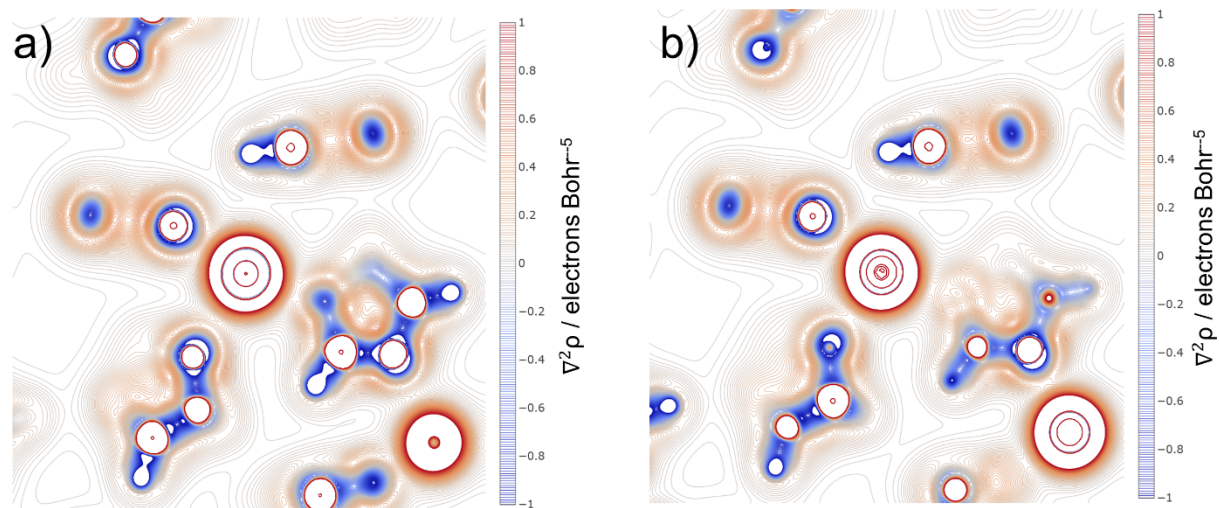
Figure 39. 2-D contour plots showing the Laplacian electron density for select regions of the: a) *sql*-Hg(Im)$_2$ and b) hypothetical *sql*-Cd(Im)$_2$ structure. The orientation of the plots is identical to that in Figures 7b,d in the main text.

148
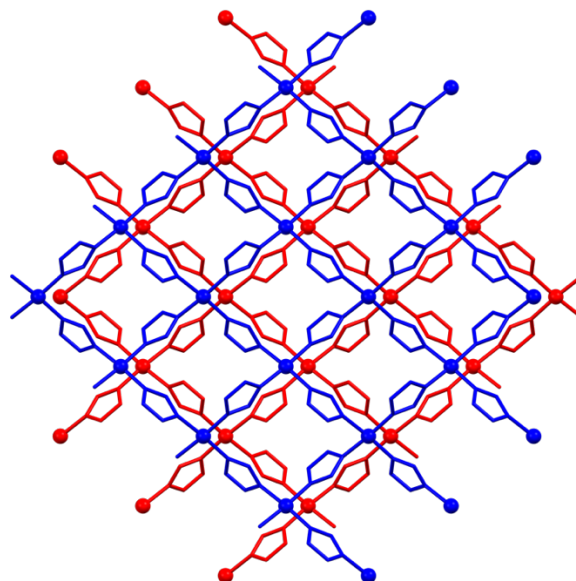
Figure 40. A view of two layers (top layer blue, bottom layer red) of the *sql*-Ni(Im)₂ framework, perpendicular to the layers and parallel to the crystallographic *c*-axis (CSD code ALIDUU). Metal atoms are shown as spheres.
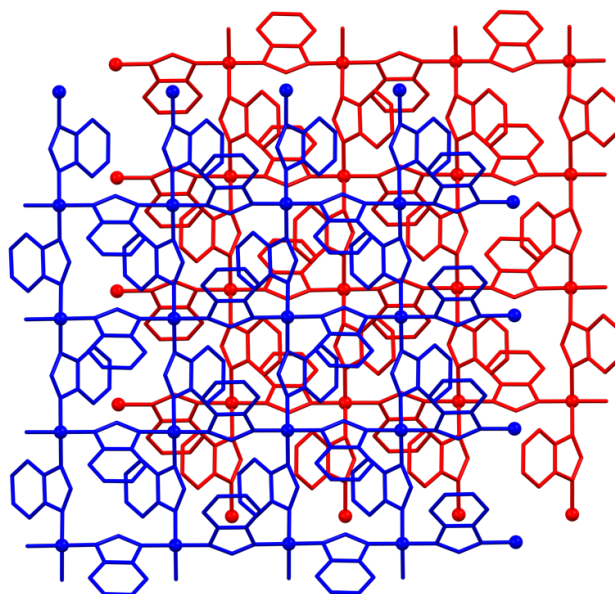
Figure 41. A view of two layers (top layer blue, bottom layer red) of the *sql*-Zn(BzIm)₂ framework, perpendicular to the layers and the crystallographic *ab*-plane (CSD code KOLYAM). Metal atoms are shown as spheres. Hydrogen atoms are omitted for clarity.
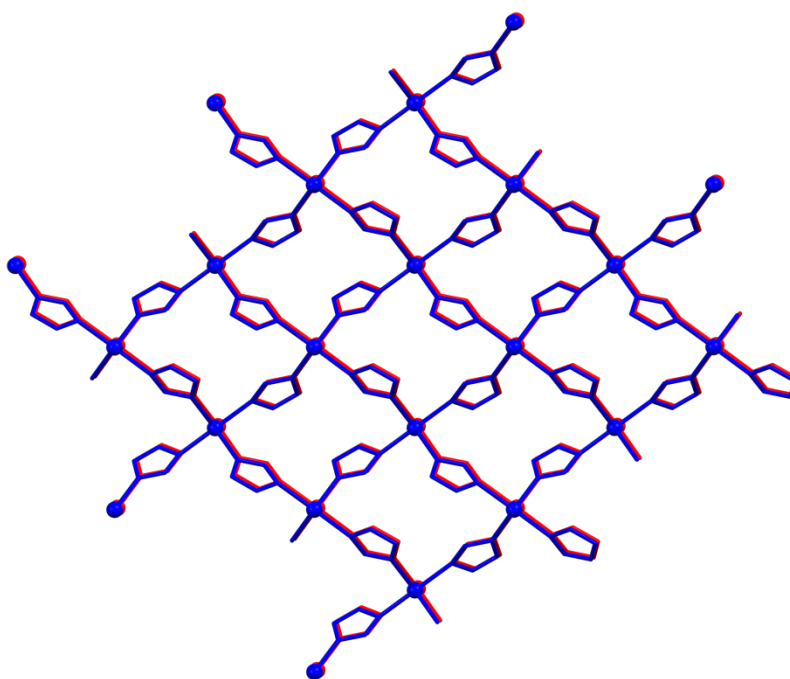
Figure 42. A view of two layers (top layer blue, bottom layer red) of the *sql*-Hg(Im)$_2$ framework, approximately normal to the planes and slightly offset from the crystallographic *c*-axis to illustrate direct stacking of the layers plane. Metal atoms are shown as spheres. Hydrogen atoms are omitted for clarity.
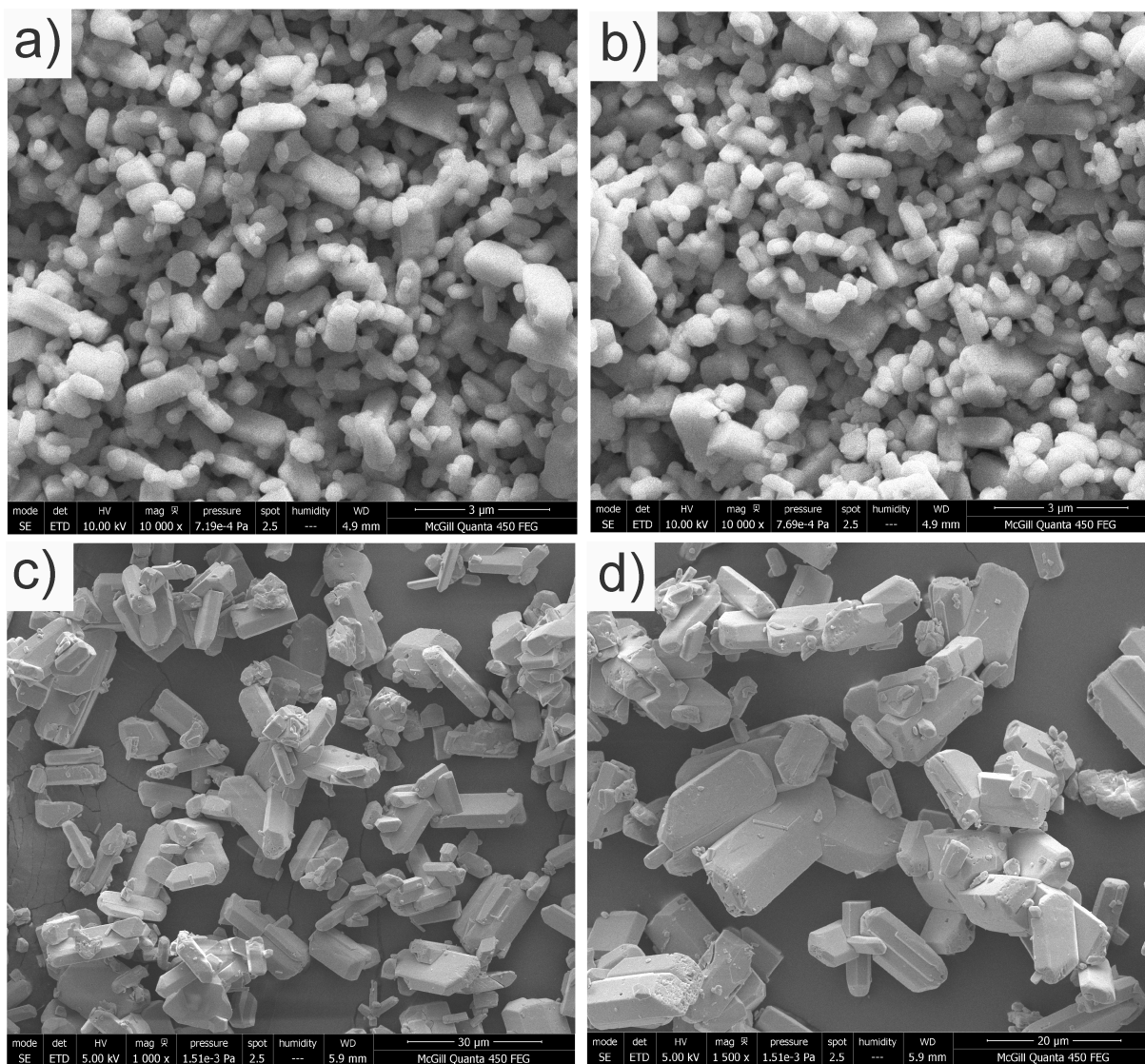
Figure 43. Scanning electron microscope images of the *sql*-Hg(Im)$_2$ framework synthesized by a,b) mechanochemical methods and by c,d) solution methods.

References

1. Anastas, P. T.; Warner, J. C., Principles of green chemistry. In Green chemistry: theory and practice, Anastas, P. T.; Warner, J. C., Eds. Oxford University Press: Oxford, UK, 1998; pp 29–56.

2. Kharissova, O. V.; Kharisov, B. I.; Oliva González, C. M.; Méndez, Y. P.; López, I., Greener synthesis of chemical compounds and materials. *R. Soc. Open Sci.* **2019,** *6* (11), 191378-191378.

3. Zink, J., Squeezing light out of crystals: Triboluminescence. *Naturwissenschaften* **1981,** *68* (10), 507-512.

4. Takacs, L., What is unique about mechanochemical reactions? *Acta Phys. Pol. A* **2014,** *126* (4), 1040-1043.

5. Rightmire, N. R.; Hanusa, T. P., Advances in organometallic synthesis with mechanochemical methods. *Dalton Trans.* **2016,** *45* (6), 2352-62.

6. Osorio, J. G.; Muzzio, F. J., Evaluation of resonant acoustic mixing performance. *Powder Technol.* **2015,** *278*, 46-56.

7. Howard, Joseph L.; Cao, Q.; Browne, D. L., Mechanochemistry as an emerging tool for molecular synthesis: what can it offer? *Chem. Sci.* **2018,** *9* (12), 3080-3094.

8. Bobet, J. L.; Even, C.; Nakamura, Y.; Akiba, E.; Darriet, B., Synthesis of magnesium and titanium hydride via reactive mechanical alloying. *J. Alloys Compd.* **2000,** *298* (1-2), 279-284.

9. Do, J. L.; Mottillo, C.; Tan, D.; Strukil, V.; Friscic, T., Mechanochemical ruthenium-catalyzed olefin metathesis. *J Am Chem Soc* **2015,** *137* (7), 2476-9.

10. Oprea, C. V.; Popa, M.; Hurduc, N., Mechanochemically Initiated Polymerizations III. Mechanochemical Polymerization of Acetonitrile by Vibratory Grinding. *Polym. J.* **1984,** *16* (3), 191-197.

11. Speight, I. R.; Huskic, I.; Arhangelskis, M.; Titi, H. M.; Stein, R. S.; Hanusa, T. P.; Friscic, T., Disappearing Polymorphs in Metal-Organic Framework Chemistry: Unexpected Stabilization of a Layered Polymorph over an Interpenetrated Three-Dimensional Structure in Mercury Imidazolate. *Chem. -Eur. J.* **2020,** *26* (8), 1811-1818.

12. Rightmire, N. R.; Bruns, D. L.; Hanusa, T. P.; Brennessel, W. W., Mechanochemical Influence on the Stereoselectivity of Halide Metathesis: Synthesis of Group 15 Tris(allyl) Complexes. *Organometallics* **2016,** *35* (11), 1698-1706.

13. Cseri, L.; Razali, M.; Pogany, P.; Szekely, G., Organic Solvents in Sustainable Synthesis and Engineering. In *Green Chemistry*, 2018; pp 513-553.

14. Tan, D.; Friščić, T., Mechanochemistry for Organic Chemists: An Update. *European Journal of Organic Chemistry* **2018,** *2018* (1), 18-33.

15. Takacs, L., M. Carey Lea, the first mechanochemist. *J. Mater. Sci.* **2004,** *39* (16/17), 4987-4993.

16. James, S. L.; Adams, C. J.; Bolm, C.; Braga, D.; Collier, P.; Friščić, T.; Grepioni, F.; Harris, K. D. M.; Hyett, G.; Jones, W.; Krebs, A.; Mack, J.; Maini, L.; Orpen, A. G.; Parkin, I. P.; Shearouse, W. C.; Steed, J. W.; Waddell, D. C., Mechanochemistry: opportunities for new and cleaner synthesis. *Chem. Soc. Rev.* **2012,** *41* (1), 413-447.

17. Orita, A.; Jiang, L.; Nakano, T.; Ma, N.; Otera, J., Solventless reaction dramatically accelerates supramolecular self-assemblyElectronic supplementary information (ESI)

available: experimental details and CD spectra. See http://www.rsc.org/suppdata/cc/b2/b203651g. *Chem. Commun.* **2002,** (13), 1362-1363.

18.   Hernández, J. G.; Frings, M.; Bolm, C., Mechanochemical Enzymatic Kinetic Resolution of Secondary Alcohols under Ball-Milling Conditions. *ChemCatChem* **2016,** *8* (10), 1769-1772.

19.   Aktoudianakis, E.; Chan, E.; Edward, A. R.; Jarosz, I.; Lee, V.; Mui, L.; Thatipamala, S. S.; Dicks, A. P., Comparing the Traditional with the Modern: A Greener, Solvent-Free Dihydropyrimidone Synthesis. *Journal of Chemical Education* **2009,** *86* (6).

20.   Leung, S. H.; Angel, S. A., Solvent-Free Wittig Reaction: A Green Organic Chemistry Laboratory Experiment. *Journal of Chemical Education* **2004,** *81* (10).

21.   Mancheño, M. J.; Royuela, S.; de la Peña, A.; Ramos, M.; Zamora, F.; Segura, J. L., Introduction to Covalent Organic Frameworks: An Advanced Organic Chemistry Experiment. *Journal of Chemical Education* **2019,** *96* (8), 1745-1751.

22.   Mascarenhas, C. M., A Two-Step Synthesis of the Laundry Detergent Perfume Additive β-Citronellyl Tosylate. *Journal of Chemical Education* **2013,** *90* (9), 1231-1234.

23.   Palleros, D. R., Solvent-Free Synthesis of Chalcones. *Journal of Chemical Education* **2004,** *81* (9).

24.   Phonchaiya, S.; Panijpan, B.; Rajviroongit, S.; Blanchfield, J. T.; Wright, T., A Facile Solvent-Free Cannizzaro Reaction. *Journal of Chemical Education* **2009,** *86* (1).

25.   Wixtrom, A.; Buhler, J.; Abdel-Fattah, T., Mechanochemical Synthesis of Two Polymorphs of the Tetrathiafulvalene-Chloranil Charge Transfer Salt: An Experiment for Organic Chemistry. *Journal of Chemical Education* **2014,** *91* (8), 1232-1235.

26.   Colacino, E.; Dayaker, G.; Morère, A.; Friščić, T., Introducing Students to Mechanochemistry via Environmentally Friendly Organic Synthesis Using a Solvent-Free Mechanochemical Preparation of the Antidiabetic Drug Tolbutamide. *Journal of Chemical Education* **2019,** *96* (4), 766-771.

27.   Sohmiya, H.; Kimura, T.; Bauchat, P.; Fujita, M.; Ando, T., Solid-State Organic Reactions Proceeding by Pulverization of Inorganic Solid-Supports. Reactions of Iodosobenzene with Unsaturated Hydrocarbons on Acid-Treated Silica Gel. *Chemistry Letters* **1991,** *20* (8), 1391-1392.

28.   Andersen, J. M.; Mack, J., Decoupling the Arrhenius equation via mechanochemistry. *Chem. Sci.* **2017,** *8* (8), 5447-5453.

29.   Perona, A.; Hoyos, P.; Farrán, Á.; Hernáiz, M. J., Current challenges and future perspectives in sustainable mechanochemical transformations of carbohydrates. *Green Chem.* **2020,** *22* (17), 5559-5583.

30.   Haehnel, A. P.; Sagara, Y.; Simon, Y. C.; Weder, C., Mechanochemistry in Polymers with Supramolecular Mechanophores. In *Polymer Mechanochemistry*, 2015; pp 345-375.

31.   Porcheddu, A.; Colacino, E.; De Luca, L.; Delogu, F., Metal-Mediated and Metal-Catalyzed Reactions Under Mechanochemical Conditions. *ACS Catal.* **2020,** *10* (15), 8344-8394.

32.   Fulmer, D. A.; Shearouse, W. C.; Medonza, S. T.; Mack, J., Solvent-free Sonogashira coupling reaction via high speed ball milling. *Green Chem.* **2009,** *11* (11).

33.   Cook, T. L.; Walker, J. A.; Mack, J., Scratching the catalytic surface of mechanochemistry: a multi-component CuAAC reaction using a copper reaction vial. *Green Chem.* **2013,** *15* (3).

34. Sawama, Y.; Yasukawa, N.; Ban, K.; Goto, R.; Niikawa, M.; Monguchi, Y.; Itoh, M.; Sajiki, H., Stainless Steel-Mediated Hydrogen Generation from Alkanes and Diethyl Ether and Its Application for Arene Reduction. *Org. Lett.* **2018,** *20* (10), 2892-2896.

35. Grätz, S.; Borchardt, L., Mechanochemical polymerization – controlling a polycondensation reaction between a diamine and a dialdehyde in a ball mill. *RSC Adv.* **2016,** *6* (69), 64799-64802.

36. Vogt, C. G.; Grätz, S.; Lukin, S.; Halasz, I.; Etter, M.; Evans, J. D.; Borchardt, L., Direct Mechanocatalysis: Palladium as Milling Media and Catalyst in the Mechanochemical Suzuki Polymerization. *Angew. Chem. Int. Ed.* **2019,** *58* (52), 18942-18947.

37. Seo, T.; Kubota, K.; Ito, H., Selective Mechanochemical Monoarylation of Unbiased Dibromoarenes by in Situ Crystallization. *J. Am. Chem. Soc.* **2020,** *142* (22), 9884-9889.

38. Do, J.-L.; Friščić, T., Chemistry 2.0: Developing a New, Solvent-Free System of Chemical Synthesis Based on Mechanochemistry. *Synlett* **2017,** *28* (16), 2066-2092.

39. Geciauskaite, A. A.; Garcia, F., Main group mechanochemistry. *Beilstein J Org Chem* **2017,** *13*, 2068-2077.

40. Reguera, E.; Fernández-Bertrán, J.; Paneque, A.; Yee-Madeira, H., Mechanochemical Reaction Between the Probe and the Matrix: A Possible Source of Errors When IR Spectra of Alkali Acid Bifluorides Are Recorded in Alkali Halide Pressed Disks. *Spectrosc. Lett.* **2004,** *37* (2), 191-199.

41. Mack, J.; Fulmer, D.; Stofel, S.; Santos, N., The first solvent-free method for the reduction of esters. *Green Chem.* **2007,** *9* (10).

42. Rightmire, N. R.; Hanusa, T. P.; Rheingold, A. L., Mechanochemical Synthesis of [1,3-(SiMe3)2C3H3]3(Al,Sc), a Base-Free Tris(allyl)aluminum Complex and Its Scandium Analogue. *Organometallics* **2014,** *33* (21), 5952-5955.

43. Koby, R. F.; Hanusa, T. P.; Schley, N. D., Mechanochemically Driven Transformations in Organotin Chemistry: Stereochemical Rearrangement, Redox Behavior, and Dispersion-Stabilized Complexes. *J Am Chem Soc* **2018,** *140* (46), 15934-15942.

44. Balaz, P.; Achimovicova, M.; Balaz, M.; Billik, P.; Cherkezova-Zheleva, Z.; Criado, J. M.; Delogu, F.; Dutkova, E.; Gaffet, E.; Gotor, F. J.; Kumar, R.; Mitov, I.; Rojac, T.; Senna, M.; Streletskii, A.; Wieczorek-Ciurowa, K., Hallmarks of mechanochemistry: from nanoparticles to technology. *Chem. Soc. Rev.* **2013,** *42* (18), 7571-7637.

45. Tsuzuki, T.; McCormick, P. G., Mechanochemical synthesis of nanoparticles. *J. Mater. Sci.* **2004,** *39* (16/17), 5143-5146.

46. Yuan, W.; O'Connor, J.; James*, S. L., Mechanochemical synthesis of homo- and hetero-rare-earth(iii) metal–organic frameworks by ball milling. *CrystEngComm* **2010,** *12* (11).

47. Rak, M. J.; Saadé, N. K.; Friščić, T.; Moores, A., Mechanosynthesis of ultra-small monodisperse amine-stabilized gold nanoparticles with controllable size. *Green Chem.* **2014,** *16* (1), 86-89.

48. Do, J.-L.; Friščić, T., Mechanochemistry: A Force of Synthesis. *ACS Cent. Sci.* **2017,** *3* (1), 13-19.

49. Wang, G.-W., Mechanochemical organic synthesis. *Chem. Soc. Rev.* **2013,** *42* (18), 7668-7700.

50. Tan, D.; Loots, L.; Friščić, T., Towards medicinal mechanochemistry: evolution of milling from pharmaceutical solid form screening to the synthesis of active pharmaceutical ingredients (APIs). *Chem. Commun.* **2016,** *52* (50), 7760-7781.

51.   Hernández, J. G.; Bolm, C., Altering Product Selectivity by Mechanochemistry. *J. Org. Chem.* **2017,** *82* (8), 4007-4019.

52.   Hernández, J. G.; Friščić, T., Metal-catalyzed organic reactions using mechanochemistry. *Tetrahedron Lett.* **2015,** *56* (29), 4253-4265.

53.   Rightmire, N. R.; Hanusa, T. P., Advances in Organometallic Synthesis with Mechanochemical Methods. *Dalton Trans.* **2016,** *45*, 2352-2362.

54.   Rightmire, N. R.; Hanusa, T. P.; Rheingold, A. L., Mechanochemical Synthesis of [1,3-(SiMe3)2C3H3]3(Al,Sc), a Base-Free Tris(allyl)aluminum Complex and Its Scandium Analogue. *Organometallics* **2014,** *33*, 5952–5955.

55.   Gečiauskaitė, A. A.; García, F., Main group mechanochemistry. *Beilstein J. Org. Chem.* **2017,** *13*, 2068-2077.

56.   Wang, J.; Ganguly, R.; Yongxin, L.; Díaz, J.; Soo, H. S.; García, F., A multi-step solvent-free mechanochemical route to indium(iii) complexes. *Dalton Trans.* **2016,** *45* (19), 7941-7946.

57.   Glavinović, M.; Krause, M.; Yang, L.; McLeod, J. A.; Liu, L.; Baines, K. M.; Friščić, T.; Lumb, J.-P., A chlorine-free protocol for processing germanium. *Sci. Adv.* **2017,** *3*, e1700149.

58.   Aleksanyan, D. V.; Churusova, S. G.; Aysin, R. R.; Klemenkova, Z. S.; Nelyubina, Y. V.; Kozlov, V. A., The first example of mechanochemical synthesis of organometallic pincer complexes. *Inorg. Chem. Commun.* **2017,** *76*, 33-35.

59.   Koby, R. F.; Hanusa, T. P.; Schley, N. D., Mechanochemically Driven Transformations in Organotin Chemistry: Stereochemical Rearrangement, Redox Behavior, and Dispersion-Stabilized Complexes. *J. Am. Chem. Soc.* **2018,** *140* (46), 15934-15942.

60.   Garay, A. L.; Pichon, A.; James, S. L., Solvent-free synthesis of metal complexes. *Chem. Soc. Rev.* **2007,** *36* (6), 846-855.

61.   Jobbágy, C.; Tunyogi, T.; Pálinkás, G.; Deák, A., A Versatile Solvent-Free Mechanochemical Route to the Synthesis of Heterometallic Dicyanoaurate-Based Coordination Polymers. *Inorg. Chem.* **2011,** *50* (15), 7301-7308.

62.   Bowmaker, G. A.; Hanna, J. V.; Hart, R. D.; Healy, P. C.; King, S. P.; Marchetti, F.; Pettinari, C.; Skelton, B. W.; Tabacaru, A.; White, A. H., Mechanochemical and solution synthesis, X-ray structure and IR and 31P solid state NMR spectroscopic studies of copper(i) thiocyanate adducts with bulky monodentate tertiary phosphine ligands. *Dalton Trans.* **2012,** *41* (25), 7513-7525.

63.   Jobbágy, C.; Molnar, M.; Baranyai, P.; Deák, A., Mechanochemical synthesis of crystalline and amorphous digold(i) helicates exhibiting anion- and phase-switchable luminescence properties. *Dalton Trans.* **2014,** *43* (31), 11807-11810.

64.   Juribašić, M.; Užarević, K.; Gracin, D.; Ćurić, M., Mechanochemical C-H bond activation: rapid and regioselective double cyclopalladation monitored by in situ Raman spectroscopy. *Chem. Commun.* **2014,** *50* (71), 10287-10290.

65.   Friščić, T., Metal-Organic Frameworks: Mechanochemical Synthesis Strategies. In *Encyclopedia of Inorganic and Bioinorganic Chemistry*, Wiley: Chichester, 2014; pp 1-19.

66.   Mottillo, C.; Friscic, T., Advances in solid-state transformations of coordination bonds: from the ball mill to the aging chamber. *Molecules* **2017,** *22* (1), 144/1-144/38.

67.   Barreda, O.; Taggart, G. A.; Rowland, C. A.; Yap, G. P. A.; Bloch, E. D., Mechanochemical Synthesis of Porous Molecular Assemblies. *Chem. Mater.* **2018**.

68.   Hanusa, T. P., 3.1 - Group 1s and 2s Metals. In *Comprehensive Coordination Chemistry II*, McCleverty, J. A.; Meyer, T. J., Eds. Pergamon: Oxford, 2003; pp 1-92.

69.   Tuulmets, A.; Panov, D., Solvation effects in partially solvated Grignard reagents. *J. Organomet. Chem.* **1999,** *575* (2), 182-186.

70.   Chmely, S. C.; Carlson, C. N.; Hanusa, T. P.; Rheingold, A. L., Classical versus Bridged Allyl Ligands in Magnesium Complexes: The Role of Solvent. *J. Am. Chem. Soc.* **2009,** *131* (18), 6344-6345.

71.   Westerhausen, M., Synthesis and Spectroscopic Properties of Bis(trimethylsilyl)amides of the Alkaline-earth Metals Magnesium, Calcium, Strontium, and Barium. *Inorg. Chem.* **1991,** *30*, 96-101.

72.   Tesh, K. F.; Hanusa, T. P.; Huffman, J. C., Ion pairing in [bis(trimethylsilyl)amido]potassium: The x-ray crystal structure of unsolvated [KN(SiMe3)2]2. *Inorg. Chem.* **1990,** *29* (8), 1584-1586.

73.   Tanner, P. S.; Burkey, D. J.; Hanusa, T. P., Cyclopentadienyl Ring Metathesis with Bis(pentamethylcyclopentadienyl)calcium as a Route to Mixed Ring Organolanthanide Complexes; the Crystal Structure of $(C_5Me_5)_2Nd(C_5H_5)$. *Polyhedron* **1995,** *14*, 331-333.

74.   Brady, E. D.; Chmely, S. C.; Jayaratne, K. C.; Hanusa, T. P.; Young, V. G., Jr., s-Block Metal Complexes of the Bis(tetramethylcyclopentadienyl) Phosphonium Diylide [Me(t-Bu)P(C5Me4)2]–. *Organometallics* **2008,** *27*, 1612-1616.

75.   Barrett, A. G. M.; Crimmin, M. R.; Hill, M. S.; Kociok-Kohn, G.; MacDougall, D. J.; Mahon, M. F.; Procopiou, P. A., Synthesis, Characterization, and Solution Lability of N-Heterocyclic Carbene Adducts of the Heavier Group 2 Bis(trimethylsilyl)amides. *Organometallics* **2008,** *27*, 3939-3946.

76.   He, X.; Noll, B. C.; Beatty, A.; Mulvey, R. E.; Henderson, K. W., Ketone Deprotonation Mediated by Mono- and Heterobimetallic Alkali and Alkaline Earth Metal Amide Bases: Structural Characterization of Potassium, Calcium, and Mixed Potassium-Calcium Enolates. *J. Am. Chem. Soc.* **2004,** *126* (24), 7444-7445.

77.   He, X.; Hurley, E.; Noll, B. C.; Henderson, K. W., Regio- and Stereoselective Enolizations Using Calcium Bis(hexamethyldisilazide) as a Base: Synthetic, Solid-State, and Solution Studies. *Organometallics* **2008,** *27* (13), 3094-3102.

78.   Harder, S., From Limestone to Catalysis: Application of Calcium Compounds as Homogeneous Catalysts. *Chem. Rev.* **2010,** *110* (7), 3852-3876.

79.   Hill, M. S.; Liptrot, D. J.; Weetman, C., Alkaline earths as main group reagents in molecular catalysis. *Chem. Soc. Rev.* **2016,** *45* (4), 972-988.

80.   Davin, J. P.; Buffet, J.-C.; Spaniol, T. P.; Okuda, J., Alkaline earth metal complexes of a chiral polyether as initiator for the ring-opening polymerization of lactide. *Dalton Trans.* **2012,** *41* (40), 12612-12618.

81.   Coles, M. P., The role of the bis-trimethylsilylamido ligand, [N{SiMe3}2]–, in main group chemistry. Part 1: Structural chemistry of the s-block elements. *Coord. Chem. Rev.* **2015,** *297-298*, 2-23.

82.   Westerhausen, M.; Schwarz, W., Molecular and crystal structures of dimeric calcium bis[bis(trimethylsilyl)amide] and calcium bis[bis(trimethylsilyl)amide].DME. *Z. Anorg. Allg. Chem.* **1991,** *604*, 127-140.

83.   Hitchcock, P. B.; Lappert, M. F.; Lawless, G. A.; Royo, B., The Synthesis and Structure of the alkaline earth metal organic compound [M(OAr)2(thf)n][M=Ca, n=3(1) or 0; M=Ba, n=4] and [{Ca(NR2)(mNR2)(thf)}2], and the X-ray Structure of (1). *J. Chem. Soc., Chem. Commun*. **1990**, 1141-1142.

84.   Drake, S. R.; Otway, D. J.; Perlepes, S. P., The synthesis of homoleptic alkaline earth complexes under mild conditions. *Main Group Metal Chem*. **1991,** *14* (5), 243-56.

85.   Bradley, D. C.; Hursthouse, M. B.; Ibrahim, A. A.; Abdul Malik, K. M.; Motevalli, M.; Möseler, R.; Powell, H.; D., R. J.; Sullivan, A. C., Synthesis and Chemistry of the Bis(trimethylsilyl)amido Bis-tetrahydrofuranates of the Group 2 Metals Magnesium, Calcium, Strontium and Barium. X-ray Crystal Structures of Mg[N(SiMe3)2]2•2THF and Related Mn[N(SiMe3)2]2•2THF. *Polyhedron* **1990,** *9* (24), 2959-2964.

86.   Gillett-Kunnath, M. M.; MacLellan, J. G.; Forsyth, C. M.; Andrews, P. C.; Deacon, G. B.; Ruhlandt-Senge, K., BiPh3-A convenient synthon for heavy alkaline-earth metal amides. *Chem. Commun*. **2008,** (37), 4490-4492.

87.   Frankland, A. D.; Hitchcock, P. B.; Lappert, M. F.; Lawless, G. A., A novel high-yield route to organic derivatives of group 2 metals; X-ray structure of [{Ba(OTf)2}4(py)14]·py (OTf = OSO2CF3) and NMR spectral characterisation of [Ba(NR2)(μ-NR2)2Na(thf)2](R = SiMe3). *J. Chem. Soc., Chem. Commun*. **1994,** (21), 2435-2436.

88.   Frankland, A. D.; Lappert, M. F., Alkaline-earth-metal arenesulfonates as precursors to organic derivatives of Group 2 metals. *J. Chem. Soc., Dalton Trans*. **1996**, 4151-4152.

89.   Hitchcock, P. B.; Lappert, M. F.; Lawless, G. A.; Royo, B., The synthesis and structure of the alkaline earth metal organic compounds [M(OAr)2(thf)][M = Ca, n= 3 (1) or 0; M = Ba, n= 4] and [{Ca(NR2)(μNR2)(thf)}2], and the X-ray structure of (1)(Ar = C6H2But2-2,6-Me-4; R = SiMe3; thf - OC4H8). *J. Chem. Soc., Chem. Commun*. **1990,** (17), 1141-1142.

90.   Tesh, K. F.; Hanusa, T. P.; Huffman, J. C., Ion Pairing in [Bis(trimethylsilyl)amido]potassium: X-ray Crystal Structure of Unsolvated [KN(SiMe3)2]2. *Inorg. Chem*. **1990,** *29*, 1584-1586.

91.   Krieck, S.; Schueler, P.; Goerls, H.; Westerhausen, M., Alkaline-Earth Metal Bis[bis(trimethylsilyl)amide] Complexes with Weakly Coordinating 2,2,5,5-Tetramethyltetrahydrofuran Ligands. *Inorg. Chem*. **2018,** *57* (21), 13937-13943.

92.   Brady, E. D.; Hanusa, T. P.; Pink, M.; Young, V. G., Jr., The First Non-coordinated Phosphonium Diylide, [Me2P(C13H8)2]–1, and its Ylidic and Cationic Counterparts: Synthesis, Structural Characterization, and Interaction with the Heavy Group 2 Metals. *Inorg. Chem*. **2000,** *39*, 6028-6037.

93.   Johns, A. M.; Chmely, S. C.; Hanusa, T. P., Solution Interaction of Potassium and Calcium Bis(trimethylsilyl)amides; Preparation of Ca[N(SiMe3)2]2 from Dibenzylcalcium. *Inorg. Chem*. **2009,** *48* (4), 1380-1384.

94.   Glock, C.; Görls, H.; Westerhausen, M., Alkyl-Substituted Amides as Ligands in Homometallic and Heterobimetallic Calcium Complexes. *Inorg. Chem*. **2009,** *48* (1), 394-399.

95.   Fischer, F.; Fendel, N.; Greiser, S.; Rademann, K.; Emmerling, F., Impact Is Important—Systematic Investigation of the Influence of Milling Balls in Mechanochemical Reactions. *Org. Process Res. Dev*. **2017,** *21* (4), 655-659.

96.   Kulla, H.; Fischer, F.; Benemann, S.; Rademann, K.; Emmerling, F., The effect of the ball to reactant ratio on mechanochemical reaction times studied by in situ PXRD. *CrystEngComm* **2017,** *19* (28), 3902-3907.

97.   McCormick, M. J.; Sockwell, S. C.; Davies, C. E. H.; Hanusa, T. P.; Huffman, J. C., Synthesis of a Monopentamethylcyclopentadienyl Halide Complex of Calcium; the X-Ray Crystal Structure of [(Me5C5)Ca(μ-I)(THF)2]2. *Organometallics* **1989,** *8*, 2044-2049.

98.   Weast, R. C., Handbook of Chemistry and Physics. Weast, R. C., Ed. Chemical Rubber Company: Cleveland, 1986; Vol. 67th, pp D-104.

99.   Makhaev, V. D.; Borisov, A. P.; Petrova, L. A., Solid-state mechanochemical synthesis of ferrocene. *J. Organomet. Chem.* **1999,** *590* (2), 222-226.

100.   Kennedy, A. R.; Mulvey, R. E.; Rowlings, R. B., Intermetallic Lithium−Magnesium Hexamethyldisilazide: Synthesis and Structure, Discovery of an Oxygen-Centered Variant, and a Reaction with Benzonitrile That Produces a Novel Amidinate Cage Compound with a Trigonal Bipyramidal Li4MgO Core. *J. Am. Chem. Soc.* **1998,** *120* (31), 7816-7824.

101.   Johns, A. M.; Chmely, S. C.; Hanusa, T. P., Solution interaction of potassium and calcium bis(trimethylsilyl)amides; preparation of Ca[N(SiMe3)2]2 from dibenzylcalcium. *Inorg Chem* **2009,** *48* (4), 1380-4.

102.   Silverman, G. S.; Rakita, P. E., *Handbook of Grignard Reagents*. Marcel Dekker, Inc.: Monticello, 1996.

103.   *Richey, H. G., Jr.*, *Grignard Reagents: New Developments*. J. Wiley and Sons., Ltd.: Chicester, 2000.

104.   Beillard, A.; Bantreil, X.; Métro, T.-X.; Martinez, J.; Lamaty, F., Alternative Technologies That Facilitate Access to Discrete Metal Complexes. *Chem. Rev.* **2019,** *119* (12), 7529-7609.

105.   Horst, C.; Chen, Y. S.; Kunz, U.; Hoffmann, U., Design, modeling and performance of a novel sonochemical reactor for heterogeneous reactions. *Chem. Eng. Sci.* **1996,** *51* (10), 1837-1846.

106.   Baig, R. B. N.; Varma, R. S., Alternative energy input: mechanochemical, microwave and ultrasound-assisted organic synthesis. *Chem. Soc. Rev.* **2012,** *41* (4), 1559-1584.

107.   Rieke, R. D.; Hudnall, P. M., Activated Metals. I. Preparation of Highly Reactive Magnesium Metal. *J. Am. Chem. Soc.* **1972,** *94*, 7178-7179.

108.   Rieke, R. D.; Li, P. T.-J.; Burns, T. P.; Uhm, S. T., Preparation of highly reactive metal powders. New procedure for the preparation of highly reactive zinc and magnesium metal powders. *J. Org. Chem.* **1981,** *46* (21), 4323-4324.

109.   Rieke, R. D.; Burns, T. P.; Wehmeyer, R. M.; Kahn, B. E., Preparation of Highly Reactive Metal Powders: Some of Their Uses in Organic and Organometallic Synthesis. *ACS Symp. Ser.* **1987,** *333*, 223-245.

110.   Burns, T. P.; Rieke, R. D., Highly reactive magnesium and its application to organic syntheses. *J. Org. Chem.* **1987,** *52* (16), 3674-3680.

111.   Rieke, R. D., Preparation of Organometallic Compounds from Highly Reactive Metal Powders. *Science* **1989,** *246*, 1260-1264.

112.   Rieke, R. D.; Hanson, M. V., New organometallic reagents using highly reactive metals. *Tetrahedron* **1997,** *53* (6), 1925-1956.

113.   Rieke, R. D., *Chemical Synthesis Using Highly Reactive Metals*. John Wiley: Hobocken, New Jersey, 2017; p 480.

114.   James, S. L.; Adams, C. J.; Bolm, C.; Braga, D.; Collier, P.; Friščić, T.; Grepioni, F.; Harris, K. D. M.; Hyett, G.; Jones, W.; Krebs, A.; Mack, J.; Maini, L.; Orpen, A. G.; Parkin, I.

P.; Shearouse, W. C.; Steed, J. W.; Waddell, D. C., Mechanochemistry: opportunities for new and cleaner synthesis. *Chem. Soc. Rev.* **2012,** *41* (1), 413-447.

115.   Howard, Joseph L.; Cao, Q.; Browne, D. L., Mechanochemistry as an emerging tool for molecular synthesis: what can it offer? *Chem. Sci.* **2018,** *9* (12), 3080-3094.

116.   Tan, D.; García, F., Main group mechanochemistry: from curiosity to established protocols. *Chem. Soc. Rev.* **2019,** *48* (8), 2274-2292.

117.   Veit, M.; Hoffmann, U., Magnesium something. *Chem. Ing. Tech.* **1996,** *68*, 1279-.

118.   Waddell, D. C.; Clark, T. D.; Mack, J., Conducting moisture sensitive reactions under mechanochemical conditions. *Tetrahedron Lett.* **2012,** *53* (34), 4510-4513.

119.   Birke, V.; Schutt, C.; Burmeier, H.; Ruck, W., Defined Mechanochemical Reductive Dechlorination of 1,3,5-Trichlorobenzene at Room Temperature in a Ball Mill. *Fresenius Environ. Bull.* **2011,** *20* (10A), 2794-2805.

120.   Rowlands, S. A.; Hall, A. K.; McCormick, P. G.; Street, R.; Hart, R. J.; Ebell, G. F.; Donecker, P., Destruction of toxic materials. *Nature* **1994,** *367* (6460), 223-223.

121.   Birke, V.; Schütt, C.; Ruck, W. K. L., Small Particle Size Magnesium in One-pot Grignard-Zerewitinoff-like Reactions Under Mechanochemical Conditions: On the Kinetics of Reductive Dechlorination of Persistent Organic Pollutants (POPs). In *Environmental Applications of Nanoscale and Microscale Reactive Metal Particles*, American Chemical Society: 2009; Vol. 1027, pp 39-54.

122.   Harrowfield, J. M.; Hart, R. J.; Whitaker, C. R., Magnesium and aromatics: mechanically-induced Grignard and McMurry reactions. *Aust. J. Chem.* **2001,** *54* (7), 423-425.

123.   Kaupp, G., Mechanochemistry: the varied applications of mechanical bond-breaking. *CrystEngComm* **2009,** *11* (3), 388-403.

124.   Huheey, J. E.; Keiter, E. A.; Keiter, R. L., *Inorg. Chem.: Principles of Structure and Reactivity*. 4th ed.; Harper Collins: New York, 1993.

125.   Ashby, E. C.; Al-Fekri, D. M., The reaction of benzotrihalides and benzal halides with magnesium. Synthetic and mechanistic studies. *J. Organomet. Chem.* **1990,** *390* (3), 275-292.

126.   Swarts, F., Some aliphatic fluorides. *Bull. Soc. Chim. Belg.* **1921,** *30*, 302-305.

127.   Respess, W. L.; Tamborski, C., A new synthesis of perfluoroaromatic Grignard reagents. *J. Organometal. Chem.* **1969,** *18* (2), 263-274.

128.   Ashby, E. C.; Nackashi, J., The preparation of organomagnesium fluorides by organometallic exchange reactions. *J. Organomet. Chem.* **1974,** *72* (1), 11-20.

129.   Paterová, J.; Skalický, M.; Rybáčková, M.; Kvíčalová, M.; Cvačka, J.; Kvíčala, J., Synthesis of 2-(perfluoroalkyl)ethyl potassium sulfates based on perfluorinated Grignard reagents. *Journal of Fluorine Chemistry* **2010,** *131* (12), 1338-1343.

130.   M. Beck, C.; Park, Y.-J.; H. Crabtree, R., Direct conversion of perfluoroalkanes and perfluoroarenes to perfluoro Grignard reagents. *Chem. Commun.* **1998,** (6), 693-694.

131.   Rieke, R. D., Preparation of highly reactive metal powders and their use in organic and organometallic synthesis. *Acc. Chem. Res.* **1977,** *10* (8), 301-306.

132.   Birke, V.; Schütt, C.; Ruck, W.K.L. Small Particle Size Magnesium in One-Pot Grignard-Zerewitinoff like Reactions Under Mechanochemical Conditions: On the Kinetics of Reductuve Dechlorination of Persistant Organic Pollutante (POPs). In Environmental Applications of Nanoscale and Microscale Reactive Metal Particles; American Chemical Society: Washington, DC, USA, 2009; Volume 1027. pp. 39-54.

133.   Bare, W. D.; Andrews, L., Formation of Grignard Species from the Reaction of Methyl Halides with Laser-Ablated Magnesium Atoms. A Matrix Infrared Study of CH3MgF, CH3MgCl, CH3MgBr, and CH3MgI. *J. Am. Chem. Soc.* **1998,** *120* (29), 7293-7301.

134.   Tjurina, L. A.; Smirnov, V. V.; Barkovskii, G. B.; Nikolaev, E. N.; Esipov, S. E.; Beletskaya, I. P., Cluster Grignard Reagents. *Organometallics* **2001,** *20* (12), 2449-2450.

135.   Tjurina, L. A.; Smirnov, V. V.; Potapov, D. A.; Nikolaev, S. A.; Esipov, S. E.; Beletskaya, I. P., Synthesis of Cluster Alkyl and Aryl Grignard Reagents in Solution. *Organometallics* **2004,** *23* (6), 1349-1351.

136.   Green, S. P.; Jones, C.; Stasch, A., Stable Magnesium(I) Compounds with Mg-Mg Bonds. *Science* **2007,** *318* (5857), 1754-1757.

137.   Bonyhady, S. J.; Jones, C.; Nembenna, S.; Stasch, A.; Edwards, A. J.; McIntyre, G. J., β-Diketiminate-Stabilized Magnesium(I) Dimers and Magnesium(II) Hydride Complexes: Synthesis, Characterization, Adduct Formation, and Reactivity Studies. *Chem.–Eur. J.* **2010,** *16* (3), 938-955.

138.   Bakewell, C.; White, A. J. P.; Crimmin, M. R., Addition of Carbon-Fluorine Bonds to a Mg(I)-Mg(I) Bond: An Equivalent of Grignard Formation in Solution. *J. Am. Chem. Soc.* **2016,** *138* (39), 12763-12766.

139.   Cahiez, G.; Moyeux, A.; Buendia, J.; Duplais, C., Manganese- or Iron-Catalyzed Homocoupling of Grignard Reagents Using Atmospheric Oxygen as an Oxidant. *J. Am. Chem. Soc.* **2007,** *129* (45), 13788-13789.

140.   Krasovskiy, A.; Tishkov, A.; del Amo, V.; Mayr, H.; Knochel, P., Transition-Metal-Free Homocoupling of Organomagnesium Compounds. *Angew. Chem. Int. Ed.* **2006,** *45* (30), 5010-5014.

141.   Xu, X.; Cheng, D.; Pei, W., Iron-Catalyzed Homocoupling of Bromide Compounds. *J. Org. Chem.* **2006,** *71* (17), 6637-6639.

142.   Zhou, Z.; Xue, W., Manganese-catalyzed oxidative homo-coupling of aryl Grignard chlorides. *J. Organomet. Chem.* **2009,** *694* (5), 599-603.

143.   Davies, D. I.; Done, J. N.; Hey, D. H., Aspects of the metallic halide-catalysed reaction of Grignard reagents with organic halides. Part II. Effect of variation in reactants. *J. Chem. Soc. C: Organic* **1969,** (10), 1392-1401.

144.   Bandari, R.; Höche, T.; Prager, A.; Dirnberger, K.; Buchmeiser, M. R., Ring-Opening Metathesis Polymerization Based Pore-Size-Selective Functionalization of Glycidyl Methacrylate Based Monolithic Media: Access to Size-Stable Nanoparticles for Ligand-Free Metal Catalysis. *Chem – Eur. J.* **2010,** *16* (15), 4650-4658.

145.   Viswanathan, G. S.; Wang, M.; Li, C.-J., A Highly Regioselective Synthesis of Polysubstituted Naphthalene Derivatives through Gallium Trichloride Catalyzed Alkyne–Aldehyde Coupling. *Angew. Chem. Int. Ed.* **2002,** *41* (12), 2138-2141.

146.   Nising, C. F.; Schmid, U. K.; Nieger, M.; Bräse, S., A New Protocol for the One-Pot Synthesis of Symmetrical Biaryls. *J. Org. Chem.* **2004,** *69* (20), 6830-6833.

147.   Frisch, M. J.; Trucks, G. W.; Schlegel, H. B.; Scuseria, G. E.; Robb, M. A.; Cheeseman, J. R.; Scalmani, G.; Barone, V.; Petersson, G. A.; Nakatsuji, H.; Li, X.; Caricato, M.; Marenich, A. V.; Bloino, J.; Janesko, B. G.; Gomperts, R.; Mennucci, B.; Hratchian, H. P.; Ortiz, J. V.; Izmaylov, A. F.; Sonnenberg, J. L.; Williams; Ding, F.; Lipparini, F.; Egidi, F.; Goings, J.; Peng, B.; Petrone, A.; Henderson, T.; Ranasinghe, D.; Zakrzewski, V. G.; Gao, J.; Rega, N.; Zheng, G.; Liang, W.; Hada, M.; Ehara, M.; Toyota, K.; Fukuda, R.; Hasegawa, J.; Ishida, M.;

Nakajima, T.; Honda, Y.; Kitao, O.; Nakai, H.; Vreven, T.; Throssell, K.; Montgomery Jr., J. A.; Peralta, J. E.; Ogliaro, F.; Bearpark, M. J.; Heyd, J. J.; Brothers, E. N.; Kudin, K. N.; Staroverov, V. N.; Keith, T. A.; Kobayashi, R.; Normand, J.; Raghavachari, K.; Rendell, A. P.; Burant, J. C.; Iyengar, S. S.; Tomasi, J.; Cossi, M.; Millam, J. M.; Klene, M.; Adamo, C.; Cammi, R.; Ochterski, J. W.; Martin, R. L.; Morokuma, K.; Farkas, O.; Foresman, J. B.; Fox, D. J. *Gaussian 16 Rev. C.01*, Wallingford, CT, 2016.

148.   Becke, A. D., Density-functional thermochemistry. III. The role of exact exchange. *J. Chem. Phys.* **1993,** *98*, 5648-5652.

149.   Grimme, S.; Antony, J.; Ehrlich, S.; Krieg, H., A consistent and accurate ab initio parametrization of density functional dispersion correction (DFT-D) for the 94 elements H-Pu. *J. Chem. Phys.* **2010,** *132*, 154104/1-154104/19.

150.   Grimme, S.; Ehrlich, S.; Goerigk, L., Effect of the damping function in dispersion corrected density functional theory. *J. Comput. Chem.* **2011,** *32* (7), 1456-1465.

151.   Weigend, F.; Ahlrichs, R., Balanced basis sets of split valence, triple zeta valence and quadruple zeta valence quality for H to Rn: Design and assessment of accuracy. *Phys. Chem. Chem. Phys.* **2005,** *7* (18), 3297-3305.

152.   Reed, A. E.; Weinstock, R. B.; Weinhold, F. J., Natural population analysis. *J. Chem. Phys.* **1985,** *83*, 735-746.

153.   Reed, A. E.; Curtiss, L. A.; Weinhold, F., Intermolecular interactions from a natural bond orbital, donor-acceptor viewpoint. *Chem. Rev.* **1988,** *88*, 899-926.

154.   Trost, B. M.; Crawley, M. L., Asymmetric Transition-Metal-Catalyzed Allylic Alkylations: Applications in Total Synthesis. *Chem. Rev.* **2003,** *103* (8), 2921-2944.

155.   Chen, Q.-A.; Chen, Z.; Dong, V. M., Rhodium-Catalyzed Enantioselective Hydroamination of Alkynes with Indolines. *J. Am. Chem. Soc.* **2015,** *137* (26), 8392-8395.

156.   Cruz, F. A.; Zhu, Y.; Tercenio, Q. D.; Shen, Z.; Dong, V. M., Alkyne Hydroheteroarylation: Enantioselective Coupling of Indoles and Alkynes via Rh-Hydride Catalysis. *J. Am. Chem. Soc.* **2017,** *139* (31), 10641-10644.

157.   Yang, X.-H.; Dong, V. M., Rhodium-Catalyzed Hydrofunctionalization: Enantioselective Coupling of Indolines and 1,3-Dienes. *J. Am. Chem. Soc.* **2017,** *139* (5), 1774-1777.

158.   Simpson, C. K.; White, R. E.; Carlson, C. N.; Wrobleski, D. A.; Kuehl, C. J.; Croce, T. A.; Steele, I. M.; Scott, B. L.; Young, V. G.; Hanusa, T. P.; Sattelberger, A. P.; John, K. D., The Role of Alkali Metal Cations in MMA Polymerization Initiated by Neutral and Anionic Allyl Lanthanide Complexes. *Organometallics* **2005,** *24* (15), 3685-3691.

159.   Chalkley, M. J.; Guard, L. M.; Hazari, N.; Hofmann, P.; Hruszkewycz, D. P.; Schmeier, T. J.; Takase, M. K., Synthesis, Electronic Structure, and Reactivity of Palladium(I) Dimers with Bridging Allyl, Cyclopentadienyl, and Indenyl Ligands. *Organometallics* **2013,** *32* (15), 4223-4238.

160.   Melvin, P. R.; Nova, A.; Balcells, D.; Dai, W.; Hazari, N.; Hruszkewycz, D. P.; Shah, H. P.; Tudge, M. T., Design of a Versatile and Improved Precatalyst Scaffold for Palladium-Catalyzed Cross-Coupling: (η3-1-tBu-indenyl)2(μ-Cl)2Pd2. *ACS Catal.* **2015,** *5* (6), 3680-3688.

161.   Dardir, A. H.; Melvin, P. R.; Davis, R. M.; Hazari, N.; Mohadjer Beromi, M., Rapidly Activating Pd-Precatalyst for Suzuki–Miyaura and Buchwald–Hartwig Couplings of Aryl Esters. *J. Org. Chem.* **2017,** *83* (1), 469-477.

162. For a detailed review of allyl chemistry see: Lichtenberg, C.; Okuda, J. Angew. Chem. Int. Ed., 2013, 52, 5228-5246. For a detailed review of silyl substituted allyl chemistry see: Solomon, S.; Layfield, R. Dalton Trans., 2010, 39, 2469-2483.

163. Harvey, M. J.; Hanusa, T. P.; Young, J. V. G., Synthesis and Crystal Structure of the Bis(allyl)calcium Complex [Ca{C3(SiMe3)2H3}2·(thf)2]. *Angew. Chem. Int. Ed.* **1999,** *38* (1-2), 217-219.

164. Carlson, C. N.; Smith, J. D.; Hanusa, T. P.; Brennessel, W. W.; Young, V. G., Homoleptic allyl complexes of chromium with trimethylsilylated ligands. Formation and molecular structure of {[1-(SiMe3)C3H4]2Cr}2, [1,3-(SiMe3)2C3H3]2Cr, and [1,1′,3-(SiMe3)3C3H2]2Cr. *J. Organomet. Chem.* **2003,** *683* (1), 191-199.

165. Quisenberry, K. T.; Smith, J. D.; Voehler, M.; Stec, D. F.; Hanusa, T. P.; Brennessel, W. W., Trimethylsilylated Allyl Complexes of Nickel. The Stabilized Bis(π-allyl)nickel Complex [η3-1,3-(SiMe3)2C3H3]2Ni and Its Mono(π-allyl)NiX (X = Br, I) Derivatives. *J. Am. Chem. Soc.* **2005,** *127* (12), 4376-4387.

166. Zhang, W.; Robins, M. J., Removal of silyl protecting groups from hydroxyl functions with ammonium fluoride in methanol. *Tetrahedron Lett.* **1992,** *33* (9), 1177-1180.

167. Scheidt, K. A.; Chen, H.; Follows, B. C.; Chemler, S. R.; Coffey, D. S.; Roush, W. R., Tris(dimethylamino)sulfonium Difluorotrimethylsilicate, a Mild Reagent for the Removal of Silicon Protecting Groups. *J. Org. Chem.* **1998,** *63* (19), 6436-6437.

168. Ferreira, F.; Vasseur, J.-J.; Morvan, F., Lewis acid deprotection of silyl-protected oligonucleotides and base-sensitive oligonucleotide analogues. *Tetrahedron Lett.* **2004,** *45* (33), 6287-6290.

169. Fraenkel, G.; Cabral, J.; Lanter, C.; Wang, J., Reorientation Dynamics within Ion-Paired Allylic Lithium Compounds: Isolation of Inversion Processes. *J. Org. Chem.* **1999,** *64* (4), 1302-1310.

170. Rightmire, N. R.; Quisenberry, K. T.; Hanusa, T. P., Balancing Adduct Formation and Ligand Coupling with the Bulky Allyl Complexes [1,3-(SiMe3)2C3H3]2M (M = Fe, Co, Ni). *Organometallics* **2014,** *33* (20), 5678-5685.

171. Bard, A. J.; Merz, A., Electrochemical reduction of allyl halides in nonaqueous solvents - a reinvestigation. *J. Am. Chem. Soc.* **1979,** *101* (11), 2959-2965.

172. Dolomanov, O. V.; Bourhis, L. J.; Gildea, R. J.; Howard, J. A. K.; Puschmann, H., OLEX2: a complete structure solution, refinement and analysis program. *J. Appl. Cryst.* **2009,** *42* (2), 339-341.

173. Sheldrick, G., SHELXT - Integrated space-group and crystal-structure determination. *Acta Crystallogr. Sect. A* **2015,** *71* (1), 3-8.

174. Sheldrick, G., Crystal structure refinement with SHELXL. *Acta Crystallogr. Sect. C* **2015,** *71* (1), 3-8.

175. Frameworks for commercial success. *Nat Chem* **2016,** *8* (11), 987.

176. Ayoub, G.; Arhangelskis, M.; Zhang, X.; Son, F.; Islamoglu, T.; Friščić, T.; Farha, O. K., Air oxidation of sulfur mustard gas simulants using a pyrene-based metal–organic framework photocatalyst. *Beilstein J. Nanotechnol.* **2019,** *10*, 2422-2427.

177. Furukawa, H.; Kim, J.; Ockwig, N. W.; O'Keeffe, M.; Yaghi, O. M., Control of Vertex Geometry, Structure Dimensionality, Functionality, and Pore Metrics in the Reticular Synthesis of Crystalline Metal−Organic Frameworks and Polyhedra. *J. Am. Chem. Soc.* **2008,** *130* (35), 11650-11661.

178.   Batten, S. R.; Champness, N. R.; Chen, X.-M.; Garcia-Martinez, J.; Kitagawa, S.; Öhrström, L.; O'Keeffe, M.; Suh, M. P.; Reedijk, J., Coordination polymers, metal–organic frameworks and the need for terminology guidelines. *CrystEngComm* **2012,** *14* (9).

179.   Pichon, A.; Lazuen-Garay, A.; James, S. L., Solvent-free synthesis of a microporous metal–organic framework. *CrystEngComm* **2006,** *8* (3).

180.   Guan, Y.; Shi, J.; Xia, M.; Zhang, J.; Pang, Z.; Marchetti, A.; Wang, X.; Cai, J.; Kong, X., Monodispersed ZIF-8 particles with enhanced performance for CO2 adsorption and heterogeneous catalysis. *Appl. Surf. Sci.* **2017,** *423*, 349-353.

181.   Titi, H. M.; Marrett, J. M.; Dayaker, G.; Arhangelskis, M.; Mottillo, C.; Morris, A. J.; Rachiero, G. P.; Friščić, T.; Rogers, R. D., Hypergolic zeolitic imidazolate frameworks (ZIFs) as next-generation solid fuels: Unlocking the latent energetic behavior of ZIFs. *Sci. Adv.* **2019,** *5* (4).

182.   Rungtaweevoranit, B.; Diercks, C. S.; Kalmutzki, M. J.; Yaghi, O. M., Spiers Memorial Lecture:. Progress and prospects of reticular chemistry. *Faraday Discuss* **2017,** *201*, 9-45.

183.   Deria, P.; Mondloch, J. E.; Karagiaridi, O.; Bury, W.; Hupp, J. T.; Farha, O. K., Beyond post-synthesis modification: evolution of metal–organic frameworks via building block replacement. *Chem. Soc. Rev.* **2014,** *43* (16), 5896-5912.

184.   Furukawa, H.; Ko, N.; Go, Y. B.; Aratani, N.; Choi, S. B.; Choi, E.; Yazaydin, A. O.; Snurr, R. Q.; O'Keeffe, M.; Kim, J.; Yaghi, O. M., Ultrahigh porosity in metal-organic frameworks. *Science* **2010,** *329* (5990), 424-8.

185.   de Lange, M. F.; Verouden, K. J. F. M.; Vlugt, T. J. H.; Gascon, J.; Kapteijn, F., Adsorption-Driven Heat Pumps: The Potential of Metal–Organic Frameworks. *Chem. Rev.* **2015,** *115* (22), 12205-12250.

186.   Tansell, A. J.; Jones, C. L.; Easun, T. L., MOF the beaten track: unusual structures and uncommon applications of metal–organic frameworks. *Chemistry Central Journal* **2017,** *11* (1).

187.   Coudert, F.-X., Responsive Metal–Organic Frameworks and Framework Materials: Under Pressure, Taking the Heat, in the Spotlight, with Friends. *Chem. Mater.* **2015,** *27* (6), 1905-1916.

188.   Schweinefuß, M. E.; Springer, S.; Baburin, I. A.; Hikov, T.; Huber, K.; Leoni, S.; Wiebcke, M., Zeolitic imidazolate framework-71 nanocrystals and a novel SOD-type polymorph: solution mediated phase transformations, phase selection via coordination modulation and a density functional theory derived energy landscape. *Dalton Trans.* **2014,** *43* (9).

189.   Coudert, F.-X.; Fuchs, A. H., Computational characterization and prediction of metal–organic framework properties. *Coord. Chem. Rev.* **2016,** *307*, 211-236.

190.   Easun, T. L.; Moreau, F.; Yan, Y.; Yang, S.; Schröder, M., Structural and dynamic studies of substrate binding in porous metal–organic frameworks. *Chem. Soc. Rev.* **2017,** *46* (1), 239-274.

191.   Arhangelskis, M.; Katsenis, A. D.; Morris, A. J.; Friščić, T., Computational evaluation of metal pentazolate frameworks: inorganic analogues of azolate metal–organic frameworks. *Chem. Sci.* **2018,** *9* (13), 3367-3375.

192.   Titi, H. M.; Arhangelskis, M.; Katsenis, A. D.; Mottillo, C.; Ayoub, G.; Do, J.-L.; Fidelli, A. M.; Rogers, R. D.; Friščić, T., Metal–Organic Frameworks as Fuels for Advanced Applications: Evaluating and Modifying the Combustion Energy of Popular MOFs. *Chem. Mater.* **2019,** *31* (13), 4882-4888.

193.   Zhang, J.; Wu, T.; Zhou, C.; Chen, S.; Feng, P.; Bu, X., Zeolitic Boron Imidazolate Frameworks. *Angew. Chem. Int. Ed.* **2009,** *48* (14), 2542-2545.

194.   Gygi, D.; Bloch, E. D.; Mason, J. A.; Hudson, M. R.; Gonzalez, M. I.; Siegelman, R. L.; Darwish, T. A.; Queen, W. L.; Brown, C. M.; Long, J. R., Hydrogen Storage in the Expanded Pore Metal–Organic Frameworks M2(dobpdc) (M = Mg, Mn, Fe, Co, Ni, Zn). *Chem. Mater.* **2016,** *28* (4), 1128-1138.

195.   Loiseau, T.; Serre, C.; Huguenard, C.; Fink, G.; Taulelle, F.; Henry, M.; Bataille, T.; Férey, G., A Rationale for the Large Breathing of the Porous Aluminum Terephthalate (MIL-53) Upon Hydration. *Chem. -Eur. J.* **2004,** *10* (6), 1373-1382.

196.   Ferey, G., A Chromium Terephthalate-Based Solid with Unusually Large Pore Volumes and Surface Area. *Science* **2005,** *309* (5743), 2040-2042.

197.   López-Cabrelles, J.; Romero, J.; Abellán, G.; Giménez-Marqués, M.; Palomino, M.; Valencia, S.; Rey, F.; Mínguez Espallargas, G., Solvent-Free Synthesis of ZIFs: A Route toward the Elusive Fe(II) Analogue of ZIF-8. *J. Am. Chem. Soc.* **2019,** *141* (17), 7173-7180.

198.   Deng, H.; Grunder, S.; Cordova, K. E.; Valente, C.; Furukawa, H.; Hmadeh, M.; Gandara, F.; Whalley, A. C.; Liu, Z.; Asahina, S.; Kazumori, H.; O'Keeffe, M.; Terasaki, O.; Stoddart, J. F.; Yaghi, O. M., Large-Pore Apertures in a Series of Metal-Organic Frameworks. *Science* **2012,** *336* (6084), 1018-1023.

199.   Zhong, G.; Liu, D.; Zhang, J., The application of ZIF-67 and its derivatives: adsorption, separation, electrochemistry and catalysts. *J. Mater. Chem. A* **2018,** *6* (5), 1887-1899.

200.   Chui, S. S., A Chemically Functionalizable Nanoporous Material [Cu3(TMA)2(H2O)3]n. *Science* **1999,** *283* (5405), 1148-1150.

201.   Bhatt, P. M.; Belmabkhout, Y.; Cadiau, A.; Adil, K.; Shekhah, O.; Shkurenko, A.; Barbour, L. J.; Eddaoudi, M., A Fine-Tuned Fluorinated MOF Addresses the Needs for Trace CO2 Removal and Air Capture Using Physisorption. *J. Am. Chem. Soc.* **2016,** *138* (29), 9301-9307.

202.   Cavka, J. H.; Jakobsen, S.; Olsbye, U.; Guillou, N.; Lamberti, C.; Bordiga, S.; Lillerud, K. P., A New Zirconium Inorganic Building Brick Forming Metal Organic Frameworks with Exceptional Stability. *J. Am. Chem. Soc.* **2008,** *130* (42), 13850-13851.

203.   Wang, T. C.; Vermeulen, N. A.; Kim, I. S.; Martinson, A. B. F.; Stoddart, J. F.; Hupp, J. T.; Farha, O. K., Scalable synthesis and post-modification of a mesoporous metal-organic framework called NU-1000. *Nat. Protoc.* **2015,** *11* (1), 149-162.

204.   Cliffe, M. J.; Wan, W.; Zou, X.; Chater, P. A.; Kleppe, A. K.; Tucker, M. G.; Wilhelm, H.; Funnell, N. P.; Coudert, F.-X.; Goodwin, A. L., Correlated defect nanoregions in a metal–organic framework. *Nat. Commun.* **2014,** *5* (1).

205.   Lammert, M.; Wharmby, M. T.; Smolders, S.; Bueken, B.; Lieb, A.; Lomachenko, K. A.; Vos, D. D.; Stock, N., Cerium-based metal organic frameworks with UiO-66 architecture: synthesis, properties and redox catalytic activity. *Chem. Commun.* **2015,** *51* (63), 12578-12581.

206.   Guo, X.; Zhu, G.; Li, Z.; Sun, F.; Yang, Z.; Qiu, S., A lanthanide metal–organic framework with high thermal stability and available Lewis-acid metal sites. *Chem. Commun.* **2006,** (30), 3172-3174.

207.   Devic, T.; Serre, C.; Audebrand, N.; Marrot, J.; Férey, G., MIL-103, A 3-D Lanthanide-Based Metal Organic Framework with Large One-Dimensional Tunnels and A High Surface Area. *J. Am. Chem. Soc.* **2005,** *127* (37), 12788-12789.

208.   Huskić, I.; Friščić, T., Understanding geology through crystal engineering: coordination complexes, coordination polymers and metal–organic frameworks as minerals. *Acta Crystallogr., Sect. B: Struct. Sci. Cryst. Eng. Mater.* **2018,** *74* (6), 539-559.

209.   Falaise, C.; Volkringer, C.; Vigier, J.-F.; Henry, N.; Beaurain, A.; Loiseau, T., Three-Dimensional MOF-Type Architectures with Tetravalent Uranium Hexanuclear Motifs (U6O8). *Chem. -Eur. J.* **2013,** *19* (17), 5324-5331.

210.   Dolgopolova, E. A.; Rice, A. M.; Shustova, N. B., Actinide-based MOFs: a middle ground in solution and solid-state structural motifs. *Chem. Commun.* **2018,** *54* (50), 6472-6483.

211.   Zhang, Y.; Lucier, B. E. G.; McKenzie, S. M.; Arhangelskis, M.; Morris, A. J.; Friščić, T.; Reid, J. W.; Terskikh, V. V.; Chen, M.; Huang, Y., Welcoming Gallium- and Indium-Fumarate MOFs to the Family: Synthesis, Comprehensive Characterization, Observation of Porous Hydrophobicity, and CO2 Dynamics. *ACS Applied Materials & Interfaces* **2018,** *10* (34), 28582-28596.

212.   Carter, K. P.; Ridenour, J. A.; Kalaj, M.; Cahill, C. L., A Thorium Metal-Organic Framework with Outstanding Thermal and Chemical Stability. *Chemistry – A European Journal* **2019,** *25* (29), 7114-7118.

213.   Gilson, S. E.; Li, P.; Szymanowski, J. E. S.; White, J.; Ray, D.; Gagliardi, L.; Farha, O. K.; Burns, P. C., In Situ Formation of Unprecedented Neptunium-Oxide Wheel Clusters Stabilized in a Metal–Organic Framework. *J. Am. Chem. Soc.* **2019,** *141* (30), 11842-11846.

214.   Robison, L.; Zhang, L.; Drout, R. J.; Li, P.; Haney, C. R.; Brikha, A.; Noh, H.; Mehdi, B. L.; Browning, N. D.; Dravid, V. P.; Cui, Q.; Islamoglu, T.; Farha, O. K., A Bismuth Metal–Organic Framework as a Contrast Agent for X-ray Computed Tomography. *ACS Applied Bio Materials* **2019,** *2* (3), 1197-1203.

215.   Park, K. S.; Ni, Z.; Cote, A. P.; Choi, J. Y.; Huang, R.; Uribe-Romo, F. J.; Chae, H. K.; O'Keeffe, M.; Yaghi, O. M., Exceptional chemical and thermal stability of zeolitic imidazolate frameworks. *Proc. Natl. Acad. Sci. U.S.A.* **2006,** *103* (27), 10186-10191.

216.   Zhang, J.-P.; Zhang, Y.-B.; Lin, J.-B.; Chen, X.-M., Metal Azolate Frameworks: From Crystal Engineering to Functional Materials. *Chem. Rev.* **2011,** *112* (2), 1001-1033.

217.   Beldon, P. J.; Fábián, L.; Stein, R. S.; Thirumurugan, A.; Cheetham, A. K.; Friščić, T., Rapid Room-Temperature Synthesis of Zeolitic Imidazolate Frameworks by Using Mechanochemistry. *Angew. Chem. Int. Ed.* **2010,** *49* (50), 9640-9643.

218.   Akimbekov, Z.; Katsenis, A. D.; Nagabhushana, G. P.; Ayoub, G.; Arhangelskis, M.; Morris, A. J.; Friščić, T.; Navrotsky, A., Experimental and Theoretical Evaluation of the Stability of True MOF Polymorphs Explains Their Mechanochemical Interconversions. *J. Am. Chem. Soc.* **2017,** *139* (23), 7952-7957.

219.   Lewis, D. W.; Ruiz-Salvador, A. R.; Gómez, A.; Rodriguez-Albelo, L. M.; Coudert, F.-X.; Slater, B.; Cheetham, A. K.; Mellot-Draznieks, C., Zeolitic imidazole frameworks: structural and energetics trends compared with their zeolite analogues. *CrystEngComm* **2009,** *11* (11).

220.   Galvelis, R.; Slater, B.; Cheetham, A. K.; Mellot-Draznieks, C., Comparison of the relative stability of zinc and lithium-boron zeolitic imidazolate frameworks. *CrystEngComm* **2012,** *14* (2), 374-378.

221.   Hughes, J. T.; Bennett, T. D.; Cheetham, A. K.; Navrotsky, A., Thermochemistry of Zeolitic Imidazolate Frameworks of Varying Porosity. *J. Am. Chem. Soc.* **2012,** *135* (2), 598-601.

222.   Schröder, C. A.; Baburin, I. A.; van Wüllen, L.; Wiebcke, M.; Leoni, S., Subtle polymorphism of zinc imidazolate frameworks: temperature-dependent ground states in the energy landscape revealed by experiment and theory. *CrystEngComm* **2013,** *15* (20), 4036-4040.

223.   Thornton, A. W.; Jelfs, K. E.; Konstas, K.; Doherty, C. M.; Hill, A. J.; Cheetham, A. K.; Bennett, T. D., Porosity in metal–organic framework glasses. *Chem. Commun.* **2016,** *52* (19), 3750-3753.

224.   Calvin, J. J.; Asplund, M.; Akimbekov, Z.; Ayoub, G.; Katsenis, A. D.; Navrotsky, A.; Friščić, T.; Woodfield, B. F., Heat capacity and thermodynamic functions of crystalline and amorphous forms of the metal organic framework zinc 2-ethylimidazolate, Zn(EtIm)2. *J. Chem. Thermodyn.* **2018,** *116*, 341-351.

225.   Arhangelskis, M.; Katsenis, A. D.; Novendra, N.; Akimbekov, Z.; Gandrath, D.; Marrett, J. M.; Ayoub, G.; Morris, A. J.; Farha, O. K.; Friščić, T.; Navrotsky, A., Theoretical Prediction and Experimental Evaluation of Topological Landscape and Thermodynamic Stability of a Fluorinated Zeolitic Imidazolate Framework. *Chem. Mater.* **2019,** *31* (10), 3777-3783.

226.   Rosen, P. F.; Calvin, J. J.; Dickson, M. S.; Katsenis, A. D.; Friščić, T.; Navrotsky, A.; Ross, N. L.; Kolesnikov, A. I.; Woodfield, B. F., Heat capacity and thermodynamic functions of crystalline forms of the metal-organic framework zinc 2-methylimidazolate, Zn(MeIm)2. *J. Chem. Thermodyn.* **2019,** *136*, 160-169.

227.   Navrotsky, A.; Petrovic, I.; Hu, Y.; Chen, C.-Y.; Davis, M. E., Little energetic limitation to microporous and mesoporous materials. *Microporous Materials* **1995,** *4* (1), 95-98.

228.   Trofymluk, O.; Levchenko, A. A.; Tolbert, S. H.; Navrotsky, A., Energetics of Mesoporous Silica: Investigation into Pore Size and Symmetry. *Chem. Mater.* **2005,** *17* (14), 3772-3783.

229.   Dunitz, J. D.; Bernstein, J., Disappearing Polymorphs. *Acc. Chem. Res.* **2002,** *28* (4), 193-200.

230.   Bučar, D.-K.; Lancaster, R. W.; Bernstein, J., Disappearing Polymorphs Revisited. *Angew. Chem. Int. Ed.* **2015,** *54* (24), 6972-6993.

231.   Tian, Y.-Q.; Xu, L.; Cai, C.-X.; Wei, J.-C.; Li, Y.-Z.; You, X.-Z., Determination of the Solvothermal Synthesis Mechanism of Metal Imidazolates by X-ray Single-Crystal Studies of a Photoluminescent Cadmium(II) Imidazolate and Its Intermediate Involving Piperazine. *Eur. J. Inorg. Chem.* **2004,** *2004* (5), 1039-1044.

232.   Tian, Y.-Q.; Yao, S.-Y.; Gu, D.; Cui, K.-H.; Guo, D.-W.; Zhang, G.; Chen, Z.-X.; Zhao, D.-Y., Cadmium Imidazolate Frameworks with Polymorphism, High Thermal Stability, and a Large Surface Area. *Chem. -Eur. J.* **2010,** *16* (4), 1137-1141.

233.   Yao, S.-Y.; Tian, Y.-Q., An exceptional self-penetrating 4-connected network derived from a (3,4)-connected net oftfa-ctopology. *CrystEngComm* **2010,** *12* (3), 697-699.

234.   Mewes, J. M.; Smits, O. R.; Kresse, G.; Schwerdtfeger, P., Copernicium: A Relativistic Noble Liquid. *Angew. Chem. Int. Ed.* **2019,** *58* (50), 17964-17968.

235.   Liu, D.-S.; Sui, Y.; Ye, G.-M.; Wang, H.-y.; Liu, J.-Q.; Chen, W.-T., Synthesis, structures and properties of three mercury coordination polymers based on 5-methyltetrazolate ligand. *J. Solid State Chem.* **2018,** *263*, 182-189.

236.   Masciocchi, N.; Ardizzoia, G. A.; Maspero, A.; LaMonica, G.; Sironi, A., Metal Pyrazolato Complexes. Synthesis, Characterization, and X-ray Powder Diffraction Studies of Group 12 Coordination Polymers. *Inorg. Chem.* **1999,** *38* (16), 3657-3664.

237.   Masciocchi, N.; Attilio Ardizzoia, G.; Brenna, S.; Castelli, F.; Galli, S.; Maspero, A.; Sironi, A., Synthesis and ab-initio XRPD structure of group 12 imidazolato polymers. *Chem. Commun.* **2003,** (16).

238.   Fernández-Bertrán, J. F.; Hernández, M. P.; Reguera, E.; Yee-Madeira, H.; Rodriguez, J.; Paneque, A.; Llopiz, J. C., Characterization of mechanochemically synthesized imidazolates of Ag+1, Zn+2, Cd+2, and Hg+2: Solid state reactivity of nd10 cations. *J. Phys. Chem. Solids* **2006,** *67* (8), 1612-1617.

239.   Rightmire, N. R.; Hanusa, T. P., Advances in organometallic synthesis with mechanochemical methods. *Dalton Trans.* **2016,** *45* (6), 2352-2362.

240.   Friščić, T.; Mottillo, C.; Titi, H. M., Mechanochemistry for Synthesis. *Angew. Chem. Int. Ed.* **2019,** *59* (3), 1018-1029.

241.   Yang, L.; Powell, D. R.; Houser, R. P., Structural variation in copper(i) complexes with pyridylmethylamide ligands: structural analysis with a new four-coordinate geometry index, τ4. *Dalton Trans.* **2007,** (9), 955-964.

242.   Okuniewski, A.; Rosiak, D.; Chojnacki, J.; Becker, B., Coordination polymers and molecular structures among complexes of mercury(II) halides with selected 1-benzoylthioureas. *Polyhedron* **2015,** *90*, 47-57.

243.   Rosiak, D.; Okuniewski, A.; Chojnacki, J., Novel complexes possessing Hg–(Cl, Br, I)···O C halogen bonding and unusual Hg 2 S 2 (Br/I) 4 kernel. The usefulness of τ4′ structural parameter. *Polyhedron* **2018,** *146*, 35-41.

244.   Masciocchi, N.; Castelli, F.; Forster, P. M.; Tafoya, M. M.; Cheetham, A. K., Synthesis and Characterization of Two Polymorphic Crystalline Phases and an Amorphous Powder of Nickel(II) Bisimidazolate. *Inorg. Chem.* **2003,** *42* (19), 6147-6152.

245.   Ma, L.; Shin, J.-Y.; Patrick, B. O.; Dolphin, D., Metal complexes of dipyrromethenes linked by rigid spacer arms. *CrystEngComm* **2008,** *10* (11).

246.   Harris, K. J.; Lupulescu, A.; Lucier, B. E. G.; Frydman, L.; Schurko, R. W., Broadband adiabatic inversion pulses for cross polarization in wideline solid-state NMR spectroscopy. *Journal of Magnetic Resonance* **2012,** *224*, 38-47.

247.   Mottillo, C.; Friscic, T., Advances in Solid-State Transformations of Coordination Bonds: From the Ball Mill to the Aging Chamber. *Molecules* **2017,** *22* (1).

248.   Užarević, K.; Wang, T. C.; Moon, S.-Y.; Fidelli, A. M.; Hupp, J. T.; Farha, O. K.; Friščić, T., Mechanochemical and solvent-free assembly of zirconium-based metal–organic frameworks. *Chem. Commun.* **2016,** *52* (10), 2133-2136.

249.   Huskić, I.; Christopherson, J.-C.; Užarević, K.; Friščić, T., In situ monitoring of vapour-induced assembly of pharmaceutical cocrystals using a benchtop powder X-ray diffractometer. *Chem. Commun.* **2016,** *52* (29), 5120-5123.

250.   Dovesi, R.; Erba, A.; Orlando, R.; Zicovich-Wilson, C. M.; Civalleri, B.; Maschio, L.; Rérat, M.; Casassa, S.; Baima, J.; Salustro, S.; Kirtman, B., Quantum-mechanical condensed matter simulations with CRYSTAL. *Wiley Interdisciplinary Reviews: Computational Molecular Science* **2018,** *8* (4).

251.   Becke, A. D., Density-functional thermochemistry. III. The role of exact exchange. *J. Chem. Phys.* **1993,** *98* (7), 5648-5652.

252.   Lee, C.; Yang, W.; Parr, R. G., Development of the Colle-Salvetti correlation-energy formula into a functional of the electron density. *Phys. Rev.* **1988,** *37* (2), 785-789.

253.   Grimme, S.; Antony, J.; Ehrlich, S.; Krieg, H., A consistent and accurate ab initio parametrization of density functional dispersion correction (DFT-D) for the 94 elements H-Pu. *J. Chem. Phys.* **2010,** *132* (15).

254.   Baburin, I. A.; Leoni, S.; Seifert, G., Enumeration of Not-Yet-Synthesized Zeolitic Zinc Imidazolate MOF Networks: A Topological and DFT Approach. *J. Phys. Chem. B* **2008,** *112* (31), 9437-9443.

255.   Alvarez, S., A cartography of the van der Waals territories. *Dalton Trans.* **2013,** *42* (24).

256.   Hu, S.-Z.; Zhou, Z.-H.; Robertson, B. E., Consistent approaches to van der Waals radii for the metallic elements. *Zeitschrift für Kristallographie* **2009,** *224* (8).

257.   Brookhart, M.; Green, M. L. H.; Parkin, G., Agostic interactions in transition metal compounds. *Proc. Natl. Acad. Sci. U.S.A.* **2007,** *104* (17), 6908-6914.

258.   Chen, Y.-C.; Tung, J.-Y.; Liu, T.-K.; Tsai, W.-J.; Lin, H.-Y.; Chang, Y.-C.; Chen, J.-H., The η1-H–C···Hg agostic interactions in the mercury complexes of N-confused porphyrin. *Dalton Trans.* **2018,** *47* (41), 14774-14784.

259.   Ilie, A.; Raţ, C. I.; Scheutzow, S.; Kiske, C.; Lux, K.; Klapötke, T. M.; Silvestru, C.; Karaghiosoff, K., Metallophilic Bonding and Agostic Interactions in Gold(I) and Silver(I) Complexes Bearing a Thiotetrazole Unit. *Inorg. Chem.* **2011,** *50* (6), 2675-2684.

260.   Izod, K.; McFarlane, W.; Tyson, B. V.; Carr, I.; Clegg, W.; Harrington, R. W., Stabilization of a Dialkylstannylene by Unusual B–H···Sn γ-Agostic-Type Interactions. A Structural, Spectroscopic, and DFT Study. *Organometallics* **2006,** *25* (5), 1135-1143.

261.   Kozelka, J., Agostic and Hydrogen-Bonding X–H…M Interactions Involving a d8 Metal Center: Recent Advances Towards Their Understanding. In *Noncovalent Forces*, 2015; pp 129-158.

262.   Bader, R. F. W., A Bond Path: A Universal Indicator of Bonded Interactions. *J. Phys. Chem. A* **1998,** *102* (37), 7314-7323.

263.   Lein, M., Characterization of agostic interactions in theory and computation. *Coord. Chem. Rev.* **2009,** *253* (5-6), 625-634.

264.   Liu, C.-S.; Chen, P.-Q.; Yang, E.-C.; Tian, J.-L.; Bu, X.-H.; Li, Z.-M.; Sun, H.-W.; Lin, Z., Silver(I) Complexes in Coordination Supramolecular System with Bulky Acridine-Based Ligands: Syntheses, Crystal Structures, and Theoretical Investigations on C–H···Ag Close Interaction. *Inorg. Chem.* **2006,** *45* (15), 5812-5821.

265.   Yeşilel, O. Z.; Günay, G.; Darcan, C.; Soylu, M. S.; Keskin, S.; Ng, S. W., An unusual 3D metal–organic framework, {[Ag4(μ4-pzdc)2(μ-en)2]·H2O}n: C–H···Ag, N–H···Ag and (O–H)···Ag interactions and an unprecedented coordination mode for pyrazine-2,3-dicarboxylate. *CrystEngComm* **2012,** *14* (8).

266.   Yuan, W.; Friščić, T.; Apperley, D.; James, S. L., High Reactivity of Metal-Organic Frameworks under Grinding Conditions: Parallels with Organic Molecular Materials. *Angew. Chem. Int. Ed.* **2010,** *49* (23), 3916-3919.

267.   Bučar, D.-K.; Day, G. M.; Halasz, I.; Zhang, G. G. Z.; Sander, J. R. G.; Reid, D. G.; MacGillivray, L. R.; Duer, M. J.; Jones, W., The curious case of (caffeine)·(benzoic acid): how heteronuclear seeding allowed the formation of an elusive cocrystal. *Chem. Sci.* **2013,** *4* (12).

268.   Clough, A. J.; Orchanian, N. M.; Skelton, J. M.; Neer, A. J.; Howard, S. A.; Downes, C. A.; Piper, L. F. J.; Walsh, A.; Melot, B. C.; Marinescu, S. C., Room Temperature Metallic

Conductivity in a Metal–Organic Framework Induced by Oxidation. *J. Am. Chem. Soc.* **2019,** *141* (41), 16323-16330.

269.   Sadakiyo, M.; Yamada, T.; Kitagawa, H., Hydrated Proton-Conductive Metal-Organic Frameworks. *ChemPlusChem* **2016,** *81* (8), 691-701.

270.   Sun, L.; Campbell, M. G.; Dincă, M., Electrically Conductive Porous Metal-Organic Frameworks. *Angew. Chem. Int. Ed.* **2016,** *55* (11), 3566-3579.

271.   Yang, Q.-F.; Cui, X.-B.; Yu, J.-H.; Lu, J.; Yu, X.-Y.; Zhang, X.; Xu, J.-Q.; Hou, Q.; Wang, T.-G., A series of metal–organic complexes constructed from in situ generated organic amines. *CrystEngComm* **2008,** *10* (11).

272.   Maddox, B., The double helix and the 'wronged heroine'. *Nature* **2003,** *421* (6921), 407-8.

273.   Moore, C., A complex legacy. *Nature Physics* **2011,** *7* (11), 828-830.

274.   Gonzalez-Sanabria, O. D. Effect of NASA Advanced Designs on Thermal Behavior of Ni-H2 Cells; Lewis Research Center, 1987. https://go.nature.com/3eTaBr1

275.   Neal, H. A.; Smith, T. L.; McCormick, J. B. Beyond Sputnik: U.S. Science Policy in the Twenty-First Century; The Univ. of Michigan Press, 2008.

276.   Matlin, S. A.; Yam, V. W. W.; Mehta, G.; Krief, A.; Hopf, H., The Need for Cultural Competence in Science: A Practical Approach to Enhancing Equality, Diversity, and Inclusion. *Angew. Chem. Int. Ed.* **2019,** *58* (10), 2912-2913.

277.   Mehta, G.; Yam, V. W. W.; Krief, A.; Hopf, H.; Matlin, S. A., The Chemical Sciences and Equality, Diversity, and Inclusion. *Angew. Chem. Int. Ed.* **2018,** *57* (45), 14690-14698.

278.   Anastas, P. T.; Zimmerman, J. B., The United Nations sustainability goals: How can sustainable chemistry contribute? *Current Opinion in Green and Sustainable Chemistry* **2018,** *13*, 150-153.

279.   Niesche, R.; Keddie, A., Foregrounding issues of equity and diversity in educational leadership. *Sch. Lead. Manag.* **2011,** *31* (1), 65-77.

280.   Royal Society of Chemistry. Inclusion & diversity strategy, 2020. https://go.nature.com/39npn8i (accessed 19 June 2020).

281.   Hamrick, K. Women, Minorities, and Persons with Disabilities in Science and Engineering, 19-304; National Science Foundation, 2019. https://www.nsf.gov/statistics/wmpd/

282.   Hamrick, K. Women, Minorities, and Persons with Disabilities in Science and Engineering, 19-304; National Science Foundation, 2019. https://www.nsf.gov/statistics/wmpd/

283.   Gvozdanovï, J.; Maes, K. Implicit bias in academia: A challenge to the meritocratic principle and to women's careers – and what to do about it; League of European Research Universities, 2018. https://go.nature.com/3hlEORc

284.   Garcia, G. A.; Johnston-Guerrero, M. P. J. Crit. Scholarsh. High. Educ. Stud. Aff. 2015, 2, 4.

285.   Zirkel, S., Is There A Place for Me? Role Models and Academic Identity among White Students and Students of Color. *Teach. Coll. Rec.* **2002,** *104* (2), 357-376.

286.   Jamieson, K. H.; Capella, J. N. Echo chamber: Rush Limbaugh and the conservative media establishment; Oxford University Press, 2008.

287.	López, N.; Erwin, C.; Binder, M.; Chavez, M. J., Making the invisible visible: advancing quantitative methods in higher education using critical race theory and intersectionality. *Race Ethn. Educ.* **2017,** *21* (2), 180-207.

288.	Museus, S. D.; Griffin, K. A., Mapping the margins in higher education: On the promise of intersectionality frameworks in research and discourse. *New Dir. Instit. Res.* **2011,** *2011* (151), 5-13.

289.	Royal Society of Chemistry. Diversity landscape of the chemical sciences; Royal Society of Chemistry, 2018. https://go.nature.com/2V7miFv

290.	Widener, A. The leaky pipeline for Black academic chemists. Chem. Eng. News, 2020. https://go.nature.com/2D3p8Dq

291.	Johnson, D. R., Campus Racial Climate Perceptions and Overall Sense of Belonging Among Racially Diverse Women in STEM Majors. *J. Coll. Stud. Dev.* **2012,** *53* (2), 336-346.

292.	O'Brien, K. R.; McAbee, S. T.; Hebl, M. R.; Rodgers, J. R., The Impact of Interpersonal Discrimination and Stress on Health and Performance for Early Career STEM Academicians. *Frontiers in Psychology* **2016,** *7.*

293.	Ong, M.; Smith, J. M.; Ko, L. T., Counterspaces for women of color in STEM higher education: Marginal and central spaces for persistence and success. *J. Res. Sci. Teach.* **2018,** *55* (2), 206-245.

294.	Kross, E.; Berman, M. G.; Mischel, W.; Smith, E. E.; Wager, T. D., Social rejection shares somatosensory representations with physical pain. *Proc. Natl. Acad. Sci. U.S.A.* **2011,** *108* (15), 6270-6275.

295.	Vincent-Ruz, P.; Binning, K.; Schunn, C. D.; Grabowski, J., The effect of math SAT on women's chemistry competency beliefs. *Chem. Educ. Res. Pract.* **2018,** *19* (1), 342-351.

296.	Witherspoon, E. B.; Vincent-Ruz, P.; Schunn, C. D., When Making the Grade Isn't Enough: The Gendered Nature of Premed Science Course Attrition. *Educ. Res.* **2019,** *48* (4), 193-204.

297.	Hsu, D. T.; Sanford, B. J.; Meyers, K. K.; Love, T. M.; Hazlett, K. E.; Walker, S. J.; Mickey, B. J.; Koeppe, R. A.; Langenecker, S. A.; Zubieta, J. K., It still hurts: altered endogenous opioid activity in the brain during social rejection and acceptance in major depressive disorder. *Molec. Psych.* **2015,** *20* (2), 193-200.

298.	Meyer, I. H., Prejudice, social stress, and mental health in lesbian, gay, and bisexual populations: Conceptual issues and research evidence. *Psychol. Bull.* **2003,** *129* (5), 674-697.

299.	National Academies of Sciences, Engineering, and Medicine. The Science of Effective Mentorship in STEMM; The National Academies Press, 2019.

300.	Estrada, M.; Hernandez, P. R.; Schultz, P. W.; Herrera, J., A Longitudinal Study of How Quality Mentorship and Research Experience Integrate Underrepresented Minorities into STEM Careers. *CBE—Life Sciences Education* **2018,** *17* (1).

301.	McCoy, D. L.; Winkle-Wagner, R.; Luedke, C. L., Colorblind mentoring? Exploring white faculty mentoring of students of color. *J. Divers. High. Educ.* **2015,** *8* (4), 225-242.

302.	Social Sciences Feminist Network Research Interest Group Humboldt J. Soc. Relat. 2017, 39, 228

303.	Jimenez, M. F.; Laverty, T. M.; Bombaci, S. P.; Wilkins, K.; Bennett, D. E.; Pejchar, L., Underrepresented faculty play a disproportionate role in advancing diversity and inclusion. *Nat. Ecol. Evol.* **2019,** *3* (7), 1030-1033.

304. Reeser, D.; Vincent-Ruz, P.; Ashwell, S.; Kemsley, J.; Yarnell, A. The secret silos of #chemtwitter. Chem. Eng. News, 2019. https://go.nature.com/3jwG4mk

305. Luc, J. G. Y.; Archer, M. A.; Arora, R. C.; Bender, E. M.; Blitz, A.; Cooke, D. T.; Hlci, T. N.; Kidane, B.; Ouzounian, M.; Varghese, T. K.; Antonoff, M. B., Does Tweeting Improve Citations? One-Year Results From the TSSMN Prospective Randomized Trial. *The Annals of Thoracic Surgery* **2021,** *111* (1), 296-300.

306. Is science only for the rich? *Nature* **2016,** *537* (7621), 466-470.

307. Wang, L. Promoting Inclusion in ACS National Awards. Chem. Eng. News, 2014. https://go.nature.com/3fSK4LS

308. Guarino, C. M.; Borden, V. M. H., Faculty Service Loads and Gender: Are Women Taking Care of the Academic Family? *Res. High. Educ.* **2017,** *58* (6), 672-694.

309. Fahy, D. The New Celebrity Scientists: Out of the Lab and Into the Limelight; Rowman & Littlefield, 2015.

310. Clayton-Pedersen, A. R.; O'Neill, N.; Musil, C. M. Making Excellence Inclusive: A Framework for Embedding Diversity and Inclusion into College and Universities' Academic Excellence Mission; Association of American Colleges and Universities, 2009.

311. Wang, L. Making invisible work in STEM more visible. Chem. Eng. News, 2019. https://go.nature.com/2WOm9FA

312. Hunt, V.; Prince, S.; Dixon-Fyle, S.; Yee, L. Delivering through Diversity; McKinsey & Company, 2018. https://go.nature.com/2WOemI4

313. Hofstra, B.; Kulkarni, V. V.; Munoz-Najar Galvez, S.; He, B.; Jurafsky, D.; McFarland, D. A., The Diversity–Innovation Paradox in Science. *Proc. Natl. Acad. Sci. U.S.A.* **2020,** *117* (17), 9284-9291.

314. López Corredoira, M. The Twilight of the Scientific Age; Brown Walker Press, 2013.

315. Pinholster, G., Journals and funders confront implicit bias in peer review. *Science* **2016,** *352* (6289), 1067-1068.

316. The Researcher Journey Through a Gender Lens; Elsevier, 2020. https://go.nature.com/2EcHsug.

317. Project Implicit. Take a Test. Project Implicit,https://implicit.harvard.edu/implicit/takeatest.html

318. Polanyi, M., The Republic of science. *Minerva* **1962,** *1* (1), 54-73.

319. David, W. I. F.; Shankland, K.; van de Streek, J.; Pidcock, E.; Motherwell, W. D. S.; Cole, J. C., DASH: a program for crystal structure determination from powder diffraction data. *J. Appl. Crystallogr.* **2006,** *39* (6), 910-915.

320. Boultif, A.; Louër, D., Powder pattern indexing with the dichotomy method. *J. Appl. Crystallogr.* **2004,** *37* (5), 724-731.

321. Pawley, G. S., Unit-cell refinement from powder diffraction scans. *J. Appl. Crystallogr.* **1981,** *14* (6), 357-361.

322. A. Coelho, Coelho Software: Brisbane, Australia 2017.

323. Rietveld, H. M., Line profiles of neutron powder-diffraction peaks for structure refinement. *Acta Crystallogr.* **1967,** *22* (1), 151-152.

324. Taylor, R. E., 13C CP/MAS: Application to glycine. *Conc. Magn. Reson.* **2004,** *22A* (2), 79-89.

325. Bertani, P.; Raya, J.; Bechinger, B., 15N chemical shift referencing in solid state NMR. *Solid State Nucl. Magn Reson* **2014,** *61-62*, 15-18.

326. Hung, I.; Rossini, A. J.; Schurko, R. W., Application of the Carr–Purcell Meiboom–Gill Pulse Sequence for the Acquisition of Solid-State NMR Spectra of Spin-1/2Nuclei. *J. Phys. Chem. A* **2004,** *108* (34), 7112-7120.

327. Kidambi, S.; Ramamoorthy, A., Quantum Chemical Calculations of Cadmium Chemical Shifts in Inorganic Complexes. *J. Phys. Chem. A* **2002,** *106* (43), 10363-10369.

328. Hayashi, S.; Hayamizu, K., Chemical Shift Standards in High-Resolution Solid-State NMR (1)13C,29Si, and1H Nuclei. *Bull. Chem. Soc. Jpn.* **1991,** *64* (2), 685-687.

329. Vinogradov, E.; Madhu, P. K.; Vega, S., High-resolution proton solid-state NMR spectroscopy by phase-modulated Lee–Goldburg experiment. *Chem. Phys. Lett.* **1999,** *314* (5-6), 443-450.

330. Salager, E.; Stein, R. S.; Steuernagel, S.; Lesage, A.; Elena, B.; Emsley, L., Enhanced sensitivity in high-resolution 1H solid-state NMR spectroscopy with DUMBO dipolar decoupling under ultra-fast MAS. *Chem. Phys. Lett.* **2009,** *469* (4-6), 336-341.

331. Laun, J.; Vilela Oliveira, D.; Bredow, T., Consistent gaussian basis sets of double- and triple-zeta valence with polarization quality of the fifth period for solid-state calculations. *J. Comp. Chem.* **2018,** *39* (19), 1285-1290.

332. Peintinger, M. F.; Oliveira, D. V.; Bredow, T., Consistent Gaussian basis sets of triple-zeta valence with polarization quality for solid-state calculations. *J. Comp. Chem.* **2013,** *34* (6), 451-459.

333. Weihrich, R.; Anusca, I., Half Antiperovskites. III. Crystallographic and Electronic Structure Effects in Sn2–xInxCo3S2. *Z. Anorg. Allg. Chem.* **2006,** *632* (8-9), 1531-1537.

334. Wadt, W. R.; Hay, P. J., Ab initio effective core potentials for molecular calculations. Potentials for main group elements Na to Bi. *J. Chem. Phys.* **1985,** *82* (1), 284-298.

335. Dou, Y.; Egdell, R. G.; Law, D. S. L.; Harrison, N. M.; Searle, B. G., An experimental and theoretical investigation of the electronic structure of CdO. *J. Phys. Cond. Matt.* **1998,** *10* (38), 8447-8458.